

# **Visual Function in Human and Experimental Glaucoma**

**Asta Vasalauskaite**

**A dissertation submitted for the degree of**

**PhD in Neuroscience**

**Cardiff School of Biosciences**

**Cardiff University**

**July 2016**

## **Acknowledgments**

First of all, I want to thank my supervisors.

I would like to thank Professor Frank Sengpiel for his endless help and support during my studies and, whose infectious positivity inspired me and kept me motivated. I am particularly grateful for the time he dedicated to listening and advising me on all aspects of my work and for never turning me away when I knocked on his office door. I would like to thank my co-supervisor Professor James Morgan for his ideas, enthusiasm and vision that shaped my studies; I believe that collaborative support from both of my supervisors uniquely enriched my PhD experience and provided me with the opportunity to explore beyond both the human and the mouse.

I am particularly grateful to my colleague and friend Dr Irina Erchova for her help, advice and many hours spent training me during my early PhD. I would have been lost without her help.

I would like to thank Dr James Tribble for his help contributing to method establishment of Chapter 3 and for being overall a great colleague, listener and a friend. I am also very grateful to Dr Julie Albon, Dr Nick White, Dr Kate Binley and everyone else in School of Optometry for their help. I thank Dr Adam Ranson and Mr Timothy Gould from School of Biosciences for their advice relating to some of the techniques presented in this thesis. Also I would like to express my gratitude to our collaborators Dr Mike Fautsch for the donation of the human tissue and Professor Marcela Vortuba for her kind donation of OPA1 mouse.

Last, but not least, I would like to thank all of my family and friends, but especially my mother Larisa, my boyfriend Ashley, my friends and unofficial proof-readers Aaron Stewart, Katherine McCrory and of course my dog and best friend Margarita for their love and support during my studies.

## Summary

Injury to optic nerve (ON) axons plays a major role in glaucoma progression. ON crush is an established model of axonal injury which results in retrograde degeneration and death of retinal ganglion cells (RGCs). However, it is unknown how signal transmission to higher visual structures such as primary visual cortex (V1) is affected after ON crush. In human glaucoma, visual function is assessed using visual field (VF) tests, but it is also not clear how the test results relate to the disease progression in the retina.

Unilateral ON crush was performed on the left eyes of adult C57BL/6 mice. V1 function of the right hemisphere was assessed longitudinally by optical imaging (OI) and in vivo calcium two-photon imaging under anaesthesia before and at 7 days, 14 days and 30 days after ON crush. Human retinas from glaucoma patients were investigated for changes in RGC density and compared to the score from the VF data obtained prior to the patients' death.

ISI and 2P experiments demonstrate a significant shift in OD towards the ipsilateral eye and significant reduction of signal magnitude in V1 in response to contralateral eye stimulation in all ON crush animals. Additionally, response magnitude to ipsilateral eye stimulation was significantly increased after ON crush. While there was significant RGC loss in human glaucoma compared to age matched controls that was correlated to mean VF loss, the scores from the individual VF test points were uncorrelated to RGC density in anatomically equivalent areas.

This work demonstrates that unilateral ON crush results in immediate loss of signal transmission from the retina to V1 via a crushed ON. A significant increase of responsiveness in V1 to non-crushed eye stimulation was observed, which indicates that injury of the ON in adulthood may evoke compensatory plasticity in V1.

## **Abbreviations**

$\Delta R/R$  difference in reflectance/reflectance

bpm beats per minute

c/deg Cycles per degree

CCD charge-coupled device

CNS central nervous system

ECG electrocardiogram

GCL ganglion cell layer

GECIs genetically encoded calcium indicators

GFAP glial fibrillary acidic protein

ILM inner limiting membrane

i.m. intramuscular

INL inner nucleus layer

IOP Intraocular pressure

IPL inner plexiform layer

ISI intrinsic signal imaging

LGN lateral geniculate nucleus

dLGN dorsal lateral geniculate nucleus

M molar concentration ( $\text{mol}/\text{dm}^3$ )

MD monocular deprivation

ME monocular enucleation

n number

NFL Nerve fibre layer

ODI ocular dominance index

OD ocular dominance

ON optic nerve

ONH optic nerve head

OPA1 optical atrophy 1

O<sub>2</sub> oxygen

PACG primary angle-closure glaucoma

PB phosphate buffer

PBS phosphate buffered saline

PFA paraformaldehyde

POAG primary open-angle glaucoma

PV parvalbumin

PV+ parvalbumin positive

RGC retinal ganglion cell

ROI region of interest

RPE retinal pigment epithelium

s.e.m. standard error of mean

s.d. standard deviation

SC superior colliculus

s.c. subcutaneous

V1 primary visual cortex

V1b primary binocular visual cortex

VF visual field

## List of Figures

<i>Figure 1.1 Human retina</i> .....	5
<i>Figure 1.2 Human visual pathway and lamination of visual cortex.</i> .....	10
<i>Figure 1.3 Morphological types of mouse RGCs.</i> .....	13
<i>Figure 1.4 The visual cortical areas and visual fields of the mouse.</i> .....	16
<i>Figure 1.5 RGC death in glaucoma</i> .....	21
<i>Figure 2.1 ISI setup and output</i> .....	41
<i>Figure 2.2 V1b response magnitudes to individual eye stimulation, in normal adult mice.</i> .....	44
<i>Figure 2.3 ISI responses immediately after unilateral ON crush</i> .....	45
<i>Figure 2.4 Response magnitudes of V1b and ODI of normal adults, and after long term follow-up after contralateral ON crush</i> .....	47
<i>Figure 2.5 ODI and individual eye response, before and after ON crush</i> .....	49
<i>Figure 2.6 Stability of ISI magnitude maps</i> .....	50
<i>Figure 2.7 ISI magnitude maps from a sham ON crush subject</i> .....	51
<i>Figure 2.8 ISI magnitude and phase maps obtained from OPA1<sup>+/-</sup> mice</i> .....	52
<i>Figure 3.1 In vivo calcium 2P microscopy imaging</i> .....	61
<i>Figure 3.2 Example of orientation tuned neurons after ON crush</i> .....	65
<i>Figure 3.3 Mean responses of orientation tuned neurons</i> .....	66
<i>Figure 3.4 PV<sup>+</sup> interneurons after ON crush</i> .....	68
<i>Figure 3.5 In vivo structural imaging of PV<sup>+</sup> interneurons in V1b.</i> .....	69
<i>Figure 4.1 VF loss in glaucoma</i> .....	75
<i>Figure 4.2 Sampling grid and VF maps</i> .....	79
<i>Figure 4.3 Hoechst stained human retina</i> .....	81
<i>Figure 4.4 Areas of retinal dissection</i> .....	83
<i>Figure 4.5 Excluded retinal samples</i> .....	86
<i>Figure 4.6 Cell count comparison with previously published data</i> .....	90
<i>Figure 4.7 RGC density maps in the GCL of average normal retinas, and in glaucoma</i> .....	92
<i>Figure 4.8 RGC density across the vertical and horizontal meridians</i> .....	93
<i>Figure 4.9 The RGC density across the vertical and horizontal axis of normal, and glaucoma retinas</i> .....	95
<i>Figure 4.10 RGC density of sample GL277, compared with maps obtained from the VF test data</i> .	97
<i>Figure 4.11 RGC density of sample GL239, compared with maps obtained from the VF test</i> .....	99
<i>Figure 4.12 The correlation of sensitivity and total deviation with RGC loss</i> .....	101
<i>Figure 4.13 The mean deviation index and pattern standard deviation in glaucoma</i> .....	103
<i>Figure 4.14 Inner retinal layer thicknesses of both glaucoma, and normal subjects</i> .....	104
<i>Figure 4.15 Inner retinal layer thicknesses in regions of variable damage, within the same glaucomatous retina</i> .....	106
<i>Figure 4.16 Inner retinal layer thicknesses in moderate, and mild glaucoma damage, and in normal samples</i> .....	107
<i>Figure 4.17 GFAP activation in human retina</i> .....	108
<i>Figure 4.18 Arcuate retinal fibres</i> .....	110
<i>Figure 5.1 Microinjection setup</i> .....	117
<i>Figure 5.2 Single cell iontophoresis of cortical neurons</i> .....	122
<i>Figure 5.3 Diolistics and Golgi stain</i> .....	123
<i>Figure 5.4 Morphology of a single mouse RGC filled with Alexa Fluor</i> .....	124
<i>Figure 5.5 Single RGC in mouse retina filled with Alexa Fluor.</i> .....	125
<i>Figure 5.6 DiI iontophoresis and astrocytes in ON</i> .....	126
<i>Figure 5.7 Human RGC fills</i> .....	128
<i>Figure 6.1 A diagram depicting effects of adult MD, ME and ON crush.</i> .....	136
<i>Figure 6.2 An overview of cortical inhibitory network</i> .....	138

## List of Tables

<i>Table 4.1 Retinal donor information</i>	77
<i>Table 4.2 The corrections applied for displaced amacrine cells</i>	82
<i>Table 4.3 Tissue summary</i>	88
<i>Table 5.1 Fluorophore excitation wavelengths</i>	120



## Table of Contents

<b>Chapter 1: Introduction</b> .....	1
<b>1.1 The human visual system</b> .....	2
1.1.1 The gross anatomy of the human eye.....	2
1.1.2 The human retina .....	3
1.1.3 RGCs in human retina .....	5
1.1.4 Human ON and lamina cribrosa.....	7
1.1.5 The SC and the LGN in humans.....	8
1.1.6 Visual cortical areas in humans .....	9
<b>1.2 The mouse visual system</b> .....	10
1.2.1 The gross anatomy of the mouse eye.....	11
1.2.2 The mouse retina .....	11
1.2.3 Mouse RGCs .....	12
1.2.4 The ON and lamina region in a mouse .....	13
1.2.5 The SC and the dLGN in mouse .....	14
1.2.6 Visual cortical areas of a mouse .....	15
<b>1.3 Glaucoma</b> .....	17
1.3.1 POAG .....	17
1.3.2 PACG.....	18
1.3.3 Other types of glaucoma .....	18
1.3.4 Glaucoma prevalence .....	18
<b>1.4 Mechanism of RGC death in glaucoma</b> .....	19
<b>1.5 Mouse models of RGC death</b> .....	21
1.5.1 ON crush .....	21
1.5.2 Inducible models of increased IOP .....	22
1.5.3 Genetic models of mouse glaucoma .....	22
<b>1.6 Plasticity of visual cortex</b> .....	23
1.6.1 OD plasticity .....	24
1.6.2 Adult plasticity.....	25
<b>1.7 ISI</b> .....	26
<b>1.8 Two-photon excitation microscopy</b> .....	27
1.8.1 Intracellular calcium in neurons.....	28
1.8.2 In Vivo two-photon calcium imaging using GECIs.....	28
1.8.3 GCaMP family calcium sensors .....	29
1.8.4 Aims of the study .....	30

<b>Chapter 2: ISI of V1b after unilateral ON crush in adult mice</b> .....	32
<b>2.1 Introduction</b> .....	33
<b>2.2 Materials and methods</b> .....	35
2.2.1 Mice.....	35
2.2.2 ON crush .....	36
2.2.3 Cranial window surgery.....	38
2.2.4 Chronic ISI procedure .....	39
2.2.5 Terminal ISI procedure .....	39
2.2.6 Periodic ISI protocol .....	40
2.2.7 Data analysis .....	42
2.2.8 Statistical analysis.....	42
<b>2.3 Results</b> .....	42
2.3.1 ISI responses in V1b of normal adult mice .....	43
2.3.2 ISI responses are diminished in V1b immediately after the unilateral ON crush	44
2.3.3 ISI responses stay diminished in V1b after long term unilateral ON crush	46
2.3.4 Responses of V1b in the same animals, before and after the unilateral ON crush	47
2.3.5 Stability of V1b responses.....	50
2.3.6 Responses of V1b after sham ON crush .....	50
2.3.7 Responses of V1b in the OPA1 <sup>+/-</sup> mice .....	51
<b>2.4 Discussion</b> .....	52
<b>2.5 Conclusion</b> .....	54
<b>Chapter 3: In vivo two-photon calcium imaging of neurons in V1b after unilateral ON crush in adult mice</b> .....	56
<b>3.1 Introduction</b> .....	57
<b>3.2 Materials and methods</b> .....	58
3.2.1 Experimental animals .....	58
3.2.2 Delivery of calcium indicator .....	59
3.2.3 Chronic in-vivo calcium two-photon laser scanning imaging.....	59
3.2.4 Quantification of PV <sup>+</sup> interneurons in V1b.....	62
3.2.5 Calcium signal data analysis.....	62
3.2.6 Statistical analysis.....	63
<b>3.3 Results</b> .....	63
3.3.1 Orientation tuned neuron responses in V1b after unilateral ON crush.....	63
3.3.2 PV <sup>+</sup> interneuron responses in V1b after unilateral ON crush.....	67

3.3.3 The density of PV+ interneurons remained unchanged in V1b, after ON crush .....	69
3.4 Discussion .....	70
Chapter 4: RGC density in human glaucoma .....	73
4.1 Introduction .....	74
4.2 Methods and Materials .....	76
4.2.1 Human tissue source.....	76
4.2.2 VF data .....	77
4.2.3 Preparation of human tissue for two-photon imaging .....	78
4.2.4 Two-photon imaging of human tissue.....	78
4.2.5 Image analysis.....	80
4.2.6 Criteria for RGC counts .....	80
4.2.7 Preparation of retinal cryosections .....	82
4.2.8 Haematoxylin and Eosin (H&E) staining.....	84
4.2.9 Immunofluorescence staining.....	84
4.2.10 Microscopy .....	85
4.2.11 Image analysis .....	85
4.2.12 Statistical analysis.....	85
4.3 Results .....	85
4.3.1 Exclusion of samples.....	85
4.3.2 Final tissue summary .....	87
4.3.3 Comparison of normal control subject RGC density with published data ....	89
4.3.4 The Density of RGCs were reduced in glaucomatous retinas .....	90
4.3.5 High variability in RGC density within the group of glaucoma subjects.....	93
4.3.6 Correlation of the density of RGCs in individual areas of glaucomatous retinas, with the VF test data within the same donor retina .....	96
4.3.7 Peak cell loss in glaucoma showed correlation with the summary findings of the VF test .....	102
4.3.8 Overall inner retinal layer thicknesses are reduced in glaucoma, compared to normal subjects.....	103
4.3.9 The thickness of inner retinal layers within the same glaucoma retina .....	104
4.4 Discussion .....	109
Chapter 5: Microinjection, Golgi and Diolistics: Single cell labelling methods to study morphology in fixation preserved tissue .....	113
5.1 Introduction .....	114
5.2 Materials and Methods .....	115
5.2.1 Animal tissue.....	115

5.2.2 Human tissue.....	116
5.2.3 General microinjection setup .....	116
5.2.4 DiI Iontophoresis .....	118
5.2.5 Alexa Fluor Iontophoresis .....	118
5.2.6 Golgi stain .....	118
5.2.7 Diolistics in fixed tissue .....	119
5.2.8 Microscopy .....	119
5.2.9 Image processing .....	120
5.3 Results .....	121
5.3.1 Neurons in mouse V1 brain slices .....	121
5.3.2 RGC morphology in mouse retina .....	123
5.3.3 RGC morphology in human retina .....	126
5.4 Discussion .....	128
Chapter 6: General Discussion .....	131
6.1 Open eye potentiation in adult visual cortex.....	133
6.2 The role of inhibition in adult plasticity .....	136
6.3 ISI and in vivo 2P calcium imaging as a measure of visual function in experimental glaucoma .....	138
6.4 RGC death in glaucoma: is it as straightforward as it appears? .....	141
6.5 Concluding thoughts .....	143
6.6 Future work .....	144
Appendix .....	146
References .....	167

# **Chapter 1: Introduction**

## **1.1 The human visual system**

The human eye is a highly specialized sensory organ that is responsible for light photoreception. The eye's structures detect light, and convert the energy received into action potentials. These action potentials are then relayed to the ON and then to the brain, where the information is processed and appreciated as vision.

### **1.1.1 The gross anatomy of the human eye**

The human eye is spherical and measures approximately 28 mm in diameter and 24 mm in length, with a total volume of 6.5 ml. The externally located pupil allows light to enter the eye and the iris, which is a coloured, circular muscle that controls the size of the pupil. The front, white, external part of the eye is the sclera, which supports the walls of the eyeball, and forms the transparent part of the eye, called the cornea. The cornea refracts light and contributes to the 2/3rds of the total focusing power (Kolb 1995). The eye movements are controlled by 6 extraocular muscles that are located in the orbit. The superior rectus and the inferior rectus move the eye upwards and downwards respectively. The medial rectus and lateral rectus move the eye inwards and outwards to the side. The superior and inferior obliques are responsible for the eye rotations (Forrester J. V., Dick A. D., McMenemy P. G., Roberts F. 2016).

The eye contains three liquid filled chambers; the anterior chamber (between the cornea and the lens), the posterior chamber (between the iris and the lens), and the vitreous chamber, which is the largest of the three. Both the anterior and posterior chamber are filled with aqueous humour, while the vitreous chamber is filled with vitreous humour (Kolb 1995). Situated between the anterior and posterior chambers

is a complex band of specialised connective tissue known as the trabecular meshwork, with the canal of Schlemm on its outer aspect.

These structures are critical in aqueous humour outflow, which is known to be affected in glaucoma, which will be discussed in detail later. The lens, together with the cornea, refracts light and focuses it on the retina. By changing its shape, the lens can change the focal distance, enabling it to focus on objects at various distances. The walls of the eye are formed by three layers (known as tunics) of different types of tissue. Sclera forms the outer shell of the eye, and it continues to the brain as dural sheath. The middle layer (choroid) is a vascular layer of the eye which is rich in blood vessels, supplied by the ophthalmic artery. The inner layer of the eye (retina) is the neural part of the eye's structure, which contains the light sensitive cells. Axons from RGCs exit the eye as II cranial nerve or ON. The ON contains the central retinal artery (a branch of the ophthalmic artery) which serves as a separate blood supply for the inner retina.

### **1.1.2 The human retina**

The human retina lines the back of the eye, and is approximately 0.2 mm in thickness. It is part of the CNS and (excluding vascular cells) only contains neurons and neuroglia that are organised in strict nuclear and neuropil layers (Figure 1.1). The outermost part of retina contains the photoreceptor cells, which are light sensitive cells, while the innermost part of retina contains RGCs, which are the output cells of the retina (Forrester J. V., Dick A. D., McMenamin P. G., Roberts F. 2016). The retina contains an area called the macula, which is a circular zone measuring 5-6 mm in diameter, situated around the fovea. The fovea is an area heavily dominated by cones, and is histologically characterized by containing multiple layers of RGCs. The

fovea is an area of 1.5mm diameter in the temporal retina, located 3 mm laterally to the optic disk. It appears slightly yellow in colour due to yellow screening xanthophyll carotenoid pigments, found in the cones. The foveola is a central 0.35mm wide depression (or pit) in the fovea, where there are no rods, but where peak cone photoreceptor density is located. The foveal pit is avascular and inner retinal layers are displaced laterally, therefore there are no RGCs in the pit itself (Figure 1.1). The optic disk is approximately 1.8 mm in diameter, and is the site where RGCs axons exit the retina. There are no retinal layers found in the optic disk, thus forming a blind spot, which is typically not perceived by human vision. The peripheral retina is the remainder of the retina (outside of the central retina), which is rich in rods and contains a single layer of RGCs. The peripheral retina ends at the ora serrata, which is a serrated margin, or transition zone, between the neural retina and non-pigmented epithelium cells.

For descriptive purposes, the retina is usually divided into nasal, temporal, superior and inferior quadrants or hemi-retina, starting from the fovea. The distance of the retina from the optic disk to the ora serrata towards the temporal side is 23-24 mm, and 18.5 mm on the nasal side. The human retina is approximately 200  $\mu\text{m}$  in thickness in the central retina, with the thickest part near ONH of 230  $\mu\text{m}$ , and 110-140  $\mu\text{m}$  in thickness in the periphery. The total area of the retina is approximately 1250  $\text{mm}^2$  (Forrester J. V., Dick A. D., McMenamin P. G., Roberts F. 2016).



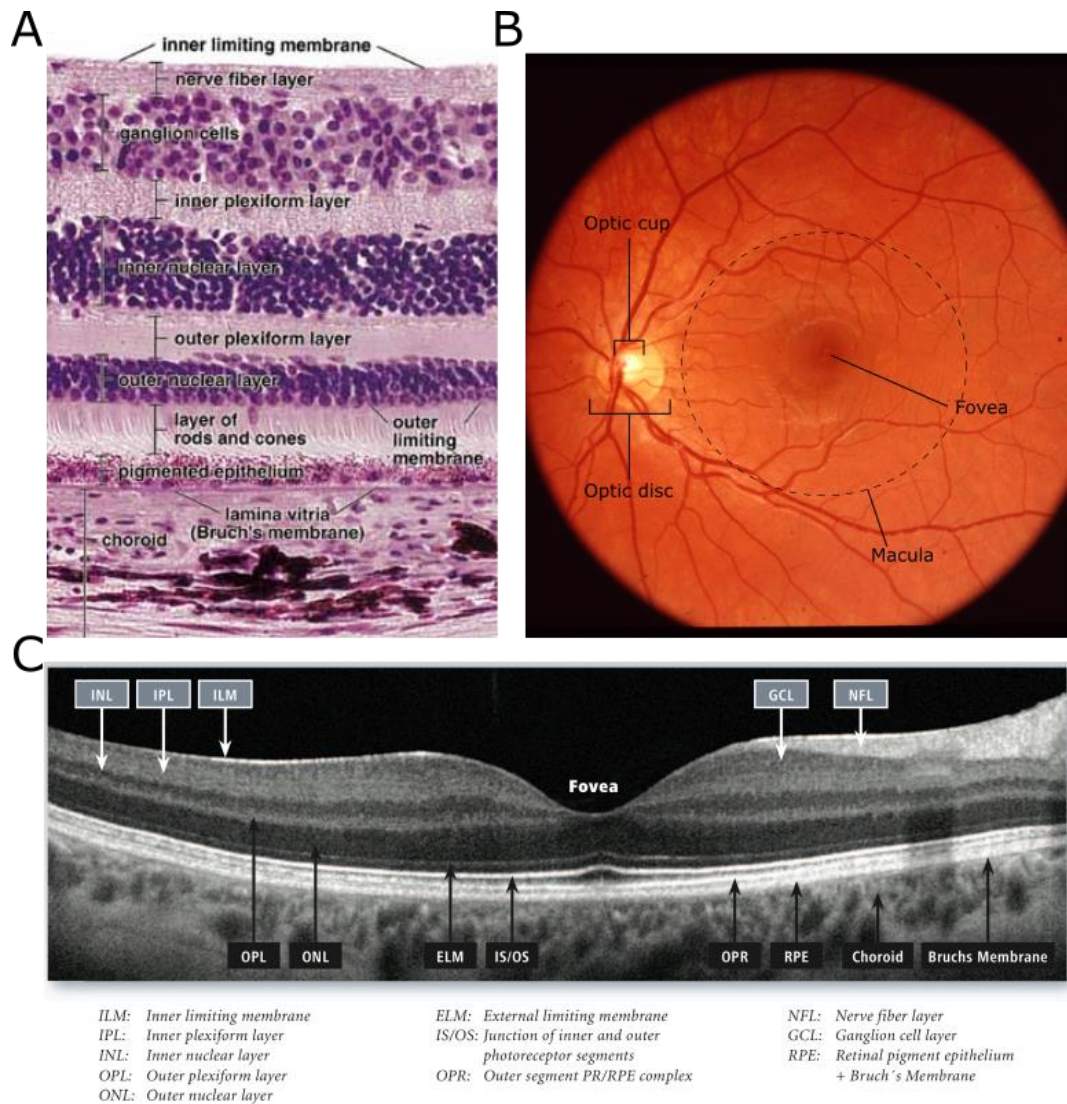


**Figure 1.1 Human retina**

(A) Laminar human retina organization visualised with H&E stain (Kolb 1995). (B) Fundus photograph of human retina of central retinal area and the fovea. (C) Optical coherence topography image of human retina.

### 1.1.3 RGCs in human retina

There are approximately 1.2 million RGCs in one human retina. Their cell bodies are mostly situated in the GCL, while their axons are found in the NFL and dendrites are found in the IPL. In the central retina, there can be up to 7 cell layers of RGCs found

in the GCL, which can result in GCL thickness of 60-80  $\mu\text{m}$ , in comparison to 10-20  $\mu\text{m}$  thickness in the peripheral retina (Forrester J. V., Dick A. D., McMenamin P. G., Roberts F. 2016). RGCs can be morphologically classified into different types: by the soma size, dendritic tree spread and branching level. Currently, there are at least 18 different types of RGCs that have been identified in human retina (Kolb *et al.* 1992). RGC's mainly receive signals from bipolar cells and amacrine cells, via synapses located in the IPL.

Human RGCs are usually separated into two main classes: midget ganglion cells, and parasol ganglion cells. Midget ganglion cells are the largest class, accounting for approximately 80 % of all RGCs. Midget ganglion cells project to parvocellular cells in the LGN, and in the retina they synapse with amacrine cells and a single midget bipolar cell. The dendritic spread of midget bipolar cells is 5-10  $\mu\text{m}$  in the central retina, and up to 100  $\mu\text{m}$  in peripheral retina. They are arranged in a mosaic shape in retina and their dendritic trees do not overlap (Dacey 1993). 10% of all human RGCs are parasol ganglion cells, which project to magnocellular cells in the LGN, and synapse with all types of bipolar cells (excluding midget bipolar cells) in the retina. Parasol RGCs have large cell bodies, and large dendritic trees of up to 200  $\mu\text{m}$  (Rodieck *et al.* 1985). Their size is directly proportional to the eccentricity (Meyer-Rüsenberg *et al.* 2006). Another class of RGCs, intrinsically photosensitive RGCs (ipRGCs), are the most recently discovered class of RGCs. ipRGCs were first identified in rodents (Hattar *et al.* 2002; Berson *et al.* 2002). They contain the photopigment melanopsin, and are not involved in image formation. ipRGCs project to supra-chiasmatic nuclei in the hypothalamus and midbrain, where they act like intrinsic photoreceptors and respond to light with a role in the control of pupillary

light reflexes and circadian rhythm (Schmidt *et al.* 2011; Ribelayga *et al.* 2014; McDougal and Gamlin 2010).

#### **1.1.4 Human ON and lamina cribrosa**

The ON is formed by 1.2 million RGC axons meeting at the optic disk. From the optic disk, axons extend along to form the ON, and pass alongside the ophthalmic artery, through the optic canal, which is located in the sphenoid bone of the orbit. The human ON can be subdivided into four main parts: intraocular (1 mm in length), orbital (25-30 mm in length), intracanalicular (4-10 mm in length), and intracranial (10 mm in length) (Forrester J. V., Dick A. D., McMenamin P. G., Roberts F. 2016).

The intraocular portion (non-myelinated portion) extends from the optic disk to the posterior of the sclera. It can be further subdivided into three areas: pars retinalis, pars choroidalis and pars scleralis. Pars scleralis, which contains lamina cribrosa, is exceptionally rich in glial cells, which account for 40% of the tissue mass (Forrester J. V., Dick A. D., McMenamin P. G., Roberts F. 2016).

Lamina cribrosa is a sieve-like connective tissue mesh, which is formed by irregular collagen fibre bundles that are continuous with the sclera. These bundles are separated from axons by a covering of glial tissue (Forrester J. V., Dick A. D., McMenamin P. G., Roberts F. 2016). Compression of lamina cribrosa sheets have been associated with the early pathogenesis of glaucoma, noted even before VF loss (Quigley *et al.* 1983). It was also found to be significantly thinner in glaucoma (Jonas *et al.* 2003). The main function of lamina cribrosa is to allow RGC axons to leave the eye and to stabilize the IOP, by forming a physical barrier between intraocular and extraocular space (Jonas *et al.* 2003). Myelination of the axons by

oligodendrocytes starts at the posterior level of pars scleralis, and posterior of lamina cribrosa. The orbital portion of the ON extends backwards towards the optic canal, and is covered by three layers of meninges: pia, arachnoid and dura mater. The intracanalicular portion of the ON passes through the optic canal, together with ophthalmic artery and sympathetic nerves (Forrester J. V., Dick A. D., McMenamin P. G., Roberts F. 2016). The ONs leave the cranial part of the optic canals, and pass backwards and slightly upwards, where they end by forming the optic chiasma. The optic chiasma is a quadrangular bundle of nerves, where partial crossing of ON fibres occurs. The fibres from the nasal hemiretina of each eye cross the midline to enter the contralateral optic tract, while fibres from the temporal hemiretina do not cross the chiasma.

### **1.1.5 The SC and the LGN in humans**

The SC are located in dorsal part of the midbrain. Fibres that project to the SC are associated with visual reflexes, automatic scanning of images and visual association pathways (Forrester J. V., Dick A. D., McMenamin P. G., Roberts F. 2016). The LGN is a part of the thalamus that is a relay station for ascending sensory information. The LGN receives inputs from both retinae and consists of 6 laminae of cells, which are numbered from 1 to 6. Nerve fibres from the nasal half of the contralateral eye's retina will terminate on cell bodies in layers 1, 4 and 6. Fibres from the temporal half of the ipsilateral eye's retina will terminate in layers 2, 3 and 5. Each RGC axon will always terminate in at least one laminae of LGN, but can terminate on up to six cells. Most of the cells from the LGN will send their fibres via the optic radiations or geniculocalcarine tracts to area 17 in the visual cortex. The

LGN has inputs from the areas 17, 18, 19, oculomotor centres and the reticular formation (Forrester J. V., Dick A. D., McMenemy P. G., Roberts F. 2016).

### **1.1.6 Visual cortical areas in humans**

The fibres from the optic radiations, which contain fibres from both eyes, enter layer IV of the visual cortex, which is located in the occipital lobe. V1 (area 17) (Figure 1.2) consists of six basic layers, and is more cellular than other areas of cortex. It is organised in OD columns, where matching projections from the left or right eye are ordered side by side in columns. Cells from layers II and III project to the secondary visual cortices (areas 18 and 19). Cells in layer V project to the SC, and layer VI cells project to the LGN (Forrester J. V., Dick A. D., McMenemy P. G., Roberts F. 2016). V1 is responsible for coding the aspects of local image features such as size, orientation, direction, and binocular differences.

Secondary visual association areas are areas that are visually responsive, but do not receive direct projections from the LGN. At least 15 secondary visual association areas have been identified so far in humans, with the potential for more to be discovered. These areas are responsible for object recognition, motion, and location of objects, as well as other complex visual tasks.



visual system is quite similar to the visual pathways of higher mammals. There are, however, some fundamental differences which will be discussed.

### **1.2.1 The gross anatomy of the mouse eye**

The eyes of a mouse are positioned laterally and the globe is approximately 3.5 mm in diameter. The mouse eye is approximately 8 times smaller than the human eye (Geng *et al.* 2011). It contains a relatively large cornea, a very large lens, and a small vitreous chamber, with a total vitreous volume of only 5  $\mu\text{l}$  (Jeon *et al.* 1998). The anterior of the eye is filled with aqueous humour, a clear liquid which supplies nutrients for the avascular cornea and the lens. The aqueous humour is secreted at the ciliary body and drained at the trabecular meshwork. The aqueous humour fills both the anterior and posterior chambers, with a total volume of 5.9  $\mu\text{l}$ .

### **1.2.2 The mouse retina**

The total retinal area in the mouse is approximately 15  $\text{mm}^2$ , and just like in humans, it is organised in nuclear and plexiform layers containing discrete populations of neurons. As the mouse is a nocturnal animal, its retina is dominated by rods (which make up 97% of all photoreceptors), which are used to see in dim light conditions. The mouse retina contains a mean density of 430,000 per  $\text{mm}^2$  of rods, and only 12,000 per  $\text{mm}^2$  of cones (Jeon *et al.* 1998). Visual acuity (the ability to determine a small distance separating two points) in typical laboratory mice, using behavioural vision tasks, was determined to be around 0.5-0.6 c/deg. This is extremely low when compared to the average human visual acuity of 60 c/deg (Chalupa and R. W. 2008).

Mouse retina lacks a discrete NFL, as seen in humans, and approximately 60% of cells in the GCL are displaced amacrine cells. It does not contain a fovea, but instead an area called area centralis, which contains the highest density of cones and rods. The rod's photosensitivity in mouse retina has been determined to peak at approximately 497-500 nm, while the two types of cone sensitivities peak at 360 nm, and 508 nm.

Mouse retina, like human retina, contain several different types of glia cells, including Müller cells (that stretch vertically through the entire retina), astrocytes, and microglia.

### **1.2.3 Mouse RGCs**

There are approximately 110,000 neurons in the GCL of a single mouse retina, of which 45,000 are RGCs, with a peak mean density of 8000 RGCs/mm<sup>2</sup> (Jeon *et al.* 1998). There have been 22 morphological types of RGCs distinguished in the mouse retina, to date (Volgyi *et al.* 2009) (Figure 1.3).

As opposed to most other mammals, where RGC soma size and dendritic tree size increases with eccentricity, this has been shown not to be true in mouse retina (Sun *et al.* 2002). Virtually all RGCs that project to ipsilateral hemisphere contribute to the binocular vision, and are located in the ventrotemporal crescent of ipsilateral eye (Chalupa and R. W. 2008).



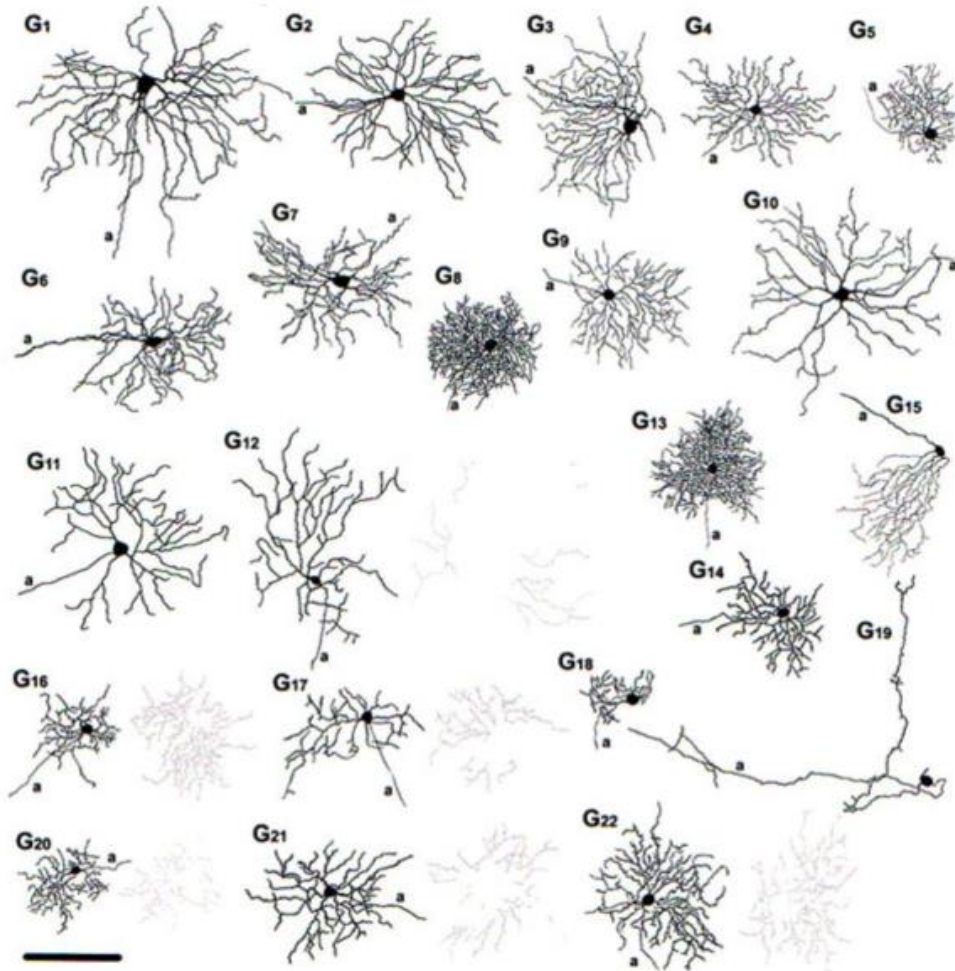


**Figure 1.3 Morphological types of mouse RGCs.**

There are at least 22 different morphological types of RGCs identified to date. At least 6 types of RGCs are bistratified, as shown in the illustration, labelled as cells G12, G16-G17, G20-G22. Axons are labelled by letter 'a'. (Volgyi et al. 2009; Kolb 1995).

#### **1.2.4 The ON and lamina region in a mouse**

The ON in a mouse can be divided into 4 separate areas: the ON head within the retina, the lamina region upon leaving the retina, the extraocular unmyelinated portion of the nerve, and the myelinated portion, which starts 0.6 mm behind the globe (May and Lutjen-Drecoll 2002). Extraocular fraction of the ON is part of the

CNS and is sheathed with three layers of meninges; pia, arachnoid, and sclera. The nerve is composed of RGC axons, astrocytes at the ON head, and astrocytes and oligodendrocytes in the extraocular portion of the nerve. The nerve also contains a small quantity of microglia and vascular cells. The central retinal artery (which is a branch of the ophthalmic artery) is responsible for the vascular supply to ON head and unmyelinated portion of ON, while the myelinated portion is supplied by blood vessels in the pia matter (Chalupa and R. W. 2008). Mice lack collagenous lamina cribrosa that is found in humans, and instead contain an analogous astrocyte rich lamina region (Howell *et al.* 2007). The ON's from both eyes meet at the optic chiasm, where the fibres cross over. In the mouse, approximately 3-4% of fibres project to the ipsilateral hemisphere, while the rest project to the contralateral hemisphere.

### **1.2.5 The SC and the dLGN in mouse**

In mice, at least 70% of RGCs project to the SC, which is a part of the tectum of the midbrain, and the inputs which terminate in the first 3 layers of SC are organised in retinotopic manner (Hofbauer and Dräger 1985; McLaughlin and O'Leary 2005). The SC is highly conserved, and is thought to be involved in gaze and eye movements (May 2006). Recently, the existence of OD columns in the SC of the mouse has been reported. This is surprising, as not even V1 in the mouse contain OD columns, that are a feature seen in higher mammals (Feinberg and Meister 2015; Ahmadlou and Heimel 2015).

The dLGN is a thalamic nucleus that relays the visual information from retina to V1. In mice, only 30% of RGCs project to dLGN. Direction selective RGCs project to

the outer shell, and the non-direction selective RGCs project to the inner core of dLGN. Axons from RGCs located in the temporal retina project to the rostolateral part of dLGN, while ventronasally located RGCs project to the dorsal part of dLGN. In humans, contralateral and ipsilateral projections to the dLGN can be distinguished easily; however, in mice they are intermingled. Ipsilateral projections to dLGN take up 14%-18% of its volume. There is also no functional diversity of mouse dLGN cells, as opposed to most other higher mammals, including rats (Chalupa and R. W. 2008).

### **1.2.6 Visual cortical areas of a mouse**

The mouse visual cortex, like the visual cortices of all mammals, is arranged in six distinct cellular layers. There are at least 11 visual areas in mouse visual cortex (Garrett *et al.* 2014) (Figure 1.4). V1 in the mouse occupies around 2-3 mm<sup>2</sup> area and is comparable to area 17 in humans (Watson 2012). V1 receives a visual input from dLGN interneuron axons that mainly project to neurons in layer IV of V1 which in turn send their outputs to layer II-III neurons. 90% of retinal inputs project to the V1 of the contralateral hemisphere in a uniform fashion, whereas 2-3% of the total inputs project to the lateral ipsilateral portion of V1, forming the binocular area of the VF. Surprisingly, the contralateral neuron drive is only 2-3 times greater in binocular area than ipsilateral (Dräger and Olsen 1980; Chalupa and R. W. 2008). In addition, the binocular field of view of the mouse only takes up 30-40 degrees of central vision, compared to 120 degrees in humans (Figure 1.4). The mouse V1b (as opposed to the higher mammals such as cat or human) does not contain OD columns, instead, neurons in the binocular zone of the mouse are organised in salt and pepper arrangement. Only approximately 40-43% of mouse neurons in V1 are orientation-

selective (Mangini and Pearlman 1980), while other neurons are non-orientated. The visual acuity of V1 neurons is determined to be around 0.5-0.6 c/deg (Porciatti *et al.* 1999; Heimel *et al.* 2007).

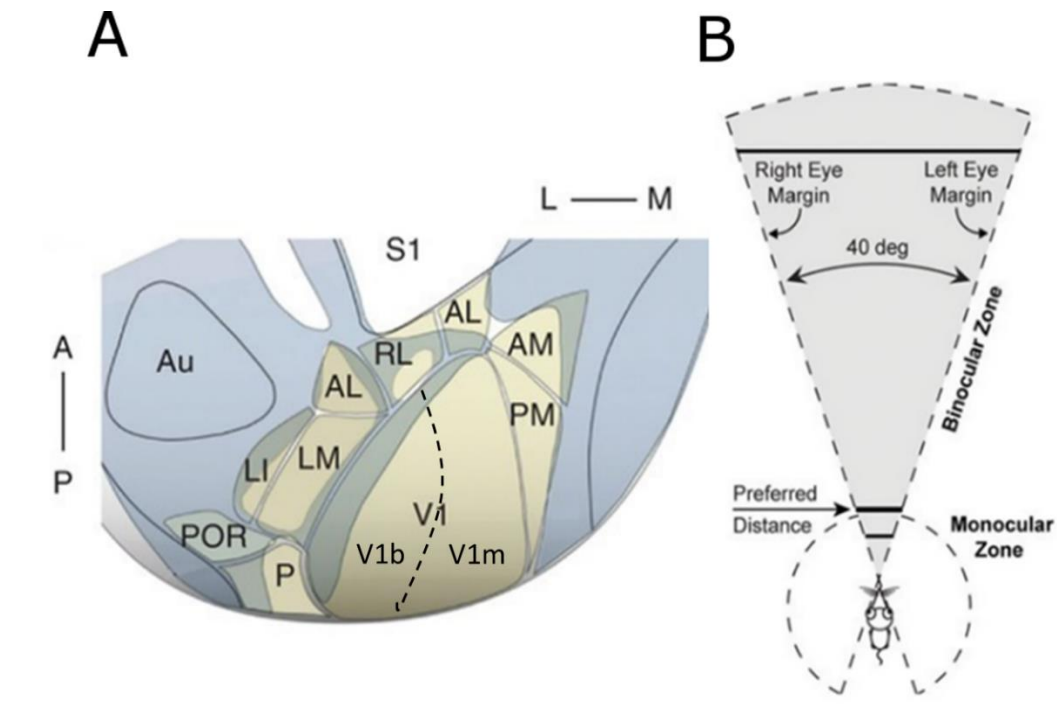


**Figure 1.4** The visual cortical areas and visual fields of the mouse.

(A) Cortical visual areas, and associated areas of the mouse. S1 – primary sensory cortex, Au – auditory cortex, AL – anterolateral area, RL – rostrolateral area, LM – lateromedial area, LI – laterointermediate area, POR – postrhinal area, P – posterior area, V1 – primary visual cortex, V1b – primary binocular visual cortex, V1m – primary monocular visual cortex, PM – posteromedial area, AM – anteromedial area. Adapted from: Carandini and Churchland 2013. (B) Binocular visual field of the mouse occupies around 40 degrees, while the rest is occupied by the monocular zone (Scholl *et al.* 2013).

### **1.3 Glaucoma**

Glaucoma is the term given to a collection of progressive ON neuropathies. It is the second leading cause of blindness in humans, worldwide (Kingman 2004). Glaucoma can be congenital, due to malformation of the anterior chamber angle, however, it occurs most commonly as a result of degenerative disease, and can be classified into primary and secondary types (Forrester J. V., Dick A. D., McMenamin P. G., Roberts F. 2016). For most types of glaucoma, elevated intraocular pressure and ageing are important risk factors. However, low or normal tension glaucoma is not uncommon.

#### **1.3.1 POAG**

POAG is slow and progressive, and manifests itself with a gradually increased IOP, which is attributed to malfunctions in the aqueous humour outflow system. The anterior chamber remains normal, but the ON does undergo classic degeneration seen in glaucoma, such as an increase in optic cup-to-disc ratio, axonal death, and thinning of NFL. POAG is the most common form of glaucoma and has been identified as having strong genetic links, with mutations on chromosome 3p in particular (Alward *et al.* 1998), as well as new mutation sites frequently being discovered (Monemi *et al.* 2005). IOP usually rises from 18-23 mmHg to 25-35mmHg, while an increase of ON cup-to-disc ratio due to axon death and defects in the VF have also been observed clinically (Forrester J. V., Dick A. D., McMenamin P. G., Roberts F. 2016). As a result of slow, mild progression, POAG is often not diagnosed until it is in its late stages, when irreversible damage to the axons of the ON and death of RGCs in retina has already occurred.

### **1.3.2 PACG**

As opposed to POAG, PACG may manifest itself acutely with an onset IOP rise of 40-80 mmHg. PACG is associated with age, as the globe becomes smaller, lens enlarges and moves into pupillary part of the eye, which creates narrow angles and a pressure build up in the anterior chamber of the eye. PACG is clinically observed by a sharp and significant increase in IOP, and optic disc swelling or papilledema (Forrester J. V., Dick A. D., McMenemy P. G., Roberts F. 2016).

### **1.3.3 Other types of glaucoma**

Congenital infantile glaucoma occurs when there is a malformation of the trabecular meshwork and Schlemm's canal at birth, and can be observed up to 3 years of age. This may cause resistance to aqueous humour outflow, thus resulting in increased IOP. It is unknown why congenital glaucoma occurs, however, it is thought that it is due to a failure of differentiation, or alterations in differential growth rates (Forrester J. V., Dick A. D., McMenemy P. G., Roberts F. 2016). This type of glaucoma is rare, occurring in 1 in 10,000 births (Francois 1980).

There are two other types of secondary glaucoma; open and closed-angle. In secondary open-angle glaucoma, the angle is usually obstructed by inflammatory cells, haemorrhage, or lens matter. In secondary closed-angle glaucoma, the chamber is closed mechanically, for example, by lens displacement, or tumour (Forrester J. V., Dick A. D., McMenemy P. G., Roberts F. 2016).

### **1.3.4 Glaucoma prevalence**

Glaucoma is the leading cause of irreversible blindness, with an estimated 60.5 million people affected by the two main types of primary glaucoma (POAG and PACG), in 2010 (Kingman 2004). The risk and subtypes of glaucoma vary across ethnicities, races and countries (Tham *et al.* 2015). In the UK, an estimated 489,000 people were affected with glaucoma in 2009, with approximately 10% of UK blindness registrations, being due to glaucoma (Nice 2009).

A meta-analysis of 50 studies was performed on people aged 40-80 years, and the total global prevalence of glaucoma was estimated to be 3.54% in 2013. POAG was found to be significantly more prevalent, accounting for a total of 3.05% prevalence, with PACG accounting for 0.50% of the global population. Glaucoma was most predominant in African people, with an estimated prevalence of 4.79%. POAG was at its highest prevalence in Africans, with 6.11%, while Asian people had the highest prevalence of PACG, at 1.2% (Tham *et al.* 2015).

Glaucoma was estimated to affect 64.3 million people worldwide in 2013, and with the accelerated rise in the ageing population, it is estimated that by the year 2020 the number of people affected will rise to 76.02 million, and 111.82 million people affected by the year 2040 (Tham *et al.* 2015).

#### **1.4 Mechanism of RGC death in glaucoma**

Independent of the type of axon injury, axons of RGC (like other axons in the CNS) do not regenerate. Furthermore, an injury to axons typically causes the death of RGCs. The mechanisms of how glaucoma progresses and leads to RGC death are not completely understood (Figure 1.5). Currently, it is thought that the first site of damage is the axon which is mechanically induced by increased IOP at the ON.

However, the general belief that an increase in IOP results in glaucoma has been strongly disputed (Vrabec and Levin 2007) as many cases have shown that patients continue to suffer from glaucoma while having low IOP, and some patients with chronic hypertension never developing glaucoma. This may be explained by a secondary degeneration in the retina. The initial insult - such an increase in IOP causes the death of directly affected axons and their cell bodies in the retina, then it is proposed that spatially neighbouring, and healthy RGCs might also be affected as a result of a secondary, or further additional degeneration (Levkovitch-Verbin *et al.* 2001; Levkovitch-Verbin *et al.* 2010). It is now widely accepted that RGCs in glaucoma and ON transection die by apoptosis, both in animal models (Quigley *et al.* 1995; Garcia-Valenzuela *et al.* 1995) and in humans (Kerrigan *et al.* 1997). It is suggested that apoptosis is the final outcome of RGC degeneration in the retina, preceded by a series of complicated, compartmentalised, degeneration of axons, synapses, and dendrites (Whitmore *et al.* 2005; Morgan 2012). It is thought that axons and dendrites can degenerate independently from each other. This hypothesis is supported by findings that showed increased autophagy in dendrites in experimental glaucoma, followed by a later, separate increase in soma (Park *et al.* 2012).



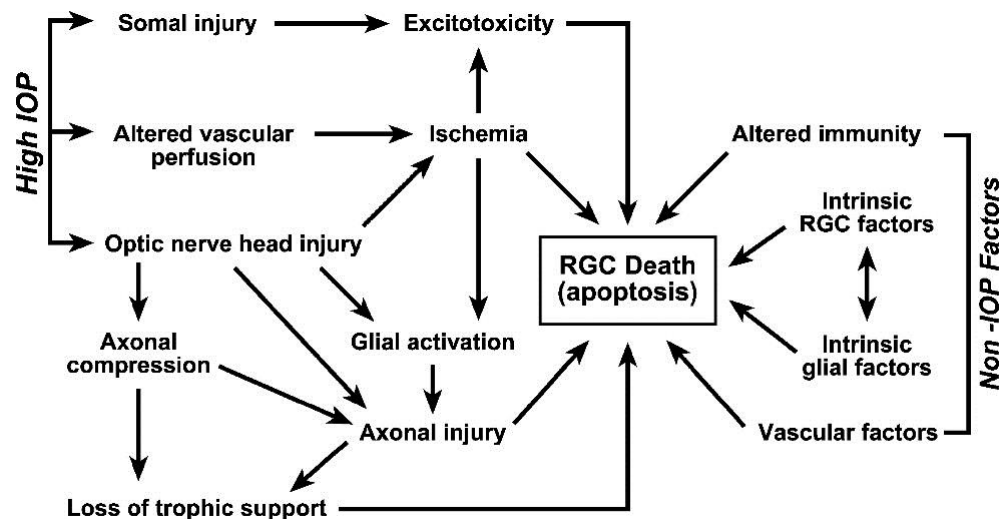


**Figure 1.5 RGC death in glaucoma**

*Suggested cascade of events leading up to RGC death by apoptosis in glaucoma. IOP and non-IOP related factors are outlined (Libby, Gould, et al. 2005).*

## 1.5 Mouse models of RGC death

Multiple genetic and induced mouse models of RGC death have been developed to study glaucoma; these will be briefly discussed below.

### 1.5.1 ON crush

ON crush is a commonly used method to induce RGC death by a mechanical injury to ON axons, by applying pressure to the nerve a few millimetres behind the globe. After an ON crush injury in adult mice, 95% of RGCs die within 2 weeks by apoptosis (or programmed death) (Berkelaar *et al.* 1994; Villegas-Perez *et al.* 1993). It has been demonstrated that short mechanical pressure applied to the ON not only causes primary mechanical damage directly, but also induces secondary degeneration to the axons that did not experience the mechanical injury (Yoles and Schwartz

1998). As early axon damage has been shown to be involved in early glaucoma damage (Howell *et al.* 2007), the ON crush method has been extensively used as an inducible RGC death model to study glaucoma.

### **1.5.2 Inducible models of increased IOP**

Inducible models of increased IOP in mice are based on chronic aqueous outflow obstruction, which results in ocular hypertension. Laser photocoagulation of the episcleral vein has often been used to mimic closed-angle glaucoma. Laser photocoagulation is usually induced unilaterally, resulting in a transient increase of IOP for 8 weeks, before returning to the baseline value (Aihara *et al.* 2003a; Mabuchi *et al.* 2003; Nakazawa *et al.* 2006). Due to the transient IOP increase, laser photocoagulation only achieves mild RGC death and molecular changes. Episcleral vein cauterisation is another method of inducing transient IOP increase for up to 6 weeks (Ruiz-Ederra and Verkman 2006). These methods are, however, associated with complications such as corneal damage, cataracts, and inflammation (McKinnon *et al.* 2009). Another successful inducible method of glaucoma is by the injection, and guidance of paramagnetic beads to block the aqueous outflow. However, this method has only been successfully achieved in rats, as the mouse eye was deemed to be too small for this method (Samsel *et al.* 2011).

### **1.5.3 Genetic models of mouse glaucoma**

DBA/2J is the most well-characterized model of spontaneous glaucoma development in mice. The DBA/2J inbred mouse strain develops an iris disease, where the pigment from the iris is detached, creating a blockage in the anterior chamber. This

blockage prevents normal drainage of aqueous humour with similar disease manifestation as seen in POAG in humans (Chalupa and R. W. 2008). These mice develop an increased IOP at 8-9 months of age, followed by a loss of RGCs, ON atrophy, and ON cupping (John *et al.* 1998; Libby, Anderson, *et al.* 2005). In addition, it has been reported that RGC death in this model occurs in a fan-shaped fashion, which may be analogous with VF loss patterns seen in human glaucoma (Jakobs *et al.* 2005). A mutation in type 11 collagen, Colla1(r/r), was also found to cause a gradual elevation of IOP in mice (Aihara *et al.* 2003b). This mutation was shown to cause an accumulation of collagen type 1 in the aqueous outflow pathway, thus creating drainage blockage, an elevation of IOP by 33%, and a loss of 28.7% of axons, at 54 weeks of age (Mabuchi *et al.* 2004). A mutation in Tyr423His myocilin was also shown to produce glaucoma-like results in mice, with a slight increase of IOP, and approximately a 20% loss of RGCs in the retina (Senatorov *et al.* 2006). Most recently Vav2/Vav3-deficient mice have been produced, that show elevated IOP, selective loss of RGCs, and ONH cupping (Fujikawa *et al.* 2010).

## **1.6 Plasticity of visual cortex**

Plasticity is the term used to describe experience-dependent changes in neural networks due to external changes, in order to adapt to a new environment. Plasticity can occur on a small synaptic scale, or large scale remodelling of networks (for example: post- injury). Plasticity is most pronounced during development and is retained throughout adulthood. During early postnatal development, cortical circuits in V1 are experience sensitive. This defined period is called the critical period. Once

the critical period for a specific sensory function is over, the plasticity is significantly reduced (Berardi *et al.* 2000).

Plasticity is a complicated process that is regulated by many genes, and occurs via several different mechanisms. The mechanisms for this process are not yet fully understood. Long-term potentiation (LTP) is a mechanism by which synapse strengthening occurs, based on recent repeated activity. The opposite, long-term depression (LTD), is a mechanism that results in synaptic weakening (Bear and Malenka 1994). In addition, neurons are also known to have the ability of homeostatic plasticity, allowing them to regulate their own activity relative to the network (Turrigiano and Nelson 2004). This is currently thought to occur via the neurons ability of synaptic scaling (Keck *et al.* 2015).

### **1.6.1 OD plasticity**

OD plasticity was first described after MD by lid suture, after eye opening in kittens induced an imbalance in cortical responses (Wiesel and Hubel 1963). It was found that if the visual signal to the contralateral eye is occluded by transient MD during the critical period of OD, it causes the cortical neurons to switch their preference from the contralateral to ipsilateral eye. Additionally a decrease in vision from the contralateral eye is observed after it is reopened (Muir and Mitchell 1973; Hubel *et al.* 1977). In normal adult mice, cortical neurons in the V1b also have a preference for the contralateral eye (Drager 1975), and just like in kittens, this can be altered by an MD during the critical period (Gordon and Stryker 1996). The OD shift is not observed in adult mice with MD paradigm after the critical period is over. The opening and closing of the critical period is activated by molecular factors, in

particular, the maturation of cortical inhibition (Huang *et al.* 1999). The maturation of inhibitory GABAergic PV+ interneurons is thought to terminate the critical period. However, it can be reopened in adults by degradation of perineuronal nets surrounding these inhibitory PV+ interneurons (Pizzorusso *et al.* 2002). Additionally, it has been shown that with certain conditions such as dark exposure (He *et al.* 2006), environmental enrichment (Greifzu *et al.* 2014), and previous MD during development (Sonja B Hofer *et al.* 2006), that the window of OD plasticity can be extended and/or reactivated in adult mice (Pizzorusso *et al.* 2002). The critical period of OD plasticity in humans can last up to 10 years of age, with the first year being the most important (Banks *et al.* 1975). In mice, OD plasticity lasts from postnatal day 19 to 33 (Gordon and Stryker 1996).

### **1.6.2 Adult plasticity**

It is accepted that an adult brain is capable of exhibiting a certain degree of plasticity that is normally seen in high levels during development. This has been famously shown in humans (Maguire *et al.* 2000), where London taxi drivers show changes in their hippocampi, related to learning new navigational skills in adulthood. The study showed that acquisition of new information induces structural changes in the adult brain, initiating neurogenesis. The visual cortex, along with other parts of the brain, constantly undergoes experience dependent network re-organization. One model of studying the visual cortex's plasticity in adults involves creating retinal lesions, thus causing a corresponding, non-responsive lesion projection zone (LPZ) in the retinotopic region of V1. During their recovery, neurons within the LPZ recover their responsiveness to visual stimuli as they receive inputs from RGCs surrounding the

retinal lesion area (Kaas *et al.* 1990; Calford *et al.* 2000; Keck *et al.* 2008). These changes have been attributed to increased dendritic turnover (Keck *et al.* 2008), and axonal sprouting within the LPZ (Yamahachi *et al.* 2009). This cortical reorganization has also been shown to occur in human patients suffering from macular degeneration. In cases of macular degeneration, where the central retina is degenerated, the V1 (which previously was associated with central vision) was found instead to be reorganised to respond to peripheral stimuli (Baker *et al.* 2005). This was found to occur in task related visual stimuli, rather than passive viewing, and is thought to occur either by cortical reorganisation, or by unmasking task-dependent cortical signals that are normally suppressed in normal V1 (Masuda *et al.* 2008).

## **1.7 ISI**

ISI is a minimally invasive method of studying the functional patterns of neural activity over large areas of the cortex, in response to a stimuli (Grinvald *et al.* 1986). ISI strictly relies on intrinsic changes, and does not require any exogenous dyes. When cortical neurons are active, the light absorption of the particular region increases, and its reflectance decreases. It is possible to capture this difference with a charge-coupled device camera. There are several separate components that contribute to the rise of intrinsic signals (Zepeda *et al.* 2004). Initially, when synaptically activated, neurons require an increased amount of oxygen, which they draw from surrounding capillaries, thus oxygenated haemoglobin is replaced with deoxyhaemoglobin. This is then followed by a local temporal increase in blood volume, lasting 10-30 seconds, which increases the concentration of oxygenated haemoglobin and decreases deoxyhaemoglobin (Hallum *et al.* 2006). ISI is based on

the ability to detect the difference in red light absorption between the oxygenated haemoglobin and deoxyhaemoglobin, blood volume, and changes in light scattering properties of the active nervous tissue.

Traditionally, ISI was performed by presenting the stimuli and acquiring images in very short intervals ('episodic' presentation). Periodic stimulation (Kalatsky and Stryker 2003) is a paradigm of ISI that uses continuous stimulus presentation and acquisition. The recorded signal is then analysed by applying Fourier transformation. This type of image analysis allows for the dissection of both heart rate and breathing rate artefacts quickly producing more robust activity maps, when compared to traditional ISI paradigms. Intrinsic signals are 10 times slower than neuronal activity, and therefore ISI has a high-spatial and low-temporal resolution (Kalatsky and Stryker 2003).

## **1.8 Two-photon excitation microscopy**

Two-photon excitation laser-scanning microscopy is a fluorescence imaging technique that can be used *in vivo*, on live tissue. It uses high-energy pulsing femtosecond near-infrared light, and for each excitation, two less-energetic photons in the infrared spectral range are simultaneously absorbed. This imaging technique achieves an increased imaging depth of up to 600  $\mu\text{m}$  (Kobat *et al.* 2011), and reduced photodamage and photobleaching (due to a focused focal volume and increased signal to noise ratio) when compared to conventional confocal microscopy (Denk *et al.* 1990). Therefore, the combination of advances in genetic modifications in mice and the development of advanced calcium sensors lead two-photon microscopy to become widely used as an advanced imaging technique in

neuroscience, as it allows in vivo imaging of the brain, and neuronal populations in their natural environment (Dombeck *et al.* 2015; Kawakami *et al.* 2013).

### **1.8.1 Intracellular calcium in neurons**

In the nervous system, neuronal activity can be observed by visualizing and quantifying influx and efflux of intracellular calcium ions within neurons. Calcium ions are an important intracellular messenger. In a neuron, calcium can be found (or stored) in the endoplasmic reticulum (ER), mitochondria, and in the cell nucleus. In addition to this, PV, calbindin-D28k, and calretinin all act as endogenous calcium buffers (Schwaller 2010). The cytosolic calcium concentration is a result of the balance between calcium influx and efflux, and the interchange of calcium within the internal compartments of the cell. Most neurons have an intracellular calcium concentration of 50-100 nM that can temporarily increase by 10-100 times when active (Berridge *et al.* 2000). In presynaptic terminals, calcium influx sets off the release of neurotransmitter-containing synaptic vesicles. It has been shown that, postsynaptically, a short-term increase of the calcium concentration in dendritic spines is critical for the induction of activity-dependent synaptic plasticity (Zucker 1999).

### **1.8.2 In Vivo two-photon calcium imaging using GECIs**

Two-photon microscopy allows the observation and quantification of the activity of dozens, or hundreds of neurons at the same time, in anesthetised, or awake and behaving mice (Huber *et al.* 2012).



There are two broad types of calcium indicators: chemical, and GECIs. These indicators measure changes in intracellular calcium concentration by acting as an exogenous calcium buffers alongside the endogenous calcium buffers (Grienberger and Konnerth 2012). There are three main methods of loading neurons in-vivo with a calcium indicator: single cell loading (Jia *et al.* 2011), bulk injection of chemical indicators (such as Oregon Green) (Garaschuk *et al.* 2006) or GECI expression by viral transfection, and in utero electroporation or by a transgenic mouse line (Grienberger and Konnerth 2012).

GECIs are most typically introduced to a neuronal population by viral transduction, using adeno-associated viruses (AAVs). Once the GECIs are transduced in the cell population of interest, neuronal activity can then be imaged using two-photon excitation microscopy for a period of several weeks (Tian *et al.* 2009). It has, however, been shown that AAVs can produce an inconsistent gradient of expression levels in the neighbouring neurons at an injection site, and the GECI expression can continue to increase with time abnormally, thus affecting some neurons (Chen *et al.* 2013).

### **1.8.3 GCaMP family calcium sensors**

GCaMP family calcium sensors are single-fluorophore GECIs that can be used to measure changes in the cytosolic free calcium concentrations in vivo. GCaMPs contain an enhanced green fluorescent protein (EGFP) as a fluorophore, which is bound by calcium-binding calmodulin and calmodulin-binding peptide M13. In the presence of calcium, calmodulin and M13 interact, evoking conformational changes in the fluorophore, prompting an increase in the emitted fluorescence (Nakai *et al.*

2001). GCaMPs can be introduced into the neuronal tissue by a transfection, using a bulk injection, and are capable of detecting up to a single action potential, and calcium changes in cell soma and dendrites (Chen *et al.* 2013). Recently, Thy1-GCaMP6s/f transgenic mice lines have been described, where mice express GCaMP6 sensors selectively, under the *Thy1* promoter, in their neurons from birth (Dana *et al.* 2014). In future, using these mice lines will eliminate the need for the extensive surgery involved in the introduction of the GCEIs to the desired area, enabling studies to be started at much younger age, and over much longer timescales.

#### **1.8.4 Aims of the study**

The aims of this study are to explore the loss of RGCs in human retina with glaucoma, and the effect of RGC loss on V1 in the mouse. To achieve this, I have employed *ex vivo* and *in vivo* two-photon laser scanning imaging, and *in vivo* functional ISI.

Chapters 2 and 3 describe the functional outcome of V1b activity after a unilateral ON crush in a mouse, which resulted in RGC loss in the retina. Chapter 2 introduces ISI as a method of longitudinal rapid detection of plasticity in V1b after an ON crush.

In Chapter 3, cellular resolution is introduced to give an insight into the same injury paradigm by utilizing longitudinal *in-vivo* calcium imaging of excitatory and inhibitory neurons.

Chapter 4 examines topographic RGC loss in the retina of human glaucoma subjects when compared to normal age matched retinas and to clinical VF data that was obtained prior to the patient's death.

Chapter 5 examines and discusses various techniques that were utilised to fully label single cell RGC morphology in fixation, in preserved human retina, in order to assess dendritic degeneration in glaucoma.

A detailed methods section and concise summary and discussion of primary findings are presented in each experimental chapter, with a comprehensive discussion of all results presented in Chapter 6.

**Chapter 2: ISI of V1b after unilateral ON  
crush in adult mice**

## 2.1 Introduction

ISI can detect small changes in the light scattering properties that occur in active neuronal tissue. While ISI is not a direct measure of neuronal activity, in mice ISI can provide a clear picture of the activity of organised networks, such as V1 (Schuett *et al.* 2002), the barrel cortex (Laaris *et al.* 2000), and even sub-cortical areas, such as the SC (Mrsic-Flogel *et al.* 2005). ISI is frequently used to study cortical plasticity, and in particular, OD plasticity in juvenile mice (Sonja B. Hofer *et al.* 2006; Ranson *et al.* 2013; Cang *et al.* 2005). It has been shown that the adult cortex, just like the juvenile cortex, is capable of reorganisation, and the formation of new connections after an injury, such as deafferentation (Wall and Egger 1971; Merzenich *et al.* 1983). In the adult visual cortex, plasticity may also be evoked by injuries, such as retinal lesions (Keck *et al.* 2008; Keck *et al.* 2011), or ME (Nys *et al.* 2014; Toldi *et al.* 1996). The ON serves as the sole retinal output, transmitting visual information from the retina, to V1, as well as other areas in the brain. It is unknown how an injury to the ON axons may affect cortical activity, or whether it would induce plasticity and reorganisation of the visual cortex. As opposed to nerves in the PNS, the mammalian ON (which is part of the CNS) is not able to regenerate after an injury, due to the inhibitory properties of myelin in the CNS (Caroni and Schwab 1988). It was hypothesised that connections within the visual cortex may be able to reorganise after partial deafferentation by an ON crush. The ON crush is a well-established model of inducing robust, but progressive, permanent RGC death in mice (Allcutt *et al.* 1984). Part of the mechanism of how the injury progresses after ON crush is by Wallerian degeneration, where the distal part of the axon degenerates, separate from the cell soma (Lawson *et al.* 1994; Lorber *et al.* 2012). It has been shown that transgenic animals with a mutation in the Wallerian pathway (Wld(S))

are more resistant to Wallerian degeneration after the ON crush (Beirowski *et al.* 2008). In addition, the same allele protects the DBA/2J mouse strain against axonal damage (Howell *et al.* 2007). The ON crush causes RGCs to die by apoptosis, mediated by inflammatory processes in the retina, as shown by observing a TUNEL assay that labels late stage apoptotic cells (Bien *et al.* 1999; Li *et al.* 1999) in the retinas of mice, that received an ON crush. Furthermore, adult mice are more susceptible to RGC loss after an ON crush than young mice, due to an increase in accompanied astrocyte death after an injury in adults (Wang *et al.* 2007). Axonal transport (Minckler *et al.* 1977), including retrograde BDNF transport from the SC (Quigley *et al.* 2000), was shown to be affected in ocular hypertension animal models. The retinal function (and thus the signal transmission within the ON) was evaluated using retinal pattern electroretinography (PERG), which is a measure of electrical activity that arises in retina in response to presentation of visual stimuli, which is then recorded at the cornea (Porciatti 2007). Following an ON crush (10-20 minutes), the PERG amplitude decreased dramatically, and remained diminished for up to 30 days, post ON crush. This was comparable to transient transmission block, that can be induced by retrobulbar lidocaine administration (Chou *et al.* 2013). Additionally, Yukita *et al.* (2015), found a decrease in another component of ERG, the positive scotopic threshold (pSTR), 3 days after an ON crush. The STR component of ERG was shown to be made up primarily of RGC responses (Bui and Fortune 2004). The reduction in pSTR correlated with the reduction of RGC specific genes (Brn3a and Brn3b), but preceded the thinning of inner retinal layers, which was observed 10 days after the injury (Yukita *et al.* 2015). This, however, does not provide an insight if the signal transmission to higher visual structures has also been affected in a similar manner.

Finally, several investigators have reported an impaired ON function in heterozygous mutation of OPA1 transcript mouse models, of autosomal dominant optic atrophy (Davies *et al.* 2007). The OPA1 mutation causes dysfunction of mitochondria fusion, which results in the significantly accelerated degeneration of the axonal ON transport function and retina (Davies *et al.* 2007), comparable to that seen in severely aged mice (White *et al.* 2009). In addition, the mice carrying this mutation were also shown to undergo significant degeneration of RGC dendrites in retina (Williams *et al.* 2010). Patients diagnosed with autosomal dominant optic atrophy are shown to exhibit anatomical degeneration in the optic disc, and ON (Votruba *et al.* 2003). Therefore we hypothesised that using ISI technique we might be able to detect and monitor ON degeneration in this disease model.

In this chapter, I set out to investigate how an acute injury, in the form of a unilateral ON crush or progressive degeneration (such as that seen in mice carrying the OPA1 mutation), may affect the functionality of V1b.

## **2.2 Materials and methods**

All procedures performed on animals were carried out in accordance with the UK Animals (Scientific Procedures) Act 1986, and the European Commission directive 2010/63/EU.

### **2.2.1 Mice**

The transgenic TD x PV mouse strain was bred in-house, on a C57BL/6 background, by crossing PV-Cre (*Pvalb<sup>tm1(cre)Arbr</sup>*) and TD Tomato (*Gt(ROSA)26Sor<sup>tm14(CAG-tdTomato)Hze</sup>*) mouse lines, obtained from a commercial provider (The Jackson Laboratory). *PV-Cre* knockin mice express Cre recombinase in PV containing

neurons, whereas TD tomato mice contain fluorescent protein (TD tomato), which is only expressed in the presence of Cre recombinase, when mouse lineage is crossed. Three aged (>12 months) adult OPA1<sup>+/-</sup> mice were donated by Professor Marcela Votruba, from the School of Optometry and Vision Sciences, Cardiff, UK. Mice were housed with same sex littermates, and kept in standard laboratory conditions (cycles of 14 hours of light, and 10 hours of darkness at 21°C), and provided with a standard laboratory diet and water *ad libitum*. Both male and female mice were used in this study, and were considered an adult if they were older than 120 days.

### **2.2.2 ON crush**

Mice enter the critical period of visual development from around P19 to P32 of their life (Gordon and Stryker 1996). In standard laboratory rearing conditions, the visual cortex remains somewhat plastic in young adults, up to approximately P110 (Lehmann and Lowel 2008; Sawtell *et al.* 2003). Only adult mice were used, as the study aimed to mimic an acute injury in a fully developed adult visual system, thus ensuring developmental factors did not interfere with the results. Time points of 2, 7, 14 and 28 days post ON crush were chosen, based on the questions asked for this project, and the available literature on this injury model. The 3 second duration of the crush was also chosen based on published literature (Gellrich *et al.* 2002; Templeton and Geisert 2012), as only mild to moderate ON injury was desired. The same investigator, using self-closing forceps, performed all ON crushes. These provided a fixed closing force (measured as 1.47 N), and ensured all ON crushes were as uniform as possible. The major advantage of this model is that due to the unilateral nature of the injury, the healthy eye can serve as a control. The ON crush model was based on practical procedure guides published by Templeton and Geisert



(Templeton and Geisert 2012) and Tang et al. (Tang et al. 2011b). All surgical recovery procedures were performed under sterile aseptic conditions, in designated surgical facilities. Instruments were sterilized by immersion in a high heat silicone bead sterilizer, while gloves and the surgical area were both sterilized using 70 % ethanol. Anaesthesia was induced using 4 % Isoflurane in oxygen, with 0.5 L/min flow rate, in an induction chamber. An injection of NSAID (1mg/kg, Metacam) was administered subcutaneously, to alleviate post-operative pain and inflammation. The mouse was transferred to a rotating platform, and placed on its side with a nose cone providing the flow of 2-2.5 % Isoflurane in 0.3 L/min Oxygen for maintenance of anaesthesia during the surgery. The conjunctiva at the temporal inferior quadrant of the eye was gently lifted with straight tip forceps, and an incision made in the conjunctiva with small tip scissors, taking care to avoid cutting any of the extra ocular muscles. The eye was then rotated towards the nose, by gripping the edge of the conjunctiva with straight forceps, and the tips of the self-closing forceps (Dumont no7) were then inserted behind the globe, in the temporal part of the eye. The ON was clamped for 3 seconds, before the forceps were withdrawn, and the eye was rotated back to its normal position. At this point, moderate to severe mydriasis should be observed, indicating a successful ON injury. Ophthalmic viscotears were gently applied onto the eye immediately (using sterile sponges), and the eye fundus inspected with an ophthalmoscope, to confirm an intact ophthalmic artery and retinal blood supply to the ON-crushed eye. Finally, an ophthalmic ointment containing 1 % Chloramphenicol was applied to the eye and the eyelid, to minimise the chance of a post-operative infection. The mouse was then allowed to recover from anaesthesia, monitored a few times on the day of surgery, and then once daily from there on after.

Direct damage to the ON produces acute pupil dilation, however, the pupil recovers its normal size and function shortly after the procedure is complete. No bleeding should be observed during the procedure, however, there is a possibility of minor bleeding due to the area being highly vascularised with blood vessels, but this should stop immediately. Entering the globe via the inferior temporal quarter gives the best chance of avoiding damage to the blood vessels (Templeton and Geisert 2012). Throughout this study, no cases were encountered where bleeding did not resolve during the procedure. Other post-operative side effects that may arise are infection and loss of muscular control, however, these are uncommon and none were observed during this study. All eyes and ONs were collected post-mortem, for further histological studies.

### **2.2.3 Cranial window surgery**

Anaesthesia was induced in an induction chamber, at 3-4 % Isoflurane with a 0.3 L/min Oxygen flow. Mice were administered with NSAID (1mg/kg, s.c., Metacam) for analgesia and dexamethasone (2mg/kg, i.m.) to prevent cerebral oedema. Mice were placed on a heating pad (to maintain their body temperature at 37°C), and placed in a stereotaxic frame.

Anaesthesia was maintained at 2-2.5 % Isoflurane, with a 0.3 L/min oxygen flow. Eyes were covered with a protective ophthalmic cream, and hairs on top of the skull were set back with liquid plaster (Germolene New Skin), before being disinfected 3 times with both 70% Ethanol, and Betadine solution. The skin on top of the skull was removed, and the edges of the incision were attached to the skull with liquid sutures (3M™ Vetbond™ Tissue Adhesive). The custom-made steel headplate was attached to the skull with dental acrylic (C&B-Metabond®), leaving the circular 6 mm skull

area of interest exposed over the V1b. A square (2.5 x 2.5 mm) craniotomy was made, and the skull flap was completely removed and replaced with glass. The glass window was produced by gluing a small square (2.5 x 2.5 mm) of glass, to a 6 mm round cover-glass, using UV curable adhesive (Norland Optical Adhesives 61). The edges of the glass were secured to the skull using liquid sutures and dental acrylic. The mouse was then placed in the heated recovery chamber, and was typically observed to be eating, and moving around within 30 minutes.

#### **2.2.4 Chronic ISI procedure**

Repeated recovery ISI recordings were performed by inducing anaesthesia with 3% isoflurane, with a 0.5-0.7 L/min oxygen flow, in an induction chamber. The mouse was then head-attached to the custom head holder, with 2 screws positioned in the implanted headplate, and placed on the stage on top of the heated blanket (set at 37°C). ISI was performed while maintaining constant anaesthesia of 0.7-0.8 % isoflurane, with a 0.3 L/min oxygen flow, and a sedative (25 µg, i.m., chlorprothixene).

#### **2.2.5 Terminal ISI procedure**

Anaesthesia was induced by placing the mouse in an induction chamber in 4 % Isoflurane, with a 0.5 L/min oxygen flow. The mouse was then removed from the induction chamber, and placed on a heating pad that was set to maintain body temperature (37°C). For terminal experiments, anaesthesia of 1.5 % Isoflurane, with a 0.3 L/min oxygen flow, was administered via a nose cone, with the supplement of a sedative (25 µg, i.m., chlorprothixene). The mouse was connected to an ECG monitor, and its heart rate, in bpm, was monitored throughout the procedure. A

normal heart rate was considered to be in the range of 350 to 550 bpm (dependent on sedative and anaesthesia level). Local anaesthetic (0.05 ml, Lidocaine) was injected under the skin, at the site of the projected incision. A subcutaneous incision was made using scissors, and the skull above posterior pole of the right cortical hemisphere was exposed. By identifying sagittal and lambdoid sutures, the approximate location of mouse visual cortex was identified, and the area cleaned of periosteum and tissue debris. The area was then sealed with 3 % agar, with a round glass window (9 mm in size) placed on top.

### **2.2.6 Periodic ISI protocol**

A light source with interchangeable bandpass filters was positioned to achieve optimal illumination of the surface cortical blood vessels, using green light (546 nm) (Figure 2.1). The CCD camera focus was manually adjusted on superficial blood vessels on the surface of the exposed brain. The filter was changed from green, to red light (700 nm) for intrinsic imaging, and camera focus was adjusted to 150-200  $\mu\text{m}$  below the cortical surface. Automatic computer controlled dual shutters were used to present stimuli to one eye at a time. The mouse was presented with a 120 s periodic stimulus, generated by VSG5 (Cambridge Research Systems), which consisted of an upwards drifting bar of 30 degrees in length, and 2-4 degrees width, presented to the binocular visual field at the rate of 0.125 Hz (Figure 2.1). Images were acquired with the Imager 3001 (Optical Imaging Inc, Mountainside, NJ), running on VDAQ software. The screen was positioned in front of the mouse at a distance of 14 cm. Each eye was presented with the same stimulus, in alternation, for 6 repetitions.

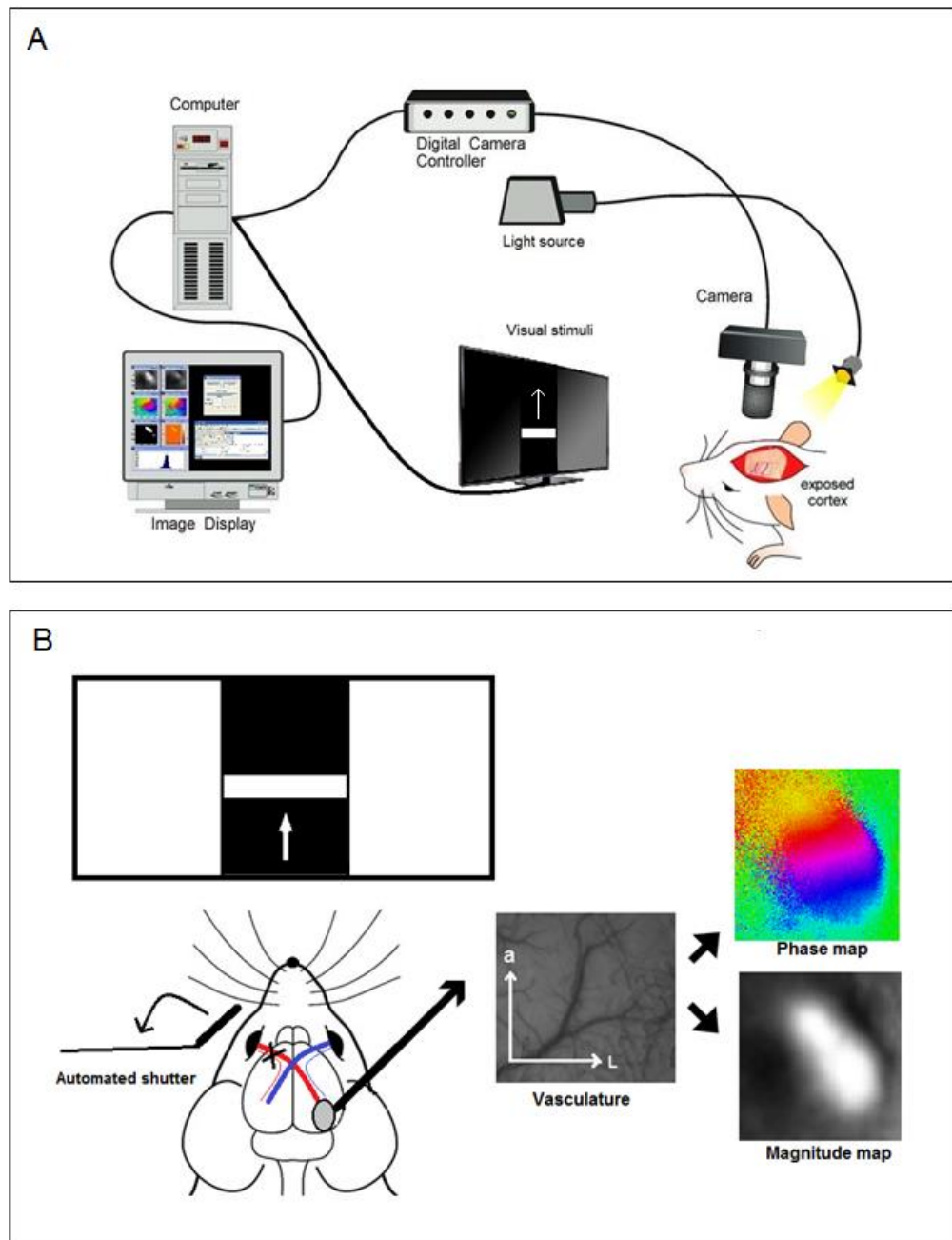


**Figure 2.1 ISI setup and output**

(A) A typical ISI setup. The mouse was presented with a stimulus. While the light source is illuminating the cortical surface, the camera is acquiring the images. The acquired images were collected by the computer, which also generated the visual stimuli. (B) The mouse was presented the visual stimuli to one eye at the time, and phase and magnitude maps were generated from the acquired images. (Key: A – anterior, L – lateral.)

### 2.2.7 Data analysis

ISI data was analysed using a custom written MATLAB script. The signal was extracted using Fast Fourier Transformation (FFT), from 6 stimulus repetitions per eye. The CCD camera acquired images at a resolution of 748 x 572 pixels, at a rate of 40 ms/frame. These were then down sampled to a resolution of 250 x 191 pixels, where one pixel represented 20 x 20  $\mu\text{m}$ . The time series of images from the 6 repetitions were averaged, and the signal was extracted using Fourier decomposition. Activity maps were generated from the amplitude and phase of the periodic signal, in a pixel-by-pixel manner. Once activity maps had been obtained, the ROI was determined, thresholding at 60 % of the maximum pixel value. The average pixel response value within the ROI was then calculated for maps from both eyes. The ODI was calculated using the following formula:

$$ODI = \frac{\textit{Contralateral} - \textit{Ipsilateral}}{\textit{Contralateral} + \textit{Ipsilateral}}$$

### 2.2.8 Statistical analysis

Numerical data was stored and analysed using Microsoft Excel software. Statistical analysis was performed using SPSS software. A Student t-test (if data were normally distributed), or a non-parametric Mann-Whitney U test was performed to compare the data sets. P values < 0.05 were accepted as significant. All data was presented as means  $\pm$  standard deviation (s.d.), unless stated otherwise.

## 2.3 Results

In the experimental ON crush group, the eye contralateral to the imaged hemisphere received the ON crush, and the ipsilateral, intact eye served as the control. These

experiments were performed on two cohorts of mice: one that was imaged once (terminal), and a chronic cohort that was imaged repeatedly. All response magnitudes are expressed in  $\Delta R/R \times 10^{-4}$ . The terminal cohort was imaged through the skull, thus the response magnitudes were much lower than that of the chronic cohort of mice, where imaging was carried out by replacing the skull flap with glass.

Remaining cell numbers in the GCL of the eye that received ON crush were quantified and it was found that 15% ( $p < 0.01$ ) of all cells are lost from GCL 7 days after ON crush and 43% ( $p < 0.001$ ) after 14 days with no further significant cell loss observed after 30 days (normal adult  $n=7$ ; 7d ON crush  $n=4$ ; 14d ON crush  $n=3$ ; 30d ON crush  $n=3$ ).

### **2.3.1 ISI responses in V1b of normal adult mice**

Normal (pre-crush) adult mice ( $n=6$ ),  $>8$  months old, had an average ODI of  $0.17 \pm 0.04$ . Presenting stimuli to the contralateral eye invariably resulted in stronger magnitude maps in V1b, in comparison to presenting stimuli to the ipsilateral eye (Figure 2.2).

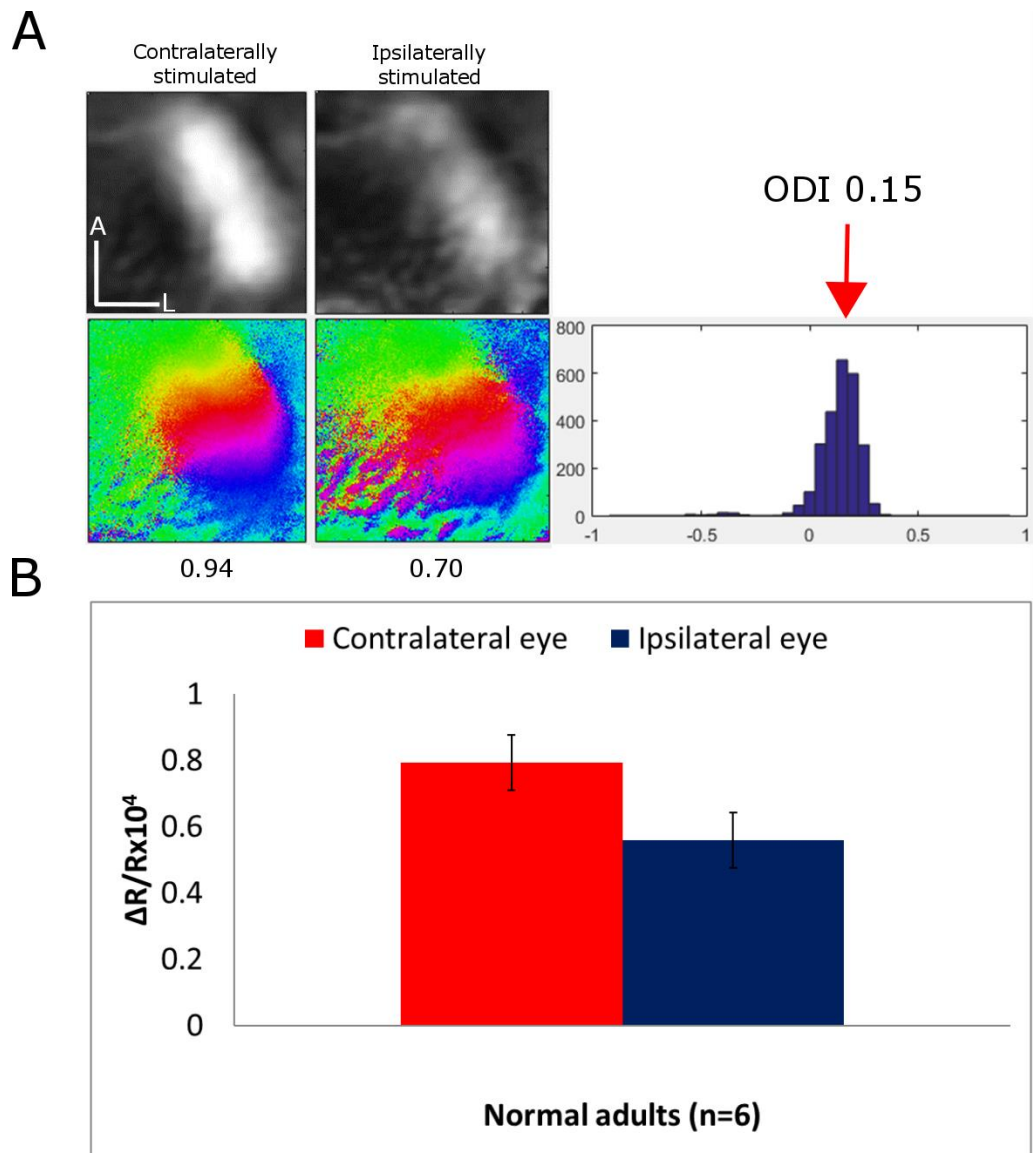


**Figure 2.2 V1b response magnitudes to individual eye stimulation, in normal adult mice.**

(A) Magnitude and phase maps in a normal adult mouse, to individual eye stimulation. (B) Average V1b response magnitudes to individual eye stimulation in normal adult mice (n=6). (Key: A – anterior, L – lateral).

### 2.3.2 ISI responses are diminished in V1b immediately after the unilateral ON crush

In the terminal cohort after completion of the first ISI session, the ON of the eye contralateral to the image cortical hemisphere was crushed immediately. Mice were



not allowed to recover from anaesthesia, however, a minimum of 30 minutes were allowed to restore the normal pupil reflex, before performing a second imaging (n=2). It was observed that the response magnitude through the contralateral eye was significantly decreased, from  $0.74 \pm 0.03$ , to near noise levels at  $0.12 \pm 0.01$ , immediately after the ON crush, while the response magnitude from the ipsilateral eye remained unchanged. As expected, a drastic ODI shift from  $0.16 \pm 0.02$ , before the ON crush, to  $-0.63 \pm 0.03$  immediately after the crush was observed (Figure 2.3).

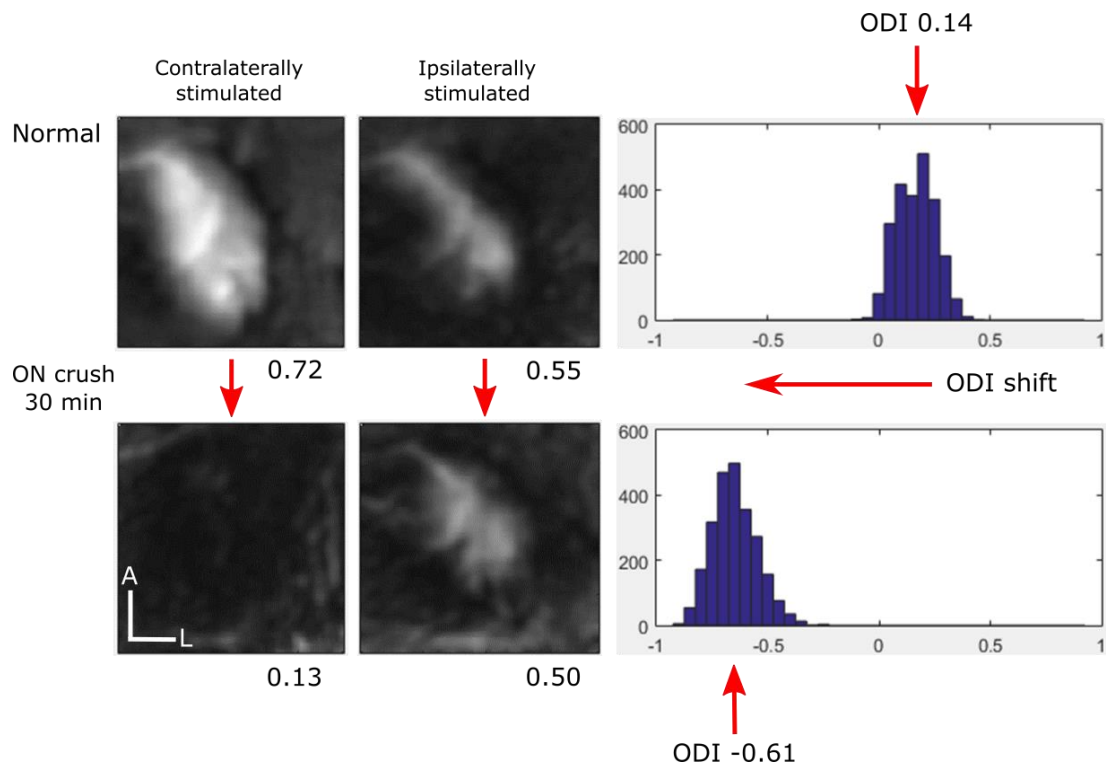


**Figure 2.3 ISI responses immediately after unilateral ON crush**

An example of binocular cortex responses, 30 minutes after the crush of the contralateral ON. A negative shift in ODI towards the ipsilateral eye was observed immediately (Key: A – anterior, L – lateral).

### **2.3.3 ISI responses stay diminished in V1b after long term unilateral ON crush**

In the terminal group, during long term follow-up (2-4 weeks) after a contralateral ON crush, a similar ODI shift towards the non-crushed eye was observed, along with an ODI of  $-0.67 \pm 0.12$  (n=7) (Figure 2.4). The ODI was shown to be significantly reduced ( $p < 0.001$ ), when compared to  $0.17 \pm 0.04$  in normal age matched animals. Response magnitudes from the eye that received the crush (n=7), were observed to be significantly decreased ( $p < 0.001$ ), to  $0.15 \pm 0.05$ , when compared to normal values of  $0.79 \pm 0.08$ , that were observed in normal adults (n=6). The response magnitude for the stimulation of the ipsilateral eye was found to have significantly increased ( $p < 0.05$ ), to  $0.72 \pm 0.15$ , when compared to a value of  $0.55 \pm 0.08$ , that was found in normal animals (n=6).

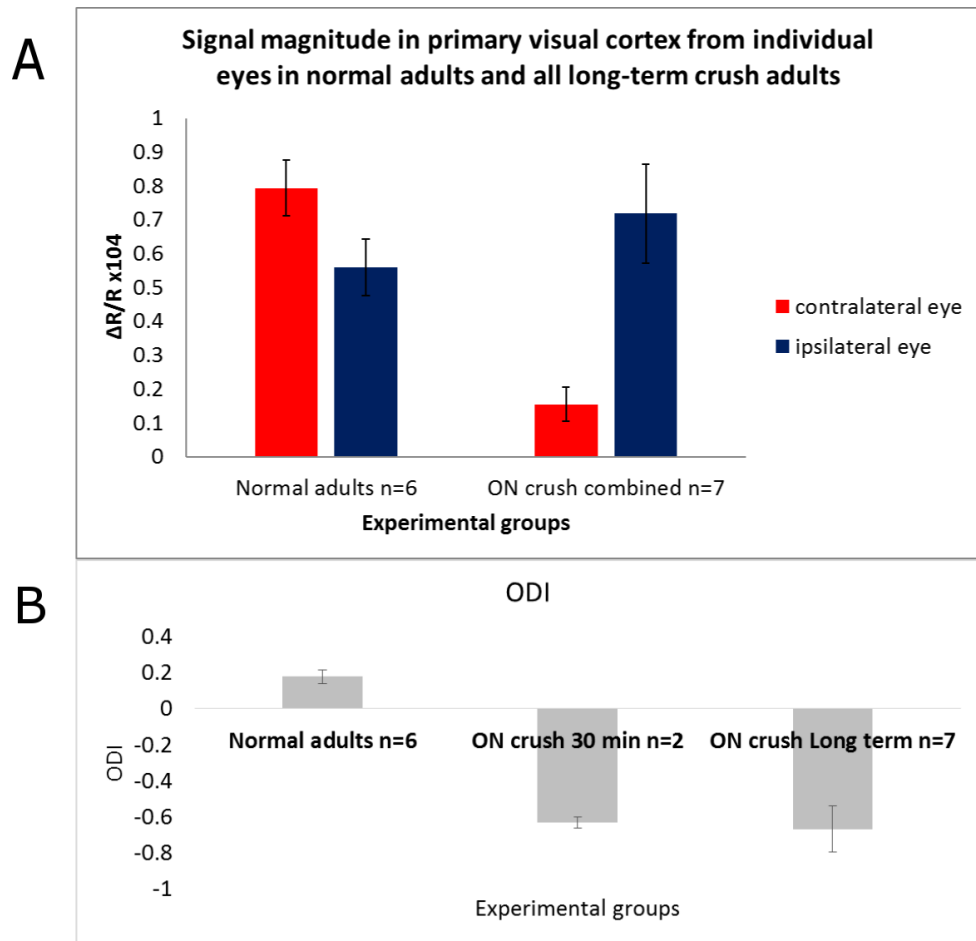


**Figure 2.4** Response magnitudes of V1b and ODI of normal adults, and after long term follow-up after contralateral ON crush

(A) Average V1b response magnitudes to individual eye stimulation in normal adults, and in contralateral ON crush groups. (B) Bar graph showing ODI of normal animals (n=6), and animals that had received an ON crush 30 mins earlier (n=2), or 2-4 weeks earlier (n=7).

### 2.3.4 Responses of V1b in the same animals, before and after the unilateral ON crush

Chronic ISI imaging was performed on the same mice (n=10), before and after the unilateral ON crush. The signal from the contralateral eye was completely abolished after the ON crush. The ODI was reduced from  $0.08 \pm 0.04$  before the crush, to  $-0.75$

$\pm 0.03$  after the crush. The signal magnitude in V1b when presenting stimuli to contralateral eye decreased dramatically, from  $1.4 \pm 0.3$ , to  $0.22 \pm 0.05$  ( $p < 0.001$ ). The signal magnitude in V1b, when presenting visual stimuli to the ipsilateral eye, increased slightly (but not significantly) from  $1.2 \pm 0.3$ , to an average of  $1.4 \pm 0.1$ , after the ON crush (Figure 2.5). There were no significant changes observed in the size of the area activated by stimulating ipsilateral eye after the ON crush.

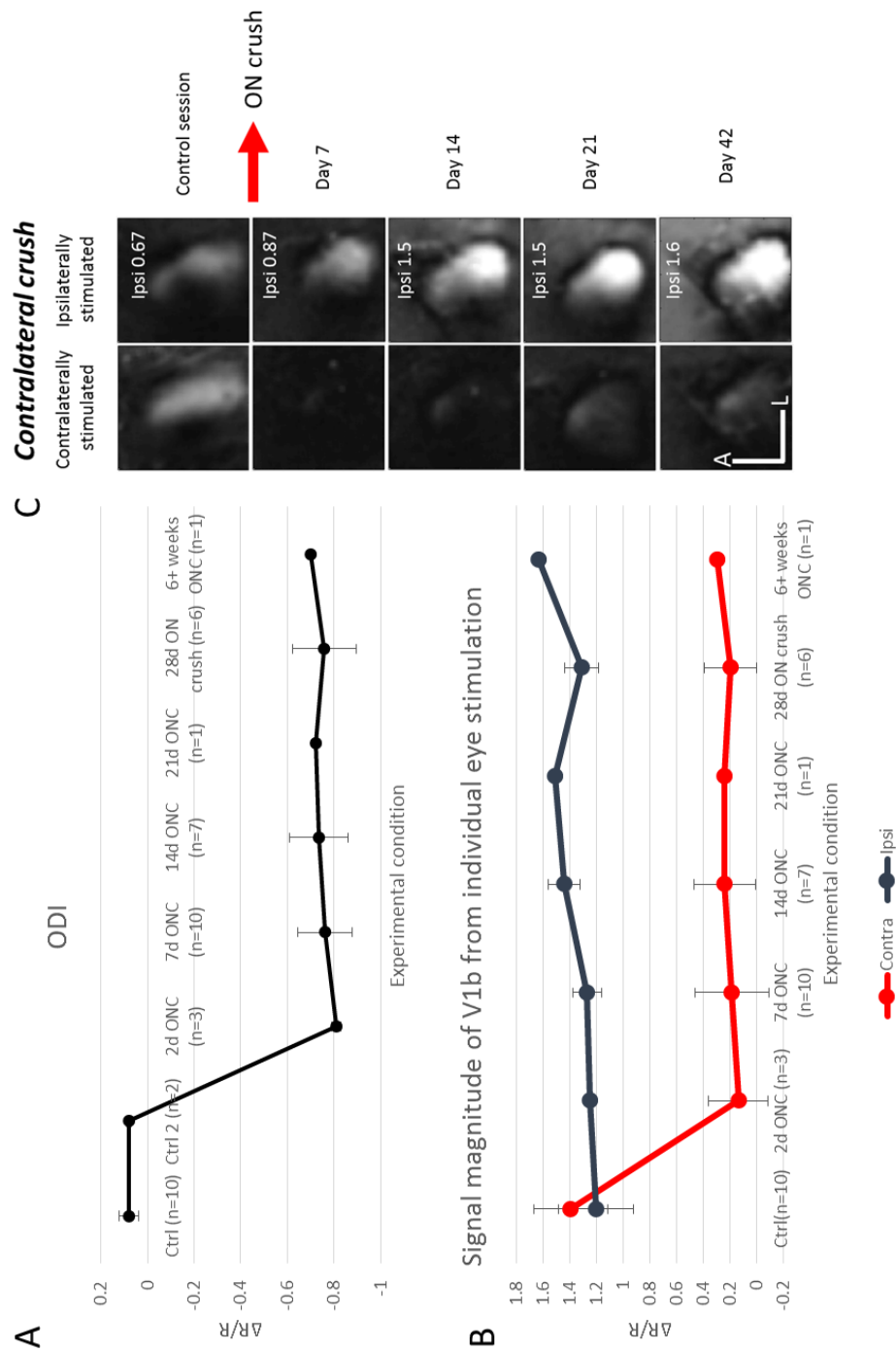
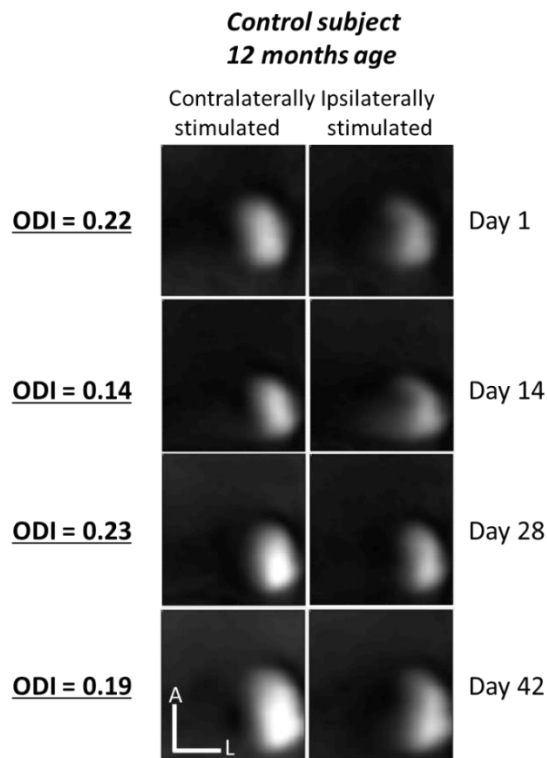


**Figure 2.5 ODI and individual eye response, before and after ON crush**

(A) ODI development before and after contralateral ON crush. (B) Signal magnitude in V1b when presenting stimuli to the contralateral (ON-crushed) eye (red line), and the intact ipsilateral eye (blue line). (C) Development of V1b magnitude maps for both eyes, before and after the ON crush. (Key: A – anterior, L – lateral.)

### 2.3.5 Stability of V1b responses

Four chronic ISI image sets were performed on the two 12-month old mice longitudinally, at biweekly intervals (Figure 2.6). The ODI was found to remain stable at  $0.19 \pm 0.04$  for mouse #1, and  $0.26 \pm 0.06$  for mouse #2, over a period of 6 weeks.



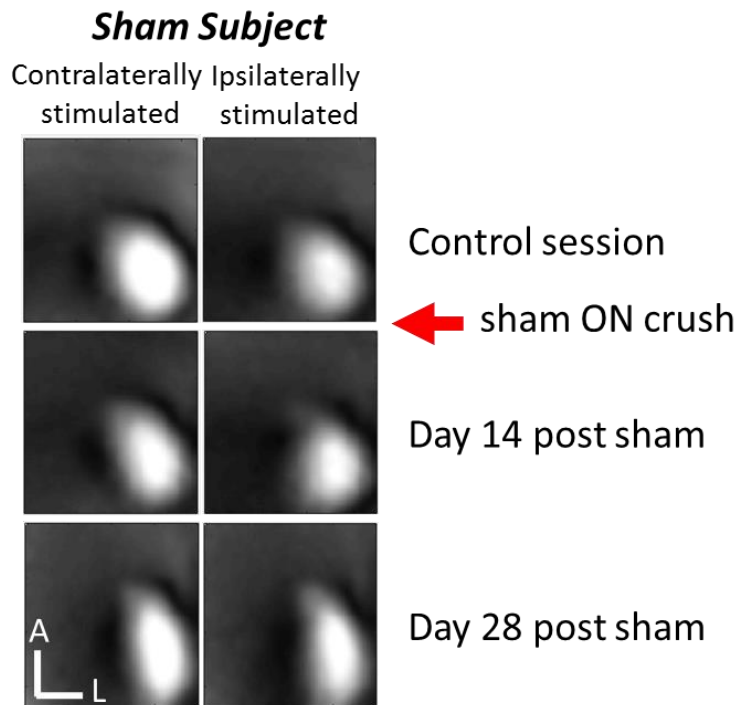
**Figure 2.6 Stability of ISI magnitude maps**

Figure panels show magnitude maps obtained from an adult mouse at biweekly time intervals, in order to demonstrate chronic ISI imaging stability. (Key: A – anterior, L – lateral).

### 2.3.6 Responses of V1b after sham ON crush

A sham surgery was performed (n=1), to verify that signal loss does not occur due to extraocular damage. The response magnitude through the contralateral, sham-

operated eye remained stable from the first to the last session, 28 days after sham ON crush (Figure 2.7).



**Figure 2.7 ISI magnitude maps from a sham ON crush subject**

Figure panels show magnitude maps obtained from a mouse that received a sham ON crush, after the first (control) imaging session. (Key: A – anterior, L – lateral.)

### 2.3.7 Responses of V1b in the OPA1<sup>+/-</sup> mice

Responses were obtained from V1b in aged adult OPA1<sup>+/-</sup> mice, using a chronic ISI protocol. The average ODI was  $0.15 \pm 0.05$ , in two 13 months old adult OPA1<sup>+/-</sup> mice (n=2) (Figure 2.8). Using a terminal ISI protocol on a single 19 months old OPA<sup>+/-</sup> mouse, an ODI of -0.02 was obtained. By comparison, under the same conditions, an ODI of 0.001 was also obtained from an age matched 15-month old control C57BL/6 mouse. No abnormal differences were observed in other parameters (such as pixel scatter or individual eye magnitudes) when compared to typical data sets from adult mice.

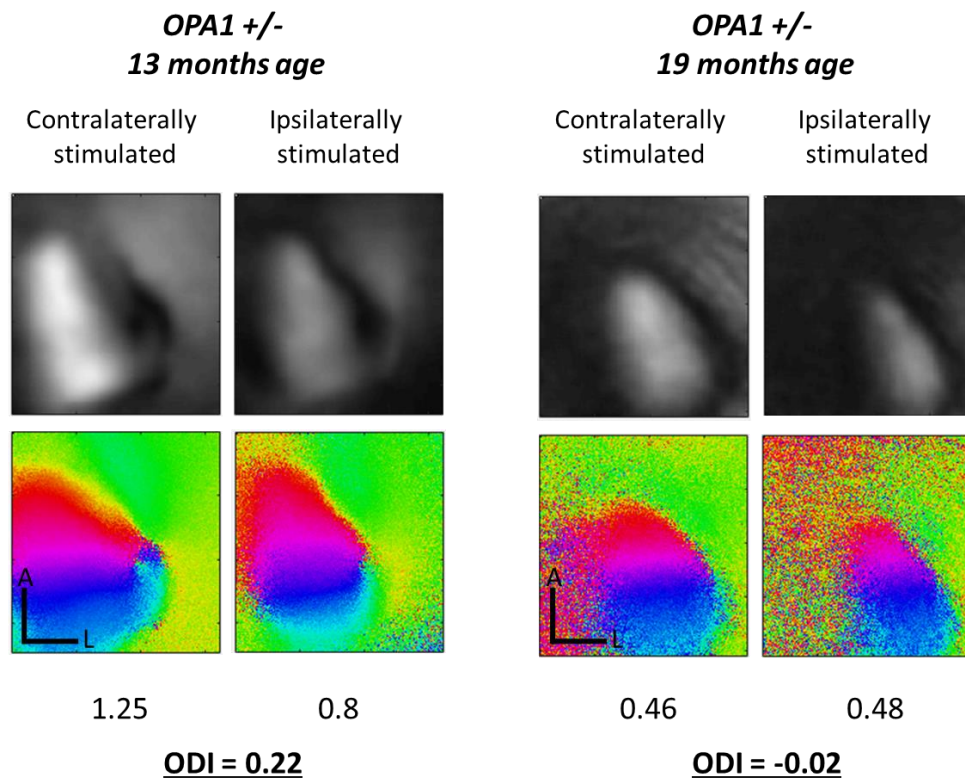


**Figure 2.8 ISI magnitude and phase maps obtained from *OPA1 +/-* mice**

Figure panels show examples of responses obtained from two adult *OPA1 +/-* mice to periodic stimuli. (Key: A – anterior, L – lateral.)

## 2.4 Discussion

The average ODI of a C57BL/6 mouse is typically reported to be around 0.2, however, the ODI values in normal mice are known to vary with age and strain (Lehmann and Lowel 2008; Ranson *et al.* 2012). The cohort of aged adult mice (>8 months old) used, had a slightly reduced ODI of  $0.17 \pm 0.04$ , when compared with an ODI of 0.22, that has been reported in juvenile mice of the same strain (Cang *et al.* 2005; Ranson *et al.* 2012). An ODI decrease indicates that the relative representation of the ipsilateral eye in adults is slightly increased, when compared to contralateral representation. This observation has been demonstrated in a study that showed in



mice, the ODI reaches its peak of 0.26, at approximately 4 months of age, and then reduces to 0.22 at 8 months of age (Lehmann and Lowel 2008). This peak is most likely linked to maturation, and the refining of cortical circuits that occurs in juvenile mice. In addition, another study from the same group also showed that the quality of recordings decreased with age, which results in high individual variability of ODI (Lehmann *et al.* 2012). This is likely to be due to the overall aging of the gross visual system, such as the reduction of retinal (Daiyas *et al.* 2003) and cortical neurons (Devaney and Johnson 1980), and clouding of the lens and cornea.

It was observed that there was both an acute, and permanent loss of transmission of signal to V1b through a crushed ON. This loss of transmission resulted in a highly significant difference in ODI between normal adult mice, and all of the ON crush groups. The transmission was lost immediately after the crush, and remained lost up to the latest time point tested, at 60 days post-crush. In contrast, the signal magnitude from the non-crushed eye initially remained unaffected, but then significantly increased 2-4 weeks after the unilateral ON crush, when compared to normal adults.

A possible mechanism behind this increase is activity-dependent network reorganisation, that is seen in mice with induced retinal lesions (Keck *et al.* 2008). It was observed that in response to photocoagulation of a small retinal area, dendritic spines in layer 5 neurons within the projected lesion zone of visual cortex, had an increased rate of turnover, and were fully replaced within a few months. On the other hand, when the retinal input was removed by complete retinal photocoagulation, these events were not observed. This would suggest that visual experience, or input to V1 is essential for this type of network reorganisation (Horton and Hocking 1998; Keck *et al.* 2008). Another mechanism which involves the removal of binocular competition, is most likely activated in parallel. It was shown that complete removal

of the visual input (for example, in ME) which removes all spontaneous and light evoked activity from retina, also eliminates the binocular competition within the V1b, allowing the remaining eye to take over and strengthen its inputs (Van Brussel *et al.* 2011).

It was reported that OPA<sup>+/-</sup> mice show significant degeneration of RGC dendritic trees in retina, around 10-15 months of age (Williams *et al.* 2010). Differences in V1b responses to periodic stimuli of 13 month old mice of OPA1<sup>+/-</sup> model of autosomal dominant atrophy, when compared to normal age matched C57BL/6 mice, were not observed. The reduced ODI in a 19 month old OPA <sup>+/-</sup> mouse is likely to be an effect of age, rather than being related to the degenerative disease that this strain of mice carry, as a similar ODI in a similarly aged wildtype mouse was observed. Younger OPA1 <sup>+/-</sup> mice retaining a normal ODI was somewhat unsurprising, as it was hypothesised that any slow dendritic degeneration in the retina (Williams *et al.* 2010) that is associated with autosomal dominant atrophy would occur long term bilaterally. I was, however, expecting to see a decrease in individual eye magnitude, or increased scatter as degeneration in retina had begun. These types of changes were, however, not evident in my data set, which should be noted, was too small (n=3) to draw strict conclusions regarding the lack of changes caused by degeneration in the retina, and the ON in V1.

## **2.5 Conclusion**

We show that acute unilateral ON injury completely abolished signal transmission to contralateral V1b. In addition, the findings summarised in this chapter suggest that severe and acute injury of the ON in adulthood may evoke plasticity, and network

reorganization, allowing the remaining eye inputs to strengthen within V1b (Lehmann and Löwel 2008).

**Chapter 3: In vivo two-photon calcium  
imaging of neurons in V1b after unilateral ON  
crush in adult mice**

### 3.1 Introduction

Neurons located in the V1b integrate information from both the left and right eyes, in such way that it allows us to have stereovision, and depth perception. In mice, the V1b is located in the lateral side of the visual area, receiving input from both the ipsilateral and contralateral eye. Rodents, as with most mammals, are also known to possess depth perception (Fox 1965). Only approximately 1 in every 10 RGCs project to the ipsilateral V1b, while most other RGCs project to the contralateral hemisphere. Due to dLGN relay input, the final eye representation in V1b results in a 2:1 ratio of the contralateral and ipsilateral eye in V1b (Coleman *et al.* 2009). Furthermore, in mice, visual areas of both hemispheres are connected via extensive interhemispheric corpus callosal connections (Cusick and Lund 1981). Approximately 70% of all cells in the V1b of the mouse will respond to stimulation of either eye, when presented with stimuli in the central 30-40° of the VF (Drager 1975).

Unlike in humans, where both eye responses are similar, in a mouse there is a distribution bias towards stronger responses obtained when visual stimuli are shown to the contralateral eye, rather than ipsilateral eye (Gordon and Stryker 1996). However, just like in higher mammals (such as cat and humans), when visual stimuli is presented via both eyes, mouse V1b neurons perform binocular integration calculations, resulting not only in signal enhancement, but also suppression, relative to monocular stimulation only (Scholl *et al.* 2013). Most neurons in V1 of L II/III of the mouse are orientation and direction selective, and can discriminate discrete spatial frequencies (Metin *et al.* 1988; Sohya *et al.* 2007), however, in rodents these neurons are not organised in columns with similar properties, as is seen in higher mammals (Hubel and Wiesel 1968). Inhibitory neurons in V1 are known to be

significantly less orientation selective than excitatory neurons (Niell and Stryker 2008). This lack of selectivity was also demonstrated to be true, using calcium imaging of GABAergic inhibitory neurons (Sohya *et al.* 2007). The maturation of inhibitory GABAergic neurons that contain PV, and the surrounding perineuronal nets, is correlated with the end of the critical period of OD plasticity (Pizzorusso *et al.* 2002). Consequently, a reduction in inhibition reopens the critical period plasticity (Harauzov *et al.* 2010). The exact mechanism of how plasticity occurs in a mature brain is not fully understood, however, several molecular pathways have been proposed (Gilbert and Li 2012), which are key in controlling the balance between the excitation and inhibition of the mature cortical network (Morishita *et al.* 2010; Woodhoo *et al.* 2009). In the following chapter, I will present a study that was undertaken in order to pin point which cells are responsible for the open eye potentiation, previously described in Chapter 2.

## **3.2 Materials and methods**

All procedures performed on animals were carried out in accordance with the UK Animals (Scientific Procedures) Act 1986, and the European Commission directive 2010/63/EU.

### **3.2.1 Experimental animals**

All of the data presented from experimental animals in this chapter have also been used to collect the data for the experiments described in Chapter 2. The ON crush was performed as described in Chapter 2.

### **3.2.2 Delivery of calcium indicator**

Cranial window surgery was performed, as described in Chapter 2.2.3. After a craniotomy was achieved successfully, 100-200 nl of solution, containing viral calcium indicator GCaMp6s (virus titre of  $10^{12-13}$ /ml, University of Pennsylvania Vector Core), was injected into V1b of the right hemisphere, at a depth of 200-300  $\mu\text{m}$ . V1b was defined using stereotaxic coordinates, of 3.2-3.5 mm lateral from lambda. The injection was performed using an UltraMicro pump with micro4 controller (WPI, USA), and a 5 $\mu\text{l}$  Hamilton syringe (Hamilton). The Hamilton syringe was adapted with RN compression fittings (Hamilton), in order to accommodate glass pulled pipettes. In order to achieve the least amount of damage to the cortex during virus delivery, sharp glass pipettes, made in-house, were used. The glass pipettes were pulled using a horizontal Sutter P-80 pipette puller (to achieve a high resistance of 80-100 M $\Omega$ ), and the tip was then broken off under the dissecting microscope, to a diameter of 20-30  $\mu\text{m}$ . After the injection, the virus was left to transfect the cells in injection area for 2-3 weeks, before the first session of imaging.

### **3.2.3 Chronic in-vivo calcium two-photon laser scanning imaging**

Mice were placed under light anaesthesia, of 0.7 % isoflurane and 0.3 L/min oxygen flow, and were sedated with Chlorprothixene (25 $\mu\text{g}$ ). The mice first underwent a protocol of periodic ISI, as described in Chapter 2, followed immediately by 2P imaging protocol (as described below).

All in vivo calcium imaging was performed on a custom built 2P microscope (MOM, Sutter Instruments), equipped with a Ti:Sapphire laser (MaiTai DeepSee, Newport SpectraPhysics) using a 20x lens, 1.00 NA Olympus (N20X-PFH) 2mm working

distance, and water dipping objective. The laser was tuned to 940 nm, and the power was maintained in the range of 25-35mW, at an indicator. An area of 270  $\mu\text{m}$  x 270  $\mu\text{m}$  was located in V1b, and imaged using a fast scan configuration at 3.5 fps (ScanImage r3.6), while the mouse was presented with visual stimuli, followed a blank screen, to one eye at a time. The visual stimuli consisted of a white, 4 degrees width bar, being presented as it drifted in black background, followed by 8 seconds of a grey background. At every separate presentation, the bar was rotated 22.5 degrees anti-clockwise, resulting in the presentation of 16 directions (Figure 3.1). The screen was tilted at 7-20°, in order to compensate for the tilt of the headplate implantation, in alignment with the horizontal eye line. The stimuli were presented to alternating eyes for 4 repetitions, and then to both eyes at the same time, for another 4 repetitions. After each imaging session, the mice were placed in a heated recovery chamber, until they were observed to move as normal, before being returned to their home cage.



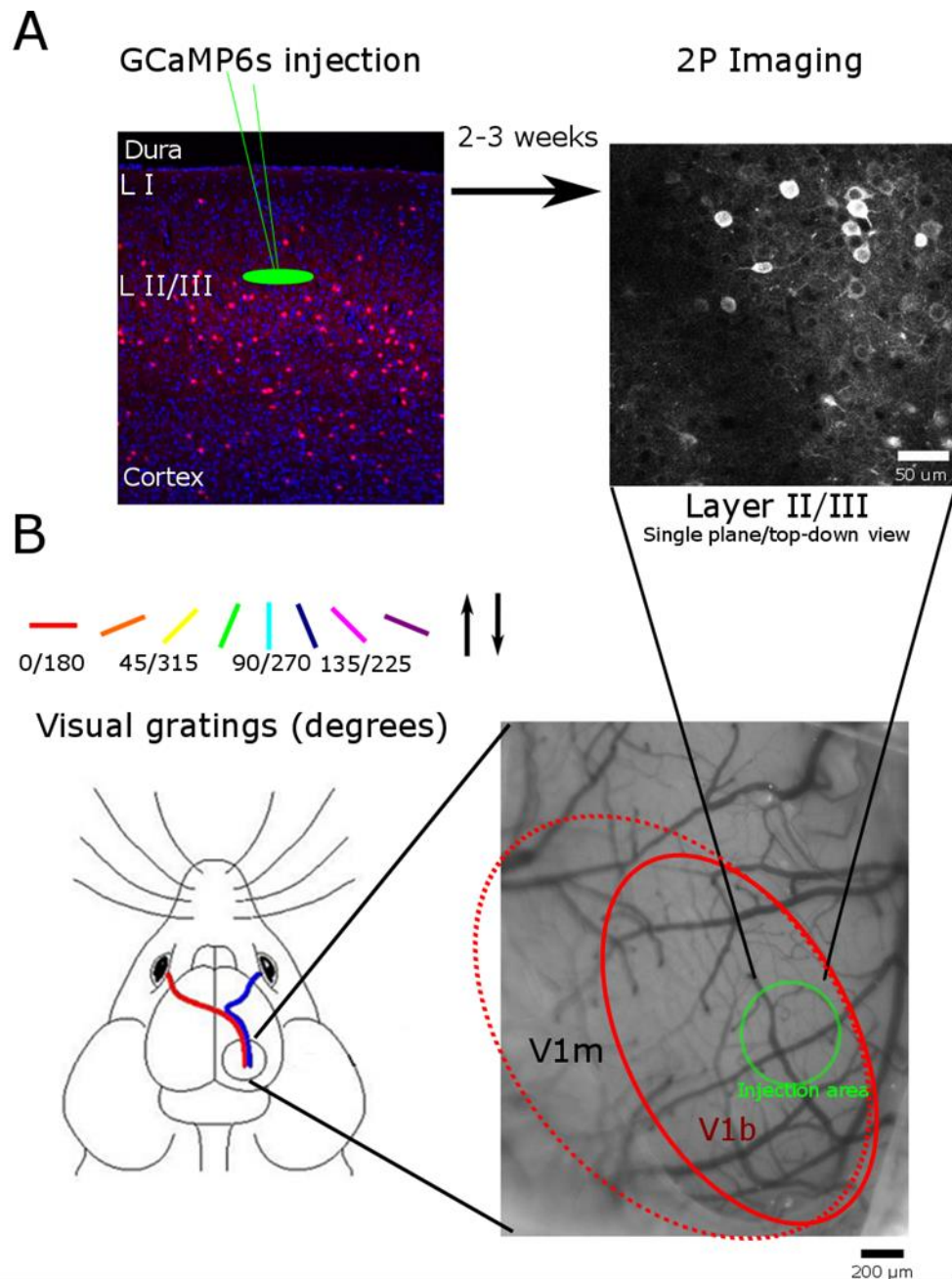


**Figure 3.1** *In vivo* calcium 2P microscopy imaging

(A) A virus was injected into L2-3 of V1b and left to transfect for 2-3 weeks. 2P imaging was performed in a single plane in LII/III. (B) During imaging sessions, a single drifting bar was presented to binocular visual field at anti-clockwise 22.5° rotations, resulting in 8 orientations and 8 opposing directions.

### 3.2.4 Quantification of PV+ interneurons in V1b

Prior to each functional imaging session, a large z-stack image of V1b was taken at 1030nm, using a two-photon microscope. Starting at the cortical surface, just below the dura, 100 slices of large 800  $\mu\text{m}$  x 800  $\mu\text{m}$  images were taken every 5  $\mu\text{m}$ , within the V1b. The Z-stacks were cropped to a depth of 350  $\mu\text{m}$ . PV+ interneurons were counted in 5 smaller areas from the z-stack, by randomly assigning a grid using, using the Grid plug-in on Image J. The counts were corrected to reflect the density of PV+ interneurons, in layer I-II per 1 mm<sup>3</sup>.

### 3.2.5 Calcium signal data analysis

Calcium signal data was collected in .tiff format files, of 256 x 256 pixels, 2ms/line. The collected files were then averaged, and further analysed with custom written scripts in MATLAB (Mathworks). The signal response (R) was expressed as:

$$\frac{\Delta F}{F_0} \times 100 \%$$

The optimal direction was estimated as the direction that elicited the highest R, and was denoted as R<sub>max</sub> at optimal direction, whereas the response in the opposing direction was denoted as R<sub>opp</sub>. The ODI was calculated, as described in chapter 2, where -1 indicates bias towards the ipsilateral eye, and +1 indicating a bias towards the contralateral eye.

The orientation selectivity index (OSI) was calculated using the following equation:

$$OSI = 1 - \text{circular variance}$$

The direction selectivity index (DSI) was calculated as:

$$DSI = \frac{R_{max} - R_{opp}}{R_{max} + R_{opp}}$$

Other parameters, such as the preferred orientation in degrees ( $\Theta^\circ$ ), and mismatch in preferred orientation between the two eyes, were also calculated.

### **3.2.6 Statistical analysis**

Data was recorded and stored in Microsoft Excel. GraphPad Prism (v 6.00) was used to make the graphs. All statistical analyses were performed using SPSS statistical package (v 23.0). Data was tested for normal distribution, and either a parametric t-test, or a non-parametric Mann-Whitney U test was used to test significance. ANOVA, or Kruskal-Wallis, test was used when comparing more than 2 groups. All data was presented as Mean  $\pm$  s.d., unless otherwise stated.

## **3.3 Results**

### **3.3.1 Orientation tuned neuron responses in V1b after unilateral ON crush**

Neurons were detected, and analysed as discrete populations at each time point. All neurons, whose maximum responses were in the top 3 quartiles (in response to stimulus that was presented to either eye) were included. Orientation tuned neurons were defined as neurons, where the OSI  $>$  0.2 (Sohya *et al.* 2007) (Figure 3.2).

In each experimental condition and time point, there were between 235 and 323 orientation tuned neurons detected from the 5 mice studied. In normal mice, the mean maximum response (at the optimal orientation) was found to be  $134 \pm 96$  %, when stimuli were presented to the contralateral eye. When visual gratings were shown to the contralateral eye after an ON crush in that eye, a significant decrease

was observed, dropping to  $108 \pm 106$  % in response maximum after 7 days ( $p < 0.05$ ),  $108 \pm 90$  % after 14 days ( $p < 0.05$ ), and  $124 \pm 95$  % 28 days ( $p = 0.06$ ), after the ON crush, when compared to pre-crush (Figure 3.3).

When visual gratings were presented via the ipsilateral eye to normal mice, the mean maximum response was found to be  $92 \pm 74$  %. The mean maximum responses were found to increase significantly when visual gratings were presented via the ipsilateral eye, rising to  $124 \pm 127$  % after 7 days ( $p < 0.001$ ),  $145 \pm 111$  % after 14 days ( $p < 0.001$ ), and to  $137 \pm 109$  % 28 days ( $p < 0.001$ ) after the ON crush.

In addition, the mean OSI of cells in response to stimulation of the contralateral (ON-crushed) eye significantly decreased from  $0.27 \pm 0.14$  in pre-crush animals to  $0.21 \pm 0.13$ , 7 days after ON crush, and remained decreased at further time points. In contrast, the OSI was found to increase significantly, from  $0.23 \pm 0.1$  in pre-crush animals to  $0.28 \pm 0.08$ , after 7 days post ON crush, when gratings were presented to the ipsilateral eye (intact eye), and remained increased at further time points. No other significant differences were detected across experimental conditions in other parameters that were analysed, such as the DSI, or mismatch between preferred orientations in the two eyes. In pre-crush animals, the mean ODI was  $0.18 \pm 0.34$ , which significantly decreased to  $-0.05 \pm 0.26$  at 7 days ( $p < 0.001$ ) post ON crush,  $-0.09 \pm 0.27$  at 14 days ( $p < 0.001$ ), and  $-0.05 \pm 0.3$  at 28 days ( $p < 0.001$ ) post ON crush.

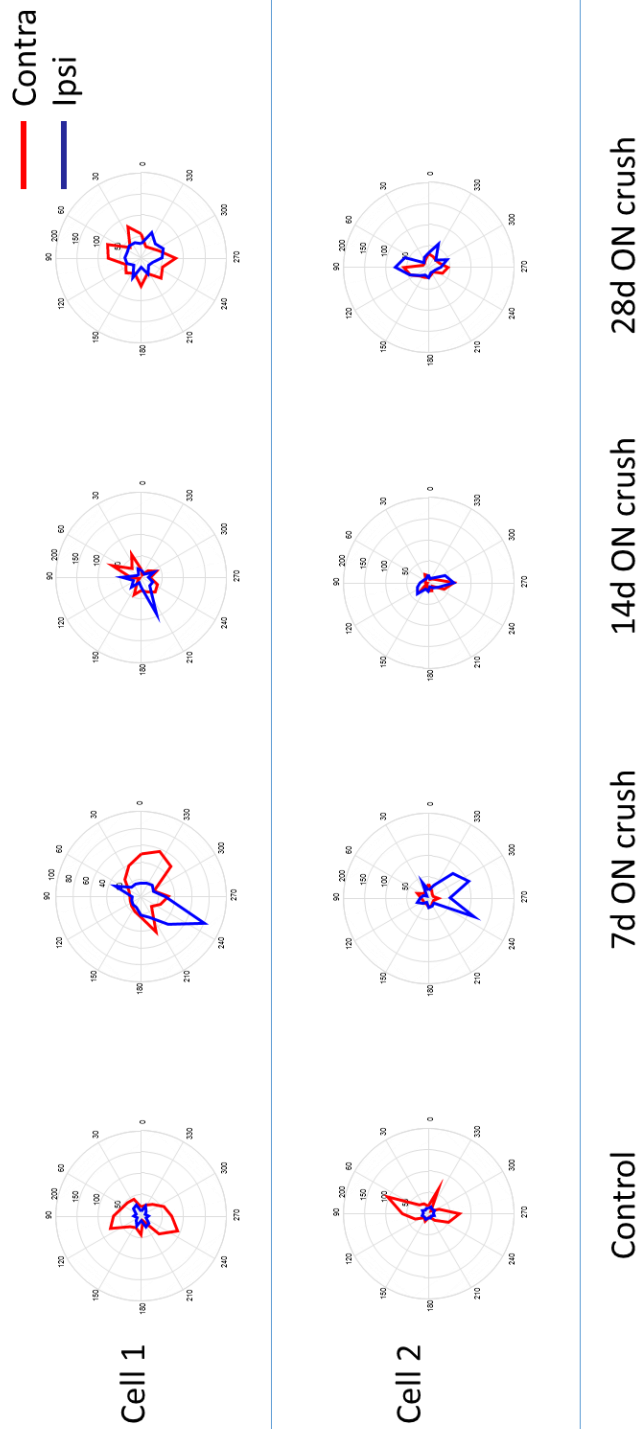


**Figure 3.2 Example of orientation tuned neurons after ON crush**

An example of traces from orientation tuned neurons across the four experimental conditions. Rmax is plotted against orientation of the drifting bar. Red – contralateral stimulation, blue – ipsilateral.

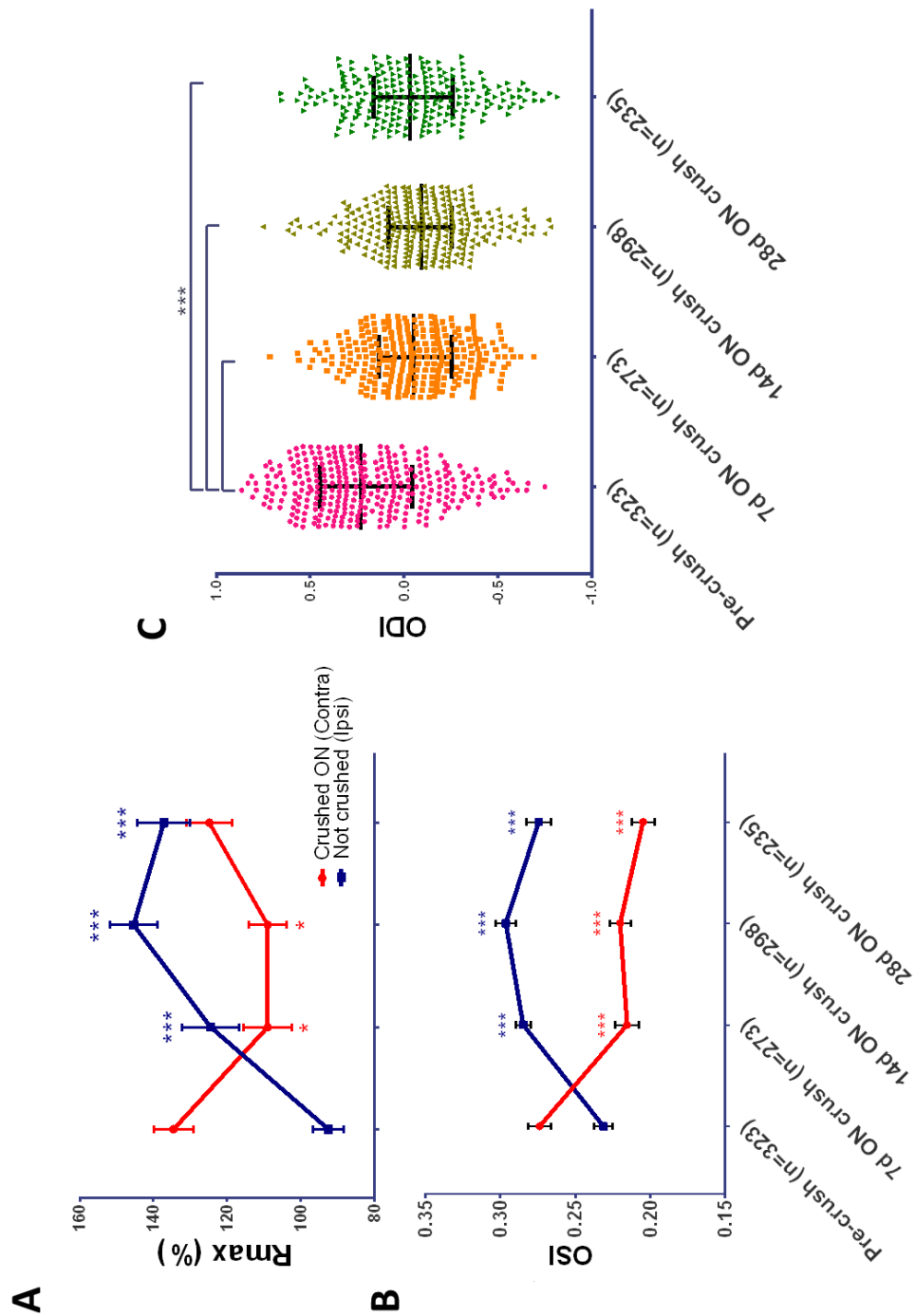


**Figure 3.3 Mean responses of orientation tuned neurons**

(A) Graph showing the mean maximum responses of orientation tuned neurons across the experimental conditions, after an ON crush (mean  $\pm$  s.e.m.). (B) Graph showing OSI values from individual orientation tuned neurons (mean  $\pm$  s.d.). (C) Graph showing OSI values from both eye stimulations, after an ON crush across the experimental conditions (mean  $\pm$  s.e.m.).

### 3.3.2 PV+ interneuron responses in V1b after unilateral ON crush

In total, 64 PV+ interneurons were detected and analysed in each imaging session, from 4 mice. Neurons whose maximum responses were in top 3 quartiles in each session, were selected for further analysis (n=48 from each session) (Figure 3.4).

In pre-crush mice, the mean maximum response of PV+ interneurons was  $70.8 \pm 40$  % to contralaterally (crushed ON) presented stimuli, which decreased significantly to  $57 \pm 22$  % after 7 days ( $p < 0.001$ ),  $55 \pm 27$  % after 14 days ( $p < 0.001$ ), and then to  $51 \pm 45$  % after 28 days ( $p < 0.001$ ) post ON crush, when compared to pre-crush responses. A significant decrease was observed in the mean maximum response of PV+ interneurons to stimuli presented to the ipsilateral (intact) eye at 14 days after ON crush ( $p < 0.05$ ), dropping from  $63 \pm 37$  %, to  $53 \pm 29$  %, when compared to pre-crush responses (Figure 3.4).

The mean ODI was  $0.05 \pm 0.17$ , for PV+ interneurons in the pre-crush group. The mean ODI of the PV+ interneuron population significantly decreased ( $p < 0.05$ ) to  $0.02 \pm 0.12$  at 7 days after the crush, and a further significant decrease ( $p < 0.001$ ) to  $0.07 \pm 0.14$ , at 28 days post crush (Figure 3.4). No significant differences were detected at other time points, or in any of the other analysed parameters (OSI, DSI and mismatch), for responses through either eye.

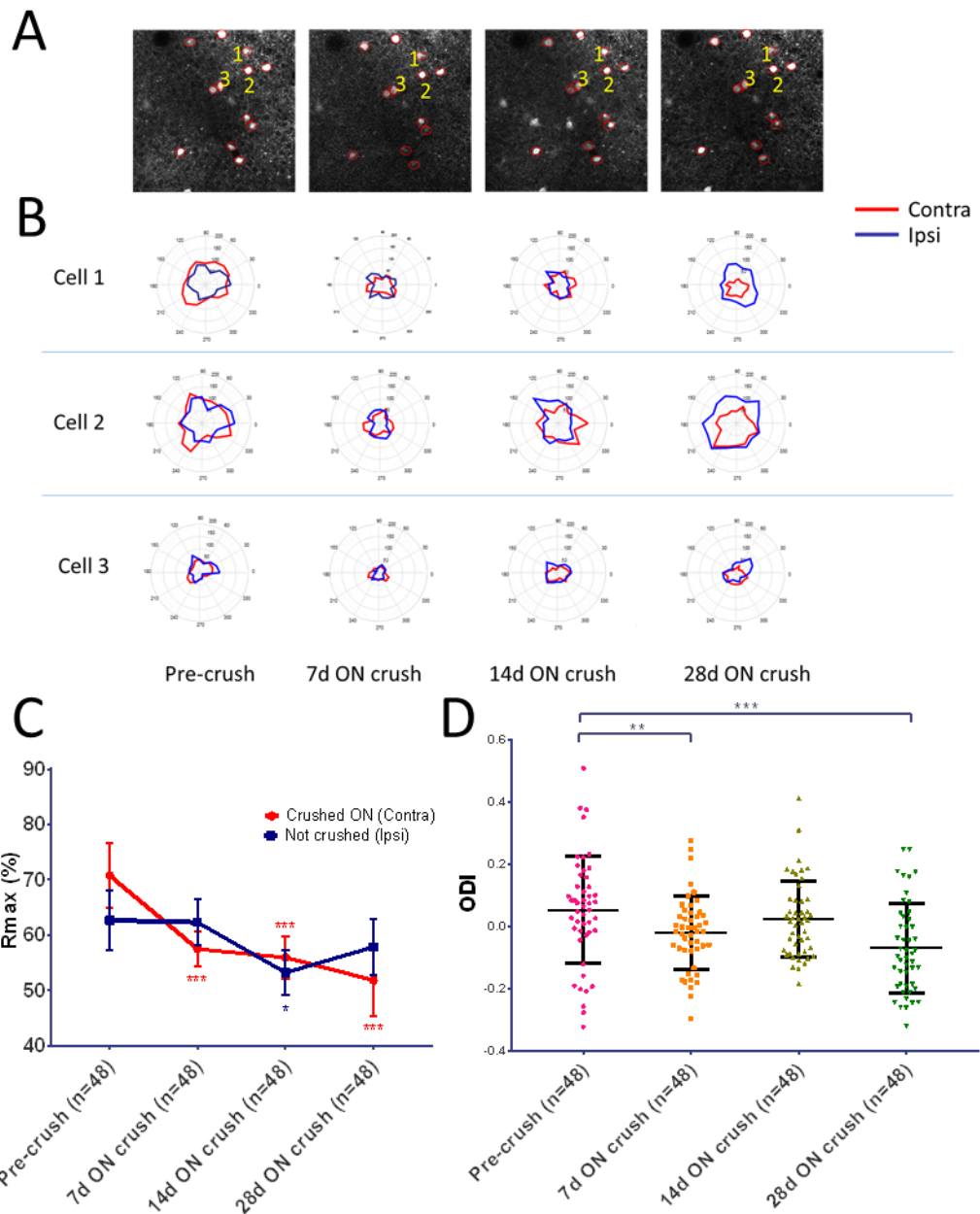


**Figure 3.4 PV+ interneurons after ON crush**

(A) Panels of 2-photon images (at 1030 nm) showing the same PV+ interneurons, easily identifiable across several discrete imaging sessions. (B) Example traces are shown for 3 cells, which correspond to the numbered cells in the images. (C) Graph showing the mean maximum responses of PV+ interneurons, when presenting stimuli via contralateral or ipsilateral eye, in various experimental conditions. (Mean  $\pm$  s.e.m.) (D) Graph showing individual ODI values of PV+ interneurons, across experimental conditions (Mean  $\pm$  s.d.). A single asterisk indicates a significant



difference at  $p < 0.05$ , while a triple asterisk indicates a significant difference at  $p < 0.001$ .

### 3.3.3 The density of PV+ interneurons remained unchanged in V1b, after ON crush

PV+ interneuron numbers were quantified in layer I-III V1b of the same mice ( $n=4$ ) longitudinally, before and after they underwent an ON crush of the contralateral eye. The mean density of PV+ interneurons in V1b in normal, pre-crush mice was  $28832 \pm 3417$  per  $1 \text{ mm}^3$ . This number remained stable after the ON crush;  $31389 \pm 2950$  at 7 days,  $30536 \pm 955$  at 14 days, and  $29762 \pm 3556$  per  $1 \text{ mm}^3$  at 28 days after post crush. There were no significant differences observed in the PV+ interneuron density within the same animals over time (Figure 3.5).

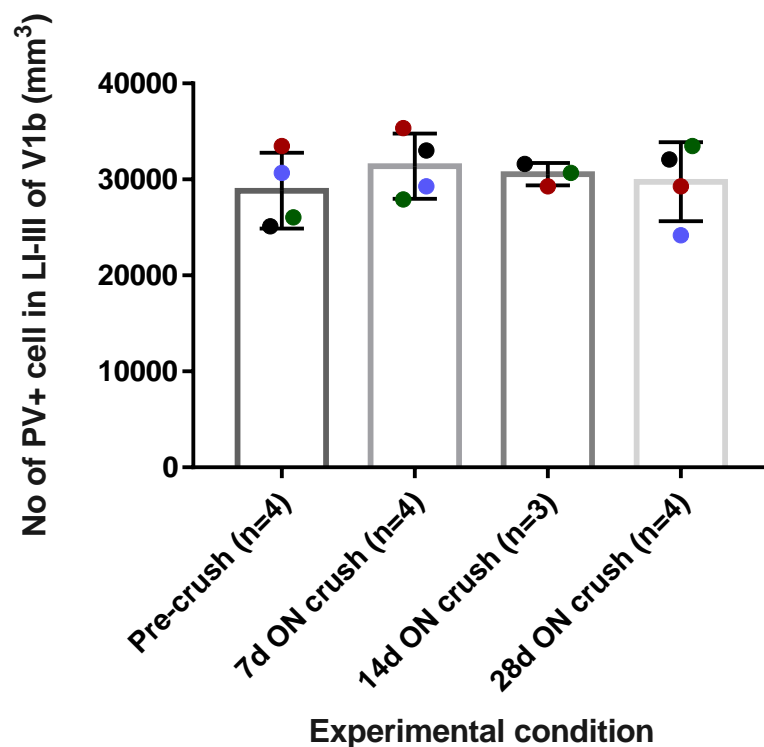


Figure 3.5 *In vivo* structural imaging of PV+ interneurons in V1b.

*The graph shows the mean density of PV+ interneurons in layer I-III of V1b after an ON crush in individual mice (n=4). Each colour represents repeated measures in the same animal (mean ± s.d.).*

### **3.4 Discussion**

It is thought that a mechanical injury to ON axons will cause an initial, direct degeneration of nerve fibres, followed by severe inflammation, which in turn causes secondary neuronal degeneration in the retina (Fitzgerald *et al.* 2009; Xie *et al.* 2010). This secondary degeneration affects axons which are not necessarily directly injured, thus resulting in progressive RGC death over time (Fitzgerald *et al.* 2010). It is currently unknown how signal transmission (from the injured ON, to its targets in V1) is affected by these stages of degeneration. Using *in vivo*, two-photon calcium imaging, I demonstrated that the response to visual stimuli presented via an injured ON, is significantly and persistently reduced after an ON crush in all cell populations. However, only the orientation tuned cell population showed a significant increase in responses through the intact eye, but not the inhibitory PV+ interneurons. This process of open eye potentiation has been extensively documented in other models of visual deprivation, such as ME (Nys *et al.* 2014), and pharmacological silencing of the retina (Frenkel and Bear 2004). In fact, in an adult mouse model of ME, it has been shown that neurons in the contralateral binocular cortex regain responsiveness as soon as 2 days after ME (Nys *et al.* 2014).

Additionally, the increase in response of orientation tuned cells is accompanied by a significant increase in OSI of neurons responding via the intact eye, along with a significant decrease in the OSI of neurons responding via the eye that received the ON crush. Both excitatory and inhibitory neurons have a broad range of OSI (Kerlin

*et al.* 2010), however, the mean OSI is lower for inhibitory neurons, as they are believed to be less tuned to one orientation (Sohya *et al.* 2007). OSI has been used to investigate the maturation of tuning properties of discrete neuronal populations during their development (Kuhlman *et al.* 2011), and after manipulations, such as MD (Rose *et al.* 2016).

In contrast to my findings in orientation tuned neurons, a significant decrease in mean maximum response of PV+ interneurons to the intact eye was observed at a single time point (14 days after ON crush). Additionally, as expected, the activity of PV+ interneurons was also decreased significantly at all experimental time points, when stimulating the eye that received the ON crush. The recorder activity decrease of PV+ interneurons likely to result in a decrease of cortical inhibition. PV+ interneurons have been shown to be involved in some types of adult visual cortex plasticity (Kaplan *et al.* 2016), but to date no study, to my knowledge, has investigated their role in adult plasticity, following an injury.

The ODI is widely used as a measure of binocularity after MD in mouse (Cang *et al.* 2005), providing an indication of bias towards either eye. It has been reported that the mean ODI value varies, and that it can depend on the method of observation used (Cang *et al.* 2005). The mean ODI of both orientation tuned, and PV+ neuron populations, was found to significantly decrease after an ON crush, which correlates with the data obtained from ISI experiments (see Chapter 2).

It was reported that the primary site of degeneration after an ON injury is the retina (Templeton and Geisert 2012), however, degeneration has also been reported in the LGN, and layers 4 and 5 of the visual cortex in rats, after a complete ON transection (You *et al.* 2012). In addition, in one human case of glaucoma, some degree of

degeneration was observed to have occurred across the whole visual pathway, including the LGN and the visual cortex (Gupta *et al.* 2006). Degeneration of the LGN was also found in induced glaucoma in monkey (Yücel *et al.* 2000). In this study, no significant change in density of PV+ interneurons was observed in V1, after ON crush. This confirms that there is no anterograde degeneration in V1, due to the ON crush, however, only one type of cell was surveyed for density (PV+ interneuron), and it was assessed for a relatively short period of time (28 days). It is however unlikely that there was cell death in other cell subtypes in V1. There were also no morphological changes observed during the *in vivo* single cell calcium imaging, of the same areas after the ON crush.

## **Chapter 4: RGC density in human glaucoma**

## 4.1 Introduction

The VF test is a standardised test used in vision clinics worldwide, to detect and assess glaucomatous damage. The current, most commonly used testing paradigm, Humphrey's field analyser (Beck *et al.* 1985), involves a static automated perimeter, where the person is asked to fixate on a fixed point, and to respond by pressing a button if they are able to detect a light presented to them, in their peripheral VF. The Humphrey's VF test can be performed in many different variations, however, most commonly either 54 or 76 test points of the SITA standard (Swedish interactive threshold algorithm) algorithm are used, as it is the fastest, most reliable method currently available (Sharma *et al.* 2000). The stimuli size may vary as well, however, most typically for patients with close to normal visual acuity, a Goldmann III circular stimulus (4 mm<sup>2</sup>) is used (Gilpin *et al.* 1990).

The reliability of the VF tests have been widely discussed, and it is accepted that results can greatly vary, even within the same patient, in a short time period (Birt *et al.* 1997; Birch *et al.* 1995). The main cause of the variability is due to fixation losses during the test (Johnson *et al.* 2002). Regardless of variable reliability, Humphrey's VF testing is a gold standard (Burnstein *et al.* 2000) for glaucoma monitoring and detection worldwide (Mitchell *et al.* 1996; Wadood *et al.* 2002).

It is thought that anatomical glaucomatous damage starts, significantly, before any functional clinical visual deficits can be detected. This is supported by evidence, that a clinically detectable loss of NFL (Sommer *et al.* 1991), and ONH (Zeyen and Caprioli 1993) precede VF defects. The deficits of NFL and the ONH have been shown to correlate in specific retinal regions, when using more advanced imaging techniques, such as optical coherence tomography (OCT) (Le *et al.* 2013; Leung *et al.* 2005; Yamagishi *et al.* 1997).

The spatial pattern loss associated with glaucoma is usually detected using automatic perimetry, and is characterised by spatial patterns typical of glaucoma (**Figure 4.1**). The relationship between the RGC loss in glaucoma, and the VF loss obtained by automated perimetry in the same patient has only been investigated once, by Kerrigan–Baumrind *et al.* 2000, however, it is still unclear if the cell loss exhibits a spatial pattern related to the field loss, and if it is the direct cause for the spatial deficits seen in automated perimetry.

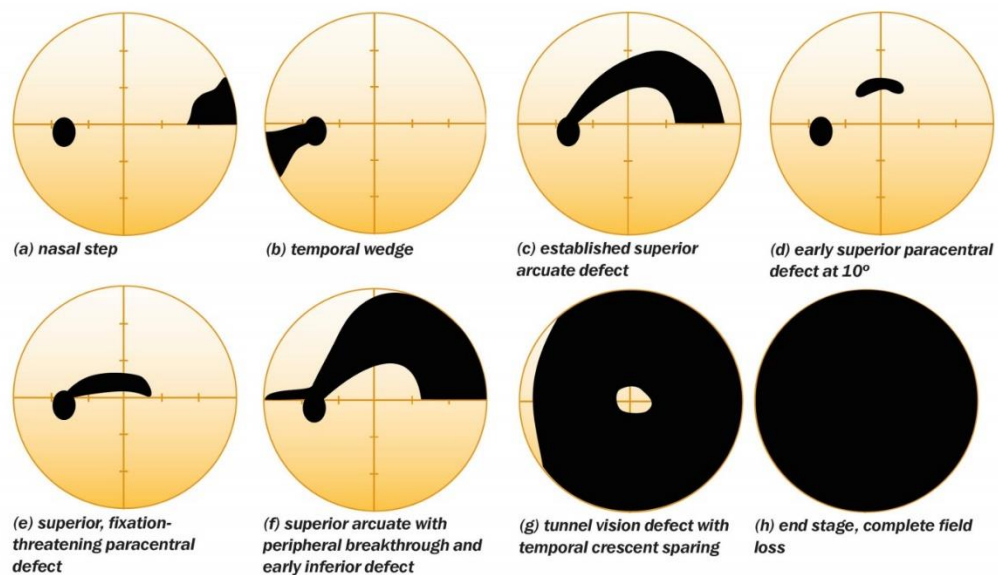


**Figure 4.1 VF loss in glaucoma**

*Characteristic VF loss in glaucoma, as detected by the VF test. (Figure adapted from: <http://www.cehjournal.org/article/visual-field-testing-for-glaucoma-a-practical-guide/>)*

In this chapter, the work that was undertaken in order to compare the histological RGC loss in human glaucoma, with RGC density in normal eyes, is detailed. In

addition, the histological RGC density in human glaucomatous eyes is correlated alongside the VF test results, from the same person.

## **4.2 Methods and Materials**

All experiments involving human tissue were performed in compliance with the Human Tissue Act, 2004.

### **4.2.1 Human tissue source**

The tissue samples that were used for this study were chosen, and age matched from the pool of the available samples. Normal (n=6) and glaucomatous (n=12) human eyes were retrieved, in accordance with the ethical approval of Lions Eye Bank, at the University of Washington, Mayo Clinic, MN, USA. All eyes were collected within 24 hours, from time of death (Table 4.1). The anterior sections of the eyes were dissected out, and the posterior cup (including the retina), placed in 1-4% PFA in 0.1M PBS. Posterior eye cups were shipped to Cardiff University, UK, in accordance with a Material Transfer Agreement (MTA), and in compliance with the Human Tissue Act 2004. The retinas were then dissected out of the posterior cups, and stored in 1-4% PFA in 0.1M PBS, at 4C°.



Sample ID	Eye	Condition	Sex	Age	Time of Death	Time of Enucleation	Time to Fixation	VFs	Therapy
GL173L	Left	Glaucoma	F	81	n/a	n/a	n/a	-	Lumigan;OD-Tru
GL173R	Right	Glaucoma	F	81	n/a	n/a	n/a	-	Lumigan;OD-Tru
GL177L	Left	Glaucoma	M	84	n/a	n/a	n/a	-	Timolol
GL177R	Right	Glaucoma	M	84	n/a	n/a	n/a	-	Timolol
GL178L	Left	Non-Glaucoma	M	77	n/a	n/a	n/a	-	Cosopt, Xalatan
GL178R	Right	Non-Glaucoma	M	77	n/a	n/a	n/a	-	Cosopt, Xalatan
GL239L	Left	Glaucoma	M	77	05/11/11 04:40	05/11/11 08:30	2h 50min	+	Xalatan
GL239R	Right	Glaucoma	M	77	05/11/11 04:40	05/11/11 08:30	2h 50min	+	Xalatan
GL272L	Left	Non-Glaucoma	F	91	7/2/14 00:22	7/2/14 02:40	2h 18min	+	Timolol
GL272R	Right	Non-Glaucoma	F	91	7/2/14 00:22	7/2/14 02:40	2h 18min	+	Timolol
GL277L	Left	Glaucoma	F	72	n/a	n/a	n/a	+	Zioptan, Xalatan
GL277R	Right	Glaucoma	F	72	n/a	n/a	n/a	+	Zioptan, Xalatan
14-0625R	Right	Normal	F	83	25/4/14	n/a	6h 30min	-	n/a
14-0865R	Right	Normal	M	66	15/6/14	n/a	10h 30min	-	n/a
14-0899L	Left	Normal	M	85	21/6/14	n/a	6h 30min	-	n/a
14-1357L	Left	Normal	M	82	19/9/14	n/a	12h	-	n/a
14-1396R	Right	Normal	M	82	29/9/14	n/a	8h	-	n/a
14-1398R	Right	Normal	M	88	30/9/14	n/a	9h 30min	-	n/a

**Table 4.1 Retinal donor information**

*This table shows the donor information of the tissue used in this study. The table lists sample IDs, condition, sex, age, time of death, fixation, presence of VFs with the sample and recorded medication taken for glaucoma.*

#### **4.2.2 VF data**

Three pairs of glaucoma samples (n=6) were supplied with clinical VF data sheets, while others were supplied with some disease treatment history. The clinical test that was applied was Humphrey's 24-2, stimulus size III, and SITA standard. The VF test data are presented, in full, in Appendix 1. Normal retinas were not observed to have any retinal pathology, and did not have any clinical history.

### **4.2.3 Preparation of human tissue for two-photon imaging**

The human tissue was fixed in 1-4% PFA in 0.1M PBS, by collaborators at The Mayo clinic, USA, upon the enucleation. The posterior section of the eye, including the sclera, retina, and the ON, were sent to Cardiff University, UK. The tissue was stored in a fixative solution, at 4°C, until further use. Retinal dissection was performed under a dissecting microscope. During the dissection, the retina was gently teased away from the sclera and RPE (using paint brushes), and a single cut was made to separate it, at the ONH. The retina was kept intact as a whole, and several peripheral cuts were made with dissecting scissors to flatten it. The dissected retina was kept in 1% PFA solution in 0.1M PBS until further use. Before imaging, Hoechst 33342 stain (Life technologies, H1399) was added, at a concentration of 1µg/ml, and incubated overnight at 4°C. The retina was then rinsed once in 0.1M PBS, before two-photon imaging. The retina was then stored in 1% PFA in 0.1M PBS Hoechst-free solution, at 4°C, in the dark, both in-between and after imaging was complete.

### **4.2.4 Two-photon imaging of human tissue**

The dissected retina was placed in a petri dish filled with 0.1 M PBS, GCL side up, and weighed down with a 'U' shaped weight with nylon strings, placed on top of it. The retinas were consistently placed in a known orientation, based on the fovea and ONH location. The fovea was used as a starting point to calculate the eccentricities. A 40x Zeiss 1 NA water immersion objective was moved according to the custom imaging grid (Figure 4.2). A single z-stack of high resolution, at magnification x40 was taken at each of the 76 anatomical locations on the retina, at 740 nm. The 76 anatomical locations were chosen to be equivalent to the 76 test point locations of the

Humphrey's 30-2 VF. The z-stack was acquired at increments of 5  $\mu\text{m}$ , in z-depth, until the cell nuclei of the INL were identifiable. The resulting image z-stack was 1024x1024 pixels, which represented an area of 350  $\mu\text{m}$  by 350  $\mu\text{m}$ .

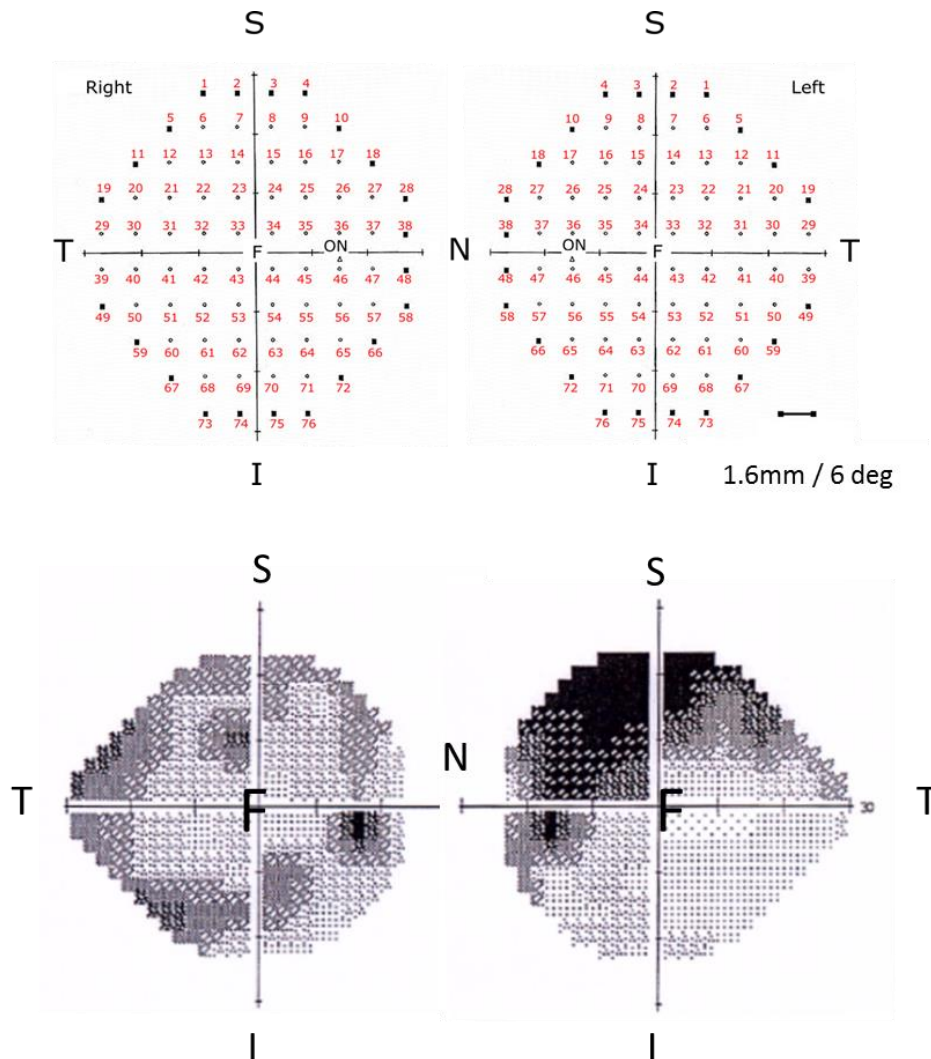


**Figure 4.2** Sampling grid and VF maps

This figure shows the anatomical locations in the right and left eyes, that are equivalent to the test points on Humphrey's 30-2 VF test. Each point is spaced at 1.62 mm, the optic nerve is labelled as ON, and the fovea as F. Retinal directions are

*indicated as S – superior, I – inferior, N – nasal, and T – temporal. All density and visual field maps are rotated and aligned based on anatomical directions for viewing.*

#### **4.2.5 Image analysis**

Post-hoc image analysis was performed using the open source image processing package, Fiji. Nuclear counts were performed manually, using the Cell Counter plug-in, on the z-stack of images. All Hoechst positive nuclei were counted in 3 ROIs (200 x 200 pixels) for each z-stack, before the counts from the 3 ROIs were averaged. The performance of various Image-J plug-ins for automated cell counting (which included ITCN, Nucleus Counter, and 3D Object Counter (v2.0)) were tested and compared, prior to the bulk analysis. None of these automated methods yielded continuously reliable results across the different images. This was mainly due to the complicated non-linear anatomical arrangement of RGCs in GCL, and the variability in cell nuclei sizes and shapes.

#### **4.2.6 Criteria for RGC counts**

GCL and INL can be readily separated by their discrete depth of lamination (Figure 4.3). Only medium-to-large cell nuclei, that were circular or round, were counted. Endothelial cells (which can be recognised by their elongated finger-like nuclei), any small nuclei, or any nuclei located in the NFL, were excluded from counting (Figure 4.3) This, however, did not eliminate the possibility that displaced amacrine cells were included in the counts, and therefore a correction for displaced amacrine cell

numbers was applied, based on published data from Curcio and Allen (1990) (Table 4.2).

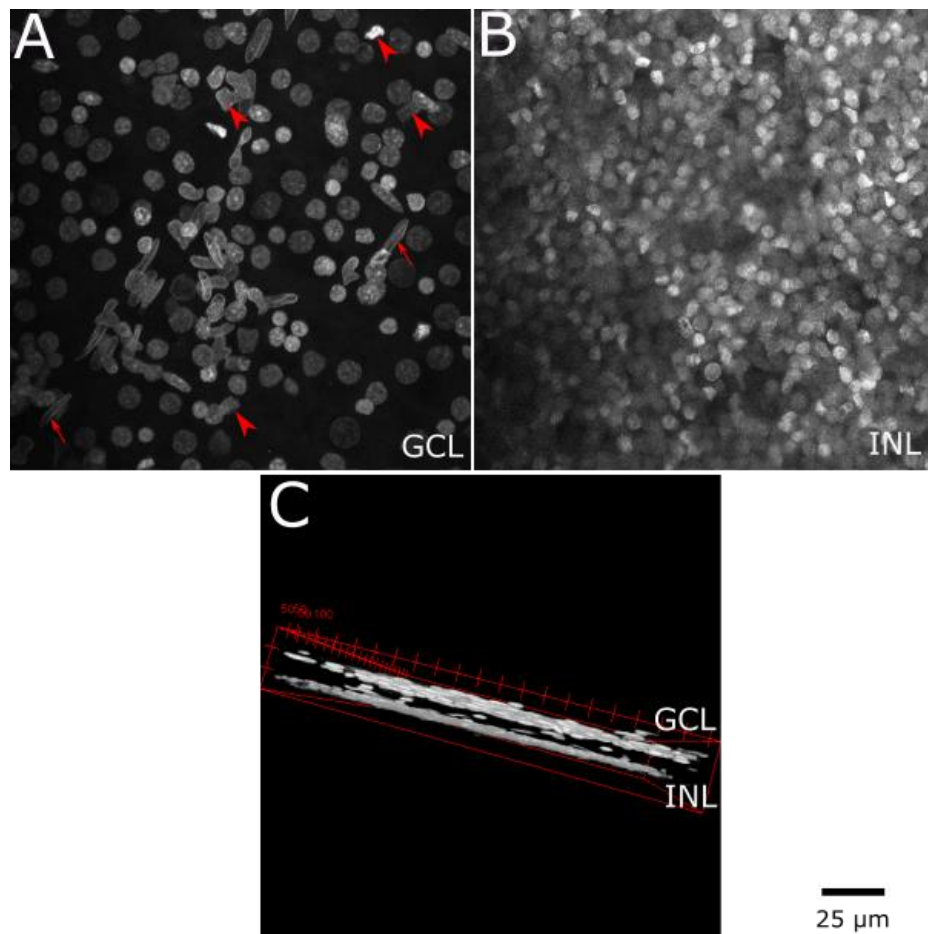


**Figure 4.3** *Hoechst stained human retina*

(A) A flatmount GCL view of the retina, (B) a flatmount INL view. Endothelial cell nuclei were marked with arrows, and other irregular cell nuclei were marked with arrowheads. Both types of cells were excluded from the counts in this study. (C) The side view of GCL to INL, demonstrates a clear distinction between the two layers. The scale bar is 25  $\mu\text{m}$ .

<b>Eccentricity from the fovea (mm)</b>	<b>Percentage of displaced amacrine neurons (%)</b>
0.8	3%
2.4	10%
4	24%
5.6	40%
7.2	45%

***Table 4.2 The corrections applied for displaced amacrine cells***

*This table summarises the corrections that were applied to each area, according to their eccentricity, based on the study Curcio and Allen (Curcio and Allen 1990).*

#### **4.2.7 Preparation of retinal cryosections**

Segments were chosen based on the scores from VF test points, with moderate and mild cell loss from each glaucoma retina, were selected and anatomically matched to segments from normal retinas (Figure 4.4) Segments of interest were dissected out, and placed in 30% Sucrose in 0.1 M PBS, overnight at 4C°. These segments were then placed in plastic cryo-molds, in the optimum cutting temperature (O.C.T.) embedding matrix (CellPath). The cryo-molds were partially submerged in isopentane, which had been cooled with liquid nitrogen, until the matrix appeared visually frozen. Samples were then wrapped in parafilm, and stored in sealed plastic specimen bags at -20 C°, until cryosectioning. Transverse, 8 µm thickness, cryosections were sectioned using a Cryostat (Leica CM3050 S), and were collected

on glass slides (Superfrost®Plus, VWR). Slides were allowed to air dry overnight, in a 37°C oven, and were stored at -20°C until further use.

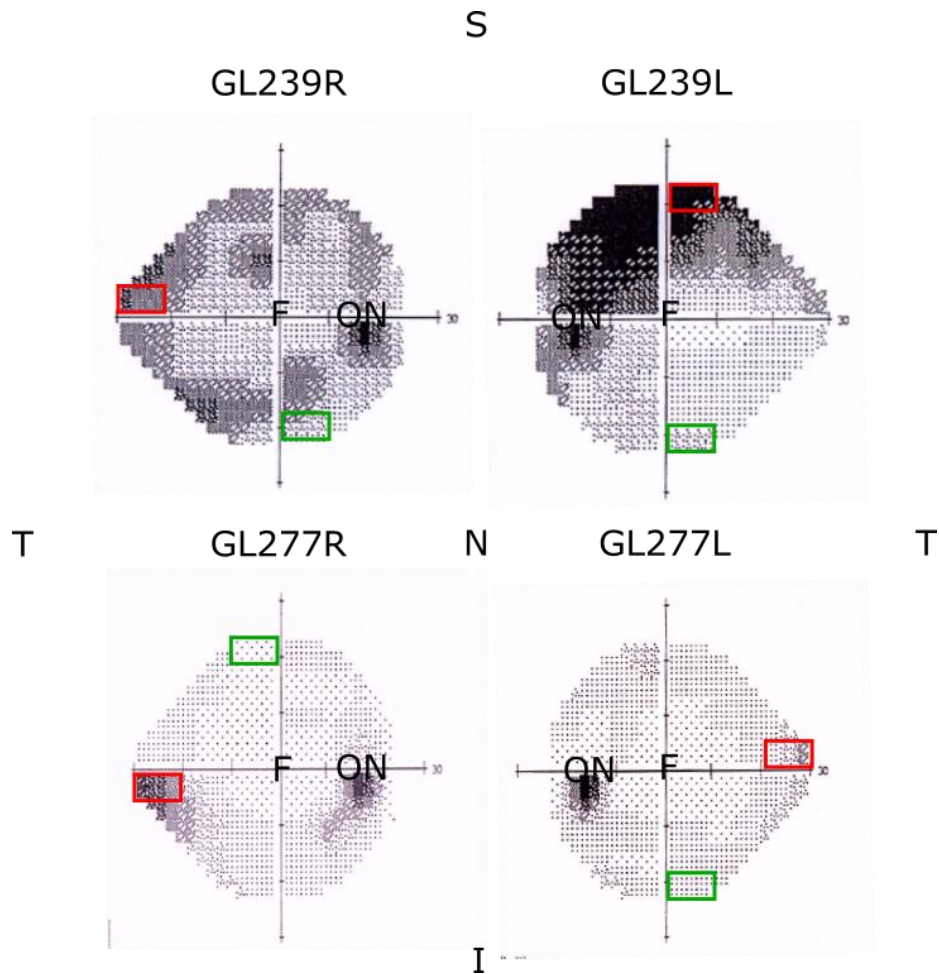


**Figure 4.4 Areas of retinal dissection**

*Retinal segments from the areas shown were dissected out from the four retinas. Moderate and mild damage areas were chosen based on VF test scores. Red rectangles indicate areas that were classified as moderate damage, and green rectangles indicate areas classified as mild damage. The optic nerve is labelled as ON, and the fovea as F. Retinal directions are indicated as S – superior, I – inferior, N – nasal, and T – temporal.*

#### **4.2.8 Haematoxylin and Eosin (H&E) staining**

H&E staining was performed on retinal cryosections, that were rinsed in 0.1 M PBS for 10 minutes, and incubated in a series of washes of tap water, Harris Haematoxylin and Eosin solutions. The slides were then dehydrated, in a series of ascending ethanol solutions, before being cleared with xylene, and a coverslip applied using DPX mountant (06522, Sigma-Aldrich).

#### **4.2.9 Immunofluorescence staining**

Immunofluorescence was performed by rinsing cryosectioned retinal slides 3 times with 0.1 M PBS, before incubating them for 1 hour in a blocking solution, which contained 5% normal goat serum (G9023, Sigma-Aldrich), 1 % bovine serum albumin (A-7906, Sigma-Aldrich), and 0.1 % Triton X-100 (X100, Sigma-Aldrich), at room temperature. The tissue was then incubated with primary anti-gial fibrillary acidic protein (GFAP), in the same blocking solution, overnight, at 4 C°. The tissue was then rinsed 3 times with 0.1 M PBS, and incubated for 1 hour with the appropriate secondary antibody, at a dilution of 1:1000, in 0.1 M PBS, at room temperature, in the dark. Retinal segments were then rinsed a final 3 times with 0.1M PBS, before being incubated in a 0.1 µg/mL solution of Hoechst 33342 (H1399, Life Technologies) nuclear stain in dH<sub>2</sub>O, for 5 minutes. Retinal sections were covered with a drop of Fluoromount™ (F4680, Sigma-Aldrich) aqueous mounting medium placed on top of the tissue, before applying a glass coverslip. The edges of glass slides and coverslips were sealed from the air, by placing a thin layer of nail polish across the edges. The stained slides were stored, in the dark, at 4 C°, and imaged within 2 weeks.



#### **4.2.10 Microscopy**

Images of the H&E stained slides were collected using a simple light microscope.

Images of the fluorescent dyes were collected using epifluorescent microscope, fitted with a standard fluorescent filter set.

#### **4.2.11 Image analysis**

Post-hoc image analysis was performed using an open source image processing package, Fiji (Image-J). Both the cell and object counts were performed using the Cell Counter plug-in.

#### **4.2.12 Statistical analysis**

Statistical analysis was performed using the SPSS statistical package. An unpaired t-test was performed if the data fulfilled the assumptions of a parametric test, such as normal distribution. A non-parametric, Mann-Whitney U test was performed to compare the other data sets, that did not fit the parametric criteria. Spearman's correlation was performed in order to correlate data sets. All values shown are mean  $\pm$  standard deviation, and the threshold for statistical significance was  $p \leq 0.05$ .

### **4.3 Results**

#### **4.3.1 Exclusion of samples**

After performing an H&E stain on retinal cryosection samples from donor GL178, they appeared to contain no photoreceptor layer, a thickened NFL, and astrocytic infiltration, as shown in Figure 4.5. This indicated that a glaucoma diagnosis prior to death was either incorrect, or secondary to another unknown pathological condition.

This sample was omitted from the study. The VF tests from donor GL272 did not show significant deficits associated with a glaucoma diagnosis, and after consulting with Professor James Morgan (Appendix 1), this donor was also omitted from the final results presented in this chapter. In summary, a total of four retinas (GL178L, GL178R, GL272L and GL272R), from 2 subjects (n=4) were completely omitted from the study, as these samples were suspected to have been misdiagnosed, and did not conform to the study's inclusion criteria, of a mild to moderate glaucoma diagnosis.

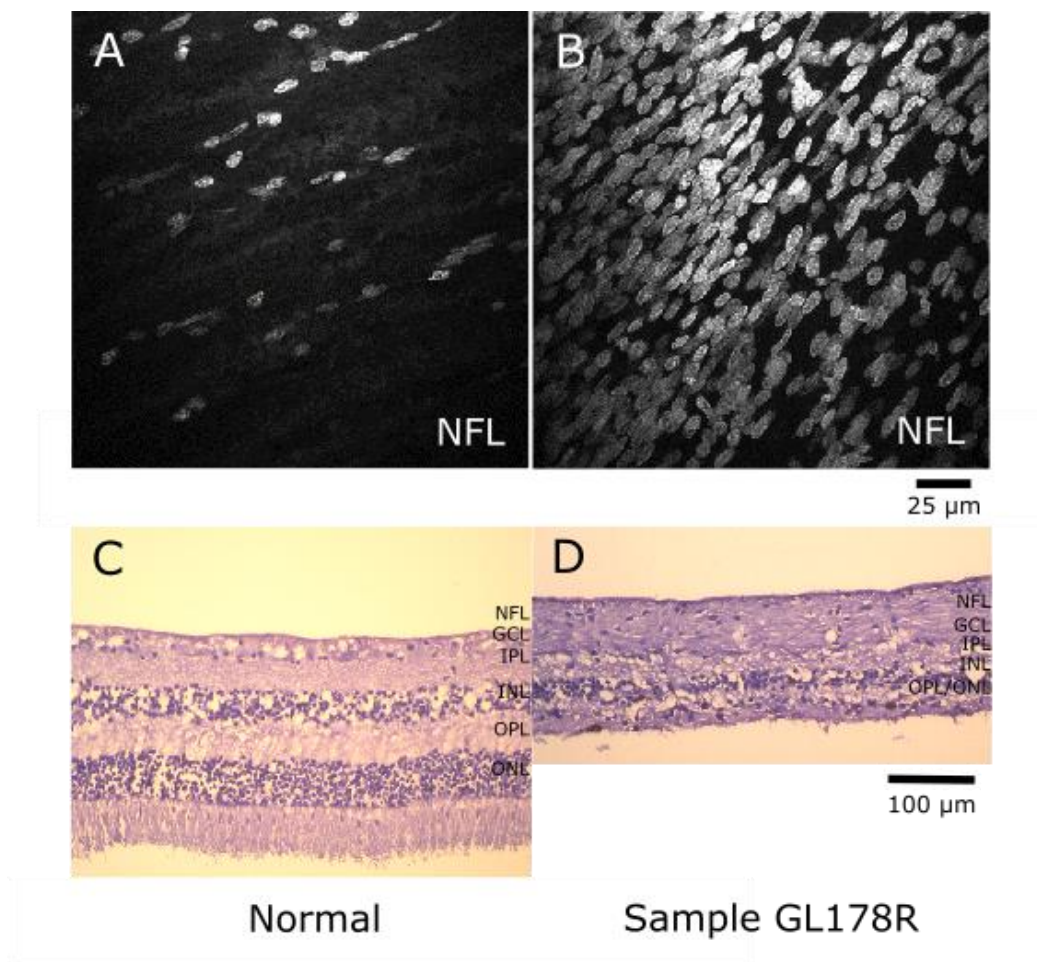


**Figure 4.5 Excluded retinal samples**

*An example of the excluded sample, GL178R. The NFL of a normal retina is shown in panel A, and the NFL of sample GL178R, is shown in panel B. The H&E stained section of normal retina is shown in panel C, and GL178R section of the retina is shown in panel D. The scale bar is 25  $\mu\text{m}$  for panels A and B, and 100  $\mu\text{m}$  for panels C and D.*

#### **4.3.2 Final tissue summary**

In the final data set, there were 6 independent retinas from normal donors, and 8 retinas from 4 glaucoma donors. The average age of the normal tissue used in this study was  $78.5 \pm 4.0$  years, and the average age of the glaucoma donor tissue was  $81 \pm 6.5$  years. A minimum of 61 areas, out of a possible 76, were imaged in each retina, with the individual sample details listed in Table 4.4. In most cases, the peak density of RGCs occurred at 0.8 mm from the fovea, except in one glaucoma sample, where the peak was found to occur at 2.4 mm eccentricity from the fovea. The quadrant of peak density was found to vary greatly, however, the peak was most commonly found in the inferior-temporal quadrant in 6 out of 14 samples.

Sample ID	Eye	Condition	Age	VFs	Areas Imaged (out of 76)	Peak RGC density (mm <sup>2</sup> ) x1000	Quadrant of peak	Eccentricity of peak (mm)
14-0625R	Right	Normal	83	-	69	23.1	S-N	0.8
14-0865R	Right	Normal	66	-	76	28.7	S-N	0.8
14-0899L	Left	Normal	85	-	75	28.8	I-T	0.8
14-1357L	Left	Normal	82	-	66	18.7	I-N	0.8
14-1396R	Right	Normal	82	-	61	23.1	I-N	0.8
14-1398R	Right	Normal	88	-	71	22.1	I-T	0.8
		<b>Mean</b>	<b>81</b>		<b>70</b>	<b>24.1</b>		
		<b>s.d.</b>	<b>±6.5</b>		<b>±5.1</b>	<b>±3.3</b>		
GL173L	Left	Glaucoma	81	-	74	25.7	I-N	0.8
GL173R	Right	Glaucoma	81	-	75	25.1	S-T	0.8
GL177L	Left	Glaucoma	84	-	71	7.5	S-N	2.4
GL177R	Right	Glaucoma	84	-	76	15.3	S-T	0.8
GL239L	Left	Glaucoma	77	+	73	12.6	I-T	0.8
GL239R	Right	Glaucoma	77	+	75	15.9	I-T	0.8
GL277L	Left	Glaucoma	72	+	75	26.7	I-T	0.8
GL277R	Right	Glaucoma	72	+	75	21.3	I-T	0.8
		<b>Mean</b>	<b>78.5</b>		<b>74</b>	<b>18.8</b>		
		<b>s.d.</b>	<b>±4.0</b>		<b>±1.5</b>	<b>±6.5</b>		

**Table 4.3 Tissue summary**

*This table lists the final tissue used in the study, including the conditions, age, presence of the VFs, the number of fields imaged, the peak of RGC density, quadrant, and eccentricity of the peak density.*

### **4.3.3 Comparison of normal control subject RGC density with published data**

The cell count data from the normal samples in this study matched closely with the data published from normal retinas by Curcio and Allen (1990), which were provided by Curcio (2013) (Figure 4.6). The significant differences at 0.8 mm eccentricity between the data sets is likely to be explained by the significantly older average donor age in this study ( $81 \pm 6.5$  years old (n=6)) than the study by Curcio and Allen (1990), in which the average donor age was  $33.8 \pm 3.5$  years old (n=5). No significant impact on any of the overall results was observed when amacrine cell correction (Table 4.2) was excluded.

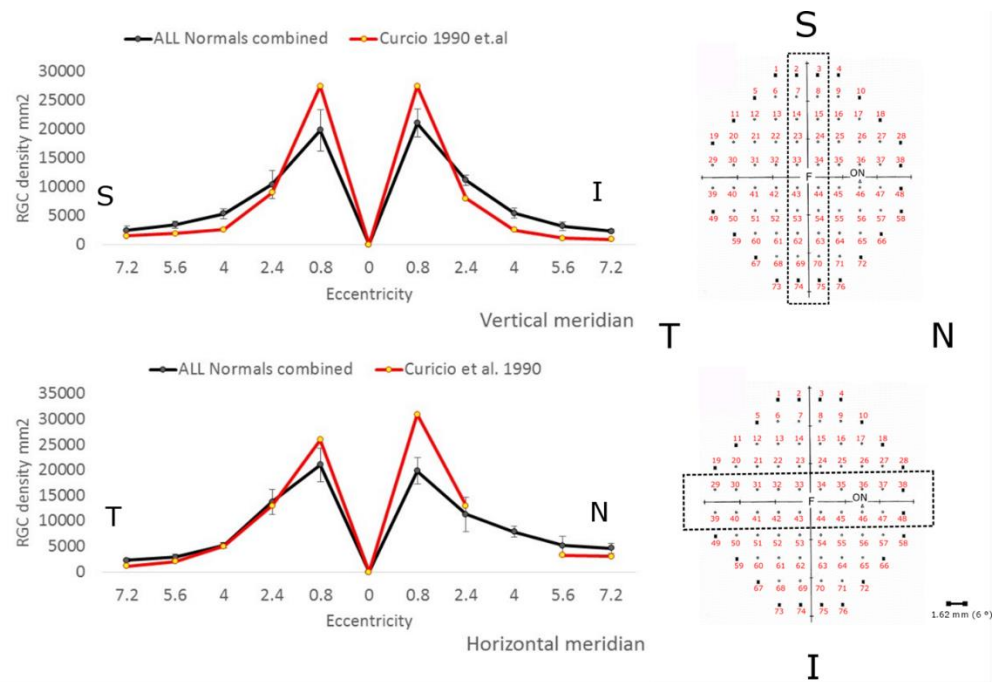


**Figure 4.6 Cell count comparison with previously published data**

The graphs show the combined normal subject RGC density count comparison across vertical and horizontal meridians, against data published by Curcio and Allen (Curcio and Allen, 1990). The diagrams on the right indicate the regions that were included. Anatomical directions are indicated as S – superior, I – inferior, N – nasal, and T – temporal.

#### 4.3.4 The Density of RGCs were reduced in glaucomatous retinas

On average, the overall density of RGCs were reduced in all glaucoma retinas (n=8), when compared to retinas from normal patients (n=6) (Figure 4.7). The percentage difference of RGC loss was also calculated in the average glaucoma (n=8), and compared to average, age-matched, normal retinas (n=6), as a reference point (Figure 4.7C). Significant cell loss was found to occur in spatial pattern, where 18 out of 76 areas were found to have a significantly reduced RGC density (Mann-Whitney U test,  $p \leq 0.05$ ) (Figure 4.7). Additionally, the overall RGC density was also

significantly reduced (Mann-Whitney U test,  $p \leq 0.05$ ) at certain eccentricities across vertical and horizontal meridians, when compared to normal, age-matched controls (Figure 4.8). The greatest cell loss across vertical axis was found to occur at 0.8 mm eccentricity in the superior hemiretina, and at 2.4 mm in the inferior hemiretina. The greatest cell loss across horizontal axis in glaucoma, however, was found to occur at all investigated eccentricities in the temporal hemiretina, from 0.8-7.2 mm.

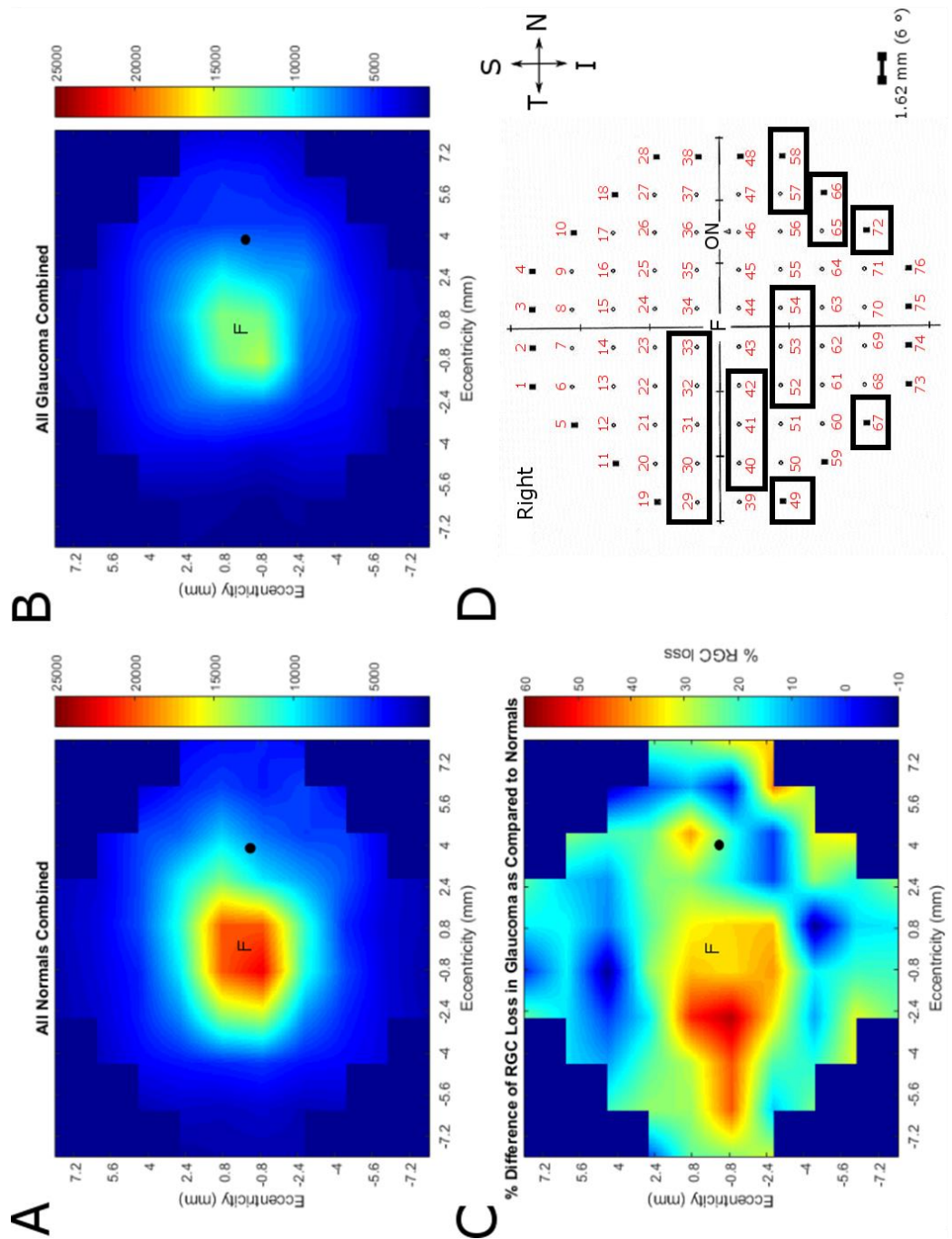


**Figure 4.7** RGC density maps in the GCL of average normal retinas, and in glaucoma

The figure shows a map depicting the combined average of normal (A), and glaucoma (B) RGC density in GCL, with red colours depicting high density, while blue depicts low density. The map of % difference of RGC loss between all normal and glaucoma samples is shown in C. Panel D shows a diagram of the anatomical sampling points, and locations where the significance value of  $p \leq 0.05$  are marked



(black square outline) (D). The graphs in panel E show RGC density along the horizontal and vertical meridians. Anatomical directions are indicated as S – superior, I – inferior, N – nasal, and T – temporal.

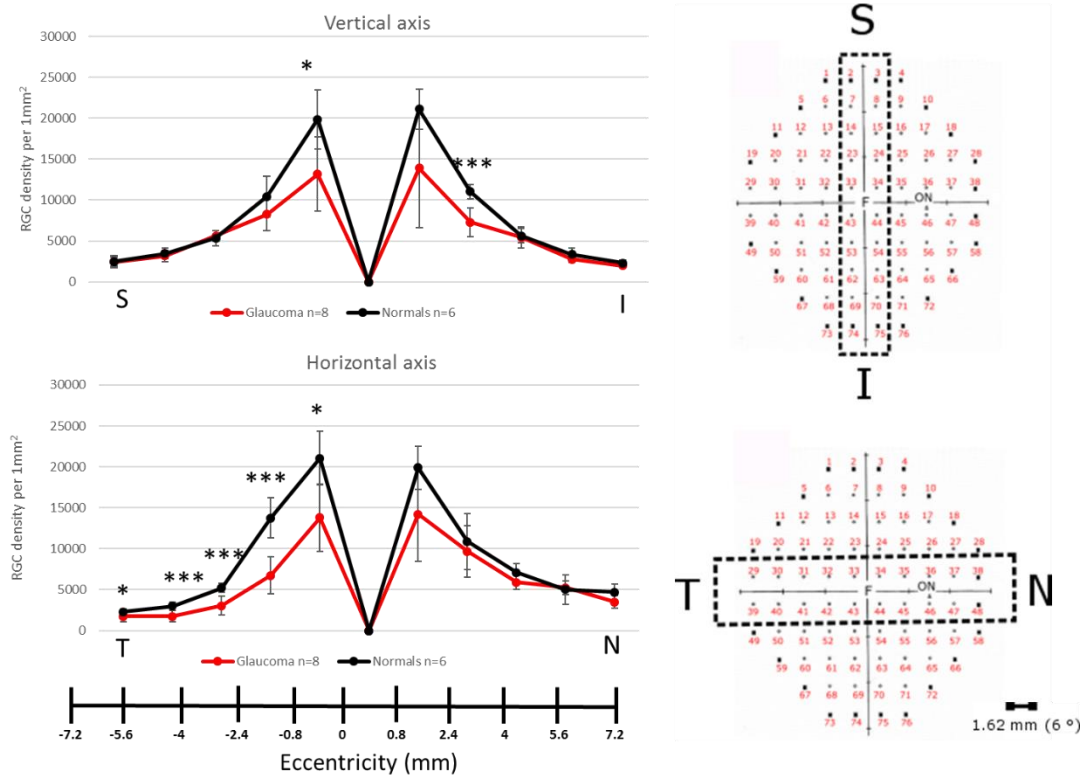


**Figure 4.8 RGC density across the vertical and horizontal meridians**

The average density of the areas around the horizontal and vertical meridians were taken, as shown in diagram next to the plotted graphs. Error bars indicate the standard deviation. Anatomical directions are indicated as S – superior, I – inferior, N – nasal, and T – temporal. \* $p \leq 0.05$  and \*\*\* $p \leq 0.001$  significance levels.

#### 4.3.5 High variability in RGC density within the group of glaucoma subjects

The coefficient of variation (CV), was calculated at each eccentricity across the vertical and horizontal meridians for both groups, using the following equation:

$$CV = \frac{s.d.}{mean} \times 100 \%$$

For the horizontal meridian, the average CV was 30.4 % in glaucoma donor samples (n=8), and 19.3 % in samples from normal donors (n=6). For the vertical meridian, the average CV for glaucoma samples was 24.4 %, and 17.9 % from normal donors. The higher CV in the glaucoma samples indicated that there was an increased variability, or spread, in data of RGC density distribution of then glaucoma samples, than in the normal samples (Figure 4.9).

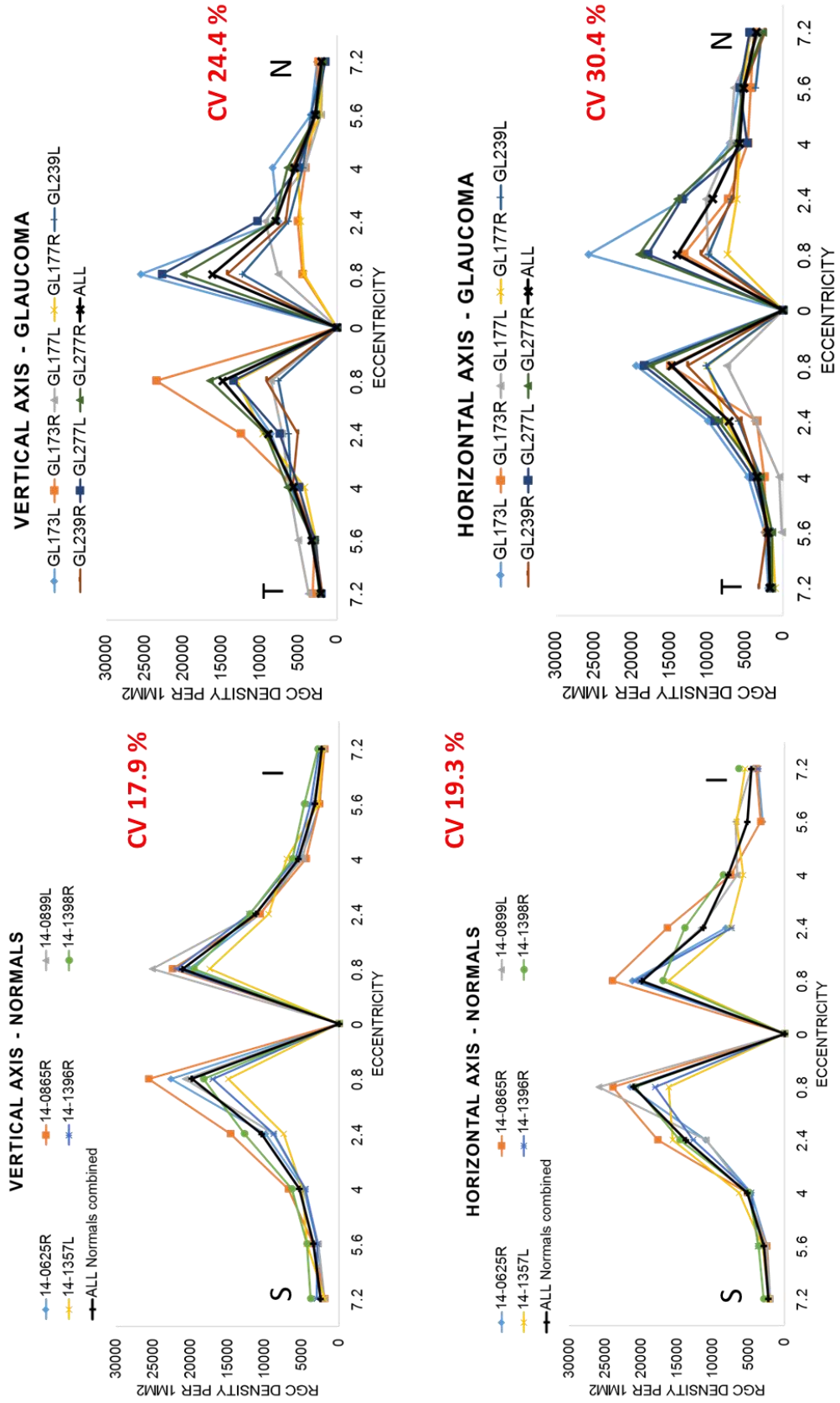
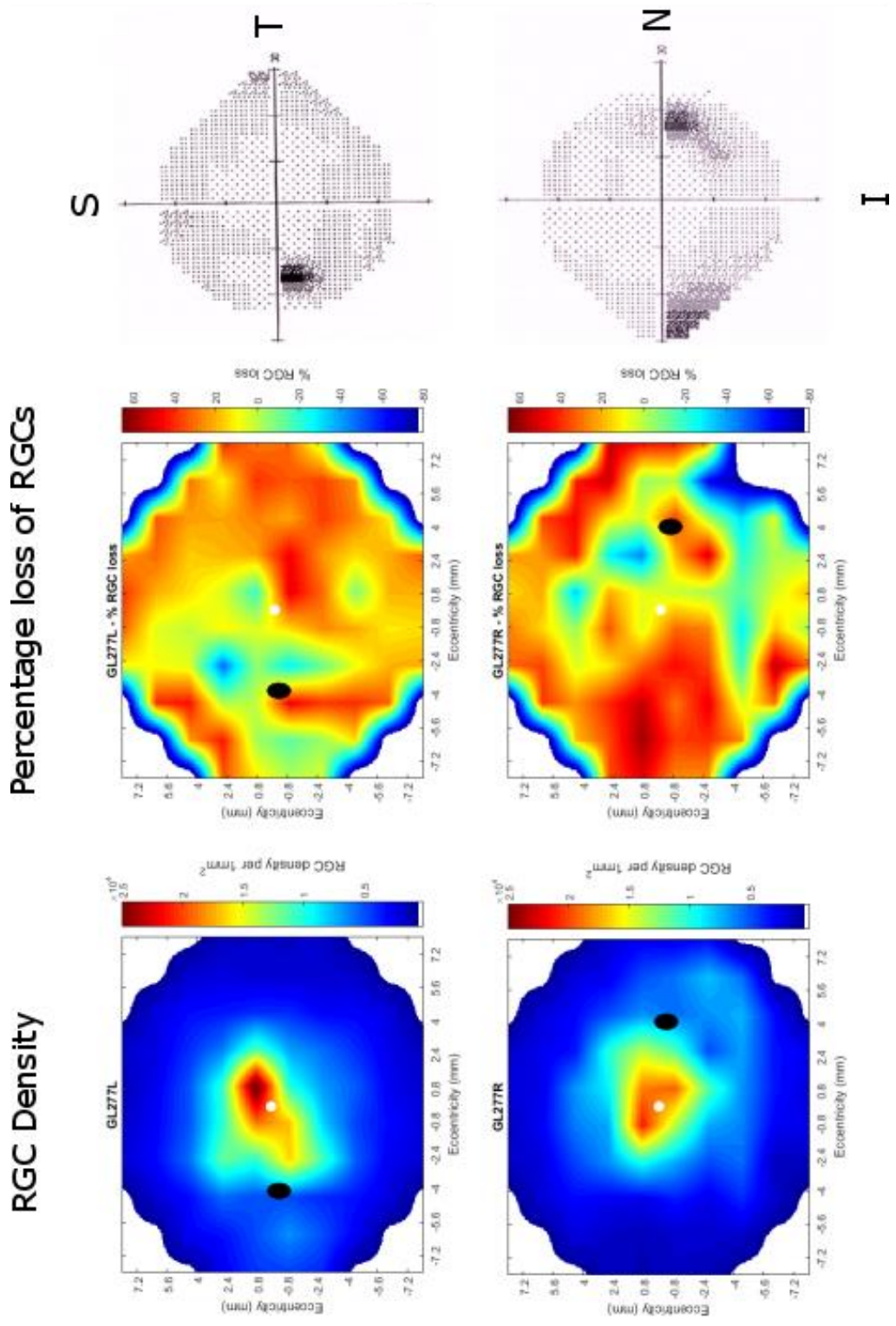


Figure 4.9 The RGC density across the vertical and horizontal axis of normal, and glaucoma retinas

*The graphs show the RGC density in GCL of the vertical and horizontal axis from each individual retinal sample. Anatomical directions are indicated as S – superior, I – inferior, N – nasal, and T – temporal.*

#### **4.3.6 Correlation of the density of RGCs in individual areas of glaucomatous retinas, with the VF test data within the same donor retina**

Sensitivity is the numerical measure obtained during VF testing expressed in decibels, it provides information on the brightness of the spot of light presented to the specific part of the retina that patient was able to correctly identify. Whereas total deviation is a measure extrapolated from an existing database of age-matched patient records, which shows mean sensitivity difference compared to age-matched population of same sex. Both sensitivity and total deviation measurements obtained from VF data (Appendix 1) were compared to the RGC density and percentage RGC loss in each individual glaucoma retina (n=4) (calculated against age matched densities of normal samples (n=6)) (Figure 4.10 and Figure 4.11). No significant correlation (Pearson's correlation) was detected in the relationship between any of the cell densities, or percentage RGC loss, when compared to the VF sensitivity and the total deviation (Figure 4.12).



*Figure 4.10 RGC density of sample GL277, compared with maps obtained from the VF test data*

*The column of maps on the left hand side displays the RGC densities of GL277 left and right retinae. The middle column displays the percentage RGC loss in individual retinas, compared to normal age-matched retinas (n=6). The right hand side column shows the maps obtained from the VF test data. The VF test maps are expressed in grey scale, where darker colours indicate a greater loss of sensitivity. The maps are rotated in correspondence to the anatomical locations listed in the figure. Anatomical directions are indicated as S – superior, I – inferior, N – nasal, and T – temporal. The white circle indicates the fovea, and the black ellipse indicates the ON.*

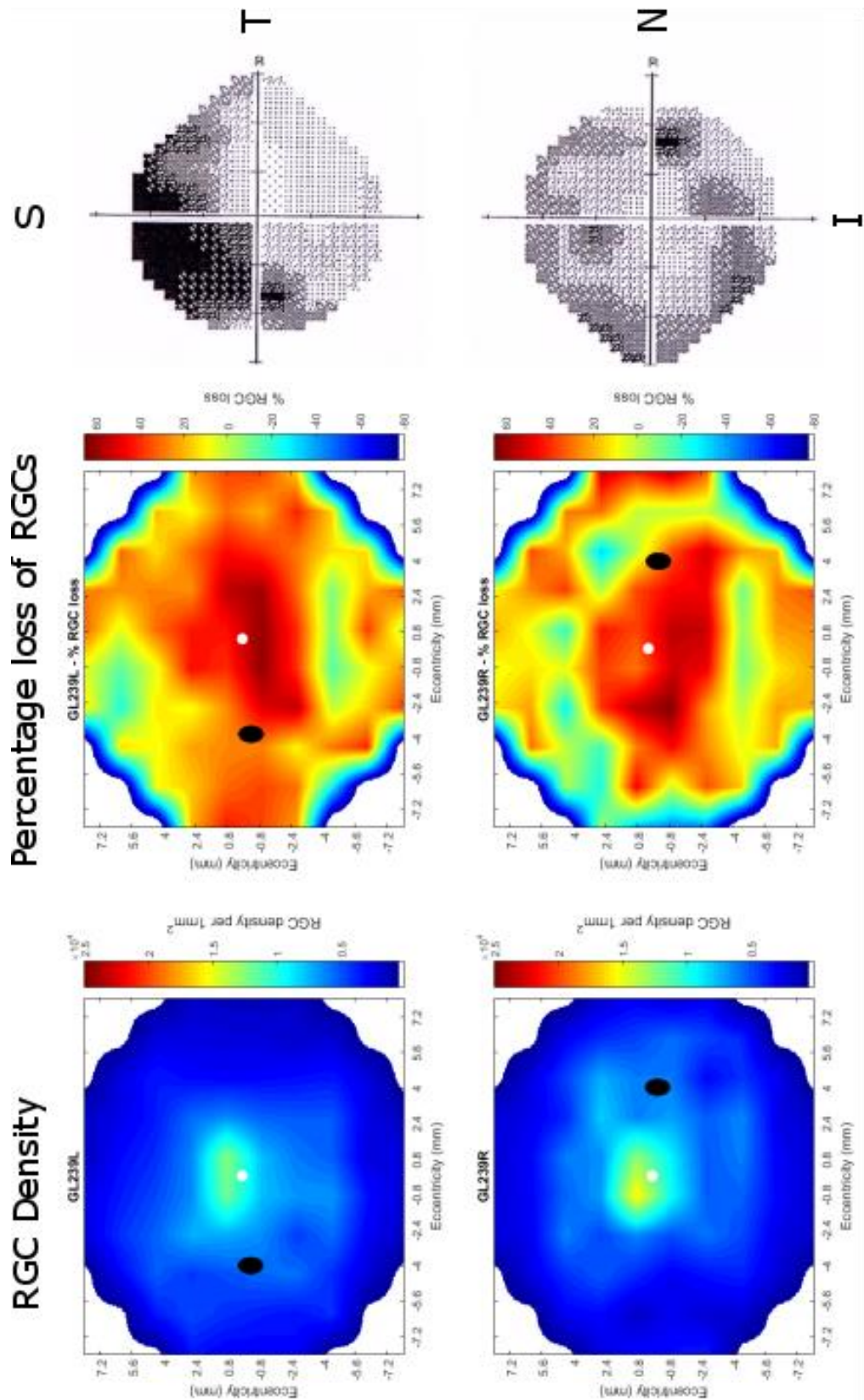


*Figure 4.11 RGC density of sample GL239, compared with maps obtained from the VF test*

*The column of maps on the left hand side displays the RGC densities of GL239 left and right retinae. The middle column displays the percentage RGC loss in individual retinas, compared to normal age-matched retinas (n=6). The right hand side column shows the maps obtained from the VF test data. The VF test maps are expressed in grey scale, where darker colours indicate a greater loss of sensitivity. The maps are rotated in correspondence to the anatomical locations listed in the figure.*

*Anatomical directions are indicated as S – superior, I – inferior, N – nasal, and T – temporal. The white circle indicates the fovea, and the black ellipse indicates the ON.*



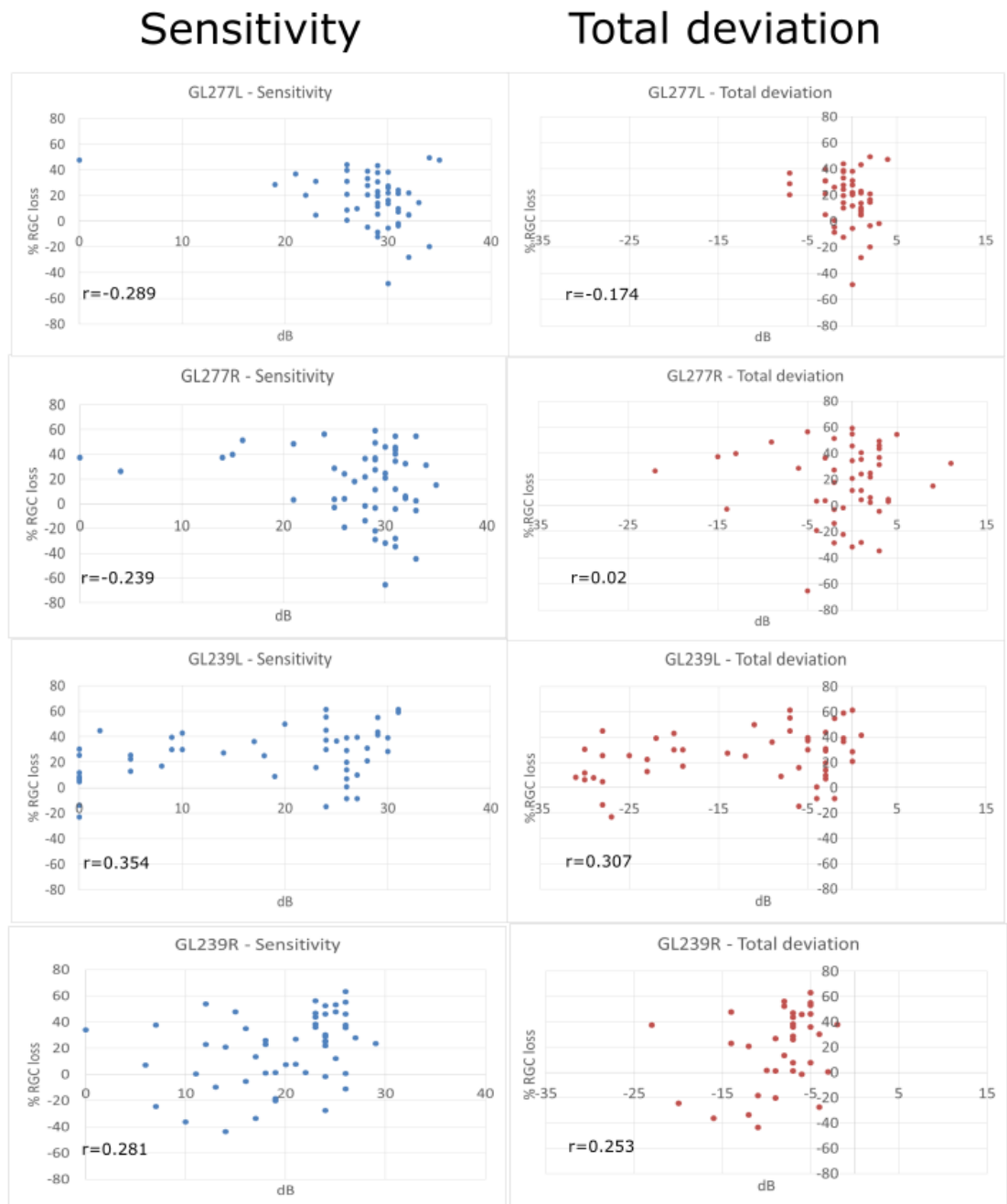


**Figure 4.12** The correlation of sensitivity and total deviation with RGC loss

The graphs show the percentage RGC loss of individual glaucoma samples plotted against VF test sensitivity (left), and total deviation from the mean of the age-matched population (right).  $R$  indicates Spearman's correlation, where 1 is a positive correlation, 0 is no correlation, and -1 is a negative correlation.

#### **4.3.7 Peak cell loss in glaucoma showed correlation with the summary findings of the VF test**

The overall mean percentage RGC loss was calculated, before using the peak RGC density to calculate if there were any statistical correlations between the clinically, commonly used general summary parameters of the mean deviation index, and the mean pattern standard deviation (PSD), which is typically used to measure focal loss in glaucoma (Appendix 1). As the human glaucoma retina sample size was small (n=4), the data did not have normal distribution, therefore Spearman's rank correlation coefficient was calculated. The peak RGC density in all four eyes was found to be highly positively correlated with the mean deviation index (rho 1), and negatively correlated with pattern standard deviation (rho -1). However, the mean percentage loss was not correlated with mean deviation index (rho 0.8), nor with pattern standard deviation (rho 0.8).

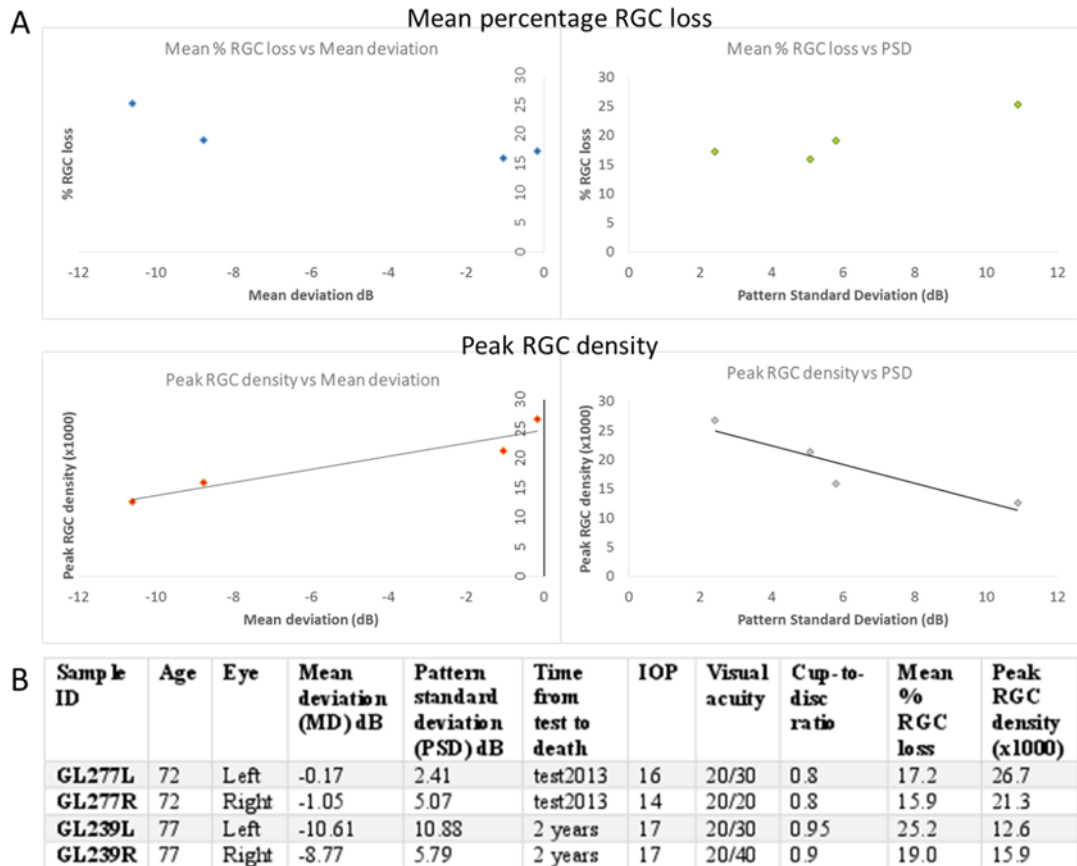


**Figure 4.13** *The mean deviation index and pattern standard deviation in glaucoma*  
 (A) A graph showing overall RGC percentage loss and peak density, plotted against the mean deviation index and PSD. Only the peak RGC density (and not cell loss) was significantly correlated with the mean deviation index and PSD. (B) A table listing the mean deviation indices, PSDs, and other average parameters for each retina.

#### 4.3.8 Overall inner retinal layer thicknesses are reduced in glaucoma, compared to normal subjects

Significant differences were found in the thickness of the inner retinal layers of glaucoma retinas, when compared to the same anatomical areas of retina in normal subjects (Figure 4.14). The ILM-GCL thickness was significantly reduced (Student t-

test,  $p \leq 0.001$ ) in glaucoma, from  $18.9 \pm 2.6 \mu\text{m}$  to  $8.7 \pm 1.5 \mu\text{m}$ . The IPL thickness was also significantly reduced (Student t-test,  $p \leq 0.001$ ), from  $26.9 \pm 3.2 \mu\text{m}$  to  $15.1 \pm 1.9 \mu\text{m}$  in glaucoma. The INL was also showed a significant reduction (Student t-test,  $p \leq 0.001$ ), from  $26.5 \pm 2.8 \mu\text{m}$  in normal retinas, down to  $19.2 \pm 1.9 \mu\text{m}$  in glaucoma.

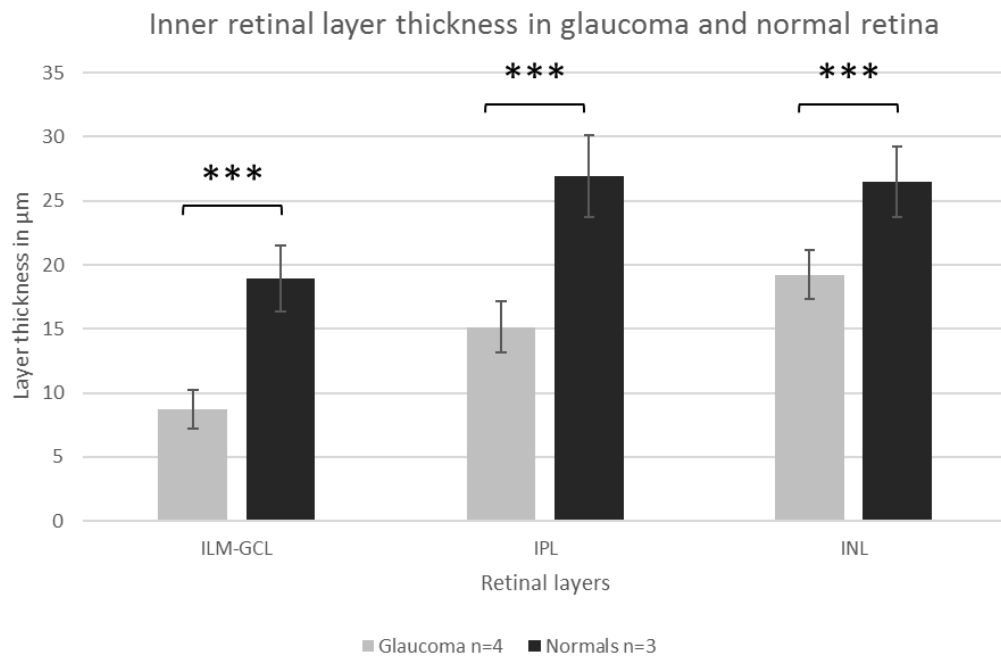


**Figure 4.14 Inner retinal layer thicknesses of both glaucoma, and normal subjects**  
The graph depicts the average layer thickness of glaucoma (n=4,) and normal (n=3) ILM to GCL, IPL and INL layers, derived from H&E stained frozen cryosections. Asterisks indicate significance level of  $p \leq 0.001$ .

#### 4.3.9 The thickness of inner retinal layers within the same glaucoma retina

Areas of mild to moderate damage were defined, based on the VF test data (Appendix 1) (Figure 4.15). The inner retinal thickness of several, separate spatial regions within the same glaucomatous eyes were measured, and their thickness was

compared within the same retina. No significant differences in layer thicknesses were observed in ILM to GCL and IPL in any of the individual samples within glaucoma (Figure 4.15). When glaucoma samples with the same degree (mild or moderate) of damage were combined and compared, no statistical differences were detected between mild or moderate damage regions in glaucoma (Figure 4.16).

Inner retinal layer thickness within glaucoma eyes

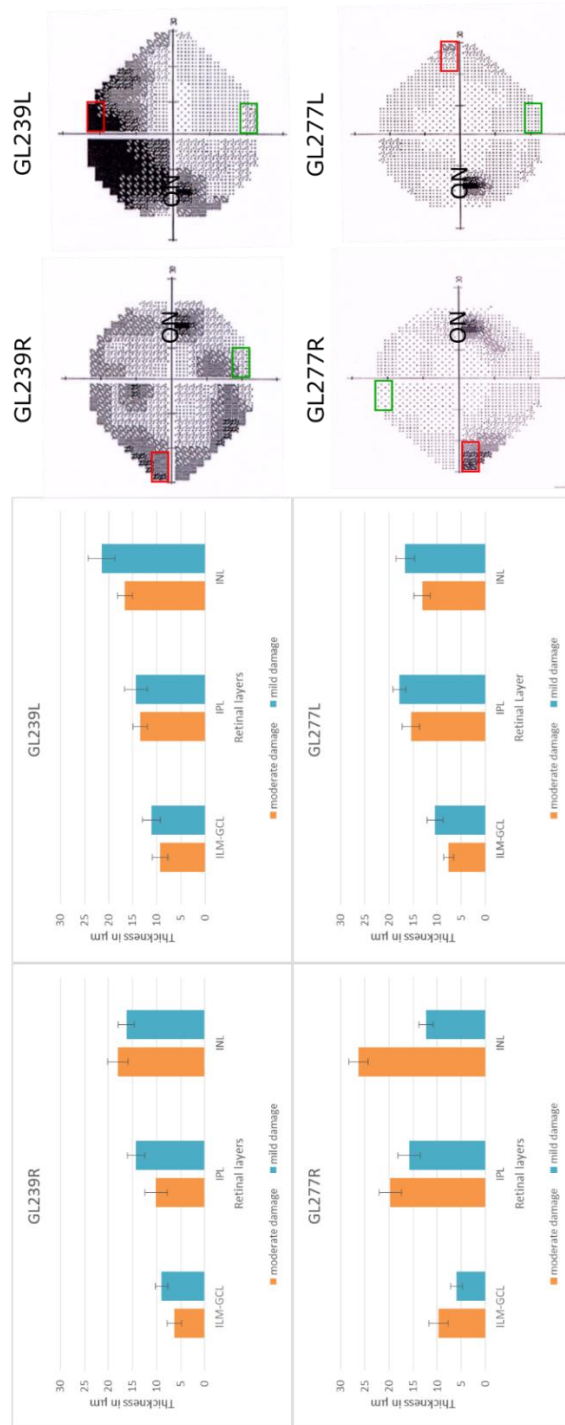


**Figure 4.15 Inner retinal layer thicknesses in regions of variable damage, within the same glaucomatous retina**

The graphs display the retinal thicknesses of ILM to GCL, IPL and INL, in moderate and mildly damaged areas of individual glaucoma retinas. The diagrams of the anatomical locations on the VF tests are shown alongside, with mildly damaged areas outlined in green and moderately damaged areas outlined in red.

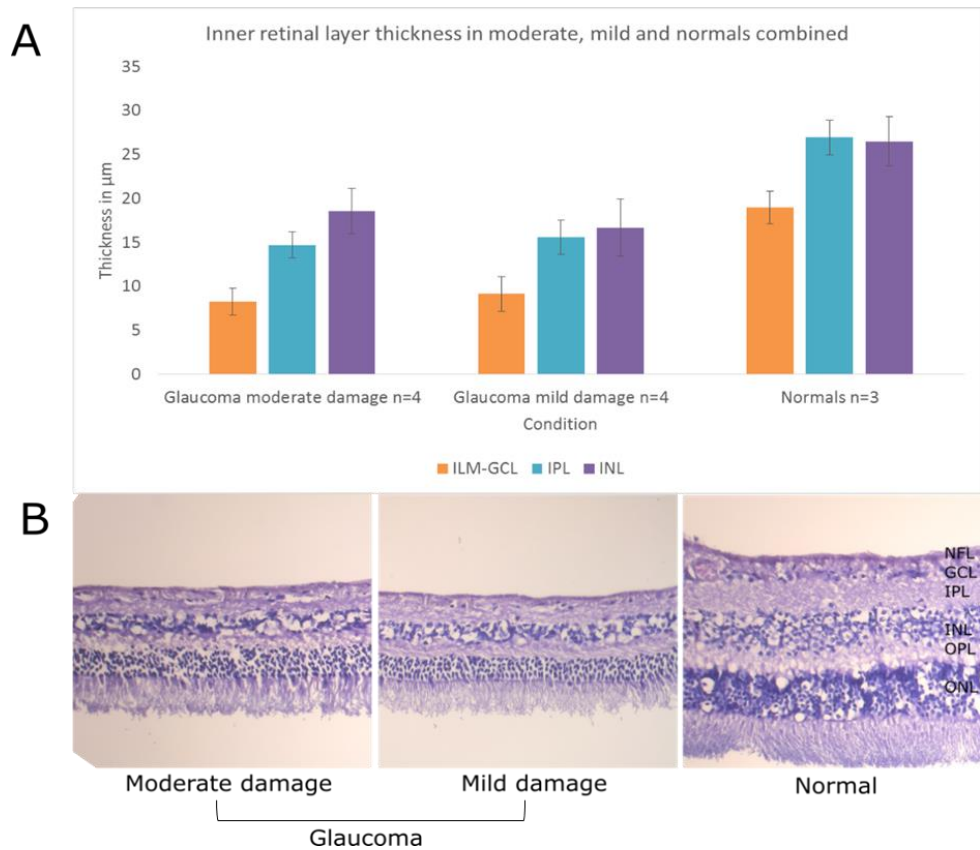


**Figure 4.16 Inner retinal layer thicknesses in moderate, and mild glaucoma damage, and in normal samples**

(A) The thicknesses of ILM-GCL, IPL and INL in moderate glaucoma damage (n=4), mild glaucoma damage (n=4), and normal retinas (n=3). (B) A number of H&E stained images, showing typical examples of moderate, and mild glaucoma, as well as normal retinal segments.

#### 4.3.10 GFAP activation in human glaucoma retina

Increased GFAP staining is associated with greater astrocytic activity and gliosis. The GFAP fluorescence intensity was measured post-hoc, in the retinal layers of ILM to IPL, and INL, separately. No marked GFAP activation was observed in

glaucoma retinas, as was shown in Figure 4.17. In fact, GFAP labelling appeared to be reduced in ILM to IPL of the glaucoma retinas, which was most likely due to their significantly reduced layer thicknesses, compared to the layer thickness in normal retinas.

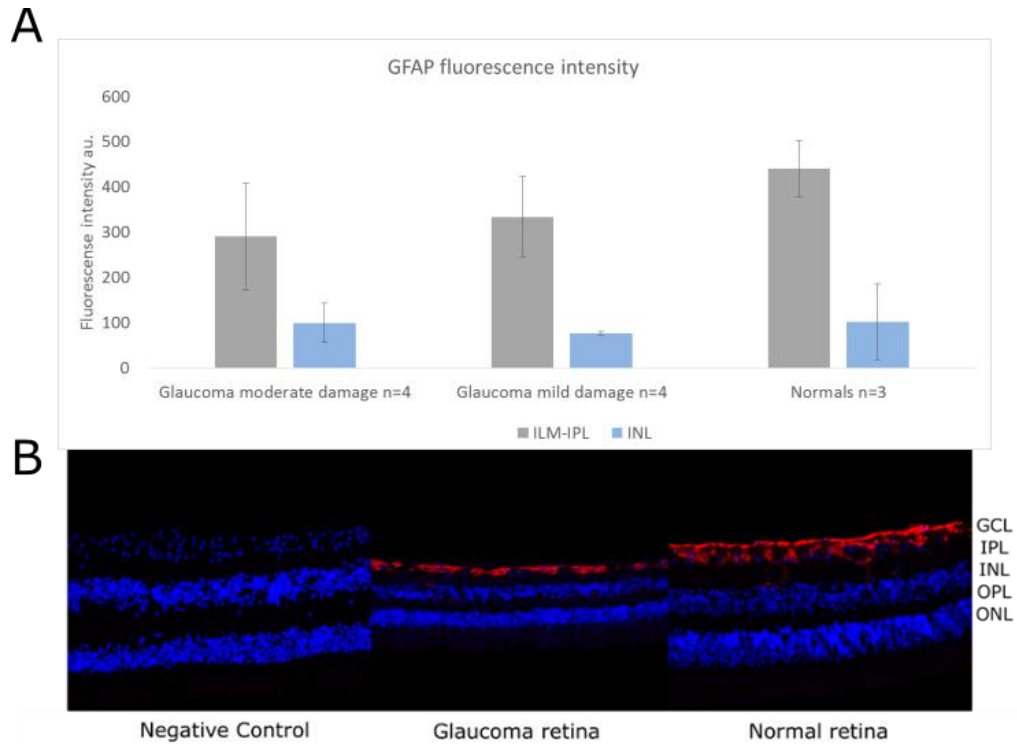


**Figure 4.17 GFAP activation in human retina**

(A) GFAP fluorescence intensity in moderate ( $n=4$ ), and mild ( $n=4$ ) glaucoma, and in the normal retina ( $n=3$ ), across ILM to IPL and INL. (B) Typical examples of images of a negative control (where the primary anti-GFAP antibody was excluded), a glaucoma retina, and a normal retina. The blue staining was from Hoechst nuclear stain, and the red staining was from GFAP.



#### 4.4 Discussion

Two pairs of donor glaucoma eyes were excluded from this study, after some of the initial experiments determined that they were unsuitable. One pair was excluded on the basis of the VF data, as it was suspected that the patient had ocular hypertension only, and not glaucoma. In 50 % of cases, ocular hypertension often leads to the development of glaucoma (Pederson and Anderson 1980), and very often treatment is administered to delay the onset of glaucoma (Kass *et al.* 2002). The peak density of RGCs in human retina was found to be located at eccentricities of less than 1 mm, similarly to what was reported in a landmark study, by Curcio and Allen (1990). In addition, the cell counts obtained from the normal human patient retina closely resembled the cell counts obtained in the same study (Curcio and Allen 1990). There was a clear reduced peak RGC density at 0.8 mm eccentricity, when comparing the obtained data set, to the data published by Curcio and Allen (1990). As previously explained, this difference was most likely to be due to the significantly different age groups that were surveyed in these studies. It is estimated that as humans age, 0.5% of the total RGC axons are lost every year (Calkins 2013), along with 0.5% of RGCs in the central retina, and a further 0.3% of RGCs in the peripheral retina (Curcio and Drucker 1993; Harman *et al.* 2000). The overall RGC density was significantly reduced in a specific spatial pattern in all glaucoma donors, when compared to all age-matched normal donors (Figure 4.7). This finding closely supports the current knowledge of glaucoma progression, in that RGC loss is selective, and follows a characteristic spatial pattern (Quigley *et al.* 1987; Glovinsky *et al.* 1991). The areas with most significant losses were located in the anatomical inferior hemiretina, and in the temporal hemiretina along the horizontal meridian (Figure 4.18). Most of the significant areas affected are supplied by the arcuate axonal fibres (Fitzgibbon and

Taylor 1996). It is thought that when arcuate axonal fibres are damaged, they are responsible for the spatial pattern of the VF loss in glaucoma (Hoyt *et al.* 1973; Schiefer *et al.* 2010) (Figure 4.18).

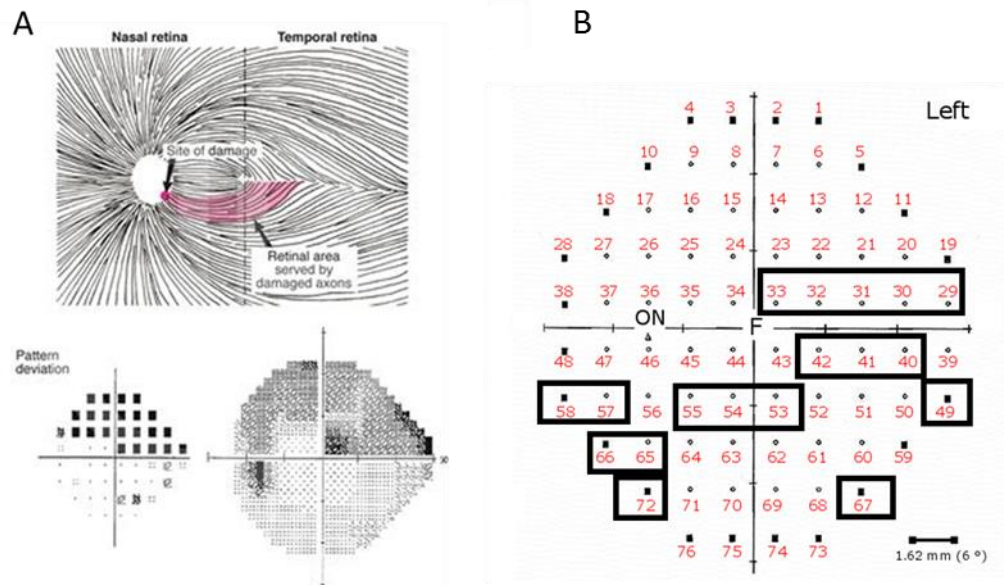


**Figure 4.18 Arcuate retinal fibres**

(A) Illustration showing arcuate retinal fibres, and corresponding VF damage in glaucoma (G. A. Cioffi 2016). (B) Areas in glaucomatous retinas that were found to have significantly reduced (outlined by a black square, Mann-Whitney U test,  $p < 0.01$ ) RGC density, compared to RGC density in normal retinas.

A high inter-individual variability in the RGC density data from glaucoma patients was observed (Figure 4.9). This is unsurprising, as the rate of glaucoma progression, and the stage of the disease, varies with each individual case. Unlike in laboratory conditions, only certain factors (such as age, and sex) can be matched for, and

controlled. This is particularly relevant to tissue that is rare, and difficult to obtain, such as retinas from well-established glaucoma patients, described in this chapter.

The most surprising finding of this study was the lack of correlation between the cell loss, or density, and the VF data in corresponding anatomical locations (Figures 4.10, and 4.11). This finding was in contrast to a previously published study, that found a correlation between cell loss and the VF test data, in the same person (Kerrigan-Baumrind *et al.* 2000). The Kerrigan-Baumrind *et al.* (2000) study had a larger sample number, 17 eyes from 13 persons, however, only 28 points out of possible 72 (that are tested in the VF test) were surveyed. They drew the conclusion that VF data was correlated with cell loss, from the strong correlation they obtained when comparing the overall percent of normal RGCs and axons remaining, and the mean deviation index obtained from the VF test data. This correlation is also true in my data set. However, the data presented by Kerrigan-Baumrind *et al.* (2000) did not mention if correlations were performed between the individual test points, and cell counts.

In this study, a weak negative trend was observed when comparing the overall mean RGC loss and mean deviation index, however, a strong statistically significant correlation was also observed between the peak RGC number and mean deviation index.

Trans-retinal degeneration in human glaucoma retinas has been reported before, by our group in Lei *et al.* 2008. It was reported that inner retinal layers were significantly reduced in glaucoma, compared to normal retinas, and that there was no difference between the areas of mild or moderate glaucoma, as per the VF tests. This finding was not unexpected, as no correlation between the cell loss and VF test in the

same anatomical locations were noted. It was predicted that taking retinal sections from areas with a lower visual sensitivity score, did not necessarily mean there would be more anatomical damage.

And finally an increase in GFAP activation in glaucoma, compared to normal retinas, was not observed, in contrary to observed GFAP activation in experimental glaucoma (Gallego *et al.* 2012). However, the absence of GFAP activation in human tissue can be most likely explained by the already substantial shrinkage of the inner retinal layers. Similar findings on GFAP immunoreactivity have been noted previously, and were attributed to the loss of axons and glial cells that surround axons in glaucoma (Wang *et al.* 2002).

The main finding presented in this chapter is that in human glaucoma the individual VF test point scores do not correlate to RGC density in anatomically equivalent areas. This is supported by a finding that the thickness of inner retina is uniformly reduced and does not differ in areas with high VF score and low VF score. The mean VF loss is in fact correlated to peak RGC density, which indicates that it is possible to assess total anatomical damage in retina using VF test. However, further investigation is required to determine whether there is a degeneration of RGCs in early stages of glaucoma e.g. dendritic degeneration (Pavlidis *et al.* 2003) and if the remaining RGCs in the glaucomatous retina are fully functional. This will be discussed in depth in Chapter 5 and 6.

**Chapter 5: Microinjection, Golgi and  
Diolistics: Single cell labelling methods to study  
morphology in fixation preserved tissue**

## 5.1 Introduction

Neuronal morphology can reveal information, such as details about network organisation, disease development, and even treatment efficacy. The neuron is the smallest processing unit of the brain, and knowing its morphological structure in both normal conditions, and disease, is essential for our understanding of various disorders, including glaucoma. It has been long understood that glaucoma is accompanied by the loss of RGCs over time. With increased knowledge about glaucoma itself, and other neurodegenerative diseases, it has been hypothesised that the loss of RGCs in glaucoma might be preceded by dendritic degeneration of the individual RGC dendrites (Gupta and Yücel 2007; Liu *et al.* 2011). This has been shown to be true in experimentally induced glaucoma in mouse (Feng *et al.* 2013; Buckingham *et al.* 2008; Williams *et al.* 2013), rat (Fu *et al.* 2009; Naskar *et al.* 2002) and in primate (Weber *et al.* 1998). To date, there has only been one study that successfully managed to demonstrate dendritic degeneration in human glaucoma (Pavlidis *et al.* 2003), however, due to the advanced stage of the samples used in the study, it is not yet known whether the degeneration occurs in the early stages of the disease. There are numerous reasons behind why there are so few studies that have successfully studied RGC morphology in human glaucoma retina. The main consideration should be the difficulty of obtaining suitable donor tissue, with a clinical history of diagnosed glaucoma. Furthermore, there are no modern, reliable methods of labelling RGCs and their dendritic trees fully, in fixed post-mortem human retina. The cell labelling methods for human RGCs that are described in the literature are technically challenging and performed on non-fixed tissue (Dacey and Petersen 1992), or, the methods used are sensitive to post-mortem fixation time, time in the fixative, and the strength of the fixative used (Kolb *et al.* 1992). These factors

are usually beyond the control of the investigators, and therefore, a robust, reliable method of labelling is required. I hypothesised that dendrites of RGCs are degenerated prior to their death in human glaucoma retina. In this chapter, various methods will be discussed, along with the attempts made to develop a protocol to label the morphology of single RGCs, in PFA fixed human retina. The protocols presented in this chapter were initially evaluated on mouse tissue, before a selected few were tested on human retinal tissue.

## **5.2 Materials and Methods**

All procedures on animals were performed in accordance with the UK Animals (Scientific Procedures) Act 1986 and European Commission directive 2010/63/EU. All experiments involving human tissue were performed *ex vivo*, in compliance with the Human Tissue Act 2004.

### **5.2.1 Animal tissue**

Adult mouse neural tissue used in this study was from the transgenic TD x PV mouse strain, which was bred in-house on C57BL/6 background by crossing PV-Cre (*Pvalb<sup>tm1(cre)Arbr</sup>*) and TD Tomato (*Gt(ROSA)26Sor<sup>tm14(CAG-tdTomato)Hze</sup>*) mouse lines obtained from commercial provider (The Jackson Laboratory). When these mouse lines are crossed their offspring express TdTomato in all cells that contain PV protein under Cre-mediated recombination. The mice were sacrificed by an approved Home Office schedule 1 method, and both eyes, ONs, and brain tissue were placed in 1-2% PFA in 0.1M PB, for up to 4 hours at 4°C.

After fixation in PFA, the retinas were dissected, and the longest cut was made to mark the temporo-inferior quarter, to keep the orientation of the retina. The brains

were sectioned into thick, 200-300  $\mu\text{m}$ , coronal sections using a vibratome. The sections that included the V1, were chosen based on anatomical hallmarks using the Allen mouse brain atlas. All tissue from this point onwards was stored at 4°C, in 0.1M PB with 0.1% sodium azide.

### **5.2.2 Human tissue**

Human tissue for this study was obtained from the Bristol CTS Eye Bank, UK, or the Mayo Clinic, Rochester, USA. Tissue obtained from the Bristol Eye Bank was lightly fixed, for 1-2 hours, in 2% PFA in 0.1M PB at 4°C, 6-48 hours after post-mortem/enucleation. Tissue obtained from the Mayo Clinic, was fixed for various lengths of times (which was beyond our control), 2-4 hours immediately after enucleation in 2% PFA in 0.1M PBS and stored at 4°C. After fixation, the retinas were stored at 4°C in 0.1M PB with 0.1% sodium azide. The retinas were then dissected into quarters, with 'v' shape cuts to mark the orientation, and peripheral macular regions were chosen for microinjection, while full quarters were used for Golgi stain.

### **5.2.3 General microinjection setup**

To visualise the individual cells for microinjections under the two-photon microscope, all tissues were stained with a nuclear dye, Hoechst 33342 (Thermofisher Scientific, H1339). In mouse tissue, Tdtomato PV+ neurons were also selected for targeted microinjection (Figure 5.1).

For microinjections, the tissue was placed in a Petri dish with 0.1M PB, with a weight made from inert silver, lined with nylon threads, placed on top of the tissue, to keep the tissue at the bottom of the dish. Sharp glass pipettes, of 80-100M $\Omega$ , were



pulled on a horizontal Sutter P-80 puller, using a custom program. Injections were driven using iontophoresis apparatus, Neurophore BH-2. Silver wire was inserted into the glass pipette, which was driven at a 45° angle, with Scientifica PatchStar micromanipulator, towards the tissue slice. A 10x water immersion objective (Olympus) was used to target, and visualise cell injection progress, under the two-photon microscope. The system was fitted with two photomultipliers, with two broad bandpass filters that permitted the user to view separate green, and red wavelength channels in real time, while the laser tuned to same wavelength. This enabled the visualization of the glass pipette approach, and dye spread in real time, also while being able to view the target cells.

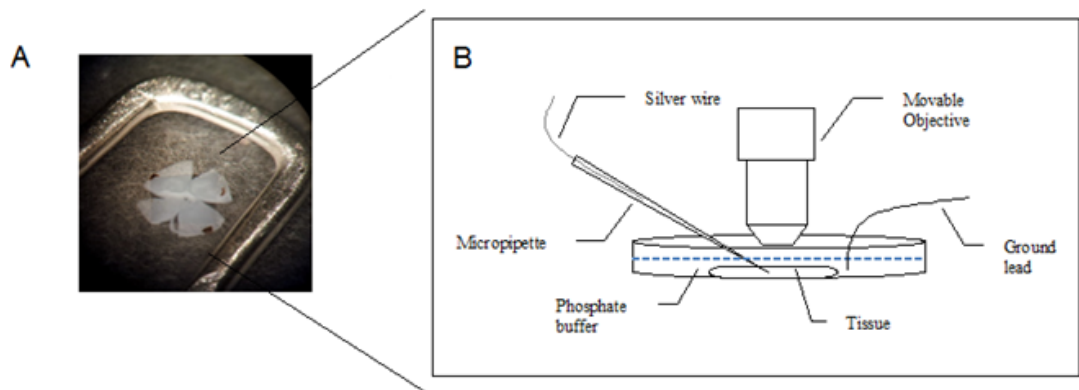


**Figure 5.1 Microinjection setup**

(A) A diagram showing the single cell microinjection set up. Tissue sections were placed in a Petri dish, with 0.1M PB as shown in. (B) A Micropipette with a silver electrode was fixed on a micromanipulator at a 45° angle, and a ground lead was inserted into the external solution.

#### **5.2.4 DiI Iontophoresis**

DiI is a fluorescent lipophilic dye, that is retained in lipophilic membranes, and is often used as a neuronal tracer. For DiI iontophoresis, the tip of the pulled glass pipette was filled with 2  $\mu$ l of 1% lipophilic DiI solution (ThermoFisher Scientific, D-3911) in 100% ethanol, and backfilled with 100% ethanol. Cells were approached and injected with a positive 5-20 nA current. The dye spread was monitored, until the distal dendrites were filled satisfactorily, before the pipette was then withdrawn.

#### **5.2.5 Alexa Fluor Iontophoresis**

Alexa Fluor is a hydrophilic fluorescent dye that is extremely bright, and is often used to fill neurons intracellularly. For single cell microinjections of Alexa Fluor dyes, the tip of the glass pipette was filled with 5mM of Alexa Fluor 568, and backfilled with 0.2M KCl in dH<sub>2</sub>O. Cells were approached using a 0 nA current, and upon the physical contact of the glass tip with the soma of the desired cell, the dye was driven with a -1nA current into the cell. Cells were filled for 15 minutes to 1 hour, until distal dendrites were observed to fill with the dye.

#### **5.2.6 Golgi stain**

In this study, the FD Rapid GolgiStain™ Kit (FD Neurotechnologies), and the glutaraldehyde-sandwich Golgi method, as described by Kolb *et al.* (1992), were used. For the glutaraldehyde-sandwich method, tissue was post-fixed in 1% PFA, and 2% glutaraldehyde, in 0.1M PB for 2-7 days, at 4°C. Tissue sections were then placed between two Whatman #50 filter papers, soaked in the fixative, placed between two glass slides, and then tied together with a thread. This ‘sandwich’ was then transferred to a solution of 5% glutaraldehyde, and 4% potassium dichromate

for 7 days at room temperature, in the dark, before being rinsed with 1% silver nitrate, and incubated in silver solution for a further 3 days under the same conditions. The tissue ‘sandwich’ was then rinsed in dH<sub>2</sub>O, and dehydrated in ascending ethanol, up to 70%, where the tissue sections were separated and carefully peeled off the filter paper. This was followed by further dehydration, to 100% ethanol, followed by clearing in xylene, and mounting on a glass slide with DPX and a coverslip. The slides were left to dry overnight, in the dark, before imaging using light microscopy.

### **5.2.7 Diolistics in fixed tissue**

1.3 µm tungsten particles (Bio-Rad) were coated with DiI, and adhered to the inside of flexible plastic tubing. The tubing was then cut into 0.5 cm segments (or bullets). These bullets were then loaded into a Helios Gene gun (Bio-Rad, USA) cartridge, positioned approximately 1 cm away from the tissue surface, and bullet contents expelled with calibrated high pressure, directly into the tissue, entering cells intracellularly, and retaining the dye in lipophilic membranes. Fixed tissue sections were then placed on Millicell cell culture inserts (Life technologies, US), in a 37°C incubator for 2-3 hours, to allow the spread of the dye to the distal processes of the cell, before imaging. Dye spread was arrested by placing the tissue in 1% PFA in 0.1 M PB solution, at 4°C.

### **5.2.8 Microscopy**

All fluorescence microscopy in this chapter was carried out using a two-photon microscope. Images were taken with a custom built two-photon microscope (MOM, Sutter Instruments), equipped with a Ti:Sapphire laser (MaiTai DeepSee, Newport

SpectraPhysics). The laser was tuned to specific wavelengths, suited to the fluorophore being imaged (Table 5.1). Cells were imaged using either a 10x 0.4NA Olympus objective, or 40x 1NA Zeiss water dipping objective, driven by a micro-stepper (Sutter Instruments) which allowed for the acquisition of stacks, at 0.5  $\mu\text{m}$  precision in the z-dimension. ScanImage r3.6.1, an open source program written in MATLAB, was used to control the objective movement and image acquisition. Golgi stain was visualised using a Leica light microscope.

<b>Fluorophore</b>	<b>Wavelength (nm)</b>
Hoechst 33342	660-710
TdTomato	1030-1040
DiI	700
Alexa Fluor 568	750-800

***Table 5.1 Fluorophore excitation wavelengths***

*Fluorophore excitation wavelengths for two-photon microscope used in this study.*

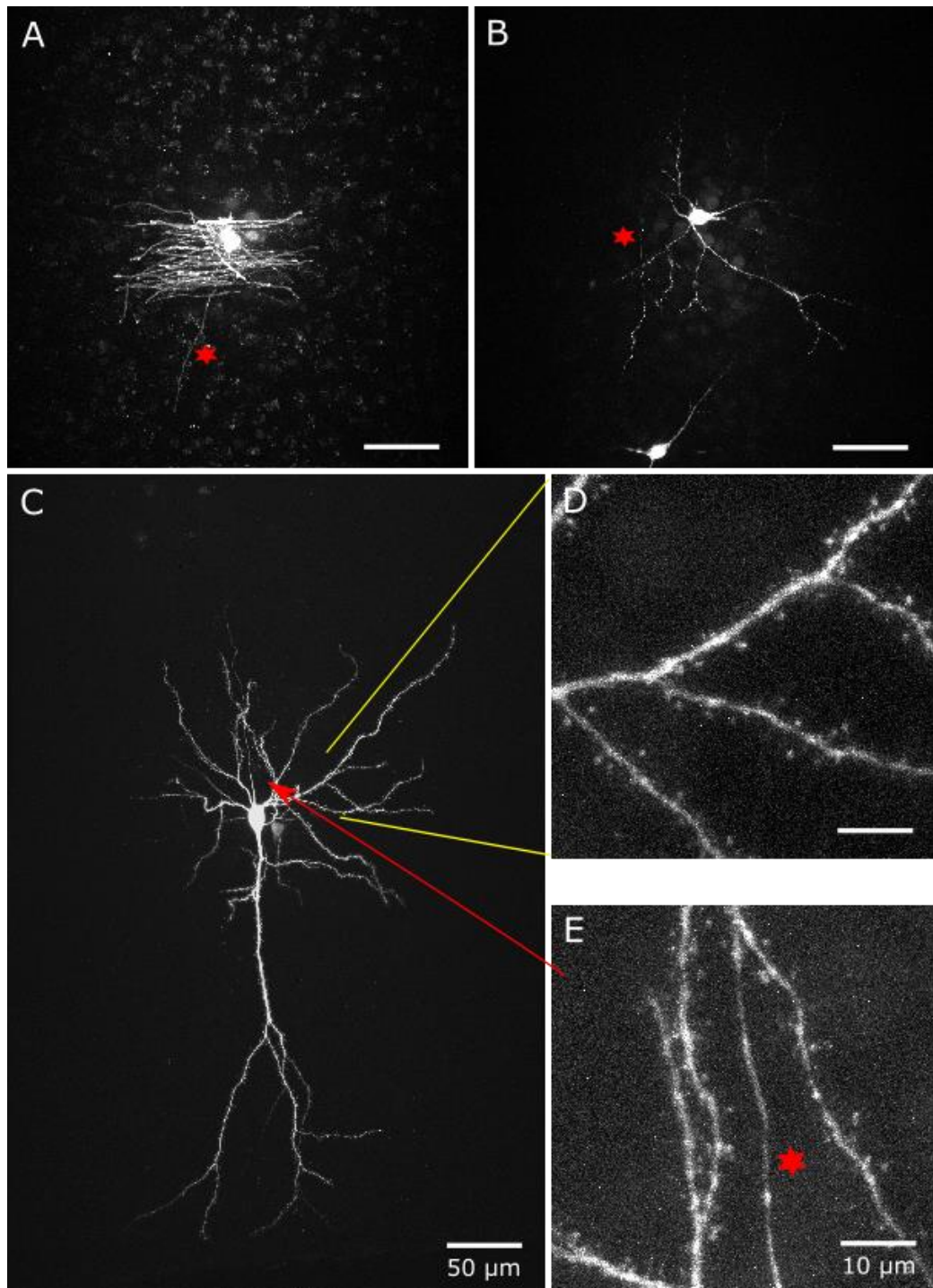
### **5.2.9 Image processing**

Image stacks were collected in .TIFF format, and were post-hoc processed using Fiji (ImageJ, NIH). Z-stacks of images were collapsed based on maximum intensity. Morphological tracing, and Scholl analysis were performed on the 2-dimensional .TIFF images that were generated from the z-stack of images, utilizing the semi-automated Simple Neurite Tracer plug-in for Fiji (Binley *et al.* 2014).

## **5.3 Results**

### **5.3.1 Neurons in mouse V1 brain slices**

Hoechst stained single cells were targeted in thick, lightly fixed, cortical sections using Alexa Fluor 568 dye, and iontophoresis. The microinjection method yielded the best results in the cortical sections, as the neurons were filled fully, including an axon, dendrites, and dendritic spines (Figure 5.2). Furthermore, cells were viable for up to 3 months after the initial fixation, as they retained comprehensive morphological details, enabling them still to be filled with dye and examined. Diolistics generated labelled single cells reasonably well (Figure 5.3), however only if the initial fixation of the cortical slices was less than 20 minutes. In addition, this also yielded over-labelled regions, where multiple clusters of cells were filled with dye, making it difficult to distinguish between the processes of individual cells. Golgi stain also achieved fair results, labelling full cells and fine processes of single cells, however, it was difficult to achieve uniform staining, instead of random, clustered staining.



**Figure 5.2 Single cell iontophoresis of cortical neurons**

Maximum projections of z-stacks of single cortical neurons (A-C) filled with Alexa Fluor dyes by iontophoresis. Dendrites and singular dendritic spines (D), and axons (E) can be observed. The axon is marked with a star. Scale bar 50  $\mu\text{m}$  in panels A-C, and 10  $\mu\text{m}$  in panels D-E.

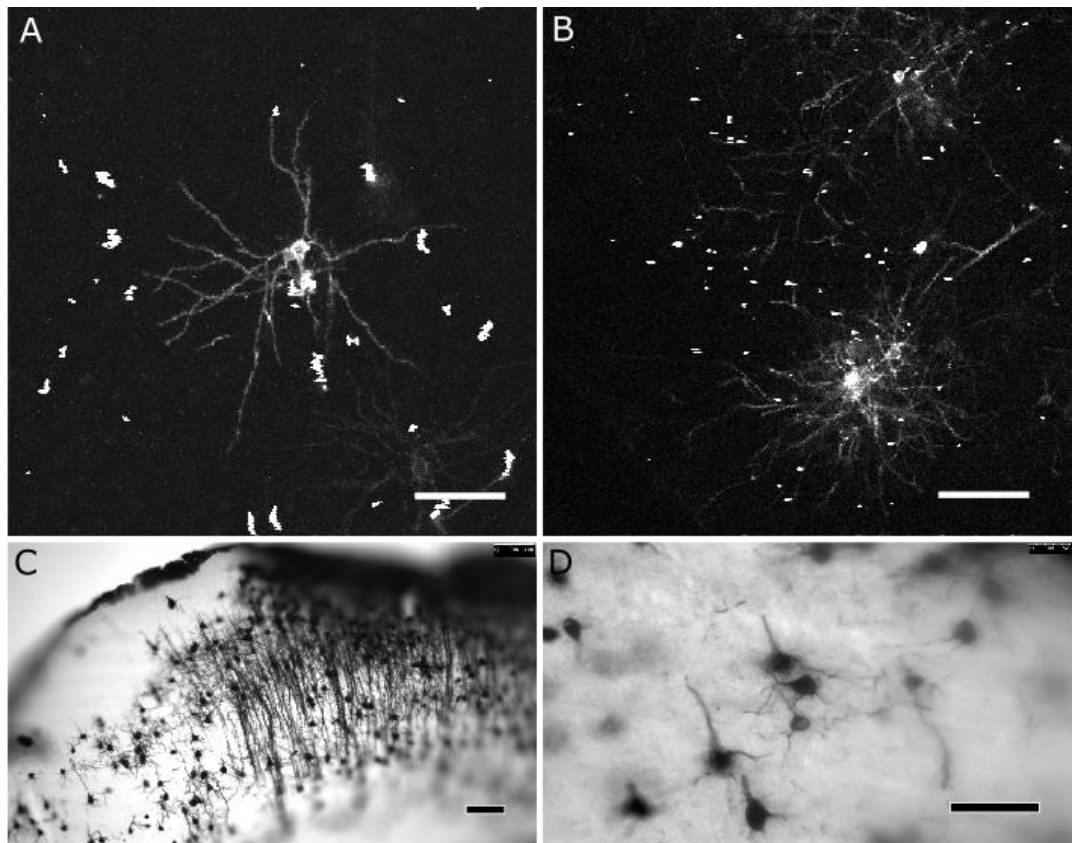


**Figure 5.3 Diolistics and Golgi stain**

*(A-B) Single neuron in fixed mouse cortical section after labelling with diolistics. (C) Clusters of neurons. (D) Several single neurons, labelled with Golgi stain. Scale bars are 50  $\mu\text{m}$ .*

### **5.3.2 RGC morphology in mouse retina**

Microinjections with Alexa Fluor dyes produced the best quality filled cells in lightly fixed mouse retina, (Figure 5.4 and Figure 5.5). In most instances, it was possible to fill the full dendritic tree, and an axon, as far as the ON head. Cells filled using this method were successfully traced, reconstructed, and analysed using Sholl analysis (Figure 5.4). This technique was also successfully utilised to fill astrocytes in lightly fixed mouse ON. Iontophoretic injection of DiI was not successful at labelling individual neurons, as in all instances there were several cell somata labelled with

DiI, which resulted in the co-labelling of several proximal dendritic trees (Figure 5.6).

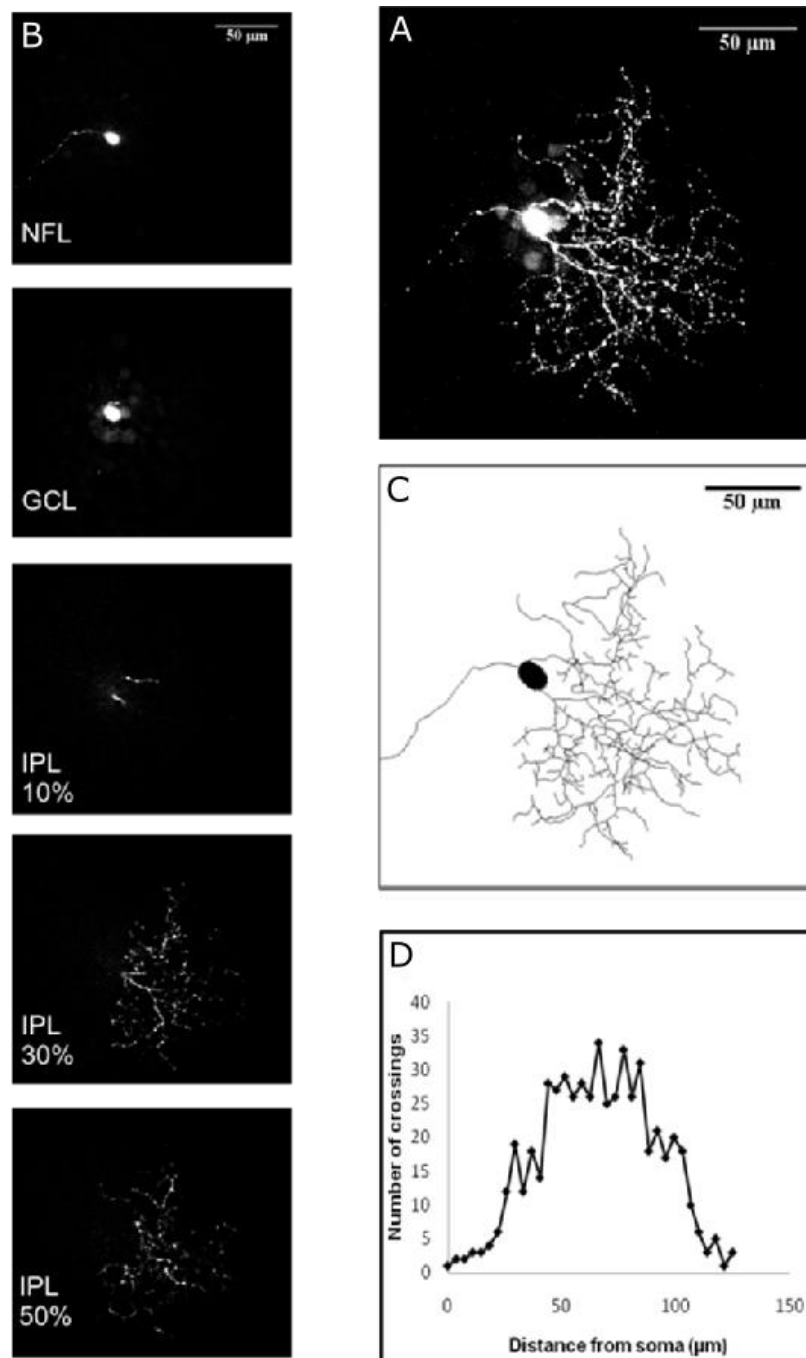


**Figure 5.4 Morphology of a single mouse RGC filled with Alexa Fluor**

(A) Single RGC filled with Alexa Fluor, (B) and panels moving through z-focus, showing the dendritic tree of the same RGC at different laminations. (C) Reconstruction of the RGC (D) and resultant profile of Sholl analysis.



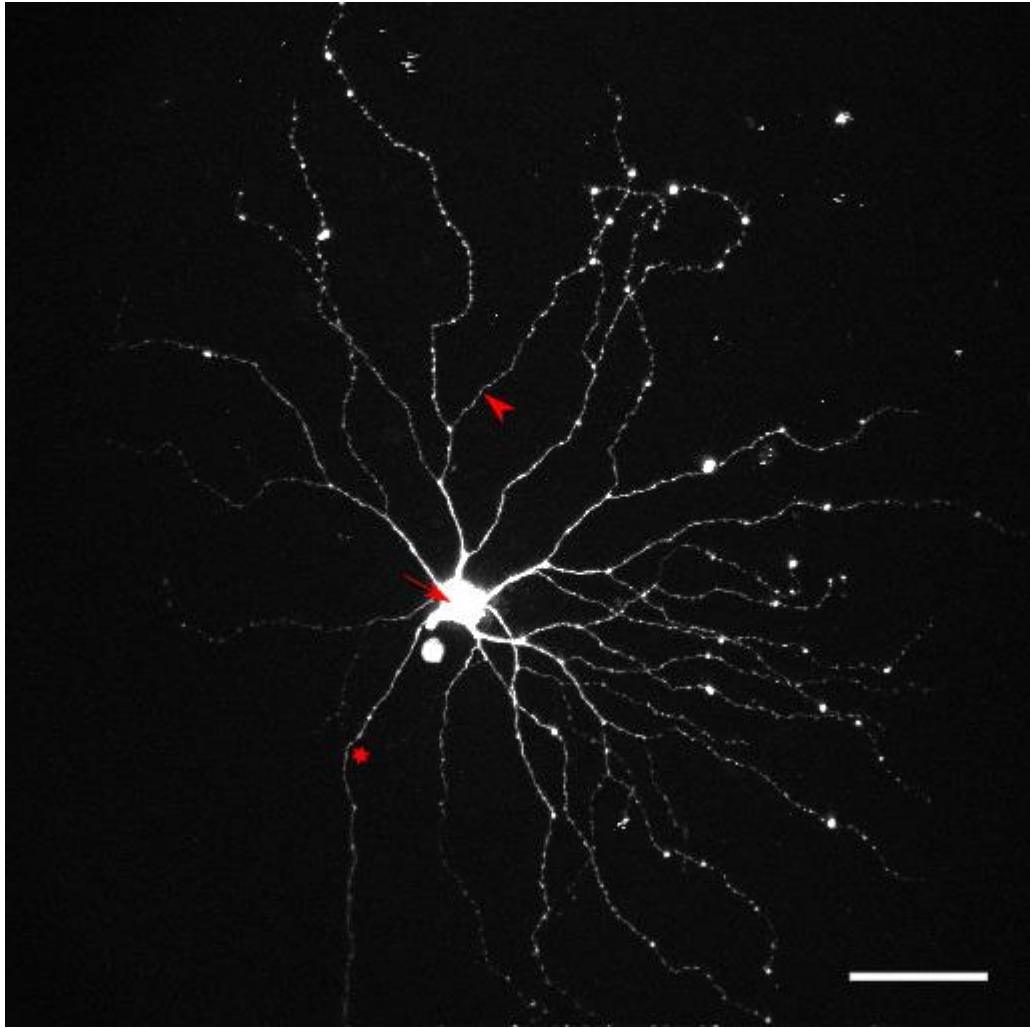


***Figure 5.5 Single RGC in mouse retina filled with Alexa Fluor.***

*An axon is marked with a star, the cell soma is marked with an arrow, and dendrite with an arrowhead. The scale bar is 50  $\mu\text{m}$ .*

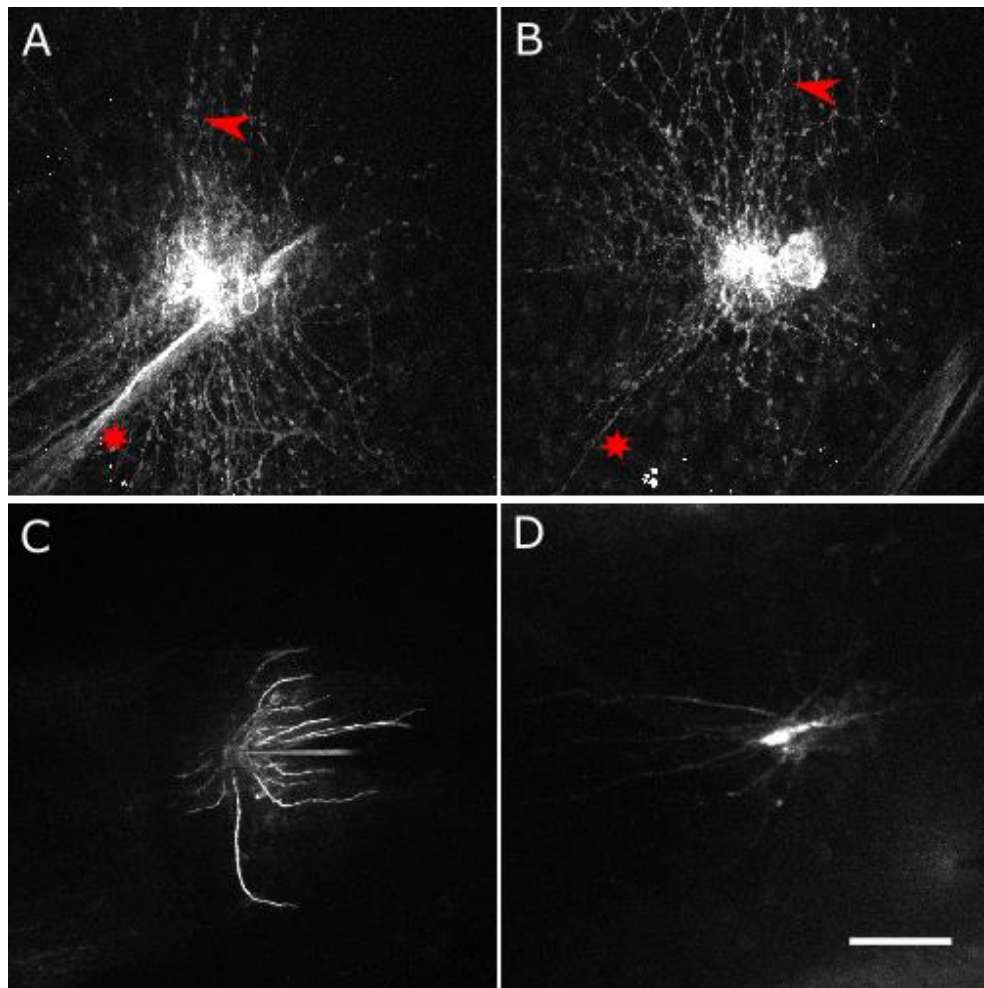


**Figure 5.6 DiI iontophoresis and astrocytes in ON**

*Clusters of cells labelled with DiI (A-B). Astrocytes labelled in the mouse ON (C-D).*

*Axon bundles are marked with a star, and dendrites are marked with arrowheads.*

*The scale bar is 50  $\mu$ m.*

### **5.3.3 RGC morphology in human retina**

As Alexa Fluor microinjections were the most successful method of single cell labelling in fixed mouse cortical, and retinal tissue, this method was chosen to label human RGCs in the retina. However, Alexa Fluor microinjections yielded poorly filled RGCs in the human retina. In cases where dye spread to processes was

achieved, only partial filling of dendritic trees was achieved, and without axon filling. Examples of RGCs filled in fixed human retina, with Alexa Fluor microinjection, are shown in Figure 5.7. In most instances, only somata and primary dendrites were filled successfully, with no further dye spread (Figure 5.7).

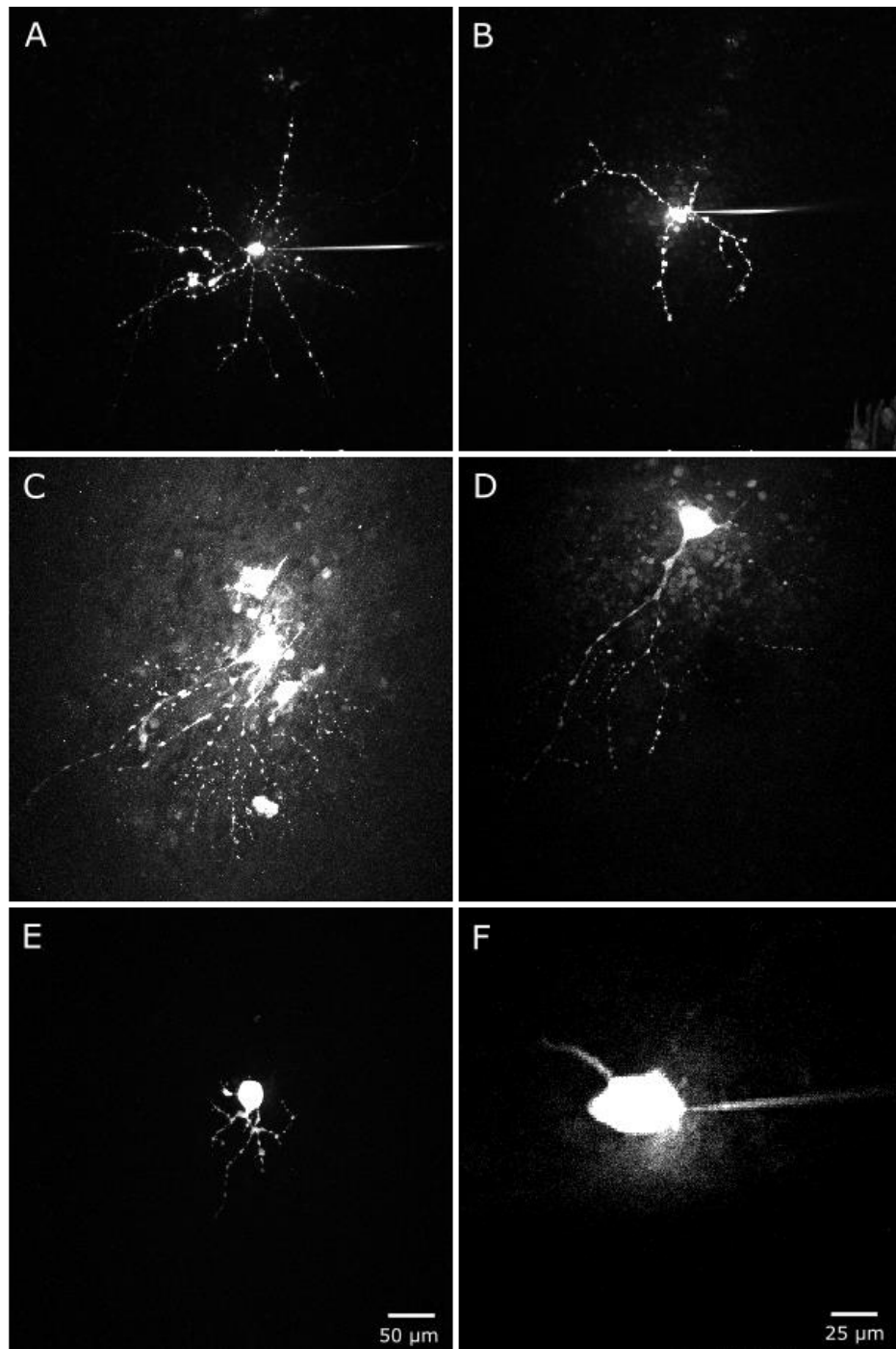


**Figure 5.7 Human RGC fills**

*Examples of human RGCs filled with Alexa Fluor dye (A-E) and example of soma fill only (F).*

#### **5.4 Discussion**

Neither DiI iontophoresis, nor Golgi or diolistics, produced good quality, fully labelled neurons, or single cell fills in mouse tissue. Single cell Alexa Fluor

iontophoresis produced the best quality labelled neurons, with fully labelled dendritic trees and axons, in fixed mouse cortical slices (Figure 5.2) and retina (Figure 5.5). This was exactly as described in Dumitriu *et al.* (2011).

Based on this, the same microinjection technique was applied to human tissue, however it only yielded partially filled RGCs (Figure 5.7). Most commonly, only cell somata were filled with the dye, and no spread to dendrites was observed. Single cell iontophoresis was a time consuming process, and was more technically demanding than many other labelling methods used in this study.

From the pilot experiments on the mouse tissue, and in agreement with Dumitriu *et al.* (2011), it was discovered that the microinjection technique required lightly fixed tissue. In view of the inconsistencies in cell labelling between the tissues, it was suspected that the quality of the human tissue was inadequate, either due to lengthy post-mortem to fixation time, or due to excessive fixation. When cross referencing this finding with studies that have successfully reported human RGC morphology, it was noted that the human tissue was reportedly fixation preserved for very short periods of time (Kolb *et al.* 1992), or not fixation preserved at all (Dacey and Petersen 1992). In addition, a recently published study that utilised the DiI iontophoresis method, reported successfully labelling a variety of single human RGCs and amacrine cells, in lightly (< 1 hour) fixation preserved tissue (Lee *et al.* 2016), thus confirming our finding that tissue fixation is the critical factor in achieving successful RGC labelling, with any of the techniques described above. These factors were uncontrollable in this study, as the tissue was collected and donated by other institutions, and there are ethical considerations, related to human tissue donation and preservation. Successful human RGC morphology labelling in heavily fixation preserved tissue was reported by Pavlidis *et al.* (2003), however, the

described method utilises DiI crystal insertion to the NFL of the retina, which relies on the presence of intact axon. Therefore, it would not be possible to analyse the dendritic morphology of cells with an injured axon, as would be seen in glaucoma.

In conclusion, this study was unable to produce a reliable protocol to fully label RGCs and their dendrites, using the fixed human retina samples that were accessible. Therefore, another more reliable method should be considered, such as scanning electron microscopy (SEM). Serial block-face SEM is a microscopy method that utilises a focused beam of electrons to scan a block of sample, while it is continuously being cut with a microtome, at a thickness such as 70 nm. SEM is technically challenging and lengthy, however, it is very accurate and produces high magnification, high quality images of cellular structures in 3D (Denk and Horstmann 2004), and has the potential of imaging dendrites. Recently, after reconstruction of the images taken with serial block-face SEM, it was possible to see the detailed morphology of astrocytes in the ON of a glaucoma model of the mouse (Nguyen *et al.* 2011). Therefore, this project is set to continue as a serial block-face SEM connectomics study.

## **Chapter 6: General Discussion**

This work presents results from studies designed to investigate the effect of RGC death on the function of V1 in mouse and correlation between visual function and loss of RGCs in glaucomatous human retina.

The main findings are:

- Following ON crush responses in V1b to stimulation of the affected eye are diminished immediately and do not recover for up to 60 days.
- The V1b responses to stimulation of the intact eye were found to either significantly rise or show a trend to increase when measured with OI.
- When stimuli were presented to the intact eye the mean maximum response significantly increased in the population of orientation tuned cells when measured using in vivo 2P calcium imaging.
- PV+ interneurons show a decrease in mean maximum response when stimulating through either of the eyes.
- A large OD shift towards the intact eye was observed using both ISI and 2P imaging paradigms.
- RGCs in human glaucoma retina were found to be lost in a spatial pattern that follows the anatomy of arcuate axon fibres in retina.
- No correlation was found between individual anatomical areas and scores from individual VF test points within the same glaucoma patient.
- A strong correlation was found between the peak RGC cell numbers and the mean deviation and pattern standard deviation within the same retina.
- No difference was found in the inner retinal layer thicknesses between mild and moderate areas of damage within the same glaucomatous retina.



- The fixation preservation is a critical step in order to achieve any success with morphological labels of RGCs in human retina.

### **6.1 Open eye potentiation in adult visual cortex**

ON crush is a widely used method of inducing RGC death in order to investigate glaucoma-like degeneration in retina (Templeton and Geisert 2012). The ISI and in vivo 2P calcium imaging experiments described in chapters 2 and 3 revealed that the ON crush induces plasticity in the visual cortex of adult mice. The loss of signal from the dominant contralateral eye due to ON crush resulted in a potentiation of the weaker intact ipsilateral eye signal within the imaged hemisphere.

Open eye potentiation in adults is a well described phenomena that can be induced by MD (Sawtell *et al.* 2003; Tagawa *et al.* 2005) and ME (Van Brussel *et al.* 2011). It is experience dependent and is absent if both eyes are visually deprived e.g. suturing both eyelids (Blais *et al.* 2008). This thus suggests that open eye potentiation might act via competitive mechanism. This work to my knowledge is the first time that open eye potentiation was demonstrated in adult mice after ON crush.

OD plasticity in adult mice after MD has been demonstrated by several different methods - visual evoked potentials (Sawtell *et al.* 2003), immediate early gene Arc expression (Tagawa *et al.* 2005), extracellular microelectrode recordings and optical imaging (Sonja B Hofer *et al.* 2006). It is thought that silencing the dominant eye by MD removes the competition and enables the potentiation of the weaker eye. It is important to note that compared to juvenile MD, in adults MD does not evoke depression of the deprived eye (Sawtell *et al.* 2003; Frenkel and Bear 2004). In adult MD open eye potentiation in adults requires visual experience and is dependent on

NMDA (N-methyl-D-aspartate) receptors (Sawtell *et al.* 2003) and CaMKII $\alpha$  (Ranson *et al.* 2012) and most likely occur via the mechanism of LTP.

The open eye potentiation in juvenile and adult animals occur via two separate mechanisms. Open eye potentiation is absent only in juvenile mice that lack TNF $\alpha$  (Kaneko *et al.* 2008; Ranson *et al.* 2012) and GluA1 (Ranson *et al.* 2013), but not in adults; it is thought to reflect a homeostatic process. In contrast, juvenile OD plasticity is normal in mice that have a point mutation in  $\alpha$ CaMKII, a kinase that is activated by Ca<sup>2+</sup> influx from NMDA receptors during LTP, but is absent in adults of this mouse strain (Ranson *et al.* 2012).

Stimulus response selective plasticity (SRP) is a type of short term upregulation (LTP) due to adaptation to one specific repeated visual stimulus (Cooke and Bear 2012) and is dependent on NMDA receptor activity (Frenkel *et al.* 2006). More recently it was reported that neither PV<sup>+</sup> interneuron activity nor NMDA receptors located in PV<sup>+</sup> interneurons are required for adult plasticity after MD but are crucial for SRP (Kaplan *et al.* 2016).

During ME all light driven and spontaneous retinal experience is removed, thus eliminating the competition (Smith and Trachtenberg 2007) and leaving behind only the ipsilateral inputs in contralateral visual cortex. In adult mice this apparent lack of competition results in reactivation and expansion of the V1b, most likely by the intact -eye potentiation (Van Brussel *et al.* 2011). This lack of competition also reduces LTD, thus allowing LTP to be more potent than in MD (Nys *et al.* 2015). In addition rearrangement of ipsilateral callosal projections has also been noted in ME (Wree *et al.* 1985).

Focal retinal injury such as by laser damage is another method of inducing plasticity in adult V1 (Keck *et al.* 2008). The reactivation of the lesion projection zone (LPZ)

that previously received the retinal inputs from damaged area occurs, most likely by takeover of the surrounding areas. Notably it was reported that this method of deprivation elicits structural changes within the cortex and not LGN. It was reported, that in the cat, binocular retinal lesions induce axonal sprouting within the LPZ (Darian-Smith and Gilbert 1994). And more recently a study in mouse reported that the dendritic spine turnover rate is increased in the cortex within the LPZ (Keck *et al.* 2008).

In the context of the discussed methods the ON crush should have an intermediate effect on the visual cortex plasticity compared to the effects of ME and MD. As shown in juvenile mice, ME of contralateral eye enhances the maturation of the ipsilateral eye, due to the lack of the cortical competition (Smith and Trachtenberg 2007). While the all meaningful signal transmission from retina might be ceased after the ON crush just like in ME, the spontaneous activity from retina is still present, as in MD and focal retinal lesion model. This in turn means that a level of LTD will be present, therefore, one might expect ON crush to induce an intermediate open eye potentiation in adults compared to MD and ME models (Figure 6.1).

In addition, verification of extent of the open-eye potentiation may be crucial; ISI has revealed only a weak significant increase, whereas single cell calcium imaging revealed much more potent intact eye potentiation. However, data obtained from single cells is likely to be more reliable as ISI only provides us with a general overview of activity.

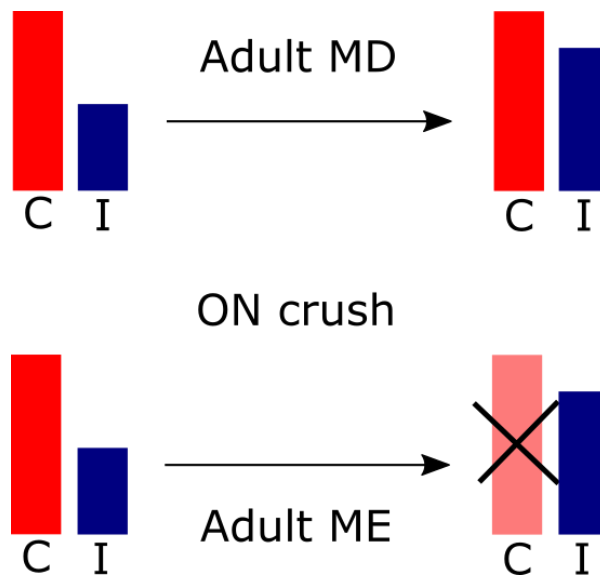


**Figure 6.1** A diagram depicting effects of adult MD, ME and ON crush.

*C* – contralateral, *I*- ipsilateral. MD -monocular deprivation, ME – monocular enucleation.

## 6.2 The role of inhibition in adult plasticity

In chapter 3 the role of inhibition was explored by using in vivo calcium imaging to investigate the activity of PV+ interneurons in layer 2/3 of V1b after ON crush.

It is thought that, in general, adult plasticity requires a decrease in cortical inhibition as shown when inhibition is reduced pharmacologically using fluoxetine (Maya Vetencourt *et al.* 2008), or by reduction of GABA transmission (Harauzov *et al.* 2010), environmental enrichment (Greifzu *et al.* 2014) and dark exposure (Huang *et al.* 2010).

Reduction of inhibition was also observed after ON crush as described in the Chapter 3 of this thesis. While the response of orientation tuned neurons was found to increase, the inhibitory PV+ interneuron activity was significantly decreased at 14 days after ON crush in response to stimulation via an intact eye.

The maturation of the inhibitory circuits in the cortex marks the closure of the critical period (Huang *et al.* 1999). PV+ interneurons are the most abundant class of inhibitory GABAergic interneurons in mouse cortex which make up 40% of all GABAergic cells in V1 (Xu *et al.* 2010) and together with somatostatin (SOM) and vasoactive intestinal polypeptide (VIP) interneurons make up almost 100% of cortical inhibitory interneurons (Rudy *et al.* 2011) (Figure 6.2). Due to the intrinsic fast spiking ability and dendrites that mostly synapse directly onto the soma of the excitatory neurons (Kepecs and Fishell 2014) the PV+ interneuron activity emerged as a potential key to modulation of OD plasticity (Kepecs and Fishell 2014). Furthermore destruction of extracellular matrix components - perineuronal nets that mostly surround PV+ interneurons enhance OD plasticity in adult rats (Pizzorusso *et al.* 2002). However, as this thesis was being prepared a study that inactivated both PV+ interneurons and NMDA receptors located on PV+ interneurons found that neither are required for adult OD plasticity (Kaplan *et al.* 2016). This study does not necessarily contradict findings presented in Chapter 3. It is simply not possible to define an exact role of PV+ interneurons in adult plasticity after ON crush from the data presented in Chapter 3. Further studies are required to investigate whether PV+ interneurons modulate the excitatory neurons directly or more likely the decrease in PV+ interneuron activity observed in chapter 3 is a result of global inhibition by GABAergic system.

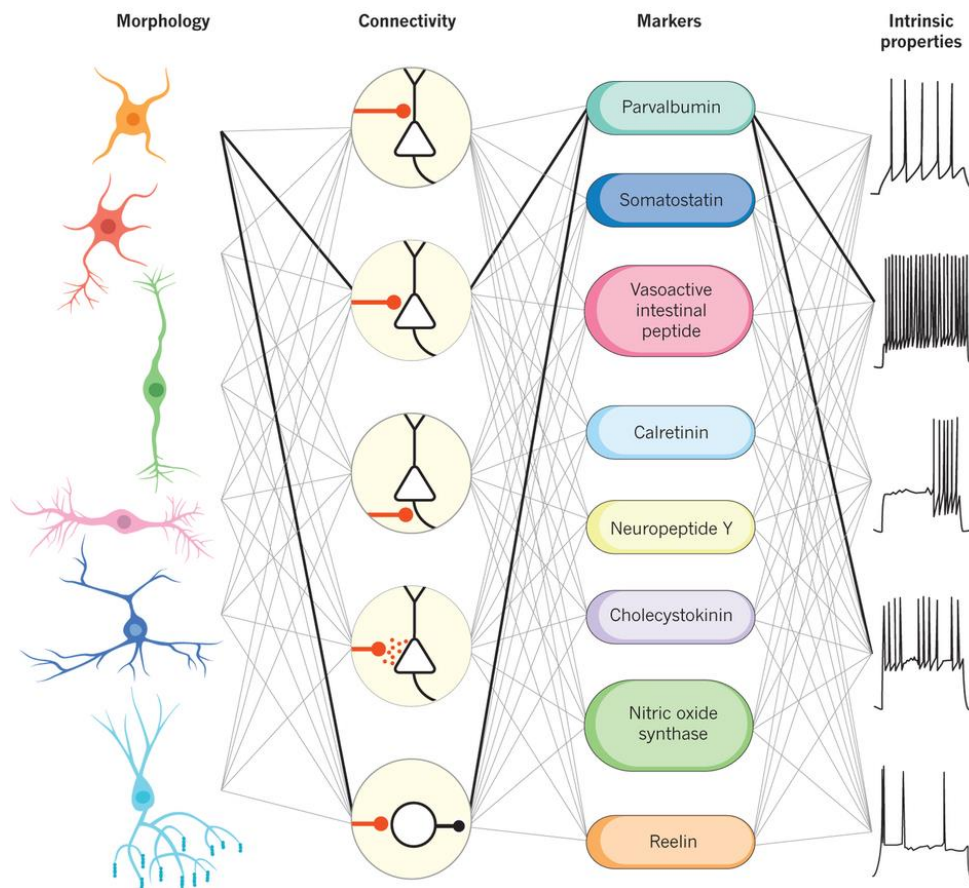


**Figure 6.2 An overview of cortical inhibitory network**

An illustration demonstrating morphological types of inhibitory neurons, their connectivity, markers and intrinsic properties (Illustration obtained from Kepecs and Fishell 2014).

### **6.3 ISI and in vivo 2P calcium imaging as a measure of visual function in experimental glaucoma**

Mounting evidence suggests that glaucoma is a neurodegenerative disease that is not limited to retina. Indeed, several studies that used fMRI have reported changes in V1 activity levels of human glaucoma both uncorrelated to retinal damage (Qing *et al.* 2010; Dai *et al.* 2013) and correlated to ONH disc damage (Duncan *et al.* 2007). In addition studies in experimental glaucoma report degeneration in SC (Chen *et al.* 2015), LGN (Yücel *et al.* 2000) and V1 (Crawford *et al.* 2001). MRI studies have

also reported LGN degeneration in human glaucoma patients (Gupta *et al.* 2009) and also wide spread degeneration of the whole visual system, including V1, was seen in post-mortem study (Gupta *et al.* 2006).

In Chapter 2 I describe how chronic ISI can be used reliably to measure the visual function and signal transmission from both eyes in normal adult mice repeatedly across a timescale of weeks or even months. ISI was first used on visual cortex of a mouse to visualize retinotopic maps (Schuett *et al.* 2002) and it quickly emerged as a powerful and fairly non-invasive imaging technique that was comparable to fMRI (Kalatsky and Stryker 2003). To date ISI has only been used to study the effects of such paradigms as eye closure by MD (Cang *et al.* 2005) and focal retinal lesions (Keck *et al.* 2008) on the function of V1. The current work to my knowledge is the first to utilise ISI as a measure of V1 function in a mouse model of RGC death.

In mouse ON crush induces a robust irreversible RGC death within 2 weeks (Templeton and Geisert 2012). ON crush shares multiple similarities with pathogenesis of glaucoma, which is the second leading cause of blindness worldwide (Kingman 2004). The current belief is that the visual function also diminishes slowly as RGCs degenerate in retina, however the data presented in this work suggest the contrary. Using ISI, I show that signal transmission ceases immediately after ON crush and does not recover when measured with ISI. In addition, this is supported by shift in ODI that was observed using both ISI and single cell 2P imaging. The reduction in V1b responsiveness after ON crush did not appear as straightforward when it was investigated using 2P calcium imaging. Some meaningful responses when stimulating cells via the eye that had received the ON crush were indeed observed using calcium imaging. This apparent discrepancy, can possibly be explained by limitations of the two imaging techniques. ISI measures global change

and might not be sensitive enough to visualize the remaining activity from a few single cells. However, it is also known that ISI is sensitive enough to visualize a small patch of inactivity within the cortex after focal retinal lesions (Keck *et al.* 2008). However, the lesion projection zone has never been imaged with any single cell technique to verify the apparent inactivity.

Thus the discrepancy between the two techniques requires further investigation.

Visual function in mice with various retina associated visual disorders usually is assessed using optokinetic responses (Davies *et al.* 2007; Thomas *et al.* 2004), and/or ERG (Bayer *et al.* 2001). These techniques do not provide information about the levels of higher visual function and thus complementary visually guided behaviour tests such as water maze are often used to assess the levels of higher processing (Doroudchi *et al.* 2011). Unfortunately, most visually guided behaviour tests also involve other sensory regions such as somatosensory (whisking) and often recruit multiple brain regions. Thus it is sometimes unclear whether rescuing retinal function also restores processing and signal transmission to visual cortex (Doroudchi *et al.* 2011) or cortex compensates the visual loss via cross-modal plasticity (Bavelier and Neville 2002).

In rats it is possible to achieve partial ON crush, and one study reported measuring visual function in V1 using VEPs that was correlated with a strength of calibrated ON crush. Spatial frequency and visual acuity decreased in non-linear fashion and strongest effects were observed after ON crush that resulted in death of most RGCs at 30 days post-crush (Klöcker *et al.* 2001). It is not possible to achieve a partial ON crush in mouse due to its much smaller size compared to rats' ON and in mouse the secondary inflammation appears to affect the whole cross-section of the nerve regardless of strength of the crush.



In summary, both ISI and 2P calcium imaging can be utilized as chronic imaging methods to investigate the signal transmission from retina to visual cortex. This is particularly beneficial in experimental setups investigating visual function recovery in retina using pharmacological and genetic treatments (Lucius *et al.* 1998; Park *et al.* 2008; de Lima *et al.* 2012) after ON crush.

#### **6.4 RGC death in glaucoma: is it as straightforward as it appears?**

As reported in Chapter 4 of this thesis, no correlation was found in RGC cell density between individual VF test points and anatomically equivalent areas within the same area in human glaucoma. In support, no morphological difference was detected between the inner retinal layer thickness between mild and moderately affected retinal areas (degree of damage was determined from the score of VF test). These findings are surprising and can be explained either by (1) inaccuracy of VF test as a measure of RGC function or (2) differential mechanism of RGC degeneration in glaucoma that is not related to the number of remaining cells – for example dendritic degeneration in remaining cells.

VF test is performed in order to monitor and track the progression of the visual loss related to glaucoma (Chauhan *et al.* 2008). However one study reported that large variations in repeat tests that could not be accounted by disease progression occurred in 16% of tested eyes (Study 1994). Most of the variability is thought to arise from lack of patient compliance and attention to the test. And this is still a factor even after the fixation losses and false positive and negative responses are tested and accounted for in automated perimetry tests (Johnson and Samuels 1997). In addition it was demonstrated that patients with VF loss in glaucoma show an increased rate of false-negative responses related to the disease progression (Bengtsson and Heijl 2000).

Studies that compared the number of remaining axons within the same eyes to VF test data both confirm (Kerrigan–Baumrind *et al.* 2000) and deny correlation (Mikelberg *et al.* 1995) of VF test points and morphological damage.

Loss of RGCs in the fovea has been reported before in experimental glaucoma in monkeys, where selective loss of large RGCs was found (Glovinsky *et al.* 1993). In this work I report no correlation between individual VF test points and RGC density, however I report correlation between peak RGC density and the absolute value of mean deviation and pattern standard deviation. Both mean and pattern standard deviations are global indices given to approximate and track the mean degree of VF damage compared to individuals of the same age, where pattern standard deviation is adjusted for other visual defects such as cataract (Forrester J. V., Dick A. D., McMenamin P. G., Roberts F. 2016). In humans peak RGC density in fovea is up to 10 times higher than in periphery (Curcio and Allen 1990; Lei *et al.* 2008), this peak is responsible for the high visual acuity of central vision (Provis *et al.* 2013). Both mouse and rat have poor visual acuity and do not have major RGC density differences between the central and peripheral retina and thus this aspect is understudied in experimental glaucoma. In fact, signs that the fovea is affected early in human glaucoma progression have been reported over 30 years ago. The focus, however has always been on vision loss in the periphery because central regions are usually significantly affected last (Anctil and Anderson 1984).

Dendritic degeneration of RGCs has been demonstrated repeatedly in experimental glaucoma in mouse (Feng *et al.* 2013), monkey (Weber *et al.* 1998) and end stage glaucoma in humans (Pavlidis *et al.* 2003). It is not clear whether axons or dendrites degenerate first in glaucoma (Morgan 2012), and furthermore it is yet to be proven

whether RGC undergo dendritic degeneration in early human glaucoma. This is however difficult due to multiple factors that were discussed in Chapter 5.

To conclude, I suggest that VF test may not be the most accurate way of measuring RGC function, especially in order to draw parallels between function and anatomy. Furthermore, when comparing anatomy and function, the remaining RGCs cannot be relied upon as a functional unit; they are most likely in a state of degeneration (Weber *et al.* 1998) due to dendritic degeneration, which precedes the cell death (Buckingham *et al.* 2008).

### **6.5 Concluding thoughts**

One of the aims of this work was an attempt to bridge the gap between retina and V1 and between the human and the mouse. First of all, assessment of visual cortex function should be considered when studying retinal degeneration, especially in studies demonstrating regeneration in retina. But more importantly, the capability of the brain to adapt to the new environment should be taken into account as it appears that in unilateral ON injury intact eye potentiation occurs simultaneously along degeneration in the affected eye's visual pathway.

It is also clear that a VF test may not be the best method of assessing retinal visual function as it is subjective and greatly relies on patients' compliance. It is evident that RGC death in human glaucoma is a complicated multistep process and it is not clear how many surviving RGCs contribute to the remaining vision assessed by VF tests in clinics.

## 6.6 Future work

Further experiments are needed to improve the precision of visual function assessment using ISI and 2P calcium imaging. This can be done using pharmacological means such as eliminating action potentials in retina using tetrodotoxin (Frenkel and Bear 2004) and lidocaine hydrochloride to silence axonal ON transport. Tetrodotoxin administration will provide some insight into how ON crush compares to ME, whereas lidocaine administration should mimic effects of ON crush on the deprived eye.

In addition, future research should be focused on assessment of ocular hypertension models such as the magnetic bead model that was discussed in the introduction (Samsel *et al.* 2011). Since the present study was completed, a research group reported a successful achievement of a magnetic microbead model in mouse, that does not occlude the anterior chamber and retains a clear visual axis (Ito *et al.* 2016). Investigating vision loss in hypertension model would be preferable as it induces partial RGC loss (McKinnon *et al.* 2009) which mimics human glaucoma more closely compared to ON crush.

Additionally, ON crush can be used as a robust and easy model of adult cortical plasticity. Experiments that utilise inactivation of activity in a subset of neurons only (e.g. VIP or Somatostatin interneurons) using designed receptors exclusively activated by designed drugs (DREADDs) (Urban and Roth 2015) might be beneficial to understand the role of inhibition in adult plasticity (Kaplan *et al.* 2016).

As for human tissue work described in this thesis, the morphology of RGCs is being currently investigated using Serial block-face SEM (Denk and Horstmann 2004). In addition, postsynaptic density staining could be utilised to quantify the density of remaining synapses RGCs make in IPL of human retinas in glaucoma. But most of

all a study that definitively answers whether dendritic degeneration actually occurs in RGCs, and whether it precedes axonal degeneration, of human retina is essential.

# Appendix

## Chapter 4: Patient VF test sheets

### GL239 1/8

**History of Present Illness** / If checked, encounter is  Management or  an Emergency, or  a Consult requested by: \_\_\_\_\_  
to provide advice or opinion regarding evaluation and / or management of \_\_\_\_\_

**Chief Complaint** glaucoma

**HPI**  includes summary of requested outside records  
Vision loss, right eye, constant past 2 years. He states that he would like to be followed here for his glaucoma. Denies eye pain, flashing lights or floaters. VCR. Referred by Winona clinic. Over the years, patient reports more difficulty reading. Distance vision has been fine and he still reports driving without difficulty. No family history of glaucoma. Was told he had glaucoma both eyes 5 years ago (Right worse than Left). Was started on Travatan at that time but had irritation and was switched to Azopt. Pressure was not at target so was switched to Xalatan and has been using for the past 3 years. He has been told he was at his target pressures on Xalatan. Per records, has also tried Betimol and Alphagan. Does not take ASA.

**Outside records:**  
9/30/09: IOP 18/18; OCT NFL: Thinning diffuse both eyes; Visual fields: Right eye sup and inf arc; Left eye dense sup arc (likely progression since 2004) and early inf arc  
8/5/09: IOP 14/14  
5/11/09: IOP 13/14  
2/23/09: IOP 12/14  
11/10/08: IOP 10/13  
8/6/08: IOP 11/11  
5/20/08: IOP 18/19  
11/16/07: IOP 16/16  
11/5/07: 18/18  
7/23/07: 16/17  
5/20/07: 17/16  
4/20/07: 18/16

**Review of Systems (ROS)** (  )

Eye	see HPI;
Neurologic	Hit head 4-5 years ago on a coat rack, dx with TIA - next day left arm and face numb briefly again. CT normal. No migraines.
Cardiovascular	negative
Respiratory	negative; no COPD, no asthma
Endocrine	negative;
ENT	negative;
General	negative;
Psychological	
Skin	negative;
Musculoskeletal	negative;
Genitourinary	
Gastrointestinal	negative;
Hem / Lymph	negative;
Immun / Allergy	negative;

See CVI of / \_\_\_\_\_ for 1 items  all other systems reviewed and negative

**Past / Family / Social Histories**

**Eye History**  Negative, unless noted **Eye FHx**  Neg., unless noted

Ant segment		Blindness	
Eyelid / Orbit		Glaucoma	
Glaucoma	Dx 2004 IOP's 31	Macula dis	
Retina-laser		Strabismus	
Retina-other		Amblyopia	
Strabismus		Other	

**Medical History**  Negative, unless noted

A		Cancer	Negative;
B		Cardiovascular	no stents
P	Xalatan, both, nightly 12/15 9pm	Diabetes	Negative;
C		Hypertension	
O		Neurologic	TIA
		Pulmonary	
		Other	

Prior drops: Travatan, Betimol, Alphagan, Azopt, Cosopt, CCT 492/498

**Comments:** \_\_\_\_\_

**Social History** (  )

Norwegian  
Nonsmoker currently, quit in 1970 (smoked for 20 years - 1/2 ppd)  
Winona - moving to Rochester  
Taught Biology, Real Estate broker, author of books now.

**Current Medications**  none

Bovine Colostrum\* (Free Text Entry) 1 one time daily.  
Co Q-10 capsule 1 capsule by mouth one time daily.  
Ester-C capsule 1 capsule by mouth one time daily.  
Lo-Dose Aspirin 81 mg tablet enteric coated 1 TABLET by mouth one time daily.  
Vitamin B-12 tablet 1 TABLET by mouth one time daily.  
Vitamin B-6 tablet 1 TABLET by mouth one time daily.  
Vitamin D-3 tablet 1 TABLET by mouth one time daily.  
Xalatan 0.005 % drops 1 drop ophthalmic every evening.  
Site: Both eyes.

These are the patient's medications as of Wednesday, December 16, 2009 at 7:53 AM.

**Allergies / Adverse Reactions** (  )

Medication :  
\*\*NO KNOWN MEDICATION ALLERGIES\*\*  
Non-Medication / Food :  
Radiology :

Allergies above current as of Wednesday, December 16, 2009 at 07:53 AM

GL239

<b>Visual Acuity (Va)</b>		<b>Habitual Prescription (Rx) # 1</b> date / /		<b>Glasses hx</b> wears glasses primarily for distance	
Distance (D) c rx #1 Comments		distance only		Comments:	
Rt	20 / 30-2 (pinhole) nh	sphere	cylinder	axis	add
Lt	20 / 50-2 (pinhole) 40	+1.00	+ 1.25	x 009	+
Preference		<b>Habitual Prescription (Rx) # 2</b> date / /			
Near (N) c rx #2 Comments		near only		Comments:	
Rt	.35 / .8 in "M" NPA (cm)	sphere	cylinder	axis	add
Lt	.39 / 1.0 in "M" NPA (cm)	+3.25	+ sphere	x	+
		Lt	+3.25	+ sphere	x
<b>Refraction 1</b> date / /		<b>Refraction 2</b> date / /		<b>Refraction Other</b>	
Rt	sphere cylinder axis D Va	Rt	sphere cylinder axis D Va	Rt	sphere cylinder axis D Va
Lt	+ 20 / +	Lt	+ 20 / +	Lt	+ 20 / +
Comments for printed prescription		Comments for printed prescription		Comments for printed prescription	
<b>Motility</b> <input type="checkbox"/> full <input type="checkbox"/> see below		<b>Alignment</b> <input type="checkbox"/> no manifest deviation in 1°		<b>Neuro - ophthalmic</b>	
Rt	H	Head Tilt		Color Ishihara Rt Lt	
Lt	H	to R to L Alignment C		Nystagmus:	
<b>Sensory</b>		Double M addox		Other Neuro - ophthalmic:	
Worth four-dot					
Titmus					
Frisby					
Preschool					
Bagolini					
<b>Fusional amplitudes: non - tropic</b>		<b>tropic / prism(s) to fuse</b>			
convergence divergence base up base down		H fuse with base break break V fuse with base break break			
Sensorimotor Comments / Report					
<b>Intraocular Pressure (IOP)</b>		<b>Pupils</b>		<b>Visual Field</b>	
Rt	IOP, in mm Hg shape size (mm) direct reaction afferent defect confrontational			Amster grid	
Lt	17 round 5 prompt none				
at08:24 via App c benox + Fluress Comments: Automated visual field completed. VCR: 12/15					
<b>Cornia</b>		<b>Gonioscopy</b>			
keratometry mires thickness sensation		via Sussman			
Lt @ 1 @ 492 um		grade 3-4 open with 1+ pigment			
Lt @ 1 @ 498 um		grade 4 open with 1+ pigment			
Dilation at09:31 with tropicamide 1.0 % Both phenylephrine 2.5 % Both Comments:					
<b>Miscellaneous Observations</b>		Persons accompanying patient spouse		<b>Key</b> Rt = Right Eye Lt = Left Eye * if other than date of record B = beta blocker H = horizontal P = prostaglandin V = vertical O = other A = alpha agonist C = carbonic anhydrase inhibitor	
Special needs, if any					
Above supporting data reviewed and noted					

Service Date/Time: 15-Dec-2009 07:58

**Exam**

General observations: Mental status: Orientation to time, place, person  WNL  other  
 Mood / affect  WNL  other

Elements below examined and within normal limits when checked

Rt Findings (describe below)		Ll Findings (describe below)
white	<input type="checkbox"/>	white
clear, no guttae	<input type="checkbox"/>	clear, no guttae
deep and quiet	<input type="checkbox"/>	deep and quiet
blue iris, no TIDs	<input type="checkbox"/>	blue iris, no TIDs
1-2+ NS, no PEX, trace PSC	<input type="checkbox"/>	1-2+ NS, no PEX, trace PSC
PVD	<input type="checkbox"/>	PVD
Distinct margins, nasalization of vessels, thin NFL, lamina cribosa visible 1.5mm disc	<input type="checkbox"/>	Distinct margins, trace peripapillary pigment, nasalization of vessels, thin NFL, lamina cribosa visible 1.6mm disc
thin rim, more prominent nasal rim	<input type="checkbox"/>	very thin rim, more prominent nasally
flat	<input type="checkbox"/>	flat fine drusen
<input type="checkbox"/> Present <input type="checkbox"/> Absent		<input type="checkbox"/> Present <input type="checkbox"/> Absent
<input type="checkbox"/> anterior segment within normal limits. no view posterior to <input type="checkbox"/> cornea <input type="checkbox"/> lens S/P <input type="checkbox"/> enucleation <input type="checkbox"/> evisceration <input type="checkbox"/> exenteration		<input type="checkbox"/> posterior segment within normal limits. no view posterior to <input type="checkbox"/> cornea <input type="checkbox"/> lens S/P <input type="checkbox"/> enucleation <input type="checkbox"/> evisceration <input type="checkbox"/> exenteration

Ocular Adnexa / globe lids, lacrimal gland / drainage, orbit  
 Conjunctiva palpebral, bulbar  
 Cornea \*\* tear film, epithelium, stroma, endothelium  
 Anterior Chamber \*\* depth, cell, flare  
 Iris \*\*  
 Lens \*\* anterior / posterior capsules, cortex, nucleus  
 Vitreous  
 Optic Disc size, appearance, nerve fiber layer  
 Cup-to-Disc Ratio 0.9 0.95  
 Retina / choroid macula  
 Macular Thickening / Edema  
 Retina / choroid vessels, post pole, periphery  
 All WNL, unless described

**Patient Education**  
 Ready to learn, no apparent learning barriers were identified; learning preferences include listening. Explained diagnosis and treatment plan; patient expressed understanding of the content.  
 Here with his wife.

**Impression / Report / Plan**  includes supervising consultant's documentation, where

Total Time (in minutes) Counseling Time (in minutes) Testing Time (in minutes) Margin Code

#1 Primary Open Angle Glaucoma, both eyes  
 CT = 492/498  
 Visual field - Right eye: double arc. Left eye: dense sup arc, int nasal step (no outside fields to compare to - only reports)  
 Photos  
 OCT NFL  
 Target may need to be 10-12  
 Will add Cosopt and reassess 6 weeks.

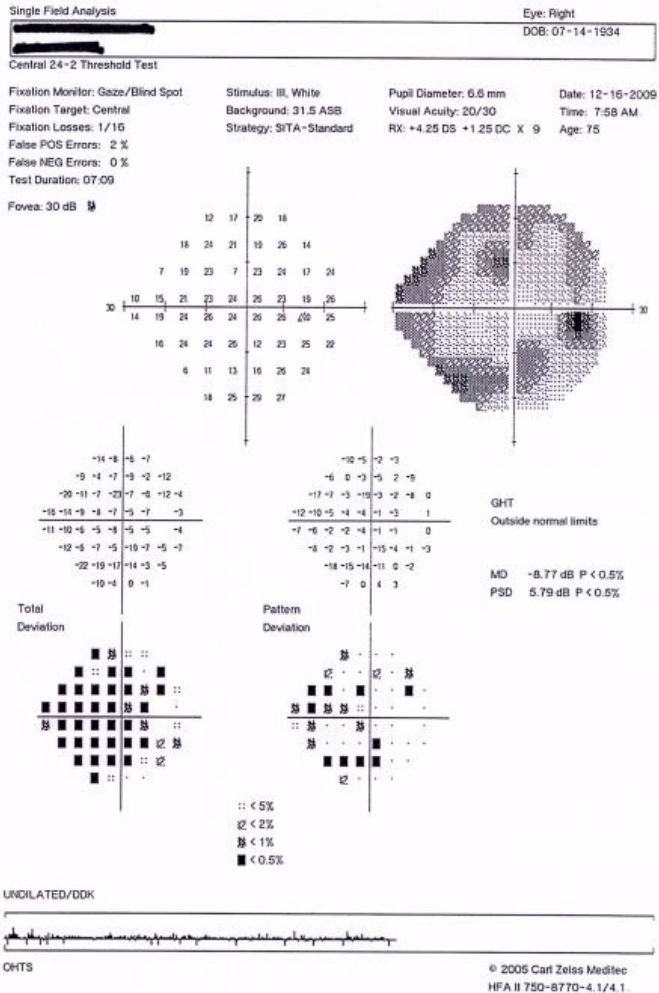
#2 Cataracts, both eyes  
 Decreases vision both eyes, left eye likely from glaucoma + cataract. Patient reports right eye vision is blurrier though - this could be from both cataract and glaucoma.

Reviewed disc photos and OCT, significant nerve fiber loss from glaucoma.

**Diagnosis**  
 #1 Primary Open Angle Glaucoma, both eyes  
 #2 Cataracts, both eyes



GL239



PATIENT COPY -  
NOT FOR DIAGNOSTIC  
PURPOSES

Exam Information  
16-Dec-2009  
12:00:00  
XC  
XC-Visual Fields

GL239

Single Field Analysis

Eye: Left

DOB: 07-14-1934

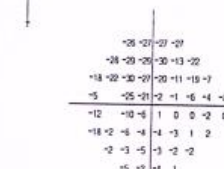
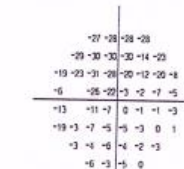
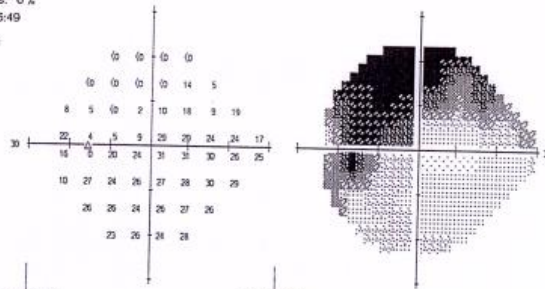
Central 24-2 Threshold Test

Fixation Monitor: Gaze/Blind Spot  
 Fixation Target: Central  
 Fixation Losses: 0/16  
 False POS Errors: 3 %  
 False NEG Errors: 0 %  
 Test Duration: 06:49  
 Fovea: 31 dB

Stimulus: III, White  
 Background: 31.5 ASB  
 Strategy: SITA-Standard

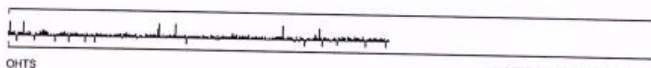
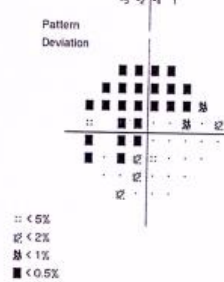
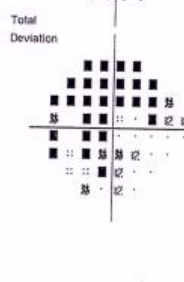
Pupil Diameter: 5.5 mm  
 Visual Acuity: 20/40  
 Rx: +4.75 DS DC X

Date: 12-16-2009  
 Time: 8:08 AM  
 Age: 75



GHT  
 Outside normal limits

MD -10.61 dB P < 0.5%  
 PSD 10.88 dB P < 0.5%



OHTS

© 2005 Carl Zeiss Meditec  
 HFA II 750-8770-4.1/4.1.

PATIENT COPY -  
 NOT FOR DIAGNOSTIC  
 PURPOSES

Exam Information  
 16-Dec-2009  
 12:00:00  
 XC  
 XC-Visual Fields

GL239 6/8

GL239

Name: ██████████  
ID: ██████████  
DOB: 7/14/1934  
Gender: Male  
Physician: ██████████

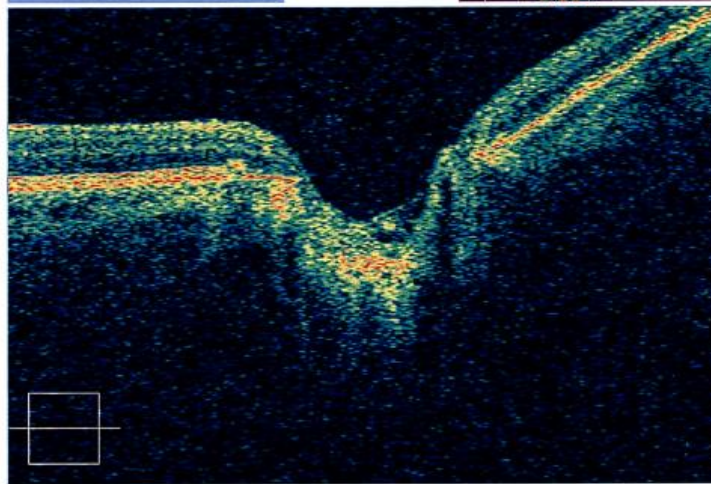
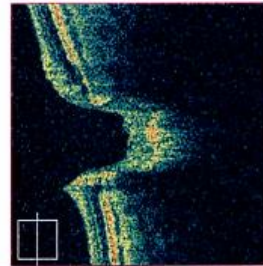
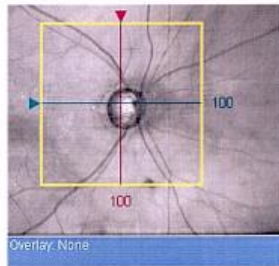
Exam Date: 12/16/2009  
Exam Time: 10:49 AM  
Technician: Operator, Cirrus  
Signal Strength: 7/10

Mayo Clinic



Advanced Visualization: Optic Disc Cube 200x200

OD  OS



Comments

Physician's Signature

SW Ver: 3.0.0.84  
Copyright 2008  
Carl Zeiss Medtec, Inc.  
All Rights Reserved  
Page 1 of 1

PATIENT COPY -  
NOT FOR DIAGNOSTIC  
PURPOSES

Exam Information  
16-Dec-2009  
00:00:00  
XC  
XC-Cirrus

GL239 7/8

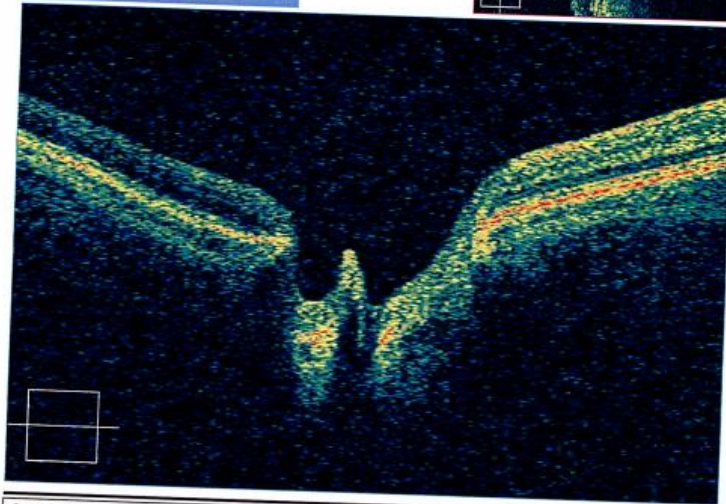
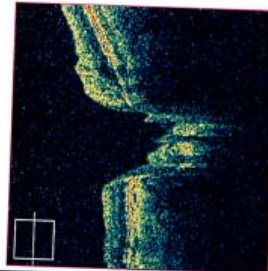
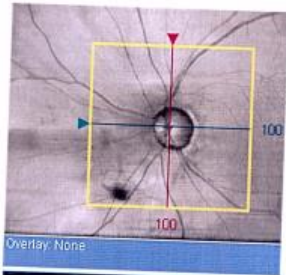
GL239

Name: ██████████  
ID: ██████████  
DOB: 7/14/1934  
Gender: Male  
Physician: ██████████  
Exam Date: 12/16/2009  
Exam Time: 10:51 AM  
Technician: Operator, Cirrus  
Signal Strength: 7/10  
Mayo Clinic



Advanced Visualization: Optic Disc Cube 200x200

OD  OS



Comments

Physician's Signature

SW Ver: 3.0.0.64  
Copyright 2008  
Carl Zeiss Medtec, Inc.  
All Rights Reserved  
Page 1 of 1

PATIENT COPY -  
NOT FOR DIAGNOSTIC  
PURPOSES

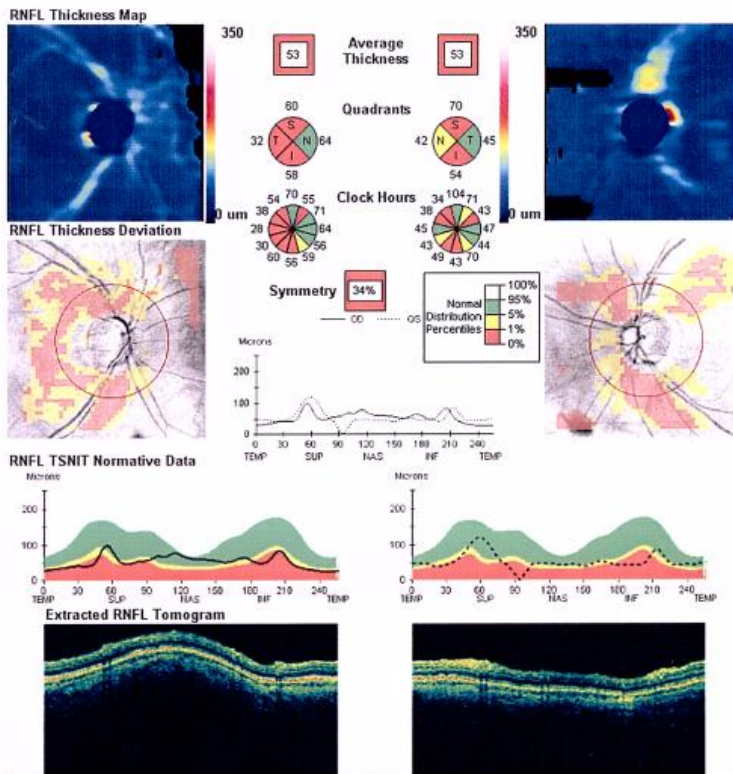
Exam Information  
16-Dec-2009  
00:00:00  
XC  
XC-Cirrus

GL239

Name: ██████████ OD OS  
 ID: ██████████ Exam Time: 10:49 AM 10:51 AM Mayo Clinic  
 DOB: 7/14/1934 Signal Strength: 7/10 7/10  
 Gender: Male Exam Date: 12/16/2009  
 Physician: Technician: Operator, Cirrus



Optic Disc Cube 200x200 OD OS



Comments

Physician's Signature

SW Ver: 3.0.0.64  
 Copyright 2008  
 Carl Zeiss Medtec, Inc.  
 All Rights Reserved  
 Page 1 of 1


PATIENT COPY -  
 NOT FOR DIAGNOSTIC  
 PURPOSES

Exam Information  
 16-Dec-2009  
 00:00:00  
 XC  
 XC-Cirrus

GL272 1/7

<b>History of Present Illness</b> // if checked, encounter is an Emergency, c a Consult requested b		<b>Review of Systems (ROS) ( / )</b>	
to evaluate Chief Complaint HPI <input type="checkbox"/> includes summary of requested outside records 79 year old female with primary open angle glaucoma, 6 month follow up. Eyes watery due to sinus infection, on medication.		Neurologic Cardiovascular Respiratory Endocrine ENT General Psychological Skin See CVI of // for † items	
<b>Past / Family / Social Histories / Medications / Allergies</b>			
Eye History <input type="checkbox"/> Negative, unless noted Ant segment IOL'S OD 1-97, OS 8-00 Eyelid / Orbit Glaucoma Retina-laser Retina-other Strabismus Amblyopia Trauma / Other Eye Medications: <input type="checkbox"/> none I II (glaucoma) A timolol 0.5%, OU, qd, 6:30am B P C O Prior drops		Medical History <input type="checkbox"/> Negative, unless noted Cancer Cardiovascular Diabetes Hypertension On med(s) Neurologic Pulmonary Other Systemic Medication † <input type="checkbox"/> none HCTZ, lipid, ASA, oclini, univasc, antihistamine, multi. vits., calcium Eye FHx <input checked="" type="checkbox"/> Neg., unless noted Blindness Glaucoma Macula dis Strabismus Amblyopia Other Social History † ) Allergies † ) <input checked="" type="checkbox"/> none known	
Comments			
<b>Visual Acuity (Va)</b>			
Distance (D) c rx #1 Comments OD 20 / 20 (pinhole) OS 20 / 40+1 (pinhole) 20/20-3 Preference Near (N) c rx #1 Comments OD .34 / .3 in "M" NPA (cm) OS .34 / .4 in "M" NPA (cm)		Habitual Prescription (Rx) # 1 date // // bifocal Glasses hx generally wears glasses all the time sphere cylinder axis add base H base V OD + x OS + x Comments:	
Refraction 1 date // // sphere cylinder axis D Va OD + x 20 / + OS + x 20 / /		Habitual Prescription (Rx) # 2 date // // sphere cylinder axis add base H base V OD + x OS + x Comments:	
Refraction 2 date // // sphere cylinder axis D Va OD + x 20 / + OS + x 20 / /		Other sphere cylinder axis D Va + x 20 / + + x 20 / /	
Comments:			
<b>Motility</b> <input type="checkbox"/> full <input type="checkbox"/> see below OD OS H H <b>Sensory</b> Worth four-dot D N Titmus Frisby Preschool Bagolini		<b>Alignment</b> <input type="checkbox"/> no manifest deviation in 1° to R Head Tilt to L Alignment C Double M addox Comments:	
<b>Neuro - ophthalmic</b> Color OD OS Ishihara Nystagmus: Other Neuro - ophthalmic:			
<b>Fusional amplitudes: non - tropic tropic / prism(s) to fuse</b> convergence divergence base up base down H fuse with base break break V fuse with base break break D N in out up down N in out up down			
<b>Sensorimotor Comments / Report</b>			

GL272 2/7

Intraocular Pressure (IOP)		Pupils			Visual Field	
	IOP, in mm Hg	shape	size (mm)	direct reaction	afferent defect	confrontational
OD	10	round	3.5	prompt	none	Amsler grid
OS	14	round	3.5	prompt	none	
#108:22 via App c benox + Fluress Comments:						
Cornea				Gonioscopy		
	keratometry	mires	thickness	sensation		
OD	@	:	@			
OS	@	:	@			
Dilation at				with		
Miscellaneous Observations				<input type="checkbox"/> separate, handwritten, yellow eye sheets in history <b>Key</b> * if other than date of record B = beta blocker H = horizontal P = prostaglandin V = vertical O = other A = alpha agonist C = carbonic anhydrase inhibitor		
Special needs, if any				Persons accompanying patient		
Above supporting data reviewed and noted				Herman, David C, MD		
<b>Exam</b>						
General observations:				Mental status: Orientation to time, place, person <input checked="" type="checkbox"/> WNL <input type="checkbox"/> other		
				Elements below examined and within		
OD Findings (describe below)		OD normal limits when checked		OS Findings (describe below)		
		<input checked="" type="checkbox"/> Ocular Adnexa / globe lids, lacrimal gland / drainage, orbit				
		<input checked="" type="checkbox"/> Conjunctiva palpebral, bulbar				
		<input checked="" type="checkbox"/> Cornea ** tear film, epithelium, stroma, endothelium				
vitreous in AC		<input type="checkbox"/> Anterior Chamber ** depth, cell, flare				
		<input checked="" type="checkbox"/> Iris **				
pciOL in position		<input type="checkbox"/> Lens ** anterior / posterior capsules, cortex, nucleus		pciOL in position		
		<input checked="" type="checkbox"/> Vitreous				
		<input checked="" type="checkbox"/> Optic Disc size, appearance, nerve fiber layer Cup-to-Disc Ratio 0.4				
		<input checked="" type="checkbox"/> Retina / choroid macula				
		<input type="checkbox"/> Retina / choroid vessels, post pole, periphery				
no view posterior to <input type="checkbox"/> cornea <input type="checkbox"/> lens		<input type="checkbox"/> All WNL, unless described		no view posterior to <input type="checkbox"/> cornea <input type="checkbox"/> lens		
S/P <input type="checkbox"/> enucleation <input type="checkbox"/> evisceration <input type="checkbox"/> exenteration				S/P <input type="checkbox"/> enucleation <input type="checkbox"/> evisceration <input type="checkbox"/> exenteration		
Time (in min): total		counseling		** via slit lamp exam/alternatively, via <input type="checkbox"/> portable slit lamp <input type="checkbox"/> pen-light inspection where necessary		
<b>Impression / Plan</b> <input type="checkbox"/> Includes supervising consultant's documentation, where appropriate						
1. POAG						
-IOP controlled. Continue current rx. Recheck 6 months.						
2. Pseudophakia OU						
<b>Contributing Authors</b>						
						

**History of Present Illness** / If checked, encounter is  Management, or  an Emergency, or  a Consult requested by: \_\_\_\_\_  
 to provide advice or opinion regarding evaluation and / or management of \_\_\_\_\_

**Chief Complaint** 1 year f/u Primary open angle glaucoma both eyes, Pseudophakia both eyes, Primary acquired melanosis left eye

**HPI**  includes summary of requested outside records  
 Tearing, left eye: x several years (plugged tear duct she says); constant. Uses OTC tears at times, couple times a week.  
 Diminished visual changes, blurs good both distance and at near.

**Review of Systems (ROS)** ( )

Eye	
Neurologic	
Cardiovascular	
Respiratory	
Endocrine	
ENT	
General	
Psychological	
Skin	
Musculoskeletal	
Genitourinary	
Gastrointestinal	
Hem / Lymph	
Immun / Allergy	

See CVI of \_\_\_\_\_ for I items  all other systems reviewed and negative

**Past / Family / Social Histories**

<b>Eye History</b> <input checked="" type="checkbox"/> Negative, unless noted	<b>Eye FHx</b> <input checked="" type="checkbox"/> Neg, unless noted
<b>Ant segment</b> IOL, right eye 1-97 (TX), left eye 8-00; YAG left eye 05/05	<b>Glaucoma</b>
<b>Eyelid / Orbit</b>	<b>Macula dis</b>
<b>Glaucoma</b>	<b>Strabismus</b>
<b>Retina-laser</b>	<b>Amblyopia</b>
<b>Retina-other</b>	<b>Other</b>
<b>Strabismus</b>	
<b>Amblyopia</b>	
<b>Trauma / Other</b>	

**Eye Medications:**  none I **II (glaucoma)**

artificial tears, both eyes, as needed	<b>A</b>	
	<b>B</b>	Timoptic 0.5%, both 1 x day 7am
	<b>P</b>	
	<b>C</b>	
	<b>O</b>	

**Medical History**  Negative, unless noted

<b>Cancer</b>	
<b>Cardiovascular</b>	no stents
<b>Diabetes</b>	
<b>Hypertension</b>	On med(s), Controlled
<b>Neurologic</b>	
<b>Pulmonary</b>	
<b>Other</b>	

**Social History** ( )

Assisted living (Grand Meadow)

**Comments:**

- Current Medications**  none
- Acetaminophen Extra Strength 500 mg tablet 2 tablets by mouth four times a day as needed.  
 Indication: Pain.  
 Instructions: take regularly for joint pain and stiffness due to degenerative joint disease and for back pain. Max 8 caps per 24 hrs.
  - Artificial Tears drops 1 drop ophthalmic as needed.  
 Site: Both eyes.  
 Indication: dryness.
  - Benzonatate [TESSALON PERLE] 200 mg capsule 1 capsule by mouth three times a day.  
 Indication: cough.
  - Calcium Carbonate 500 mg (1,250 mg) tablet 1 tablet by mouth two times a day.  
 Indication: osteoporosis.
  - Clarin 10 mg tablet 1 tablet by mouth one time daily.
  - Detrol LA 4 mg capsule sustained release 24 hour 1 capsule by mouth one time daily.
  - Flaxseed Oil 1,030 mg capsule 1 capsule by mouth three times a day.
  - Glucosamine-MSM Complex tablet 1 tablet by mouth three times a day.
  - Hydrochlorothiazide 25 mg tablet 1 tablet by mouth one time daily.
  - Melatonin 3 mg tablet 1-2 tablets by mouth every bedtime.  
 Indication: Sleep.
  - Milk of Magnesia 800 mg/5 mL suspension 2.5 mL by mouth as needed.  
 Indication: Constipation.
  - Multivitamin with Iron-Min capsule 1 tablet by mouth one time daily.
  - Norflex 100 mg tablet sustained release 1 tablet by mouth two times a day.
  - Robitussin DM\* (Free Text Entry) 5 mL by mouth as needed.  
 Indication: Cough/wheeze.
  - Senokot-S 8.6-50 mg tablet 1 tablet by mouth one time daily as needed.  
 Indication: constipation.  
 Instructions: Use while taking narcotics, hold for loose stools.
  - Timolol Maleate [TIEMOPTIC] 0.5 % drops 1 drop ophthalmic one time daily #15 drop.  
 Site: Both eyes.
  - Toprol XL 50 mg tablet sustained release 24 hour 1 tablet by mouth one time daily.  
 Indication: blood pressure.  
 Instructions: to get average below 140/90.
  - Trazodone 50 mg tablet 1 tablet by mouth every bedtime.  
 Indication: Sleep.
  - Vitamin D-3 1000 unit tablet 1 tablet by mouth every morning.
  - Zocor 40 mg tablet 1 tablet by mouth one time daily.

GL272

[continued...]

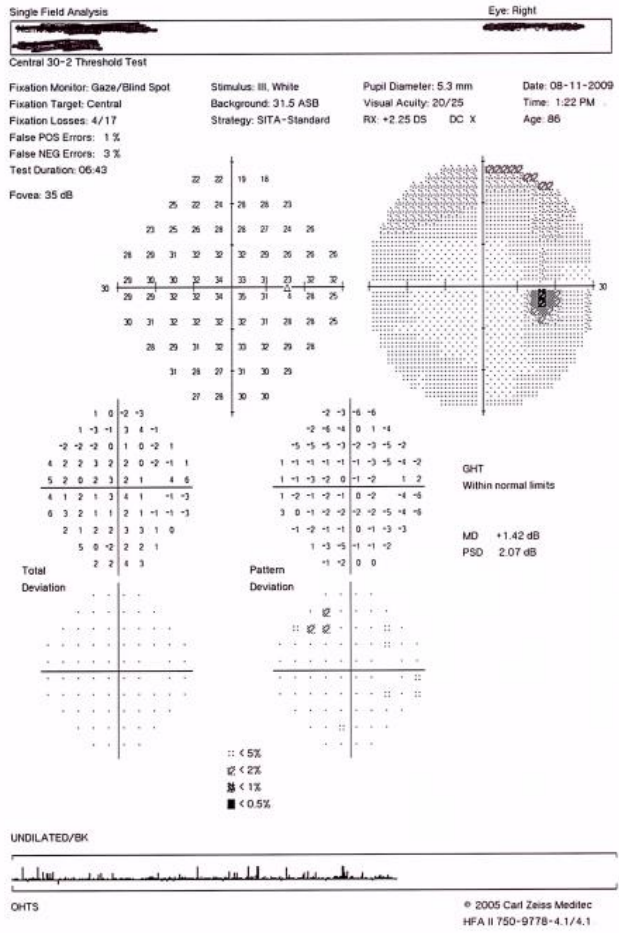




<b>General observations:</b> Healthy-appearing		<b>Mental status:</b> Orientation to time, place, person <input checked="" type="checkbox"/> WNL <input type="checkbox"/> other Mood / affect <input type="checkbox"/> WNL <input type="checkbox"/> other	
<b>Elements below examined and within</b>		<b>Elements below examined and within</b>	
<b>Rt Findings (describe below)</b> Krukenberg's like spindle centrally Small plug of vitreous to temporal paraentesis @ 8:30 No transillumination defects pciOL in position c central posterior capsular opening Healthy rim Flat <input type="checkbox"/> Present <input type="checkbox"/> Absent	<b>Rt normal limits when checked</b> <input type="checkbox"/> Ocular Adnexa / globe lids, lacrimal gland / drainage, orbit <input type="checkbox"/> Conjunctiva palpebral, bulbar <input type="checkbox"/> Cornea ** tear film, epithelium, stroma, endothelium <input type="checkbox"/> Anterior Chamber ** depth, cell, flare <input type="checkbox"/> Iris ** <input type="checkbox"/> Lens ** anterior / posterior capsules, cortex, nucleus <input type="checkbox"/> Vitreous <input type="checkbox"/> Optic Disc size, appearance, nerve fiber layer Cup-to-Disc Ratio 0.4 <input type="checkbox"/> Retina / choroid macula <input type="checkbox"/> Macular Thickening / Edema <input type="checkbox"/> Retina / choroid vessels, post pole, periphery	<b>Lt Findings (describe below)</b> Flat scattered brown pigment on bulbar conjunctiva adjacent to limbus intertemporally, ~ 3x3mm Deep and quiet No transillumination defects pciOL in position c central posterior capsular opening Flat <input type="checkbox"/> Present <input type="checkbox"/> Absent	<input type="checkbox"/> posterior segment within normal limits. no view posterior to <input type="checkbox"/> cornea <input type="checkbox"/> lens S/P <input type="checkbox"/> enucleation <input type="checkbox"/> evisceration <input type="checkbox"/> exenteration
** via slit lamp exam alternatively, via <input type="checkbox"/> portable slit lamp or <input type="checkbox"/> pen-light inspection where necessary			
<b>Impression / Report / Plan</b> <input type="checkbox"/> includes supervising consultant's documentation, where		via slit lamp exam alternatively, via <input type="checkbox"/> portable slit lamp or <input type="checkbox"/> pen-light inspection where necessary	
Total Time (in minutes)	Counseling Time (in minutes)	Testing Time (in minutes)	Margin Code
#1 Primary open angle glaucoma, both eyes No family history of glaucoma. Intraocular pressures stable. Some inferior thinning of left disc. Visual field (04/06; automated; reliable): OU = normal. Visual field (08/08; automated; reliable): OD = normal; OS = superior constriction Visual field (08/09; automated; reliable): OU = normal Plan: continue present management (0.5% Timoptic OU q day).			
#2 Pseudophakia, both eyes Stable.			
#3 Primary acquired melanosis, left eye No change compared to 04/92 photos. No other pigmented areas on conjunctiva. Observe.			
#4 Epiphora Punctal dilation / irrigation performed on left canalicular system (08/10): left system partially blocked, mostly reflux through superior punctum. Plan: defers surgical consult. Continue present management (0.5% Timoptic OU q day). Recheck 1 year.			
<b>Diagnosis</b> #1 Primary open angle glaucoma, both eyes #2 Pseudophakia, both eyes #3 Primary acquired melanosis, left eye #4 Epiphora			

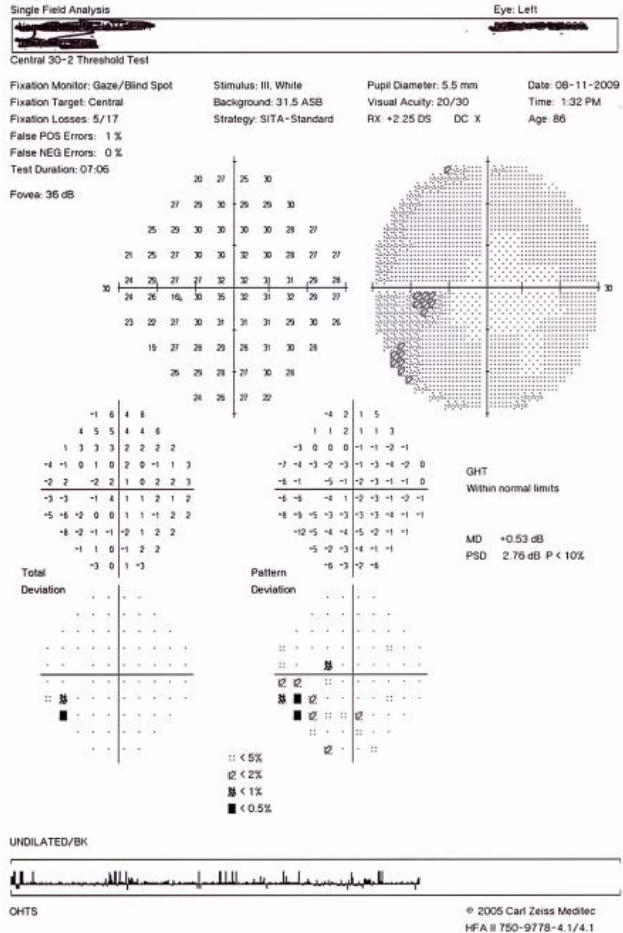
GL272

*Glenn*



**Exam Information**  
 11-Aug-2009  
 13:33:00  
 XC  
 XC-HFA

GL272



Exam Information  
 11-Aug-2009  
 13:33:00  
 XC  
 XC-HFA

6/28/2013

**Allergies / Adverse Reactions(+)**  
 Medication : MORPHINE - Nausea & Vomiting  
 LEVAQUIN - Rash

Allergies above current as of Friday, 28-Jun-2013 at 07:13.

---

**Visual Acuity (Va)** c rx #1  
 Distance (D) Comments  
 Rt 20 / 40 (pinhole) 40+2  
 Lt 20 / 25+2 (pinhole)  
 Preference

**Habitual Prescription (Rx) # 1** date:  
 Glasses rx generally wears glasses all the time  
 trifocal sphere cylinder axis add base H base V  
 Rt -4.00 + 1.00 x 110 + 2.50 4 down  
 Lt -4.50 + 0.50 x 051 + 2.50 6 up  
 Comments: gl x 2 years

**Habitual Prescription (Rx) # 2** date:  
 sphere cylinder axis add base H base V  
 Rt + x x +  
 Lt + x x +  
 Comments: Preferred +3.0 over manifest for near.

---

**Refraction 1** manifest date: 28-Jun-2013  
 sphere cylinder axis D Va add N Va in "M" vertex base H base V  
 Rt -4.00 + 0.75 x 133 20 / 25-2 + 3.00 .40 / .4 4 down  
 Lt -4.75 + 1.00 x 059 20 / 25+1 + 3.00 .40 / .4 5 up  
 Comments: Patient requests refraction; billing complete.

---

**Refraction 2** date:  
 sphere cylinder axis D Va add N Va in "M" vertex base H base V  
 Rt + x x 20 / + / /  
 Lt + x x 20 / + / /  
 Comments:  
 Comments for printed prescription

**Refraction Other**  
 sphere cylinder axis D Va  
 + x x 20 /  
 + x x 20 /

---

**Motility**  full  see below  
 Rt Lt  
 H H

**Alignment**  no manifest deviation in 1°  
 D cc MR  
 D Rh  
 2 Rh  
 D sc MR  
 3 Exo  
 8 Rh  
 N cc ACT to R Head Tilt to L  
 0  
 0  
 Double Maddox alternates fixation, fused and preferred 4 down and 5 up  
 Alignment Comments:

**Neuro - ophthalmic**  
 Color Ishihara Rt Lt  
 Nystagmus:  
 Other Neuro - ophthalmic:

---

**Fusional amplitudes: non - tropic** base up base down D H fuse with base break break V fuse with base break break  
 D convergence divergence  
 N in out in out up down up down

**tropic / prismatic** to fuse

---

**Sensorimotor Comments / Report**

---

**Intraocular Pressure (IOP)** Pupils Visual Field  
 IOP, in mm Hg shape size (mm) direct reaction afferent defect confrontational  
 Rt 21 round 3 prompt none full to finger count  
 Lt 21 round 3 prompt none full to finger count  
 Amisler grid

at08-02 via App c benox + Fluress Comments:

---

**Cornia** Gonioscopy  
 keratometry mires thickness sensation via Koeppel  
 Rt @ : @ 600 um  
 Lt @ : @ 605 um

Dilation at 09:03 with tropicamide 1.0 % Both Comments: Dilation protocol : no exclusions identified, pupil(s) dilated.

---

**Miscellaneous Observations** Key Rt = Right Eye Lt = Left Eye  
 Special needs, if any Persons accompanying patient  
 \* If other than date of record B = beta blocker  
 H = horizontal P = prostaglandin  
 V = vertical O = other  
 A = alpha agonist C = carbonic anhydrase inhibitor

Above supporting data reviewed and noted by \_\_\_\_\_

8/8/2013

**Allergies / Adverse Reactions ( )**

Medication:  
 MORPHINE - Nausea & Vomiting  
 LEVAQUIN - Rash  
 TRAVATAN Z - Other; burning sensation  
 LUMIGAN - Other; burning sensation

Allergies above current as of Thursday, 08-Aug-2013 at 10:58.

Visual Acuity (Va)		Habitual Prescription (Rx) # 1 date:				
Distance (D) c rx #1		Bifocal Glasses hx				
Comments		sphere cylinder axis add base H base V				
Rt 20 / 50+2 (pinhole) 20-1		Rt -4.00 + 1.00 x 135 + 3.00	4 down			
Lt 20 / 50+1 (pinhole) nh		Lt -4.75 + 1.00 x 060 + 3.00	5 down			
Near (N) c rx #1		Habitual Prescription (Rx) # 2 date:				
Comments		sphere cylinder axis add base H base V				
Rt .39 / .6 in "M" NPA (cm)		Rt				
Lt .38 / .8 in "M" NPA (cm)		Lt				
<b>Refraction 1</b> date:		<b>Refraction 2</b> date:				
sphere cylinder axis D Va	add N Va in "M" vertex base H base V	sphere cylinder axis D Va	add N Va in "M" vertex base H base V			
Rt + / x / 20 / +	/ / /	Rt + / x / 20 / +	/ / /			
Lt + / x / 20 / +	/ / /	Lt + / x / 20 / +	/ / /			
Comments for printed prescription		Comments for printed prescription				
<b>Motility</b> <input checked="" type="checkbox"/> full <input type="checkbox"/> sup below		<b>Alignment</b> <input type="checkbox"/> no manifest deviation in 1"				
Rt Lt		<table border="1" style="width: 100%; height: 40px;"> <tr> <td style="width: 33%;"></td> <td style="width: 34%;"></td> <td style="width: 33%;"></td> </tr> </table>				
H H		to R Head Tilt to L Alignment Comments:				
<b>Sensory</b>		<b>Neuro - ophthalmic</b>				
Worth four-dot		Color Ishihara Rt Lt				
D N Titmus Frisby Preschool Bagolini		Nystagmus:				
		Other Neuro - ophthalmic:				
<b>Fusional amplitudes: non - tropic / prism(s) to fuse</b>						
convergence divergence base up base down		H fuse with base break break	V fuse with base break break			
D N		D in out	up down			
		N in out	up down			
<b>Sensorimotor Comments / Report</b>						
<b>Intraocular Pressure (IOP)</b>		<b>Pupils</b>				
IOP, in mm Hg	shape size (mm) direct reaction afferent defect	confrontational Amsler grid				
Rt 16	round 3.5 prompt none	full to finger count				
Lt 16	round 3.5 prompt none	full to finger count				
at 10:59 via App c bonox + Fluress. Comments: Automated visual field completed.						
<b>Cornea</b>		<b>Gonioscopy</b>				
keratometry mires thickness sensation		via Sussman				
Rt		grade 5, minimal pigment				
Lt		grade 5, minimal pigment				
Dilation at 11:03 with cyclopentolate 1.0 % Both phenylephrine 2.5 % Both Comments: Dilation protocol; no exclusions identified, pupil(s) dilated.						
<b>Miscellaneous Observations</b>		<b>Key</b>				
Special needs, if any	Persons accompanying patient	H = horizontal	B = beta blocker			
Above supporting data reviewed and noted by _____		V = vertical	P = prostaglandin			
		A = alpha agonist	O = other			
			C = carbonic anhydrase inhibitor			

Observations: \_\_\_\_\_ Mental status: Orientation to time, place, person  WNL  other  
 Apparent distress: \_\_\_\_\_ Mood / affect  WNL  other

Rt Findings (describe below)	Elements below examined and within normal limits when checked	Lt Findings (describe below)
trace injection	<input type="checkbox"/> Ocular Adnexa / globe lids, lacrimal gland / drainage, orbit	trace injection
no K spindle, decreased tear film	<input type="checkbox"/> Conjunctiva palpebral, bulbar	no K spindle, decreased tear film
deep and quiet	<input type="checkbox"/> Cornea ** tear film, epithelium, stroma, endothelium	deep and quiet
blue iris, poor dilation, no TIDs	<input type="checkbox"/> Anterior Chamber ** depth, cell, flare	blue iris, poor dilation, no TIDs
1+ Nuclear sclerosis, no PXE	<input type="checkbox"/> Iris **	1+ Nuclear sclerosis, no PXE
quiet	<input type="checkbox"/> Lens ** anterior / posterior capsules, cortex, nucleus	quiet
2.2mm disc, no hemorrhage	<input type="checkbox"/> Vitreous	2.1mm disc, no hemorrhage
flat	<input type="checkbox"/> Optic Disc size, appearance, nerve fiber layer	flat
flat 360, no lesion	<input type="checkbox"/> Cup-to-Disc Ratio 0.8	flat 360, no lesion
	<input type="checkbox"/> Retina / choroid macula	
	<input type="checkbox"/> Macular Thickening / Edema	
	<input type="checkbox"/> Retina / choroid vessels, post pole, periphery	

anterior segment within normal limits.  All WNL, unless described  
 no view posterior to cornea  lens  posterior segment within normal limits.  
 S/P  enucleation  evisceration  exenteration  
 S/P  enucleation  evisceration  exenteration

\*\* via slit lamp exam; alternatively, via  portable slit lamp or  pen-light inspection where necessary

2/8/2013

**Patient Education**  
 Ready to learn, no apparent learning barriers were identified; learning preferences include listening. Explained diagnosis and treatment plan; patient expressed understanding of the content.

**Eye Medications & Impression/Report/Plan**  includes supervising consultant's documentation, where applicable

Total Time (in minutes)	Counseling Time (in minutes)	Testing Time (in minutes)	Margin Code
<b>Eye Medications</b>			
<b>Impression / Report / Plan</b>			
#1 Open angle glaucoma, both eyes based on cup to disc, high normal pressures, + past steroid use, + raynauds. Prior treatment/interventions: No surgery or lasers, Lumigan and Travatan - did not tolerate due to burning. Timex 21/21 CCT: 600/605 No FH			
Disc photos consistent with exam OCT int: signal 59/64, int thickness 59/64 RIGHT: mod thinning 1, 9-10 and severe thinning 6, 11-12 LEFT: mod thinning 12,6 severe 7, 11 SITA (B/D) RIGHT: FN0%, dense inferior arcuate LEFT: FN 0%, suspicious for inferior arc, possible early sup nasal changes			
#2 Cataract, both eyes not visually significant, observe			
#3 Dry eye syndrome, both eyes			
Impression: Had burning reaction to Lumigan and Travaprost (Sept 2012). She has lung cancer and is undergoing treatment so might avoid Timolol, at least initially. Discussed option of trying Xalatan despite prior adverse and she is willing to try.			
Plan: - Try Xioptan, if too expensive will try Xalatan (both scripts given) - recheck 4-6wks, for IOP, will call sooner if not tolerating drops. - Also discussed SLT option - to consider - Preservative free artificial tears 4-6x per day and pm - obtain outside records to check prior IOP			

**Diagnosis**  
 #1 Open angle glaucoma, both eyes  
 #2 Cataract, both eyes  
 #3 Dry eye syndrome, both eyes

**Other / Office Procedure**  
 The following tests have been completed and need interpretation. OCT nerve, Fundus photos  
 The following tests have been completed and need interpretation.  
 Sita visual field  
 Procedural pause conducted to verify: correct patient identity, procedure to be performed and as applicable, correct side and site, correct patient position, and availability of implants, special equipment or special requirements.

**Contributing Authors**

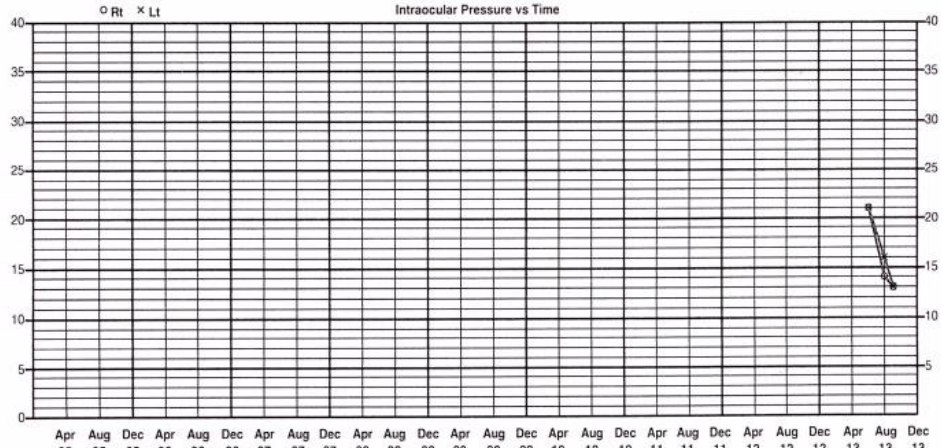
# GL277 4/6

## Life History

Glaucoma  
 Ant segment  
 Retina - laser  
 Retina - other

9/17/2013

Date of Exam	Visual Acuity		IOP		Thickness		Cup / Disc		Glaucoma Drops					Prior Drops	Field	Diurnal	Photo
	Rt	Lt	Rt	Lt	Rt	Lt	Rt	Lt	A	B	P	C	O				
9/17/2013	20 / 60	20 / 40+2	13	13					<input type="checkbox"/>	<input checked="" type="checkbox"/>	<input type="checkbox"/>	<input type="checkbox"/>					
8/8/2013	20 / 50+2	20 / 30+1	14	16			0.8	0.8	<input type="checkbox"/>	<input type="checkbox"/>	<input type="checkbox"/>	<input type="checkbox"/>					x
6/28/2013	20 / 40	20 / 25+2	21	21	600	605	0.8	0.8	<input type="checkbox"/>	<input type="checkbox"/>	<input type="checkbox"/>	<input type="checkbox"/>	Ci 600/605				



	Apr 05	Aug 05	Dec 05	Apr 06	Aug 06	Dec 06	Apr 07	Aug 07	Dec 07	Apr 08	Aug 08	Dec 08	Apr 09	Aug 09	Dec 09	Apr 10	Aug 10	Dec 10	Apr 11	Aug 11	Dec 11	Apr 12	Aug 12	Dec 12	Apr 13	Aug 13	Dec 13	
A																												
B																												
P																												
C																												
O																												

Eye Medication vs Time

Key: A = alpha agonist; B = beta blocker; P = prostaglandin; C = carbonic anhydrase inhibitor; O = other; Rt = Right Eye; Lt = Left Eye

Printed by 10882367 at 21-Jan-2015 10:21  
 Performed at Mayo Clinic in Rochester





MLEB 15-0117  
Rec'd 1-2/15

Mayo  
Clinic

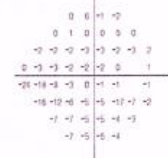
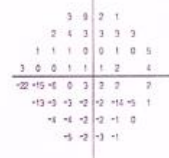
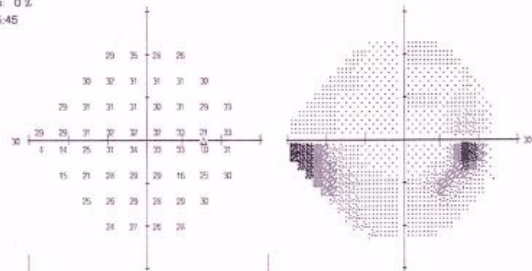
25  
10

Single Field Analysis Eye: Right  
Name: [REDACTED]  
ID: [REDACTED]

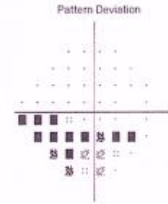
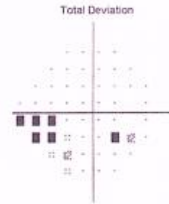
Central 24-2 Threshold Test

Fixation Monitor: Gaze/Blind Spot	Stimulus: Ill. White	Pupil Diameter: 4.2 mm	Date: 08-08-2013
Fixation Target: Central	Background: 31.5 ASB	Visual Acuity: 20/20	Time: 10:13 AM
Fixation Losses: 0/15	Strategy: SITA-Standard	RX: -0.25 DS DC X	Age: 71
False POS Errors: 4 %			
False NEG Errors: 0 %			
Test Duration: 05:45			

Fovea: 35 dB

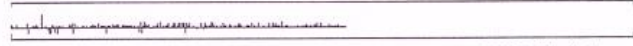


GHT  
Outside normal limits  
VFI: 95%  
MD: -1.05 dB  
PSD: 5.07 dB P < 0.5%



MAYO CLINIC  
ROCHESTER, MN

UNDILATED/WAV



© 2007 Carl Zeiss Meditec  
HFA II 750-12871-4.2.2/4.2.2



May 2013  
HFA II

26 1  
26 1

Single Field Analysis

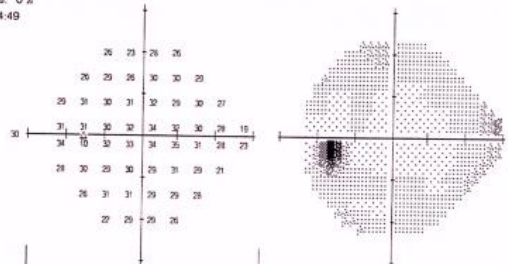
Eye: Left

Name: [REDACTED]

Central 24-2 Threshold Test

Fixation Monitor: Gaze/Blind Spot  
 Fixation Target: Central  
 Fixation Losses: 3/15 xx  
 False POS Errors: 3 %  
 False NEG Errors: 0 %  
 Test Duration: 04:49  
 Fovea: 37 dB

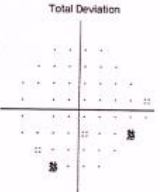
Stimulus: III White  
 Background: 31.5 ASB  
 Strategy: SITA-Standard  
 Pupil Diameter: 4.3 mm  
 Visual Acuity: 20/30  
 RX: -1.00 DS DC X  
 Date: 08-08-2013  
 Time: 10:23 AM  
 Age: 71



1	-3	2	0				
-1	1	-2	1	2	1		
1	3	0	1	1	-1	0	-1
2	0	1	2	0	0	-1	-7
5	1	2	2	4	1	-1	-3
-2	0	-1	-2	-3	-1	-1	-7
-3	1	0	-2	-1	-1		
-7	0	0	-3				

-1	-5	0	-2				
-3	-1	-4	-1	0	-1		
0	1	-2	-1	-1	-2	-3	
0	-2	-1	0	-1	-2	-3	-5
3	-1	0	0	2	-1	-3	-5
-3	-2	-3	-4	-5	-3	-3	
-5	-1	-2	-4	-3	-3		
-3	-2	-2	-3				

\*\*\* Low Test Reliability \*\*\*  
 GHT  
 Outside normal limits  
 VFI 98%  
 MD -0.17 dB  
 PSD 2.41 dB P < 5%



UNDILATED/WAV

MAYO CLINIC  
 ROCHESTER, MN

## References

Ahmadlou, M. and Heimel, J.A. (2015). Preference for concentric orientations in the mouse superior colliculus. *Nature communications* **6**:6773.

Aihara, M., Lindsey, J.D. and Weinreb, R.N. (2003a). Experimental mouse ocular hypertension: establishment of the model. *Investigative ophthalmology & visual science* **44**:4314–4320.

Aihara, M., Lindsey, J.D. and Weinreb, R.N. (2003b). Ocular hypertension in mice with a targeted type I collagen mutation. *Investigative ophthalmology & visual science* **44**:1581–1585.

Allcutt, D., Berry, M. and Sievers, J. (1984). A quantitative comparison of the reactions of retinal ganglion cells to optic nerve crush in neonatal and adult mice. *Brain research* **318**:219–230.

Alward, W.L.M., Fingert, J.H., Coote, M.A., Johnson, A.T., Lerner, S.F., Junqua, D., Durcan, F.J., *et al.* (1998). Clinical Features Associated with Mutations in the Chromosome 1 Open-Angle Glaucoma Gene (GLC1A). *New England Journal of Medicine* [Online] **338**:1022–1027. Available at: <http://dx.doi.org/10.1056/NEJM199804093381503>.

Anctil, J.L. and Anderson, D.R. (1984). Early foveal involvement and generalized depression of the visual field in glaucoma. *Archives of ophthalmology* [Online] **102**:363–70. Available at: <http://www.ncbi.nlm.nih.gov/pubmed/6703983>.

Baker, C.I., Peli, E., Knouf, N. and Kanwisher, N.G. (2005). Reorganization of visual processing in macular degeneration. *Journal of Neuroscience* [Online] **25**:614–618. Available at: <http://www.scopus.com/inward/record.url?eid=2-s2.0-12744253415&partnerID=40&md5=176f8160cb039290e4192c13f2d606e7>.

Banks, M.S., Aslin, R.N. and Letson, R.D. (1975). Sensitive period for the development of human binocular vision. *Science* [Online] **190**:675–677. Available at: <http://www.ncbi.nlm.nih.gov/pubmed/1188363>.

Bavelier, D. and Neville, H.J. (2002). Cross-modal plasticity: where and how? *Nature reviews. Neuroscience* [Online] **3**:443–52. Available at: <http://www.ncbi.nlm.nih.gov/pubmed/12042879>.

Bayer, A.U., Neuhardt, T., May, A.C., Martus, P., Maag, K.P., Brodie, S., Lütjen-Drecoll, E., *et al.* (2001). Retinal morphology and ERG response in the DBA/2NNia mouse model of angle-closure glaucoma. *Investigative Ophthalmology and Visual Science* **42**:1258–1265.

Bear, M.F. and Malenka, R.C. (1994). Synaptic plasticity: LTP and LTD. *Current Opinion in Neurobiology* [Online] **4**:389–399. Available at: <http://www.sciencedirect.com/science/article/pii/0959438894901015>.

Beck, R.W., Bergstrom, T.J. and Lighter, P.R. (1985). A Clinical Comparison of Visual Field Testing With a New Automated Perimeter, the Humphrey Field Analyzer, and the Goldmann Perimeter. *Ophthalmology* [Online] **92**:77–82. Available at: <http://www.sciencedirect.com/science/article/pii/S0161642085340654>.

- Beirowski, B., Babetto, E., Coleman, M.P. and Martin, K.R. (2008). The WldS gene delays axonal but not somatic degeneration in a rat glaucoma model. *The European journal of neuroscience* **28**:1166–1179.
- Bengtsson, B. and Heijl, A. (2000). False-negative responses in glaucoma perimetry: Indicators of patient performance or test reliability? *Investigative Ophthalmology and Visual Science* **41**:2201–2204.
- Berardi, N., Pizzorusso, T. and Maffei, L. (2000). Critical periods during sensory development. *Current Opinion in Neurobiology* **10**:138–145.
- Berkelaar, M., Clarke, D.B., Wang, Y.C., Bray, G.M. and Aguayo, A.J. (1994). Axotomy results in delayed death and apoptosis of retinal ganglion cells in adult rats. *The Journal of neuroscience : the official journal of the Society for Neuroscience* **14**:4368–4374.
- Berridge, M.J., Lipp, P. and Bootman, M.D. (2000). The versatility and universality of calcium signalling. *Nat Rev Mol Cell Biol* [Online] **1**:11–21. Available at: <http://dx.doi.org/10.1038/35036035>.
- Berson, D.M., Dunn, F.A. and Takao, M. (2002). Phototransduction by retinal ganglion cells that set the circadian clock. *Science (New York, N.Y.)* **295**:1070–1073.
- Bien, A., Seidenbecher, C.I., Bockers, T.M., Sabel, B.A. and Kreutz, M.R. (1999). Apoptotic versus necrotic characteristics of retinal ganglion cell death after partial optic nerve injury. *Journal of neurotrauma* **16**:153–163.
- Binley, K.E., Ng, W.S., Tribble, J.R., Song, B. and Morgan, J.E. (2014). Sholl analysis: a quantitative comparison of semi-automated methods. *Journal of neuroscience methods* [Online] **225**:65–70. Available at: <http://www.ncbi.nlm.nih.gov/pubmed/24485871>.
- Birch, M.K., Wishart, P.K. and O'Donnell, N.P. (1995). Determining Progressive Visual Field Loss in Serial Humphrey Visual Fields. *Ophthalmology* [Online] **102**:1227–1235. Available at: <http://www.sciencedirect.com/science/article/pii/S0161642095308858>.
- Birt, C.M., Shin, D.H., Samudrala, V., Hughes, B.A., Kim, C. and Lee, D. (1997). Analysis of Reliability Indices from Humphrey Visual Field Tests in an Urban Glaucoma Population. *Ophthalmology* [Online] **104**:1126–1130. Available at: <http://www.sciencedirect.com/science/article/pii/S0161642097301730>.
- Blais, B.S., Frenkel, M.Y., Kuindersma, S.R., Muhammad, R., Shouval, H.Z., Cooper, L.N. and Bear, M.F. (2008). Recovery from monocular deprivation using binocular deprivation. *Journal of neurophysiology* **100**:2217–2224.
- Van Brussel, L., Gerits, A. and Arckens, L. (2011). Evidence for cross-modal plasticity in adult mouse visual cortex following monocular enucleation. *Cerebral cortex (New York, N.Y. : 1991)* [Online] **21**:2133–46. Available at: <http://www.ncbi.nlm.nih.gov/pubmed/21310780>.
- Buckingham, B.P., Inman, D.M., Lambert, W., Oglesby, E., Calkins, D.J., Steele, M.R., Vetter, M.L., *et al.* (2008). Progressive Ganglion Cell Degeneration Precedes Neuronal Loss in a Mouse Model of Glaucoma. *The Journal of Neuroscience* [Online] **28**:2735–2744. Available at:

<http://www.jneurosci.org/content/28/11/2735.abstract>.

Bui, B. V and Fortune, B. (2004). Ganglion cell contributions to the rat full-field electroretinogram. *The Journal of physiology* **555**:153–173.

Burnstein, Y., Elish, N.J., Magbalon, M. and Higginbotham, E.J. (2000). Comparison of frequency doubling perimetry with Humphrey visual field analysis in a glaucoma practice. *American Journal of Ophthalmology* [Online] **129**:328–333. Available at: <http://www.sciencedirect.com/science/article/pii/S0002939499003645>.

Calford, M.B., Wang, C., Taglianetti, V., Waleszczyk, W.J., Burke, W. and Dreher, B. (2000). Plasticity in adult cat visual cortex (area 17) following circumscribed monocular lesions of all retinal layers. *The Journal of Physiology* [Online] **524**:587–602. Available at: <http://dx.doi.org/10.1111/j.1469-7793.2000.t01-1-00587.x>.

Calkins, D.J. (2013). Age-related changes in the visual pathways: blame it on the axon. *Investigative Ophthalmology & Visual Science* [Online] **54**:ORSF37-41. Available at: <http://www.pubmedcentral.nih.gov/articlerender.fcgi?artid=3864377&tool=pmcentrez&rendertype=abstract>.

Cang, J., Kalatsky, V. a, Löwel, S. and Stryker, M.P. (2005). Optical imaging of the intrinsic signal as a measure of cortical plasticity in the mouse. *Visual neuroscience* [Online] **22**:685–691. Available at: <http://www.ncbi.nlm.nih.gov/pubmed/16332279> <http://www.pubmedcentral.nih.gov/articlerender.fcgi?artid=PMC2553096>.

Carandini, M. and Churchland, A.K. (2013). Probing perceptual decisions in rodents. *Nat Neurosci* [Online] **16**:824–831. Available at: <http://dx.doi.org/10.1038/nn.3410>.

Caroni, P. and Schwab, M.E. (1988). Antibody against myelin associated inhibitor of neurite growth neutralizes nonpermissive substrate properties of CNS white matter. *Neuron* [Online] **1**:85–96. Available at: <http://www.sciencedirect.com/science/article/pii/0896627388902127>.

Chalupa, L.M. ;Williams and R. W. (2008). *Eye, Retina, and Visual System of the Mouse*. 18th ed. Cambridge, Mass, MIT press.

Chauhan, B.C., Garway-Heath, D.F., Goñi, F.J., Rossetti, L., Bengtsson, B., Viswanathan, A.C. and Heijl, A. (2008). Practical recommendations for measuring rates of visual field change in glaucoma. *The British journal of ophthalmology* [Online] **92**:569–73. Available at: <http://bj.o.bmj.com/content/92/4/569.abstract>.

Chen, H., Zhao, Y., Liu, M., Feng, L., Zhen, P., Yi, J., Liang, P., *et al.* (2015). Progressive degeneration of retinal and superior collicular functions in mice with sustained ocular hypertension. *Investigative Ophthalmology and Visual Science* **56**:1971–1984.

Chen, T.-W., Wardill, T.J., Sun, Y., Pulver, S.R., Renninger, S.L., Baohan, A., Schreiter, E.R., *et al.* (2013). Ultrasensitive fluorescent proteins for imaging neuronal activity. *Nature* [Online] **499**:295–300. Available at: <http://dx.doi.org/10.1038/nature12354>.

Chou, T.-H., Park, K.K., Luo, X. and Porciatti, V. (2013). Retrograde Signaling in the Optic Nerve Is Necessary for Electrical Responsiveness of Retinal Ganglion

CellsPERG and Axon Transport. *Investigative Ophthalmology & Visual Science* [Online] **54**:1236–1243. Available at: <http://dx.doi.org/10.1167/iovs.12-11188>.

Coleman, J.E., Law, K. and Bear, M.F. (2009). Anatomical origins of ocular dominance in mouse primary visual cortex. *Neuroscience* **161**:561–571.

Cooke, S.F. and Bear, M.F. (2012). Stimulus-selective response plasticity in the visual cortex: an assay for the assessment of pathophysiology and treatment of cognitive impairment associated with psychiatric disorders. *Biological psychiatry* **71**:487–495.

Crawford, M.L.J., Harwerth, R.S., Smith, E.L., Mills, S. and Ewing, B. (2001). Experimental glaucoma in primates: Changes in cytochrome oxidase blobs in V1 cortex. *Investigative Ophthalmology and Visual Science* **42**:358–364.

Curcio (2013). *Curcio 1990* [Online]. Available at: [https://www.cis.uab.edu/curcio/GanglionCellTopography/Curcio\\_JCompNeurol1990\\_GCtopo\\_F6.xls](https://www.cis.uab.edu/curcio/GanglionCellTopography/Curcio_JCompNeurol1990_GCtopo_F6.xls).

Curcio, C.A. and Allen, K.A. (1990). Topography of ganglion cells in human retina. *The Journal of comparative neurology* **300**:5–25.

Curcio, C.A. and Drucker, D.N. (1993). Retinal ganglion cells in Alzheimer's disease and aging. *Annals of neurology* **33**:248–57.

Cusick, C.G. and Lund, R.D. (1981). The distribution of the callosal projection to the occipital visual cortex in rats and mice. *Brain Research* **214**:239–259.

Dacey, D.M. (1993). The mosaic of midget ganglion cells in the human retina. *The Journal of neuroscience : the official journal of the Society for Neuroscience* **13**:5334–5355.

Dacey, D.M. and Petersen, M.R. (1992). Dendritic field size and morphology of midget and parasol ganglion cells of the human retina. *Proceedings of the National Academy of Sciences of the United States of America* **89**:9666–9670.

Dai, H., Morelli, J.N., Ai, F., Yin, D., Hu, C., Xu, D. and Li, Y. (2013). Resting-state functional MRI: Functional connectivity analysis of the visual cortex in primary open-angle glaucoma patients. *Human Brain Mapping* **34**:2455–2463.

Dana, H., Chen, T.-W., Hu, A., Shields, B.C., Guo, C., Looger, L.L., Kim, D.S., *et al.* (2014). Thy1-GCaMP6 Transgenic Mice for Neuronal Population Imaging In Vivo. *PLoS ONE* [Online] **9**:e108697. Available at: <http://dx.doi.org/10.1371/journal.pone.0108697>.

Danias, J., Lee, K.C., Zamora, M.F., Chen, B., Shen, F., Filippopoulos, T., Su, Y., *et al.* (2003). Quantitative Analysis of Retinal Ganglion Cell (RGC) Loss in Aging DBA/2NNia Glaucomatous Mice: Comparison with RGC Loss in Aging C57/BL6 Mice. *Investigative Ophthalmology and Visual Science* **44**:5151–5162.

Darian-Smith, C. and Gilbert, C.D. (1994). Axonal sprouting accompanies functional reorganization in adult cat striate cortex. *Nature* **368**:737–740.

Davies, V.J., Hollins, A.J., Piechota, M.J., Yip, W., Davies, J.R., White, K.E., Nicols, P.P., *et al.* (2007). Opa1 deficiency in a mouse model of autosomal dominant optic atrophy impairs mitochondrial morphology, optic nerve structure and visual

function. *Human Molecular Genetics* **16**:1307–1318.

Denk, W. and Horstmann, H. (2004). Serial block-face scanning electron microscopy to reconstruct three-dimensional tissue nanostructure. *PLoS Biology* **2**.

Denk, W., Strickler, J.H. and Webb, W.W. (1990). Two-photon laser scanning fluorescence microscopy. *Science* [Online] **248**:73–76. Available at: <http://www.sciencemag.org/content/248/4951/73.abstract>.

Devaney, K.O. and Johnson, H. a (1980). Neuron loss in the aging visual cortex of man. *Journal of gerontology* [Online] **35**:836–41. Available at: <http://www.ncbi.nlm.nih.gov/pubmed/7440924>.

Dombeck, D.A., Khabbaz, A.N., Collman, F., Adelman, T.L. and Tank, D.W. (2015). Imaging Large-Scale Neural Activity with Cellular Resolution in Awake, Mobile Mice. *Neuron* [Online] **56**:43–57. Available at: <http://dx.doi.org/10.1016/j.neuron.2007.08.003>.

Doroudchi, M.M., Greenberg, K.P., Liu, J., Silka, K. a, Boyden, E.S., Lockridge, J. a, Arman, a C., *et al.* (2011). Virally delivered channelrhodopsin-2 safely and effectively restores visual function in multiple mouse models of blindness. *Molecular therapy* **19**:1220–9.

Drager, U.C. (1975). Receptive fields of single cells and topography in mouse visual cortex. *J Comp Neurol* [Online] **160**:269–290. Available at: <http://www.ncbi.nlm.nih.gov/pubmed/1112925>.

Dräger, U.C. and Olsen, J.F. (1980). Origins of crossed and uncrossed retinal projections in pigmented and albino mice. *The Journal of Comparative Neurology* [Online] **191**:383–412. Available at: <http://dx.doi.org/10.1002/cne.901910306>.

Dumitriu, D., Rodriguez, A. and Morrison, J.H. (2011). High-throughput, detailed, cell-specific neuroanatomy of dendritic spines using microinjection and confocal microscopy. *Nature protocols* [Online] **6**:1391–1411. Available at: <http://www.pubmedcentral.nih.gov/articlerender.fcgi?artid=3566769&tool=pmcentrez&rendertype=abstract>.

Duncan, R.O., Sample, P.A., Weinreb, R.N., Bowd, C. and Zangwill, L.M. (2007). Retinotopic organization of primary visual cortex in glaucoma: A method for comparing cortical function with damage to the optic disk. *Investigative Ophthalmology and Visual Science* **48**:733–744.

Feinberg, E.H. and Meister, M. (2015). Orientation columns in the mouse superior colliculus. *Nature* [Online] **519**:229–232. Available at: <http://dx.doi.org/10.1038/nature14103>.

Feng, L., Zhao, Y., Yoshida, M., Chen, H., Yang, J.F., Kim, T.S., Cang, J., *et al.* (2013). Sustained Ocular Hypertension Induces Dendritic Degeneration of Mouse Retinal Ganglion Cells That Depends on Cell Type and Location. *Investigative Ophthalmology & Visual Science* [Online] **54**:1106–1117. Available at: <http://www.ncbi.nlm.nih.gov/pmc/articles/PMC3567754/>.

Fitzgerald, M., Bartlett, C. a, Harvey, A.R. and Dunlop, S. a (2010). Early events of secondary degeneration after partial optic nerve transection: an immunohistochemical study. *Journal of neurotrauma* **27**:439–452.

- Fitzgibbon, T. and Taylor, S.F. (1996). Retinotopy of the human retinal nerve fibre layer and optic nerve head. *The Journal of comparative neurology* **375**:238–251.
- Forrester J. V., Dick A. D., McMenamin P. G., Roberts F., P.E. (2016). *The Eye: Basic Sciences in Practice*. Available at: <http://linkinghub.elsevier.com/retrieve/pii/B9780702055546000101>.
- Fox, M.W. (1965). The visual cliff test for the study of visual depth perception in the mouse. *Animal Behaviour* [Online] **13**:232–IN3. Available at: <http://www.sciencedirect.com/science/article/pii/0003347265900400>.
- Francois, J. (1980). Congenital glaucoma and its inheritance. *Ophthalmologica. Journal international d'ophtalmologie. International journal of ophthalmology. Zeitschrift fur Augenheilkunde* **181**:61–73.
- Frenkel, M.Y. and Bear, M.F. (2004). How monocular deprivation shifts ocular dominance in visual cortex of young mice. *Neuron* **44**:917–923.
- Frenkel, M.Y., Sawtell, N.B., Diogo, A.C.M., Yoon, B., Neve, R.L. and Bear, M.F. (2006). Instructive Effect of Visual Experience in Mouse Visual Cortex. *Neuron* **51**:339–349.
- Fu, Q., Li, X., Shi, J., Xu, G., Wen, W., Lee, D.S. and So, K.-F. (2009). Synaptic Degeneration of Retinal Ganglion Cells in a Rat Ocular Hypertension Glaucoma Model. *Cellular and Molecular Neurobiology* [Online] **29**:575–581. Available at: <http://dx.doi.org/10.1007/s10571-009-9349-7>.
- Fujikawa, K., Iwata, T., Inoue, K., Akahori, M., Kadotani, H., Fukaya, M., Watanabe, M., *et al.* (2010). VAV2 and VAV3 as candidate disease genes for spontaneous glaucoma in mice and humans. *PloS one* **5**:e9050.
- G. A. Cioffi, M. (2016). *Aao.org*. [Online]. Available at: <http://www.aao.org/image/i-arcuate-scotoma-i> [Accessed: 2 January 2017].
- Gallego, B.I., Salazar, J.J., de Hoz, R., Rojas, B., Ramírez, A.I., Salinas-Navarro, M., Ortín-Martínez, A., *et al.* (2012). IOP induces upregulation of GFAP and MHC-II and microglia reactivity in mice retina contralateral to experimental glaucoma. *Journal of neuroinflammation* **9**:92.
- Garaschuk, O., Milos, R.-I. and Konnerth, A. (2006). Targeted bulk-loading of fluorescent indicators for two-photon brain imaging in vivo. *Nat. Protocols* [Online] **1**:380–386. Available at: <http://dx.doi.org/10.1038/nprot.2006.58>.
- Garcia-Valenzuela, E., Shareef, S., Walsh, J. and Sharma, S.C. (1995). Programmed cell death of retinal ganglion cells during experimental glaucoma. *Experimental Eye Research* [Online] **61**:33–44. Available at: <http://www.sciencedirect.com/science/article/pii/S0014483595800565>.
- Garrett, M.E., Nauhaus, I., Marshel, J.H. and Callaway, E.M. (2014). Topography and areal organization of mouse visual cortex. *The Journal of neuroscience : the official journal of the Society for Neuroscience* **34**:12587–12600.
- Gellrich, N.-C., Schimming, R., Zerfowski, M. and Eysel, U.T. (2002). Quantification of histological changes after calibrated crush of the intraorbital optic nerve in rats. *The British journal of ophthalmology* [Online] **86**:233–7. Available at: <http://www.pubmedcentral.nih.gov/articlerender.fcgi?artid=1771007&tool=pmcentre>



z&rendertype=abstract.

Geng, Y., Schery, L.A., Sharma, R., Dubra, A., Ahmad, K., Libby, R.T. and Williams, D.R. (2011). Optical properties of the mouse eye. *Biomedical Optics Express* [Online] **2**:717–738. Available at: <http://www.ncbi.nlm.nih.gov/pmc/articles/PMC3072116/>.

Gilbert, C.D. and Li, W. (2012). Adult Visual Cortical Plasticity. *Neuron* [Online] **75**:250–264. Available at: <http://www.sciencedirect.com/science/article/pii/S0896627312005922>.

Gilpin, L.B., Stewart, W.C., Hunt, H.H. and Broom, C.D. (1990). Threshold variability using different Goldmann stimulus sizes. *Acta Ophthalmologica* [Online] **68**:674–676. Available at: <http://dx.doi.org/10.1111/j.1755-3768.1990.tb01692.x>.

Glovinsky, Y., Quigley, H. a and Dunkelberger, G.R. (1991). Retinal ganglion cell loss is size dependent in experimental glaucoma. *Investigative ophthalmology & visual science* [Online] **32**:484–91. Available at: <http://www.ncbi.nlm.nih.gov/pubmed/2001923>.

Glovinsky, Y., Quigley, H. a and Pease, M.E. (1993). Foveal ganglion cell loss is size dependent in experimental glaucoma. *Investigative ophthalmology & visual science* [Online] **34**:395–400. Available at: <http://www.ncbi.nlm.nih.gov/pubmed/8440594>.

Gordon, J.A. and Stryker, M.P. (1996). Experience-Dependent Plasticity of Binocular Responses in the Primary Visual Cortex of the Mouse. *The Journal of Neuroscience* [Online] **16**:3274–3286. Available at: <http://www.jneurosci.org/content/16/10/3274.abstract>.

Greifzu, F., Pielecka-Fortuna, J., Kalogeraki, E., Krempler, K., Favaro, P.D., Schlüter, O.M. and Löwel, S. (2014). Environmental enrichment extends ocular dominance plasticity into adulthood and protects from stroke-induced impairments of plasticity. *Proceedings of the National Academy of Sciences* [Online] **111**:1150–1155. Available at: <http://www.pnas.org/content/111/3/1150.abstract>.

Grienberger, C. and Konnerth, A. (2012). Imaging Calcium in Neurons. *Neuron* [Online] **73**:862–885. Available at: <http://www.sciencedirect.com/science/article/pii/S0896627312001729>.

Grinvald, A., Lieke, E., Frostig, R.D., Gilbert, C.D. and Wiesel, T.N. (1986). Functional architecture of cortex revealed by optical imaging of intrinsic signals. *Nature* [Online] **324**:361–364. Available at: <http://www.scopus.com/inward/record.url?eid=2-s2.0-0022997296&partnerID=40&md5=52127641d91b5b202a2ac0670196e1a3>.

Gupta, N., Ang, L.-C.C., Noël de Tilly, L., Bidaisee, L. and Yücel, Y.H. (2006). Human glaucoma and neural degeneration in intracranial optic nerve, lateral geniculate nucleus, and visual cortex. *The British journal of ophthalmology* [Online] **90**:674–8. Available at: <http://www.pubmedcentral.nih.gov/articlerender.fcgi?artid=1860237&tool=pmcentrez&rendertype=abstract%5Cnhttp://www.ncbi.nlm.nih.gov/pubmed/16464969%5Cnhttp://bjo.bmj.com/cgi/doi/10.1136/bjo.2005.086769>.

Gupta, N., Greenberg, G., de Tilly, L.N., Gray, B., Polemidiotis, M. and Yücel, Y.H.

(2009). Atrophy of the lateral geniculate nucleus in human glaucoma detected by magnetic resonance imaging. *The British journal of ophthalmology* [Online] **93**:56–60. Available at: <http://www.pubmedcentral.nih.gov/articlerender.fcgi?artid=2605243&tool=pmcentrez&rendertype=abstract>.

Gupta, N. and Yücel, Y.H. (2007). Glaucoma as a neurodegenerative disease. *Current Opinion in Ophthalmology* [Online] **18**. Available at: [http://journals.lww.com/ophthalmology/Fulltext/2007/03000/Glaucoma\\_as\\_a\\_neurodegenerative\\_disease.4.aspx](http://journals.lww.com/ophthalmology/Fulltext/2007/03000/Glaucoma_as_a_neurodegenerative_disease.4.aspx).

Hallum, L.E., Chen, S.C., Cloherty, S.L., Morley, J.W., Suaning, G.J. and Lovell, N.H. (2006). Functional Optical Imaging of Intrinsic Signals in Cerebral Cortex. In: *Wiley Encyclopedia of Biomedical Engineering*. John Wiley & Sons, Inc. Available at: <http://dx.doi.org/10.1002/9780471740360.ebs1588>.

Harauzov, A., Spolidoro, M., DiCristo, G., De Pasquale, R., Cancedda, L., Pizzorusso, T., Viegi, A., *et al.* (2010). Reducing intracortical inhibition in the adult visual cortex promotes ocular dominance plasticity. *The Journal of neuroscience : the official journal of the Society for Neuroscience* **30**:361–371.

Harman, a, Abrahams, B., Moore, S. and Hoskins, R. (2000). Neuronal density in the human retinal ganglion cell layer from 16-77 years. *The Anatomical record* **260**:124–131.

Hattar, S., Liao, H.W., Takao, M., Berson, D.M. and Yau, K.W. (2002). Melanopsin-containing retinal ganglion cells: architecture, projections, and intrinsic photosensitivity. *Science (New York, N.Y.)* **295**:1065–1070.

He, H.-Y., Hodos, W. and Quinlan, E.M. (2006). Visual Deprivation Reactivates Rapid Ocular Dominance Plasticity in Adult Visual Cortex. *The Journal of Neuroscience* [Online] **26**:2951–2955. Available at: <http://www.jneurosci.org/content/26/11/2951.abstract>.

Heimel, J.A., Hartman, R.J., Hermans, J.M. and Levelt, C.N. (2007). Screening mouse vision with intrinsic signal optical imaging. *The European journal of neuroscience* **25**:795–804.

Hofbauer, A. and Dräger, U.C. (1985). Depth segregation of retinal ganglion cells projecting to mouse superior colliculus. *The Journal of Comparative Neurology* [Online] **234**:465–474. Available at: <http://dx.doi.org/10.1002/cne.902340405>.

Hofer, S.B., Mrsic-Flogel, T.D., Bonhoeffer, T. and Hubener, M. (2006). Prior experience enhances plasticity in adult visual cortex. *Nat Neurosci* [Online] **9**:127–132. Available at: <http://dx.doi.org/10.1038/nn1610>.

Hofer, S.B., Mrsic-Flogel, T.D., Bonhoeffer, T. and Hübener, M. (2006). Lifelong learning: ocular dominance plasticity in mouse visual cortex. *Current Opinion in Neurobiology* **16**:451–459.

Howell, G.R., Libby, R.T., Jakobs, T.C., Smith, R.S., Phalan, F.C., Barter, J.W., Barbay, J.M., *et al.* (2007). Axons of retinal ganglion cells are insulated in the optic nerve early in DBA/2J glaucoma. *The Journal of Cell Biology* [Online] **179**:1523–1537. Available at: <http://jcb.rupress.org/content/179/7/1523.abstract>.

- Hoyt, W.F., Frisen, L. and Newman, N.M. (1973). Fundoscopy of Nerve Fiber Layer Defects in Glaucoma. *Investigative Ophthalmology & Visual Science* **12**:814–829.
- Huang, S., Gu, Y., Quinlan, E.M. and Kirkwood, A. (2010). A Refractory Period for Rejuvenating GABAergic Synaptic Transmission and Ocular Dominance Plasticity with Dark Exposure. *Journal of Neuroscience* [Online] **30**:16636–16642. Available at: <http://www.jneurosci.org/cgi/doi/10.1523/JNEUROSCI.4384-10.2010> %5Cnpapers2://publication/doi/10.1523/JNEUROSCI.4384-10.2010.
- Huang, Z.J., Kirkwood, A., Pizzorusso, T., Porciatti, V., Morales, B., Bear, M.F., Maffei, L., *et al.* (1999). BDNF regulates the maturation of inhibition and the critical period of plasticity in mouse visual cortex. *Cell* **98**:739–755.
- Hubel, D.H. (1988). Eye, brain, and vision (Scientific American Library). *New York*.
- Hubel, D.H. and Wiesel, T.N. (1968). Receptive fields and functional architecture of monkey striate cortex. *The Journal of physiology* **195**:215–243.
- Hubel, D.H., Wiesel, T.N. and LeVay, S. (1977). Plasticity of Ocular Dominance Columns in Monkey Striate Cortex. *Philosophical Transactions of the Royal Society of London B: Biological Sciences* [Online] **278**:377–409. Available at: <http://rsta.royalsocietypublishing.org/content/278/961/377.abstract>.
- Huber, D., Gutnisky, D.A., Peron, S., O'Connor, D.H., Wiegert, J.S., Tian, L., Oertner, T.G., *et al.* (2012). Multiple dynamic representations in the motor cortex during sensorimotor learning. *Nature* [Online] **484**:473–478. Available at: <http://dx.doi.org/10.1038/nature11039>.
- Ito, Y.A., Belforte, N., Cueva Vargas, J.L. and Di Polo, A. (2016). A Magnetic Microbead Occlusion Model to Induce Ocular Hypertension-Dependent Glaucoma in Mice. *Journal of visualized experiments : JoVE*.
- Jakobs, T.C., Libby, R.T., Ben, Y., John, S.W.M. and Masland, R.H. (2005). Retinal ganglion cell degeneration is topological but not cell type specific in DBA/2J mice. *The Journal of cell biology* **171**:313–325.
- Jeon, C.-J., Strettoi, E. and Masland, R.H. (1998). The Major Cell Populations of the Mouse Retina. *The Journal of Neuroscience* [Online] **18**:8936–8946. Available at: <http://www.jneurosci.org/content/18/21/8936.abstract>.
- Jia, H., Rochefort, N.L., Chen, X. and Konnerth, A. (2011). In vivo two-photon imaging of sensory-evoked dendritic calcium signals in cortical neurons. *Nat. Protocols* [Online] **6**:28–35. Available at: <http://dx.doi.org/10.1038/nprot.2010.169>.
- John, S.W., Smith, R.S., Savinova, O. V, Hawes, N.L., Chang, B., Turnbull, D., Davisson, M., *et al.* (1998). Essential iris atrophy, pigment dispersion, and glaucoma in DBA/2J mice. *Investigative ophthalmology & visual science* **39**:951–962.
- Johnson, C.A., Keltner, J.L., Cello, K.E., Edwards, M., Kass, M.A., Gordon, M.O., Budenz, D.L., *et al.* (2002). Baseline visual field characteristics in the ocular hypertension treatment study. *Ophthalmology* [Online] **109**:432–437. Available at: <http://www.sciencedirect.com/science/article/pii/S0161642001009484>.
- Johnson, C.A. and Samuels, S.J. (1997). Screening for glaucomatous visual field loss with frequency-doubling perimetry. *Investigative Ophthalmology and Visual Science* **38**:413–425.

Jonas, J.B., Berenshtein, E. and Holbach, L. (2003). Anatomic Relationship between Lamina Cribrosa, Intraocular Space, and Cerebrospinal Fluid Space. *Investigative Ophthalmology & Visual Science* [Online] **44**:5189–5195. Available at: <http://dx.doi.org/10.1167/iovs.03-0174>.

Kaas, J.H., Krubitzer, L.A., Chino, Y.M., Langston, A.L., Polley, E.H. and Blair, N. (1990). Reorganization of retinotopic cortical maps in adult mammals after lesions of the retina. *Science (New York, N.Y.)* **248**:229–231.

Kalatsky, V.A. and Stryker, M.P. (2003). New Paradigm for Optical Imaging: Temporally Encoded Maps of Intrinsic Signal. *Neuron* [Online] **38**:529–545. Available at: <http://www.sciencedirect.com/science/article/pii/S0896627303002861>.

Kaneko, M., Stellwagen, D., Malenka, R.C. and Stryker, M.P. (2008). Tumor necrosis factor-alpha mediates one component of competitive, experience-dependent plasticity in developing visual cortex. *Neuron* [Online] **58**:673–80. Available at: <http://www.pubmedcentral.nih.gov/articlerender.fcgi?artid=2884387&tool=pmcentrez&rendertype=abstract>.

Kaplan, E.S., Cooke, S.F., Komorowski, R.W., Chubykin, A.A., Thomazeau, A., Khibnik, L.A., Gavornik, J.P., *et al.* (2016). Contrasting roles for parvalbumin-expressing inhibitory neurons in two forms of adult visual cortical plasticity Mrsic-Flogel, T. D. (ed.). *eLife* [Online] **5**:e11450. Available at: <https://dx.doi.org/10.7554/eLife.11450>.

Kass, M.A., Heuer, D.K., Higginbotham, E.J., Johnson, C.A., Keltner, J.L., Miller, J.P., Parrish, R.K., *et al.* (2002). The Ocular Hypertension Treatment Study: a randomized trial determines that topical ocular hypotensive medication delays or prevents the onset of primary open-angle glaucoma. *Archives of ophthalmology* [Online] **120**:701-713-830. Available at: <http://archophth.jamanetwork.com/article.aspx?doi=10.1001/archophth.120.6.701>.

Katz, L.C. and Crowley, J.C. (2002). Development of cortical circuits: lessons from ocular dominance columns. *Nature reviews. Neuroscience* [Online] **3**:34–42. Available at: <http://www.ncbi.nlm.nih.gov/pubmed/11823803>.

Kawakami, R., Sawada, K., Sato, A., Hibi, T., Kozawa, Y., Sato, S., Yokoyama, H., *et al.* (2013). Visualizing hippocampal neurons with in vivo two-photon microscopy using a 1030 nm picosecond pulse laser. *Sci. Rep.* [Online] **3**. Available at: <http://dx.doi.org/10.1038/srep01014>.

Keck, T., Keller, G.B., Jacobsen, R.I., Eysel, U.T., Bonhoeffer, T. and Hübener, M. (2015). Synaptic Scaling and Homeostatic Plasticity in the Mouse Visual Cortex In Vivo. *Neuron* [Online] **80**:327–334. Available at: <http://dx.doi.org/10.1016/j.neuron.2013.08.018>.

Keck, T., Mrsic-Flogel, T.D., Vaz Afonso, M., Eysel, U.T., Bonhoeffer, T. and Hübener, M. (2008). Massive restructuring of neuronal circuits during functional reorganization of adult visual cortex. *Nat Neurosci* [Online] **11**:1162–1167. Available at: <http://dx.doi.org/10.1038/nn.2181>.

Keck, T., Scheuss, V., Jacobsen, R.I., Wierenga, C.J., Eysel, U.T., Bonhoeffer, T. and Hübener, M. (2011). Loss of Sensory Input Causes Rapid Structural Changes of Inhibitory Neurons in Adult Mouse Visual Cortex. *Neuron* [Online] **71**:869–882.

Available at: <http://www.sciencedirect.com/science/article/pii/S0896627311005642>.

Kepecs, A. and Fishell, G. (2014). Interneuron cell types are fit to function. *Nature* [Online] **505**:318–326. Available at: <http://www.nature.com/doifinder/10.1038/nature12983>.

Kerlin, A.M., Andermann, M.L., Berezovskii, V.K. and Reid, R.C. (2010). Broadly Tuned Response Properties of Diverse Inhibitory Neuron Subtypes in Mouse Visual Cortex. *Neuron* **67**:858–871.

Kerrigan–Baumrind, L.A., Quigley, H.A., Pease, M.E., Kerrigan, D.F. and Mitchell, R.S. (2000). Number of Ganglion Cells in Glaucoma Eyes Compared with Threshold Visual Field Tests in the Same Persons. *Investigative Ophthalmology & Visual Science* **41**:741–748.

Kerrigan, L.A., Zack, D.J., Quigley, H.A., Smith, S.D., Pease, M.E., LA, K., DJ, Z., *et al.* (1997). TUNEL-positive ganglion cells in human primary open-angle glaucoma. *Archives of ophthalmology (Chicago, Ill. : 1960)* [Online] **115**:1031–1035. Available at: <http://dx.doi.org/10.1001/archoph.1997.01100160201010>.

Kingman, S. (2004). Glaucoma is second leading cause of blindness globally. *Bulletin of the World Health Organization* [Online] **82**:887–888. Available at: <http://www.ncbi.nlm.nih.gov/pmc/articles/PMC2623060/>.

Klöcker, N., Zerfowski, M., Gellrich, N.C. and Bähr, M. (2001). Morphological and functional analysis of an incomplete CNS fiber tract lesion: Graded crush of the rat optic nerve. *Journal of Neuroscience Methods* **110**:147–153.

Kobat, D., Horton, N.G. and Xu, C. (2011). In vivo two-photon microscopy to 1.6-mm depth in mouse cortex. *Journal of Biomedical Optics* [Online] **16**:106014. Available at: <http://dx.doi.org/10.1117/1.3646209>.

Kolb, H. (1995). Gross Anatomy of the Eye. In: Kolb, H., Fernandez, E. and Nelson, R. (eds.) Salt Lake City (UT).

Kolb, H., Linberg, K. a and Fisher, S.K. (1992). Neurons of the human retina: a Golgi study. *The Journal of comparative neurology* **318**:147–187.

Kuhlman, S.J., Tring, E. and Trachtenberg, J.T. (2011). Fast-spiking interneurons have an initial orientation bias that is lost with vision. *Nature neuroscience* [Online] **14**:1121–1123. Available at: <http://dx.doi.org/10.1038/nn.2890>.

Laaris, N., Carlson, G.C. and Keller, A. (2000). Thalamic-evoked synaptic interactions in barrel cortex revealed by optical imaging. *The Journal of neuroscience : the official journal of the Society for Neuroscience* **20**:1529–1537.

Lawson, L.J., Frost, L., Risbridger, J., Fearn, S. and Perry, V.H. (1994). Quantification of the mononuclear phagocyte response to Wallerian degeneration of the optic nerve. *Journal of neurocytology* **23**:729–744.

Le, P. V, Tan, O., Chopra, V., Francis, B.A., Ragab, O., Varma, R. and Huang, D. (2013). Regional Correlation Among Ganglion Cell Complex, Nerve Fiber Layer, and Visual Field Loss in Glaucoma. *Investigative Ophthalmology & Visual Science* [Online] **54**:4287–4295. Available at: <http://www.ncbi.nlm.nih.gov/pmc/articles/PMC3691052/>.

- Lee, S.C.S., Weltzien, F., Madigan, M.C., Martin, P.R. and Gr??nert, U. (2016). Identification of AII amacrine, displaced amacrine, and bistratified ganglion cell types in human retina with antibodies against calretinin. *Journal of Comparative Neurology* **524**:39–53.
- Lehmann, K. and Lowel, S. (2008). Age-dependent ocular dominance plasticity in adult mice. *PLoS one* **3**:e3120.
- Lehmann, K., Schmidt, K.F. and Löwel, S. (2012). Vision and visual plasticity in ageing mice. *Restorative Neurology and Neuroscience* **30**:161–178.
- Lei, Y., Garrahan, N., Hermann, B., Becker, D.L., Hernandez, M.R., Boulton, M.E. and Morgan, J.E. (2008). Quantification of retinal transneuronal degeneration in human glaucoma: A novel multiphoton-DAPI approach. *Investigative Ophthalmology and Visual Science* **49**:1940–1945.
- Leung, C.K.S., Chan, W.-M., Yung, W.-H., Ng, A.C.K., Woo, J., Tsang, M.-K. and Tse, R.K.K. (2005). Comparison of macular and peripapillary measurements for the detection of glaucoma: An Optical Coherence Tomography study. *Ophthalmology* [Online] **112**:391–400. Available at: <http://www.sciencedirect.com/science/article/pii/S0161642004016549>.
- Levkovitch-Verbin, H., Dardik, R., Vander, S. and Melamed, S. (2010). Mechanism of retinal ganglion cells death in secondary degeneration of the optic nerve. *Experimental Eye Research* [Online] **91**:127–134. Available at: <http://www.sciencedirect.com/science/article/pii/S0014483509003431>.
- Levkovitch-Verbin, H., Quigley, H.A., Kerrigan-Baumrind, L.A., D’Anna, S.A., Kerrigan, D. and Pease, M.E. (2001). Optic nerve transection in monkeys may result in secondary degeneration of retinal ganglion cells. *Investigative ophthalmology & visual science* **42**:975–982.
- Li, Y., Schlamp, C.L. and Nickells, R.W. (1999). Experimental induction of retinal ganglion cell death in adult mice. *Investigative ophthalmology & visual science* **40**:1004–1008.
- Libby, R.T., Anderson, M.G., Pang, I.-H., Robinson, Z.H., Savinova, O. V, Cosma, I.M., Snow, A., *et al.* (2005). Inherited glaucoma in DBA/2J mice: pertinent disease features for studying the neurodegeneration. *Visual neuroscience* **22**:637–648.
- Libby, R.T., Gould, D.B., Anderson, M.G. and John, S.W.M. (2005). Complex genetics of glaucoma susceptibility. *Annual Review of Genomics and Human Genetics* [Online] **6**:15–44. Available at: <http://dx.doi.org/10.1146/annurev.genom.6.080604.162209>.
- de Lima, S., Koriyama, Y., Kurimoto, T., Oliveira, J.T., Yin, Y., Li, Y., Gilbert, H.-Y., *et al.* (2012). Full-length axon regeneration in the adult mouse optic nerve and partial recovery of simple visual behaviors. *Proceedings of the National Academy of Sciences of the United States of America* [Online] **109**:9149–54. Available at: <http://www.pubmedcentral.nih.gov/articlerender.fcgi?artid=3384191&tool=pmcentrez&rendertype=abstract>.
- Liu, M., Duggan, J., Salt, T.E. and Cordeiro, M.F. (2011). Dendritic changes in visual pathways in glaucoma and other neurodegenerative conditions. *Experimental Eye Research* [Online] **92**:244–250. Available at:

<http://www.sciencedirect.com/science/article/pii/S0014483511000340>.

Lorber, B., Tassoni, A., Bull, N.D., Moschos, M.M. and Martin, K.R. (2012). Retinal ganglion cell survival and axon regeneration in WldS transgenic rats after optic nerve crush and lens injury. *BMC neuroscience* **13**:56.

Lucius, R., Gallinat, S., Rosenstiel, P., Herdegen, T., Sievers, J. and Unger, T. (1998). The angiotensin II type 2 (AT2) receptor promotes axonal regeneration in the optic nerve of adult rats. *The Journal of experimental medicine* [Online] **188**:661–70. Available at:

<http://www.pubmedcentral.nih.gov/articlerender.fcgi?artid=2213348&tool=pmcentrez&rendertype=abstract>.

Mabuchi, F., Aihara, M., Mackey, M.R., Lindsey, J.D. and Weinreb, R.N. (2003). Optic nerve damage in experimental mouse ocular hypertension. *Investigative ophthalmology & visual science* **44**:4321–4330.

Mabuchi, F., Lindsey, J.D., Aihara, M., Mackey, M.R. and Weinreb, R.N. (2004). Optic nerve damage in mice with a targeted type I collagen mutation. *Investigative ophthalmology & visual science* **45**:1841–1845.

Maguire, E.A., Gadian, D.G., Johnsrude, I.S., Good, C.D., Ashburner, J., Frackowiak, R.S.J. and Frith, C.D. (2000). Navigation-related structural change in the hippocampi of taxi drivers. *Proceedings of the National Academy of Sciences* [Online] **97**:4398–4403. Available at:

<http://www.pnas.org/content/97/8/4398.abstract>.

Mangini, N.J. and Pearlman, A.L. (1980). Laminar distribution of receptive field properties in the primary visual cortex of the mouse. *The Journal of comparative neurology* **193**:203–222.

Masuda, Y., Dumoulin, S.O., Nakadomari, S. and Wandell, B.A. (2008). V1 projection zone signals in human macular degeneration depend on task, not stimulus. *Cerebral Cortex* **18**:2483–2493.

May, C.A. and Lutjen-Drecoll, E. (2002). Morphology of the murine optic nerve. *Investigative ophthalmology & visual science* **43**:2206–2212.

May, P.J. (2006). The mammalian superior colliculus: laminar structure and connections. *Progress in brain research* **151**:321–378.

Maya Vetencourt, J.F., Sale, A., Viegi, A., Baroncelli, L., De Pasquale, R., O’Leary, O.F., Castrén, E., *et al.* (2008). The antidepressant fluoxetine restores plasticity in the adult visual cortex. *Science (New York, N.Y.)* [Online] **320**:385–8. Available at: <http://www.ncbi.nlm.nih.gov/pubmed/18420937>.

McDougal, D.H. and Gamlin, P.D. (2010). The influence of intrinsically-photosensitive retinal ganglion cells on the spectral sensitivity and response dynamics of the human pupillary light reflex. *Vision research* **50**:72–87.

McKinnon, S.J., Schlamp, C.L. and Nickells, R.W. (2009). Mouse models of retinal ganglion cell death and glaucoma. *Experimental eye research* [Online] **88**:816–824. Available at: <http://www.ncbi.nlm.nih.gov/pmc/articles/PMC3056071/>.

McLaughlin, T. and O’Leary, D.D.M. (2005). Molecular gradients and development of retinotopic maps. *Annual Review of Neuroscience* [Online] **28**:327–55. Available

at:

<http://www.annualreviews.org/doi/abs/10.1146/annurev.neuro.28.061604.135714%5Cnhttp://www.ncbi.nlm.nih.gov/pubmed/16022599>.

Merzenich, M.M., Kaas, J.H., Wall, J., Nelson, R.J., Sur, M. and Felleman, D. (1983). Topographic reorganization of somatosensory cortical areas 3b and 1 in adult monkeys following restricted deafferentation. *Neuroscience* [Online] **8**:33–55. Available at: <http://www.sciencedirect.com/science/article/pii/0306452283900246>.

Metin, C., Godement, P. and Imbert, M. (1988). The primary visual cortex in the mouse: receptive field properties and functional organization. *Experimental brain research* **69**:594–612.

Meyer-Rüsenberg, B., Pavlidis, M., Stupp, T. and Thanos, S. (2006). Pathological changes in human retinal ganglion cells associated with diabetic and hypertensive retinopathy. *Graefe's Archive for Clinical and Experimental Ophthalmology* [Online] **245**:1009–1018. Available at: <http://dx.doi.org/10.1007/s00417-006-0489-x>.

Mikelberg, F.S., Yidegiligne, H.M. and Schulzer, M. (1995). Optic nerve axon count and axon diameter in patients with ocular hypertension and normal visual fields. *Ophthalmology* [Online] **102**:342–348. Available at: <http://www.ncbi.nlm.nih.gov/pubmed/7862423>.

Minckler, D.S., Bunt, A.H. and Johanson, G.W. (1977). Orthograde and retrograde axoplasmic transport during acute ocular hypertension in the monkey. *Investigative ophthalmology & visual science* **16**:426–441.

Mitchell, P., Smith, W., Attebo, K. and Healey, P.R. (1996). Prevalence of Open-angle Glaucoma in Australia: The Blue Mountains Eye Study. *Ophthalmology* [Online] **103**:1661–1669. Available at: <http://www.sciencedirect.com/science/article/pii/S0161642096304491>.

Monemi, S., Spaeth, G., DaSilva, A., Popinchalk, S., Ilitchev, E., Liebmann, J., Ritch, R., *et al.* (2005). Identification of a novel adult-onset primary open-angle glaucoma (POAG) gene on 5q22.1. *Human Molecular Genetics* [Online] **14**:725–733. Available at: <http://hmg.oxfordjournals.org/content/14/6/725.abstract>.

Morgan, J.E. (2012). Retina ganglion cell degeneration in glaucoma: an opportunity missed? A review. *Clinical & Experimental Ophthalmology* [Online] **40**:364–368. Available at: <http://dx.doi.org/10.1111/j.1442-9071.2012.02789.x>.

Morishita, H., Miwa, J.M., Heintz, N. and Hensch, T.K. (2010). Lynx1, a cholinergic brake, limits plasticity in adult visual cortex. *Science (New York, N.Y.)* [Online] **330**:1238–40. Available at: <http://www.pubmedcentral.nih.gov/articlerender.fcgi?artid=3387538&tool=pmcentrez&rendertype=abstract>.

Mrsic-Flogel, T.D., Hofer, S.B., Creutzfeldt, C., Cloez-Tayarani, I., Changeux, J.-P., Bonhoeffer, T. and Hubener, M. (2005). Altered map of visual space in the superior colliculus of mice lacking early retinal waves. *The Journal of neuroscience : the official journal of the Society for Neuroscience* **25**:6921–6928.

Muir, D.W. and Mitchell, D.E. (1973). Visual Resolution and Experience: Acuity Deficits in Cats Following Early Selective Visual Deprivation. *American Association for the Advancement of Science* **180**:420–422.



- Nakai, J., Ohkura, M. and Imoto, K. (2001). A high signal-to-noise Ca(2+) probe composed of a single green fluorescent protein. *Nature biotechnology* **19**:137–141.
- Nakazawa, T., Nakazawa, C., Matsubara, A., Noda, K., Hisatomi, T., She, H., Michaud, N., *et al.* (2006). Tumor necrosis factor-alpha mediates oligodendrocyte death and delayed retinal ganglion cell loss in a mouse model of glaucoma. *The Journal of neuroscience : the official journal of the Society for Neuroscience* **26**:12633–12641.
- Naskar, R., Wissing, M. and Thanos, S. (2002). Detection of Early Neuron Degeneration and Accompanying Microglial Responses in the Retina of a Rat Model of Glaucoma. *Investigative Ophthalmology & Visual Science* **43**:2962–2968.
- Nguyen, J. V, Soto, I., Kim, K.-Y., Bushong, E. a, Oglesby, E., Valiente-Soriano, F.J., Yang, Z., *et al.* (2011). Myelination transition zone astrocytes are constitutively phagocytic and have synuclein dependent reactivity in glaucoma. *Proceedings of the National Academy of Sciences of the United States of America* **108**:1176–1181.
- Nice, I. (2009). Glaucoma : diagnosis and management of chronic open angle glaucoma and ocular hypertension Costing report Implementing NICE guidance. **85**:1–39.
- Niell, C.M. and Stryker, M.P. (2008). Highly Selective Receptive Fields in Mouse Visual Cortex. *Journal of Neuroscience* [Online] **28**:7520–7536. Available at: <http://www.jneurosci.org/cgi/doi/10.1523/JNEUROSCI.0623-08.2008>.
- Nys, J., Aerts, J., Ytebrouck, E., Vreysen, S., Laeremans, A. and Arckens, L. (2014). The cross-modal aspect of mouse visual cortex plasticity induced by monocular enucleation is age dependent. *Journal of Comparative Neurology* [Online] **522**:950–970. Available at: <http://dx.doi.org/10.1002/cne.23455>.
- Nys, J., Scheyltjens, I. and Arckens, L. (2015). Visual system plasticity in mammals: the story of monocular enucleation-induced vision loss. *Frontiers in systems neuroscience* **9**:60.
- Park, H.-Y.L., Kim, J.H. and Park, C.K. (2012). Activation of autophagy induces retinal ganglion cell death in a chronic hypertensive glaucoma model. *Cell Death Dis* [Online] **3**:e290. Available at: <http://dx.doi.org/10.1038/cddis.2012.26>.
- Park, K.K., Liu, K., Hu, Y., Smith, P.D., Wang, C., Cai, B., Xu, B., *et al.* (2008). Promoting axon regeneration in the adult CNS by modulation of the PTEN/mTOR pathway. *Science (New York, N.Y.)* [Online] **322**:963–6. Available at: <http://www.pubmedcentral.nih.gov/articlerender.fcgi?artid=2652400&tool=pmcentrez&rendertype=abstract>.
- Pavlidis, M., Stupp, T., Naskar, R., Cengiz, C. and Thanos, S. (2003). Retinal Ganglion Cells Resistant to Advanced Glaucoma: A Postmortem Study of Human Retinas with the Carbocyanine Dye DiI. *Investigative Ophthalmology & Visual Science* [Online] **44**:5196–5205. Available at: <http://dx.doi.org/10.1167/iovs.03-0614>.
- Pederson, J.E. and Anderson, D.R. (1980). The Mode of Progressive Disc Cupping in Ocular Hypertension and Glaucoma. *Archives of ophthalmology* **98**:490–495.
- Pizzorusso, T., Medini, P., Berardi, N., Chierzi, S., Fawcett, J.W. and Maffei, L.

- (2002). Reactivation of Ocular Dominance Plasticity in the Adult Visual Cortex. *Science* [Online] **298**:1248–1251. Available at: <http://www.sciencemag.org/content/298/5596/1248.abstract>.
- Porciatti, V. (2007). The mouse pattern electroretinogram. *Documenta Ophthalmologica* **115**:145–153.
- Porciatti, V., Pizzorusso, T. and Maffei, L. (1999). The visual physiology of the wild type mouse determined with pattern VEPs. *Vision research* **39**:3071–3081.
- Provis, J.M., Dubis, A.M., Maddess, T. and Carroll, J. (2013). Adaptation of the central retina for high acuity vision: Cones, the fovea and the a vascular zone. *Progress in Retinal and Eye Research* **35**:63–81.
- Qing, G., Zhang, S., Wang, B. and Wang, N. (2010). Functional MRI signal changes in primary visual cortex corresponding to the central normal visual field of patients with primary open-angle glaucoma. *Investigative Ophthalmology and Visual Science* **51**:4627–4634.
- Quigley, H.A., Hohman, R.M., Addicks, E.M., Massof, R.W. and Green, W.R. (1983). Morphologic changes in the lamina cribrosa correlated with neural loss in open-angle glaucoma. *American journal of ophthalmology* **95**:673–691.
- Quigley, H.A., McKinnon, S.J., Zack, D.J., Pease, M.E., Kerrigan–Baumrind, L.A., Kerrigan, D.F. and Mitchell, R.S. (2000). Retrograde Axonal Transport of BDNF in Retinal Ganglion Cells Is Blocked by Acute IOP Elevation in Rats. *Investigative Ophthalmology & Visual Science* **41**:3460–3466.
- Quigley, H.A., Nickells, R.W., Kerrigan, L.A., Pease, M.E., Thibault, D.J. and Zack, D.J. (1995). Retinal ganglion cell death in experimental glaucoma and after axotomy occurs by apoptosis. *Investigative Ophthalmology & Visual Science* **36**:774–786.
- Quigley, H.A., Sanchez, R.M., Dunkelberger, G.R., L'Hernault, N.L. and Baginski, T.A. (1987). Chronic glaucoma selectively damages large optic nerve fibers. *Investigative Ophthalmology and Visual Science* **28**:913–920.
- Ranson, A., Cheetham, C.E.J., Fox, K. and Sengpiel, F. (2012). Homeostatic plasticity mechanisms are required for juvenile, but not adult, ocular dominance plasticity. *Proceedings of the National Academy of Sciences of the United States of America* [Online] **109**:1311–1316. Available at: <http://www.ncbi.nlm.nih.gov/pubmed/22232689>.
- Ranson, A., Sengpiel, F. and Fox, K. (2013). The Role of GluA1 in Ocular Dominance Plasticity in the Mouse Visual Cortex. *The Journal of Neuroscience* [Online] **33**:15220–15225. Available at: <http://www.jneurosci.org/content/33/38/15220.abstract>.
- Ribelayga, C., Zhang, Z., Vidal, A. and Zimmerman, R. (2014). A circadian clock in intrinsically photosensitive retinal ganglion cells is required for normal visual function. *Investigative Ophthalmology & Visual Science* **55**:1234.
- Rodieck, R.W., Binmoeller, K.F. and Dineen, J. (1985). Parasol and midget ganglion cells of the human retina. *The Journal of comparative neurology* **233**:115–132.
- Rose, T., Jaepel, J., Hübener, M. and Bonhoeffer, T. (2016). Cell-specific restoration of stimulus preference after monocular deprivation in the visual cortex. *Science*

352:1319–1322.

Rudy, B., Fishell, G., Lee, S. and Hjerling-Leffler, J. (2011). Three groups of interneurons account for nearly 100% of neocortical GABAergic neurons. *Developmental Neurobiology* **71**:45–61.

Ruiz-Ederra, J. and Verkman, A.S. (2006). Mouse model of sustained elevation in intraocular pressure produced by episcleral vein occlusion. *Experimental eye research* **82**:879–884.

Samsel, P. a, Kisiswa, L., Erichsen, J.T., Cross, S.D. and Morgan, J.E. (2011). A novel method for the induction of experimental glaucoma using magnetic microspheres. *Investigative ophthalmology & visual science* [Online] **52**:1671–5. Available at: <http://www.ncbi.nlm.nih.gov/pubmed/20926815>.

Sawtell, N.B., Frenkel, M.Y., Philpot, B.D., Nakazawa, K., Tonegawa, S. and Bear, M.F. (2003). NMDA receptor-dependent ocular dominance plasticity in adult visual cortex. *Neuron* [Online] **38**:977–985. Available at: [http://www.ncbi.nlm.nih.gov/entrez/query.fcgi?cmd=Retrieve&db=PubMed&dopt=Citation&list\\_uids=12818182](http://www.ncbi.nlm.nih.gov/entrez/query.fcgi?cmd=Retrieve&db=PubMed&dopt=Citation&list_uids=12818182).

Schiefer, U., Papageorgiou, E., Sample, P.A., Pascual, J.P., Selig, B., Krapp, E. and Paetzold, J. (2010). Spatial pattern of glaucomatous visual field loss obtained with regionally condensed stimulus arrangements. *Investigative Ophthalmology and Visual Science* **51**:5685–5689.

Schmidt, T.M., Chen, S.-K. and Hattar, S. (2011). Intrinsically photosensitive retinal ganglion cells: many subtypes, diverse functions. *Trends in neurosciences* [Online] **34**:572–580. Available at: <http://www.ncbi.nlm.nih.gov/pmc/articles/PMC3200463/>.

Scholl, B., Burge, J. and Priebe, N.J. (2013). Binocular integration and disparity selectivity in mouse primary visual cortex. *Journal of Neurophysiology* [Online] **109**:3013–3024. Available at: <http://jn.physiology.org/content/109/12/3013.abstract>.

Schuett, S., Bonhoeffer, T. and Hübener, M. (2002). Mapping Retinotopic Structure in Mouse Visual Cortex with Optical Imaging. *The Journal of Neuroscience* [Online] **22**:6549–6559. Available at: <http://www.jneurosci.org/content/22/15/6549.abstract>.

Schwaller, B. (2010). Cytosolic Ca<sup>2+</sup> Buffers. *Cold Spring Harbor Perspectives in Biology* [Online] **2**. Available at: <http://cshperspectives.cshlp.org/content/2/11/a004051.abstract>.

Senatorov, V., Malyukova, I., Fariss, R., Wawrousek, E.F., Swaminathan, S., Sharan, S.K. and Tomarev, S. (2006). Expression of mutated mouse myocilin induces open-angle glaucoma in transgenic mice. *The Journal of neuroscience : the official journal of the Society for Neuroscience* **26**:11903–11914.

Sharma, A.K., Goldberg, I., Graham, S.L. and Mohsin, M. (2000). Comparison of the Humphrey Swedish Interactive Thresholding Algorithm (SITA) and Full Threshold Strategies. *Journal of Glaucoma* [Online] **9**. Available at: [http://journals.lww.com/glaucomajournal/Fulltext/2000/02000/Comparison\\_of\\_the\\_Humphrey\\_Swedish\\_Interactive.5.aspx](http://journals.lww.com/glaucomajournal/Fulltext/2000/02000/Comparison_of_the_Humphrey_Swedish_Interactive.5.aspx).

Smith, S.L. and Trachtenberg, J.T. (2007). Experience-dependent binocular

competition in the visual cortex begins at eye opening. *Nature neuroscience* **10**:370–375.

Sohya, K., Kameyama, K., Yanagawa, Y., Obata, K. and Tsumoto, T. (2007). GABAergic neurons are less selective to stimulus orientation than excitatory neurons in layer II/III of visual cortex, as revealed by in vivo functional Ca<sup>2+</sup> imaging in transgenic mice. *The Journal of neuroscience : the official journal of the Society for Neuroscience* **27**:2145–2149.

Sommer, A., Katz, J. and HA, Q. (1991). Clinically detectable nerve fiber atrophy precedes the onset of glaucomatous field loss. *Archives of Ophthalmology* [Online] **109**:77–83. Available at: <http://dx.doi.org/10.1001/archophth.1991.01080010079037>.

Study, A.G.I. (1994). Advanced Glaucoma Intervention Study (AGIS): 2. Visual Field Test Scoring and Reliability. *Ophthalmology* **101**:1445–1455.

Sun, W., Li, N. and He, S. (2002). Large-scale morphological survey of mouse retinal ganglion cells. *The Journal of comparative neurology* **451**:115–126.

Tagawa, Y., Kanold, P.O., Majdan, M. and Shatz, C.J. (2005). Multiple periods of functional ocular dominance plasticity in mouse visual cortex. *Nature neuroscience* **8**:380–388.

Templeton, J.P. and Geisert, E.E. (2012). A practical approach to optic nerve crush in the mouse. *Molecular vision* [Online] **18**:2147–52. Available at: <http://www.pubmedcentral.nih.gov/articlerender.fcgi?artid=3413441&tool=pmcentrez&rendertype=abstract>.

Tham, Y.-C., Li, X., Wong, T.Y., Quigley, H.A., Aung, T. and Cheng, C.-Y. (2015). Global Prevalence of Glaucoma and Projections of Glaucoma Burden through 2040. *Ophthalmology* [Online] **121**:2081–2090. Available at: <http://dx.doi.org/10.1016/j.ophtha.2014.05.013>.

Thomas, B.B., Seiler, M.J., Saddy, S.R., Coffey, P.J. and Aramant, R.B. (2004). Optokinetic test to evaluate visual acuity of each eye independently. *Journal of Neuroscience Methods* **138**:7–13.

Tian, L., Hires, S.A., Mao, T., Huber, D., Chiappe, M.E., Chalasani, S.H., Petreanu, L., *et al.* (2009). Imaging neural activity in worms, flies and mice with improved GCaMP calcium indicators. *Nat Meth* [Online] **6**:875–881. Available at: <http://dx.doi.org/10.1038/nmeth.1398>.

Toldi, J., Fehér, O. and Wolff, J.-R. (1996). Neuronal plasticity induced by neonatal monocular (and binocular) enucleation. *Progress in Neurobiology* [Online] **48**:191–218. Available at: <http://www.sciencedirect.com/science/article/pii/0301008295000380>.

Turrigiano, G.G. and Nelson, S.B. (2004). Homeostatic plasticity in the developing nervous system. *Nat Rev Neurosci* [Online] **5**:97–107. Available at: <http://dx.doi.org/10.1038/nrn1327>.

Urban, D.J. and Roth, B.L. (2015). DREADDs (Designer Receptors Exclusively Activated by Designer Drugs): Chemogenetic Tools with Therapeutic Utility. *Annual Review of Pharmacology and Toxicology* [Online] **55**:399–417. Available at: <http://www.annualreviews.org/doi/abs/10.1146/annurev-pharmtox-010814->

124803%5Cn.

Villegas-Perez, M.P., Vidal-Sanz, M., Rasminsky, M., Bray, G.M. and Aguayo, A.J. (1993). Rapid and protracted phases of retinal ganglion cell loss follow axotomy in the optic nerve of adult rats. *Journal of neurobiology* **24**:23–36.

Volgyi, B., Chheda, S. and Bloomfield, S.A. (2009). Tracer coupling patterns of the ganglion cell subtypes in the mouse retina. *The Journal of comparative neurology* **512**:664–687.

Votruba, M., Thiselton, D. and Bhattacharya, S.S. (2003). Optic disc morphology of patients with OPA1 autosomal dominant optic atrophy. *The British journal of ophthalmology* [Online] **87**:48–53. Available at: <http://www.pubmedcentral.nih.gov/articlerender.fcgi?artid=1771445&tool=pmcentrez&rendertype=abstract>.

Vrabec, J.P. and Levin, L.A. (2007). The neurobiology of cell death in glaucoma. *Eye* [Online] **21**:S11–S14. Available at: <http://dx.doi.org/10.1038/sj.eye.6702880>.

Wadood, A.C., Azuara-Blanco, A., Aspinall, P., Taguri, A. and King, A.J.W. (2002). Sensitivity and specificity of frequency-doubling technology, tendency-oriented perimetry, and Humphrey Swedish interactive threshold algorithm-fast perimetry in a glaucoma practice1. *American Journal of Ophthalmology* [Online] **133**:327–332. Available at: <http://www.sciencedirect.com/science/article/pii/S0002939401014246>.

Wall, P.D. and Egger, M.D. (1971). Formation of New Connexions in Adult Rat Brains after Partial Deafferentation. *Nature* [Online] **232**:542–545. Available at: <http://dx.doi.org/10.1038/232542a0>.

Wang, A.L., Yuan, M. and Neufeld, A.H. (2007). Age-related changes in neuronal susceptibility to damage: comparison of the retinal ganglion cells of young and old mice before and after optic nerve crush. *Annals of the New York Academy of Sciences* **1097**:64–66.

Wang, L., Cioffi, G.A., Cull, G., Dong, J. and Fortune, B. (2002). Immunohistologic evidence for retinal glial cell changes in human glaucoma. *Investigative Ophthalmology and Visual Science* **43**:1088–1094.

Watson, C. (2012). Chapter 25 - Visual System. In: Puelles, C. W. P. B. T.-T. M. N. S. (ed.) San Diego: Academic Press, pp. 646–652. Available at: <http://www.sciencedirect.com/science/article/pii/B9780123694973100251>.

Weber, A.J., Kaufman, P.L. and Hubbard, W.C. (1998). Morphology of single ganglion cells in the glaucomatous primate retina. *Investigative Ophthalmology & Visual Science* **39**:2304–2320.

White, K.E., Davies, V.J., Hogan, V.E., Piechota, M.J., Nichols, P.P., Turnbull, D.M. and Votruba, M. (2009). OPA1 deficiency associated with increased autophagy in retinal ganglion cells in a murine model of dominant optic atrophy. *Investigative ophthalmology & visual science* **50**:2567–2571.

Whitmore, A. V, Libby, R.T. and John, S.W.M. (2005). Glaucoma: Thinking in new ways—a role for autonomous axonal self-destruction and other compartmentalised processes? *Progress in Retinal and Eye Research* [Online] **24**:639–662. Available at: <http://www.sciencedirect.com/science/article/pii/S1350946205000224>.

Wiesel, T.N. and Hubel, D.H. (1963). Single-Cell Responses in Striate Cortex of Kittens Deprived of Vision in One Eye. *Journal of neurophysiology* [Online] **26**:1003–1017. Available at: <http://dinshi.com/wp-content/uploads/2014/03/Wiesel-Striate-cortex-responses-in-deprived-eye-J-Neurophys-1963.pdf>.

Williams, P.A., Howell, G.R., Barbay, J.M., Braine, C.E., Sousa, G.L., John, S.W.M. and Morgan, J.E. (2013). Retinal Ganglion Cell Dendritic Atrophy in DBA/2J Glaucoma. *PLoS ONE* [Online] **8**:e72282. Available at: <http://dx.doi.org/10.1371%2Fjournal.pone.0072282>.

Williams, P.A., Morgan, J.E. and Votruba, M. (2010). Opa1 deficiency in a mouse model of dominant optic atrophy leads to retinal ganglion cell dendropathy. *Brain* **133**:2942–2951.

Woodhoo, A., Alonso, M.B.D., Droggiti, A., Turmaine, M., D'Antonio, M., Parkinson, D.B., Wilton, D.K., *et al.* (2009). Notch controls embryonic Schwann cell differentiation, postnatal myelination and adult plasticity. *Nat Neurosci* [Online] **12**:839–847. Available at: <http://www.pubmedcentral.nih.gov/articlerender.fcgi?artid=2782951&tool=pmcentrez&rendertype=abstract>.

Wree, A., Kulig, G., Gutmann, P. and Zilles, K. (1985). Modification of callosal afferents of the primary visual cortex ipsilateral to the remaining eye in rats monocularly enucleated at different stages of ontogeny. *Cell and Tissue Research* **242**:433–436.

Xu, X., Roby, K.D. and Callaway, E.M. (2010). Immunochemical characterization of inhibitory mouse cortical neurons: Three chemically distinct classes of inhibitory cells. *Journal of Comparative Neurology* **518**:389–404.

Yamagishi, N., Anton, A., Sample, P.A., Zangwill, L., Lopez, A. and Weinreb, R.N. (1997). Mapping structural damage of the optic disk to visual field defect in glaucoma. *American Journal of Ophthalmology* [Online] **123**:667–676. Available at: <http://www.scopus.com/inward/record.url?eid=2-s2.0-0030922693&partnerID=40&md5=b144f85fa1abf0e07d1a0802545ff318>.

Yamahachi, H., Marik, S.A., McManus, J.N.J., Denk, W. and Gilbert, C.D. (2009). Rapid axonal sprouting and pruning accompany functional reorganization in primary visual cortex. *Neuron* **64**:719–729.

Yoles, E. and Schwartz, M. (1998). Degeneration of spared axons following partial white matter lesion: implications for optic nerve neuropathies. *Experimental neurology* **153**:1–7.

You, Y., Gupta, V.K., Graham, S.L. and Klistorner, A. (2012). Anterograde Degeneration along the Visual Pathway after Optic Nerve Injury. *PLoS ONE* **7**.

Yücel, Y.H., Zhang, Q., Gupta, N., Kaufman, P.L. and Weinreb, R.N. (2000). Loss of neurons in magnocellular and parvocellular layers of the lateral geniculate nucleus in glaucoma. *Archives of ophthalmology* **118**:378–384.

Yukita, M., Machida, S., Nishiguchi, K.M., Tsuda, S., Yokoyama, Y., Yasuda, M., Maruyama, K., *et al.* (2015). Molecular, anatomical and functional changes in the retinal ganglion cells after optic nerve crush in mice. *Documenta ophthalmologica. Advances in ophthalmology* **130**:149–156.

Zepeda, A., Arias, C. and Sengpiel, F. (2004). Optical imaging of intrinsic signals: recent developments in the methodology and its applications. *Journal of Neuroscience Methods* [Online] **136**:1–21. Available at: <http://www.sciencedirect.com/science/article/pii/S0165027004000974>.

Zeyen, T. and Caprioli, J. (1993). Progression of disc and field damage in early glaucoma. *Archives of Ophthalmology* [Online] **111**:62–65. Available at: <http://dx.doi.org/10.1001/archopht.1993.01090010066028>.

Zucker, R.S. (1999). Calcium- and activity-dependent synaptic plasticity. *Current Opinion in Neurobiology* [Online] **9**:305–313. Available at: <http://www.sciencedirect.com/science/article/pii/S0959438899800452>.